CERN 68-7
Volume II
29 February 1968

ORGANISATION EUROPÉENNE POUR LA RECHERCHE NUCLÉAIRE
CERN EUROPEAN ORGANIZATION FOR NUCLEAR RESEARCH

TOPICAL CONFERENCE ON HIGH-ENERGY COLLISIONS OF HADRONS

sponsored by

The International Union of Pure and Applied Physics (IUPAP)

CERN, Geneva, 15 - 18 January 1968

PROCEEDINGS

Volume II: Contributed papers

GENEVA
1968

V O L U M E II

TABLE OF CONTENTS

(The page numbers referred to are those in brackets)

CONTRIBUTED PAPERS - Theoretical

CONTRIBUTED PAPERS - Experimental

V O L U M E I

TABLE OF CONTENTS

(The page numbers referred to are those in brackets)

*) Paper presented by L. Van Hove due to illness of the author.

SPECIAL SESSION

INVITED PAPERS - Theoretical

---

*) Not included in these Proceedings, to be published in the Proceedings of Sixth International Conference on High Energy Accelerators, Cambridge, USA, September 11-15, 1967.

**) Not included in these Proceedings, an extended version of this paper, written by J.D. Jackson and G.E. Hite, will be published in Physical Review.

INVITED PAPERS - Experimental

REGGE RESIDUA, FORM FACTORS, AND COMPOSITE PARTICLES

R. C. Arnold and S. Fenster,

High Energy Physics Division
Argonne National Laboratory
Argonne, Illinois 60439

1. INTRODUCTION

1.1 The Van Hove formula

It was observed by Van Hove[1] in 1966 that for small $|t|$, the relation

$$\frac{d\sigma}{dt} \underset{s \to \infty}{\sim} [\, G_E(t)]^4 \qquad (1)$$

for proton-proton scattering is apparently very well satisfied experimentally. He gave a derivation based on a quark model, wherein both the strong and electromagnetic interaction amplitudes of the quarks were assumed to be slowly varying with t compared to the variation of the structure factors. This picture is quite analogous to the deuteron's properties. We will refer to (1) as the Van Hove formula, to emphasize the small momentum transfer spirit in which it will be regarded in this work.[2]

In Figure 1 we present the right and left sides of relation (1), using data for proton-proton scattering at 20 GeV/c,[3] and the proton magnetic form factor G_M.[4] The agreement is very impressive for a strong interaction dynamics result.

1.2 Regge pole residua and form factors

We wish to explore the significance of a relation such as (1) (generalized to other hadrons, as well as nucleons) in the context of the analysis of singularities in the angular momentum plane of high energy scattering amplitudes. In particular suppose that a Pomeranchuk

Regge pole, with $\alpha(0) = 1$, is responsible for the high energy asymptotic behavior at small $|t|$ of elastic scattering amplitudes. Then if the Van Hove formula is to be satisfied, this pole must have the following two properties:

(a) $\alpha(t)$ remains very close to 1 for the range of t under consideration (i.e., the pole must be fixed, or nearly so);

(b) The pole residue $\beta(t)$ must have factors proportional to the electromagnetic form factors of the hadrons to which the pole couples, e.g., $\beta_{12}(t) \propto G_{E_1}(t)\, G_{E_2}(t)$.

Property (a) is necessary if $d\sigma/dt$ is to become asymptotically a function of t only for the range of t under consideration (e.g., $|t| < .50\ \text{GeV}^2$); property (b) then yields the relation (1) since

$$\frac{d\sigma}{dt} \underset{s \to \infty}{\to} s^{2\alpha(t)-2}\,[\beta(t)]^2 \quad .$$

A natural question to ask is this; do all the <u>other</u> Regge poles (e.g., $\rho, \omega, A_2, \ldots$) have residua given in such a way by the electromagnetic form factors? We will consider a model wherein this can be answered; we will also be able to discuss corrections to the Van Hove formula, and whether all corrections die out for large enough energy. We also show in the model that relations such as (1) hold even if there are singularities near $\alpha = 1$ other than poles which dominate the asymptotic quark-quark scattering behavior.

1.3 <u>Outline of model</u>

We consider the known low-mass hadrons to be composed of three quarks (baryons) or quark and antiquark (mesons). To simplify the discussion[5] we will later take a meson mass around $M_\omega \approx .80\,\text{GeV}$ and baryon mass around $M_\Sigma \approx 1.2\ \text{GeV}$; this will permit us to introduce quarks of mass M slightly above $\frac{M_\omega}{2}$ (e.g., .42 GeV) and ultimately consider a moderately weak-binding limit.[6] However, the initial discussion is independent of these details.

The Regge poles, and other singularities in the ℓ plane, will be introduced as singularities in the $Q\bar{Q} \to Q\bar{Q}$ t channel.

The QQ, $Q\bar{Q}$ scattering amplitudes at high energies and Q form factors are to be input quantities from which we derive the hadron properties using an approach which is essentially the impulse approximation generalized to the complex angular momentum plane. In practice, the $Q\bar{Q}$ Regge pole reduced residua are taken as constants over the t region of interest ($|t| < .50$ GeV^2), and the trajectories taken as straight lines passing through known resonances in the J plane. The formulation of the model relies on analyticity and unitarity rather than nonrelativistic ideas.

Assuming the t channel in hadron-hadron scattering is dominated by $Q\bar{Q}$ states, corresponding to the picture of hadrons with a quark structure, a coupled channel N/D formulation for amplitudes in the t-channel at complex angular momentum is constructed, continued when necessary to binding energies for which anomalous thresholds appear. We will find that near each singularity ℓ_s in the ℓ plane where the QQ or $Q\bar{Q}$ scattering amplitude $A_{11}(\ell, t)$ has an infinity, the (hadron)$_j$-(hadron)$_k$ scattering amplitude A_{jk} can be factored into 3 terms:

$$A_{jk}(\ell, t) \cong [D_{1j}(\ell_s, t)]^T A_{11}(\ell, t) D_{1k}(\ell_s, t) \qquad (2)$$

for ℓ near ℓ_s, where the D_{1j} contain the structure parameters of hadron j. (The transpose notation refers only to spin indices, when present.) This generalizes the Van Hove formula, which is obtained from singularities with $\ell = 1$, as $D_{1j}(1, t)$ is closely related to the electromagnetic form factor of hadron j, the two coinciding when the quark form factors are constants.

2. TRIPLE FACTORIZATION AT SINGULARITIES

Consider the elastic scattering of hadron j on hadron k, in a system composed of hadrons and quarks. We define a suitably normalized scattering amplitude $A_{jk}(\ell, t)$, whose relation to differential cross-

sections will be specified later, to be obtained from an N/D formalism (with proper threshold and analytic properties built in) as:

$$\underline{A}(\ell, t) = \underline{N}(\ell, t)\underline{D}^{-1}(\ell, t), \tag{3}$$

where $\underline{D}$ has only a right hand (unitarity) cut in t and $\underline{N}$ has only left hand or anomalous cuts. Let channel 1 be $Q\bar{Q}$, and let $\rho_j(\ell, t)$ be the phase space for channel j with appropriate threshold factors. We follow to a great extent the approach of Blankenbecler, Cook and Goldberger,[7] who treated Regge poles in a coupled channel formalism including composite particles. The unitarity condition, keeping many coupled two-body channels, imposes the relation

$$\underline{D}(\ell, t) = \underline{I} - \frac{1}{\pi}\int_{4M^2}^{\infty} \frac{dt'}{t' - t - i\epsilon}\underline{\rho}(\ell, t')\underline{N}(\ell, t') \tag{4}$$

where $\underline{\rho}$ is the diagonal matrix of phase space factors; $4M^2$ is the lowest normal threshold. (The lower limit will be extended to the anomalous threshold when the continuation is performed to obtain weak binding.)

The input quantities for this formalism can be taken as $\underline{B}(\ell, t)$, the left hand or "dynamical" contributions to the amplitude, representing a generalization of the Born approximation for processes such as $j + \bar{j} \to k + \bar{k}$ in the t channel. The N function satisfies a linear integral equation whose kernel and inhomogeneous term are determined by $\underline{B}$. The hadron structure information is contained in the B_{1j}'s in a way well-known from deuteron theory.[8] These functions arise from the partial wave projection of the following graphs:

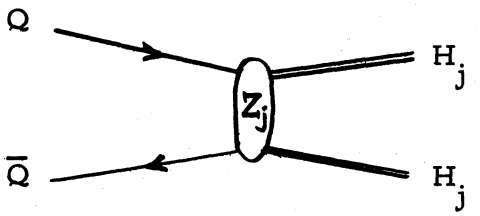

These contain the wave function of hadron H_j as a composite of quark Q with state Z_j. In the meson case we take Z to be $\bar{Q}$, whence for mesons

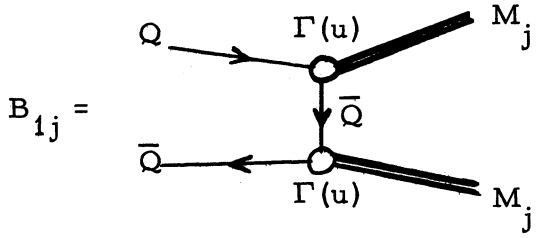

where u is the square of the invariant momentum transfer between Q and M_j.

The vertex functions $\Gamma_j(u)$ now are essentially the wave function [of M_j as a bound state of $Q\bar{Q}$] in momentum space divided by a factor representing the bound state pole. [8]

In accordance with the idea that hadron reactions at high energy are mediated by Q interactions, we postulate $B_{jk} = 0$ unless either j or k = 1 (absence of "direct" hadron-hadron potentials). However, B_{11} is assumed arbitrarily strong. Now we make the following observations:

(A) If the vertex Γ_j refers to bound state wave functions which vanish rapidly enough at small distances, B_{1j} will drop off rapidly with increasing t.

(B) Since the hadron masses are assumed appreciably larger than the quark mass M, $4M^2$ is the lowest normal threshold. [In the weak binding configuration the anomalous threshold will be $t_0 < 4M^2$.] Thus the thresholds $t_k (k > 1)$ which define the support of ρ_k will be high, and presumably in a region of t where B_{1j} is small.

(C) We assume the singularities in B_{11} are at high mass (short range $Q\bar{Q}$ forces).

As a consequence of (A), (B) and (C), we can (for j, $k \neq 1$) approximate N_{1j} by B_{1j}; and further, D_{j1} and $(D_{jk}-1)$ for j, $k \neq 1$ will have magnitudes much less than D_{1j}, so we can ignore the former two classes of terms in computing D^{-1}. We obtain an upper-triangular

form for D, with only the top row and diagonal elements nonzero, and all terms but D_{11} on the diagonal are unity. This yields a determinant equal to the determinant of the (1, 1) channel only, i. e., quark-antiquark dynamics determine the pole positions (zeros of det D). The form of D^{-1} is the same as the form of D, with $(D^{-1})_{11} = (D_{11})^{-1}$, and $(D^{-1})_{1j} = -(D_{11})^{-1}D_{1j}$.

The meson-meson scattering amplitude, computed using these expressions, can be written in the form:

$$A_{jk} = -(N_{1j})^{T}D_{1k} + (D_{1j})^{T}A_{11}D_{1k} \tag{5}$$

where the transpose notation refers only to possible spin indices in the channels specified by the explicit subscript notation. [In obtaining this expression it is necessary to use the proof of Bjorken and Nauenberg[9] that a symmetric input B (as we assume) necessarily yields a symmetric.] At any singularity of the quark-antiquark scattering amplitude A_{11}, e. g., poles (or branch points yielding an infinity) in the ℓ plane, the second term dominates yielding equation (2).

For later reference, the amplitude for t channel annihilation of mesons into quark and antiquark is given by:

$$A_{1j} = N_{1j} - A_{11}D_{1j} \tag{6}$$

The second term in (5), which gives the contributions for $Q\bar{Q}$ scattering singularities, is generated by diagrams of the following form:

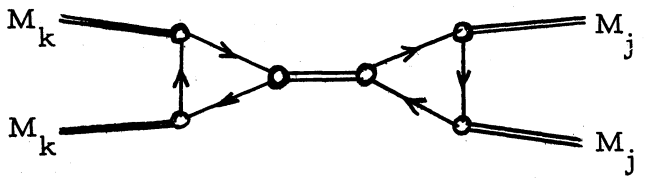

Note that these diagrams are exactly those given by Van Hove[1] in his derivation.

The first term in (5) can be shown to be generated by the box diagrams (since the imaginary part of this term is $N^{+}\rho N$, which is the imaginary part of the box):

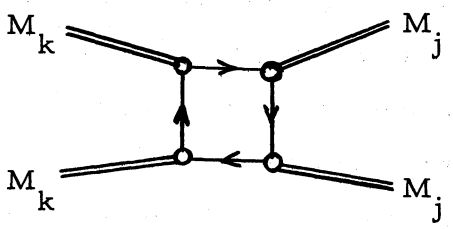

A similar explanation can be attached to the two terms in (6); the second involves $Q\bar{Q}$ scattering, while the first is just the Born term.

For our particular case involving $Q\bar{Q}$ states with spin 1/2 quarks, it can be shown that the first term in (5) contributes an asymptotic term in the meson-meson s channel scattering amplitude of order s^{-1} compared to the Pomeranchuk singularity, and can always be ignored asymptotically.

The expression (2) now exhibits a form of relativistic impulse approximation, since D_{1j} is calculated directly from the wave functions of the hadrons through Γ_j.

3. FORM FACTORS

Let G_j be the j^{th} hadron form factor (set of $2s_j + 1$ form factors, if hadron j has spin s_j). Then using coupled channel unitarity, writing G as a column matrix with elements G_j,

$$\mathrm{Im}G(t) = A^{+}(1,t)\,\rho\,(1,t)G(t) \tag{7}$$

We assume only $Q\bar{Q}$ states dominate the absorptive parts in the t channel for all processes, as in scattering. In addition, unsubtracted dispersion relations are assumed for the form factors. Using the expressions (6) for the relevant amplitudes in (7), and noting that $\mathrm{Im}D = -\rho N$, we can obtain

$$G_j(t) = [\,D_{1j}(1,t)\,]^{T} G_1(t) \tag{8}$$

exhibiting the factorization of the j^{th} hadron form factor into products of quark form factor [presumably dominated by vector meson poles, where det $D(1,t) = 0$] and structure factor $D_{1j}(1,t)$.

Now (8) together with (2) imply the Van Hove formula if G_1 and the residua of A_{11} are constant; but a correction is obtained to the VH formula in general which depends on the relative t dependence of the strong and electromagnetic properties of the quark. This faithfully reflects the physical assumptions implicit in the simple derivations given originally.[1] The empirical data on high energy scattering shown in Figure 1, together with the form factor data, suggest that this correction must be unimportant in fact.

The relation (8) has another consequence. If the normalization appropriate to charge conservation is chosen, then $G_{1E}(0) = G_j(0) = 1$ (here, E denotes the quark electric form factor).

Taking j to be a meson, the condition $D_{1j}(1,0) = 1$ implied by these relations can be interpreted as imposing a condition on the magnitude of the wave function normalizations, or Γ functions. It can be shown that in the extreme weak binding limit this condition is identical to that of the zero-range model of Freund and Predazzi,[10] and thus our model contains theirs as a special case.

The condition that $D_{1k}(1,0)$ is a universal constant for all hadrons guarantees the retention of universality and symmetry properties as in a nonrelativistic bound-state quark model, but (strictly speaking) only for singularities near $\ell = 1$ such as the Pomeranchuk singularity.

Now our theory of Regge residua in general can be stated as follows: Let the vertex function Γ_j (related to wave functions of hadron j) be parametrized with any number of parameters; e.g., a sum of poles (cf. Gourdin et al., Ref. 8), leading to a sum of Legendre functions for B_{1j}. These parameters can be determined (in principle) by accurate enough measurements of the electromagnetic form factor $D_{1j}(1,t)$. Then the expression for B_{1j} exhibits explicitly the dependence

on ℓ, from which we obtain $D_{1j}(\ell, t)$ at the position of Regge poles (or cuts) in $Q\bar{Q}$ scattering amplitudes $A_{11}(\ell, t)$. The meson-meson residua then are obtained from equation (2).

We will explore the consequences in detail of a zero-range approximation for Γ which contains only one parameter: the binding energy of the $Q\bar{Q}$ pair constituting the meson.

4. STRUCTURE FACTORS AND CONTINUATIONS

4.1 D functions (structure factors) for meson residua

The reaction $MM \to Q\bar{Q}$ for spinless mesons and spin 1/2 quarks can be described with two invariant amplitudes, A and B, as in $\pi\pi \to N\bar{N}$. The latter reaction has been discussed extensively by Frazer and Fulco[11] and by Singh;[12] starting with the normal-threshold (tight binding) case we can carry over their kinematics directly to $MM \to Q\bar{Q}$. If Λ is the absolute value of the sum of quark and antiquark helicities ($\Lambda = 0$ or 1), B^{Λ}_{1j} are the appropriate parital wave projections (with threshold factors extracted), and assuming $A = 0$ [as we have only a positive parity spin 1/2 pole as in $\pi\pi \to N\bar{N}$], from ref. (12) one obtains:

$$B^{0}_{1j}(\ell, t) = (pq)^{-\ell} \int du\, Z\, Q_{\ell}(Z)\, \mathrm{disc}_u B(u,t)$$
$$B^{1}_{1j}(\ell, t) = \frac{1}{2}(pq)^{-\ell} \int du [Q_{\ell+1}(Z) - Q_{\ell-1}(Z)]\, \mathrm{disc}_u B(u,t) \qquad (9)$$

and

$$Z(u) = (u + p^2 + q^2)/2pq\ ;$$
$$p = (t/4 - \mu^2)^{1/2}, \quad q = (t/4 - M^2)^{1/2}.$$

Now if the zero-range approximation for the wave function is used (Γ constant), the discontinuity is concentrated only at $u = M^2$ and we obtain

$$B^{0}_{1j}(\ell, t) = \Gamma_j^2 (pq)^{-\ell} Z_0 Q_{\ell}(Z_0)$$
$$B^{1}_{1j}(\ell, t) = \Gamma_j^2 (pq)^{-\ell} [Q_{\ell+1}(Z_0) - Q_{\ell-1}(Z_0)]/2 \qquad (10)$$

where

$$Z_0 = (M^2 + p^2 + q^2)/2pq \quad .$$

In the general case we can parametrize Γ^2 by a sum of poles, [8] and the resulting B's will be sums of terms of the form (10). The continuation in angular momentum (in the normal threshold case) is now simple, since the Q functions are analytic in ℓ and damp out at infinity sufficiently rapidly to insure uniqueness via Carlson's theorem.

For practical applications, instead of using a multi-pole form for Γ which naturally damps out at high t we will use a zero-range approximation as given in (10), and after the D functions are expressed in terms of these B's, the masses continued to the weak binding region and the dominant anomalous threshold contribution exhibited, the t region above the normal threshold will be dropped. [13] The explicit form of the elements of the channel 1 phase space matrix, chosen to take into account the normal threshold behavior of the partial waves in the t channel and the analytic properties at t = 0 of the helicity amplitudes, are:

$$\rho_1^+(\ell, t) = \frac{2[q(t)]^{2\ell+1}}{\sqrt{t}}$$

$$\rho_1^-(\ell, t) = \left(\frac{t}{4M^2}\right) \frac{2[q(t)]^{2\ell+1}}{\sqrt{t}}$$

Finally, the result of the above continuation (keeping only the anomalous region) is:

$$D_j^+(\ell, t) = \Gamma_j^2 \cdot \frac{2}{\pi} \int_{t_0}^{4M^2} \frac{dt'q'}{\sqrt{t'}(t' - t)} Z_0(t') P_\ell[Z_0(t')] (q'/p')^\ell$$

$$D_j^-(\ell, t) = \Gamma_j^2 \cdot \frac{1}{\pi} \int_{t_0}^{4M^2} \frac{dt'q'}{\sqrt{t'}(t'-t)} \{P_{\ell+1}[Z_0(t')] - P_{\ell-1}[Z_0(t')]\} \times (q'/p')^\ell (t'/4M^2) \quad , \tag{11}$$

where

$$t_0 = \frac{\mu^2}{M^2}(4M^2 - \mu^2) \quad .$$

[The notation (±) has been introduced instead of $\Lambda = (0, 1)$.]

For $M = .425$ GeV and $\mu = .80$ GeV, $t_0 = .29$ GeV; this gives roughly the same binding energy as Freund and Predazzi[10] obtain to fit the coupling constants. With this set of masses we obtain (assuming a constant quark form factor) a satisfactory fit to the pion form factor $F_\pi(t)$, as shown in Figure 2, taking F_π from the VH formula and high energy πp scattering data. (Also shown in Fig. 2 is the empirical proton form factor G_{Mp}, which drops off somewhat more rapidly, illustrating a probable difference in structure between proton and pion.)

With the same masses, putting $\ell = \alpha_\rho(t) \cong .5 + 1.0\,t$, we find $D^+(\ell, t)$ from (11) to be comparatively flat for $|t| < .50$ GeV^2, and D^- remains small compared to D^+. These D's, for ρ exchange (e.g., in charge exchange reactions), are shown in Figure 3. (The relative normalization between Figs. 2 and 3 is significant, but not the absolute normalization.) If the binding energy is much smaller, one obtains similar behavior for the form factors and the residua. This is illustrated in Figure 4, where the value $M = .41$ GeV is used and the $D^\pm$ calculated both for $\ell = 1$ and $\ell = \alpha_\rho(t)$ (arbitrary absolute normalization).

The qualitative behavior of these functions can be seen from the expressions (11). For very small t_0, the integrands are sharply peaked at the lower limit from the $(t')^{-1/2}$ factor. At the lower limit, however, $Z_0 = 1$ and there is no variation of the P_ℓ factor as ℓ changes. Near $t' = 0$ the factor $(q'/p')^\ell$ becomes $(M/\mu)^\ell$, which changes by only 40% when ℓ varies over the range $0 < \ell < 0.5$ [as $\alpha_\rho(t)$ does for $|t| < .50$], and is significant only for precise symmetry considerations. The D's therefore differ only slightly for $\ell = \alpha_\rho(t)$ compared to $\ell = 1$. At the same time, we find $|D^-| \ll |D^+|$ since the integrand of D^- vanishes at the lower limit. As the binding energy is increased, the contribution of higher t' becomes more important; the ℓ dependence becomes significant, and D^+ does not dominate so much over D^-.

It may be noted that expressions (10), inserted in the D integrals before continuation, are just the lowest order ($Q\bar{Q}$ intermediate states)

expressions for the vertex functions of a spin ℓ elementary meson coupling to spinless mesons, with constant vertices in the triangle diagram.

4.2 Effect of quark properties on meson residua

In order to compute the Regge residua in meson-meson scattering, given the D functions, we must assume some properties of the channel 1 ($Q\bar{Q}$) scattering amplitudes A_{11}. If we assume slowly varying reduced residua in channel 1, which have similar spin-amplitude ratios for each pole, we can relate the A_{11} residua to the electromagnetic properties of the quarks, e.g., magnetic moments. In this case we can write, near each pole under consideration,

$$\underset{\sim}{T}_{11}(\ell, t) \equiv \underset{\sim}{\rho}_1^{1/2} \underset{\sim}{A}_{11}(\ell, t) \underset{\sim}{\rho}_1^{1/2} = \underset{\sim}{\beta}_1(t)/[\ell - \alpha(t)] \qquad (12)$$

where $\alpha(t)$ is the pole trajectory in the ℓ plane, and $\underset{\sim}{\beta}_1$ is essentially constant. (We neglect signature here.)

Since residua factorize in helicity indices, we can express $\underset{\sim}{\beta}_1$ as:

$$\underset{\sim}{\beta}_1 = \begin{pmatrix} \gamma_1^2 & \gamma_1\gamma_2 \\ \gamma_1\gamma_2 & \gamma_2^2 \end{pmatrix}$$

If we examine the unitarity equation (7) for the quark e.m. form factors, near the lowest vector meson pole (assuming it dominates the quark form factor), we find that

$$\frac{G_{1-}(0)}{G_{1+}(0)} = \frac{\gamma_2}{\gamma_1} \quad .$$

This relation connects the magnetic moment to charge ratio of the quark with the residue $\underset{\sim}{\beta}_1$ appearing in hadron residua, through (2) and (12), leaving only an overall normalization factor independent of s or t.

If the quark is pure Dirac particle, i.e. with no anomalous magnetic moment, then $G_-(0)/G_+(0) = 1$. We find then the contribution

from terms involving D^- in meson-meson scattering are quantitatively unimportant because $|D^-| \ll |D^+|$ for moderately weak ($\sim$ 50 MeV) binding; e.g., for ρ exchange

$$[\beta_\rho(t)]_{jk} \cong D_j^+[a_\rho(t), t] \times D_k^+[a_\rho(t), t].$$

In particular, from Figure 3, this means the $(\rho\,\pi\pi)$ vertex should be slowly varying with t compared to typical electromagnetic form factors. If we assume a similar situation holds for the nucleon vertex, then we find agreement with phenomenological analysis[14] of $\pi^- p \to \pi^0 n$, wherein constant residua give a good fit for $|t| < .50\,\mathrm{GeV}^2$.

We remark again that the same model leads to a Pomeranchon residue which (on the contrary) drops off sharply like the electromagnetic form factor (cf. Fig. 2), as suggested by the Van Hove formula, (1).

At this point it is appropriate to record the connection between differential s-channel meson-meson cross-sections and A_{22}. If

$$\left(\frac{d\sigma}{d\Omega}\right)_{22} = \frac{1}{s}|F|^2, \quad \text{then}$$

$$F \underset{s \to \infty}{\to} (s/s_0)^a [D^T(a,t)\beta_1 D(a,t)](2a+1)\left[\frac{1 \pm \exp(-i\pi a)}{\sin \pi a}\right] \qquad (13)$$

for each pole, where we have restored the signature factor; s_0 is the scale factor[15] appropriate for $Q\bar{Q}$ scattering, presumably in the neighborhood of $2M^2$.

4.3 Baryon vertices

Since the baryons are assumed conventionally to have a three-quark structure, the formulation of the vertex functions and their relation to wave functions is not such a well-known procedure as with the mesons. Consequently, we cannot rely on previous work and we will only treat the baryons in a simplified way, which is similar to the mesons.

Guided by SU(6) baryon wave function symmetry with all quarks in relative S-waves, we suppose that when a baryon emits a (virtual) quark the remaining part (QQ state)[16] A has 1^+ or 0^+ quantum numbers only, and the $(A\bar{Q}B)$ coupling has the simplest possible, i.e., non-derivative form. Then the kinematics for $B\bar{B} \to Q\bar{Q}$ resemble those in $N\bar{N} \to Y\bar{Y}$ with scalar and axial vector exchange with non-derivative coupling. This case can now be treated with the formalism of Chan,[17] who considered exchange of Regge and elementary poles in $N\bar{N} \to Y\bar{Y}$.

In a zero-range approximation for the $(A\bar{Q}B)$ vertex, we obtain a pole structure (similar to the meson case) for Chan's invariant amplitudes F_1 and F_4, yielding with normal thresholds

$$[\rho_1 B^J_{13}]_{11} = C_1 Q_J[Z_A(t)]$$

$$[\rho_1 B^J_{13}]_{22} = C_4 Q_J[Z_A(t)]$$

where $Z_A(t) = (M_A^2 + q^2 + n^2)/(2qn)$; C_1 and C_4 are residua;

and $$[\rho_1 B^J_{13}]_{12} = [\rho_1 B^J_{13}]_{21} = 0$$

where (in all the above) channel 3 refers to $N\bar{N}$, $n^2 = t/4 - M_B^2$ where M_B is the baryon mass, and the second set of subscripts refers to helicity indices as defined by GGMW.[18]

Finally, inserting these in the expressions for $[D_{13}]_{jk}$ and analytically continuing in baryon mass (and/or A mass) to describe weak binding, keeping only the anomalous region, we obtain:

$$[D_{13}]_{11} = C_1 D_0(\ell, t) \ ;$$

$$[D_{13}]_{22} = C_4 D_0(\ell, t) \ ;$$

and

$$[D_{13}]_{12} = [D_{13}]_{21} = 0$$

where

$$D_0(\ell, t) = \frac{1}{\pi} \int_{t_A}^{4M^2} \frac{dt'q'}{\sqrt{t'(t' - t)}} \left(\frac{q'}{n'}\right)^{\ell} P_\ell[Z_A(t')]$$

The lower limit t_A is that value of t which makes $Z_A = +1$.

Since both spin terms have the same t-dependence in this approximation we see immediately that both the electric and magnetic form factors of the nucleon have the same t-dependence, in agreement with experiment. Furthermore, the qualitative properties (ℓ and t dependence) of these D_{13} are similar to those of D^{+}_{12} which, as previously discussed, leads to satisfactory agreement with $\pi^- p$ charge exchange data, as well as yielding the Van Hove formula for πN scattering.

The residua C_1 and C_4 can, in principle, be fixed from electromagnetic properties of nucleons. However, we see that such a procedure would lead to a ratio of helicity-flip to helicity non-flip which is independent of the trajectory; this is undesirable, since the ratio as determined in $\pi^- p \to \pi^0 n$ is much larger[19] than that of the static nucleon properties, i. e., magnetic moment. This means that our simple baryon model is not quite adequate to describe the details of the accepted phenomenological residue fits.

5. CONCLUDING DISCUSSION

The central point of our model has been the generalized impulse approximation formula (2). This equation follows from one-channel dominance for exchange processes and one of the following assumptions: (a) spin 1/2 constituents and asymptotically high energies, or: (b) dominance of singularities above $\ell = 0$ in the ℓ plane (usually relevant at high energies) in the scattering of constituents. Such a formula is already enough to obtain the Van Hove relation (1) when diffraction singularities (near $\ell = 1$) dominate, and constituents' form factors and scattering amplitudes vary weakly with t.

To draw further conclusions concerning moving Regge poles one needs additional dynamical assumptions. In particular, if moderately weak binding is assumed such that the anomalous region ($t_0 < t' < 4M^2$) is most important in the D functions (equivalently, in the form factors), our general formulation allows a connection to be made between form factors and residua, represented by equations (8) and (13).

This assumption is not necessary if one is willing to parametrize with sufficient freedom the input Born terms. Thus, using the general form (9), one can use (2) together with (8) in the normal case, and avoid the assumption of anomalous thresholds (weak binding) altogether. However, in such a case it would be difficult to justify the one-channel approximation.

When we specialize to the weak-binding case we find consistency between: (a) Diffraction (Pomeranchuk) residua falling with t (like electromagnetic form factors) in agreement with asymptotic πp elastic scattering data; (b) Residua for ρ exchange varying slowly with t, as indicated by $\pi^- p$ charge-exchange data; (c) Absolute value of strong-interaction coupling constants, as computed by Freund and Predazzi,[10] all with a binding energy of around 50 MeV.

Finally, we find that it is not possible to use a simple ZRA and extrapolate from t = 0 to the vector meson poles, as one would like to do in pole models. A more detailed model for the Γ's is necessary.

1) L. Van Hove, at 1966 Topical Conference on Two-Body Reactions at High Energy at Stony Brook, L.I., N. Y. (CERN preprint, 1966).

2) This relation was first postulated for large momentum transfer by Wu and Yang, [Phys. Rev. 137, B708 (1965)] and later discussed for all momentum transfer by Chou and Yang at the International Conference on High Energy Physics and Nuclear Structure, Weizmann Institute, Israel, 1967 (State Univ. of N. Y. at Stony Brook preprint, 1967) in terms of a droplet model for high energy hadron reactions. Such a model is not appropriate, however, for a discussion of Regge poles. The essential idea common to both types of models has been stated clearly by Feynman, in a remark at the XIIIth International Conference on High Energy Physics, Session 6 (Univ. of Calif. Press, Berkeley and Los Angeles, 1967).

3) Small angle pp and π p data were taken from K. J. Foley et al., Phys. Rev. Letters 11, 425 (1963); form factor data was obtained from the compilation of Hand, Miller and Wilson, Rev. Mod. Phys. 35, 335 (1963).

4) The Sachs magnetic form factor G_M has been plotted since this is more accurately determined than the electric form factor G_E; quark models suggest the two are proportional, in agreement with experiment to date. In the case of the scattering data we have chosen pp data only, ignoring $p\bar{p}$ results, since the former seem to be approaching an asymptotic behavior more rapidly than the latter, indicating that for $p\bar{p}$ a simple singularity in the ℓ plane is not yet dominant (e.g., at 12 GeV/c).

5) We will find later that with weak binding there is a correlation between meson mass and the width of the forward peak obtained with $\beta(t)$. If the mass is too small (i.e., μ_π) the peak is too narrow. Therefore, we use a meson mass around M_ω.

6) We offer no explanation concerning the experimental nonexistence of light quarks.

7) R. Blankenbecler, L. F. Cook, Jr., and M. L. Goldberger, Phys. Rev. 128, 2440 (1962).

8) F. Gross, Phys. Rev. 134, B405 (1964); ibid. 136, B140 (1964). See also M. Gourdin, M. LeBellac, F. M. Renard and J. Tran Thanh Van, Nuovo Cimento 37, 524 (1965); and for a discussion of basic principles, R. Blankenbecler and Y. Nambu, Nuovo Cimento 18, 595 (1960).

9) Bjorken and Nauenberg, Phys. Rev. 121, 1250 (1961).

10) P. G. O. Freund and E. Predazzi, Physics 3, 81 (1967).

11) W. R. Frazer and J. R. Fulco, Phys. Rev. 117, 1603 (1960); ibid., p. 1069.

12) V. Singh, Phys. Rev. 129, 1889 (1963).

13) The expressions from the ZRA, (10), lead to a logarithmic divergence in D if taken literally at large t. A more realistic approximation for the wave functions would agree with the ZRA in the small t region but provide a damping necessary for larger t. If we keep only the anomalous region our procedure would yield the same physics.

14) The relatively slow variation of ρ residua can be noticed in the fits of Phillips and Rarita [Phys. Rev. 139, B1326 (1965)] and early considerations of Logan [Phys. Rev. Letters 14, 414 (1965)]. We ignore the "crossover phenomenon" discussed by Phillips and Rarita, and suggest the charge-exchange fits of Yokosawa [Phys. Rev. 159, 1431 (1967)] as our reference point.

15) For moving poles ($\alpha \neq 1$), the choice of S_0 is important, especially in comparing symmetry predictions. This has been discussed by

James and Watson [Phys. Rev. Letters 18, 179 (1967)] using a simple bound state picture. Changing S_0 in a purely phenomenological approach from S_{01} to S_{02} introduces a multiplicative factor $(S_{01}/S_{02})^{\alpha(t)}$ for each pole, resulting in a different residue. In our model, on the other hand, the residua are obtained unambiguously from the D functions and S_0 is the same for any hadron reaction. We find that in the extreme weak-binding limit, the result of James and Watson appears in our model via the threshold factor $(p')^{-\ell}$ in the meson D function integrand which may be approximated by $\mu^{-\ell}$ for sufficiently weak binding. A similar factor occurs with baryon vertices. In our approach we use a degenerate (mean) meson-mass and would not make a correction when comparing π with K data, but such factors become important when comparing MB and BB reactions.

16) We are well aware that there is no QQ bound state, A. We use the single-particle Born term only as a guide.

17) C. H. Chan, Phys. Rev. 133, B431 (1964).

18) M. L. Goldberger, M. T. Grisaru, S. W. MacDowell, and D. Y. Wong, Phys. Rev. 120, 2250 (1960); referred to in text as GGMW.

19) G. Hohler, J. Baacke, H. Schlaile, and P. Sonderegger, Physics Letters 20, 79 (1966); B. R. Desai, Phys. Rev. 142, 1255 (1966).

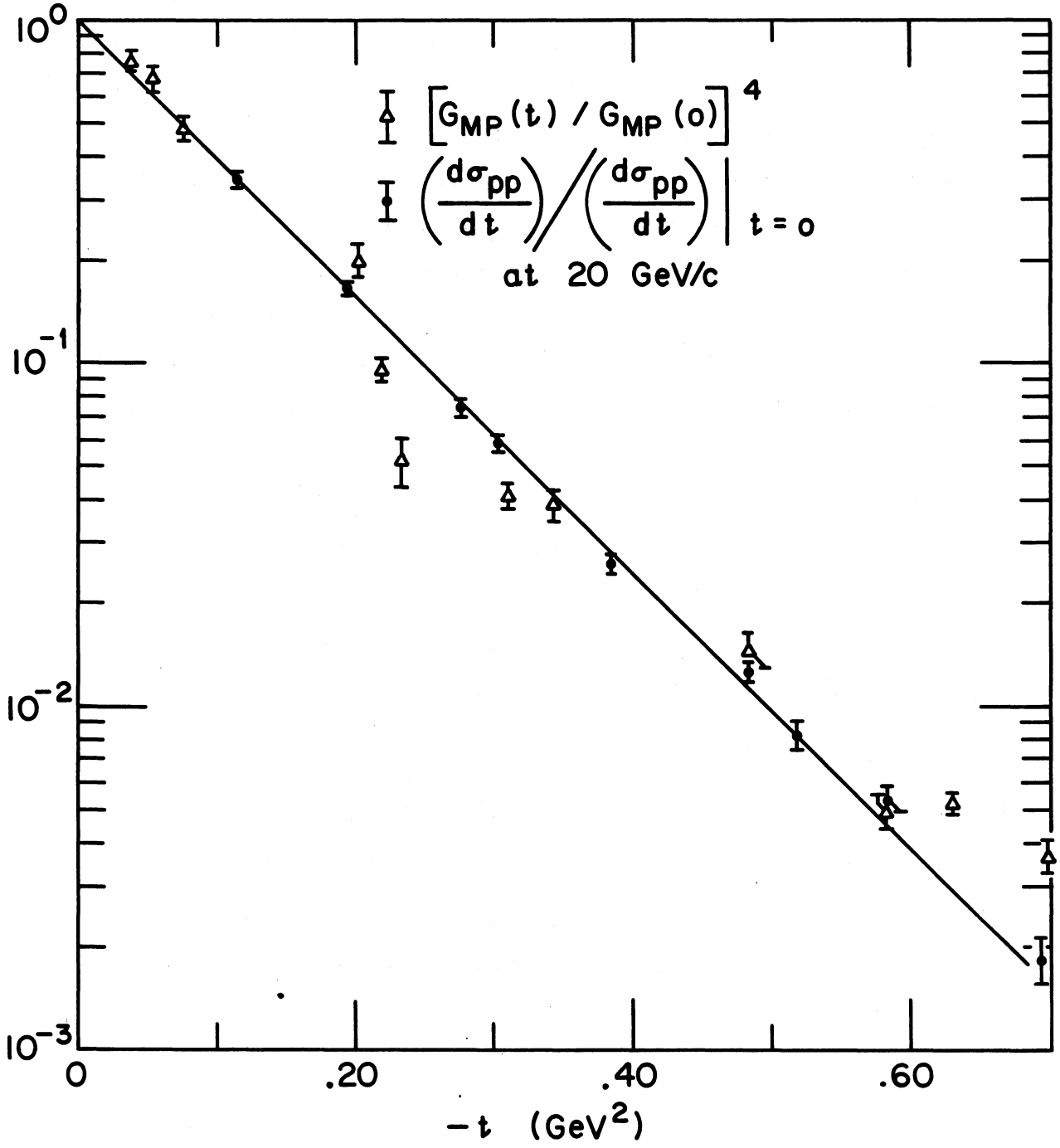

Figure 1.

Comparison of Differential Cross Section for p-p elastic scattering as a function of t at 20 GeV/c with prediction of Van Hove relation (Eq. 1), using magnetic Sachs form factor of proton as representative electromagnetic form factor. Data sources are given in references 2 and 3. The straight line is to guide the eye only.

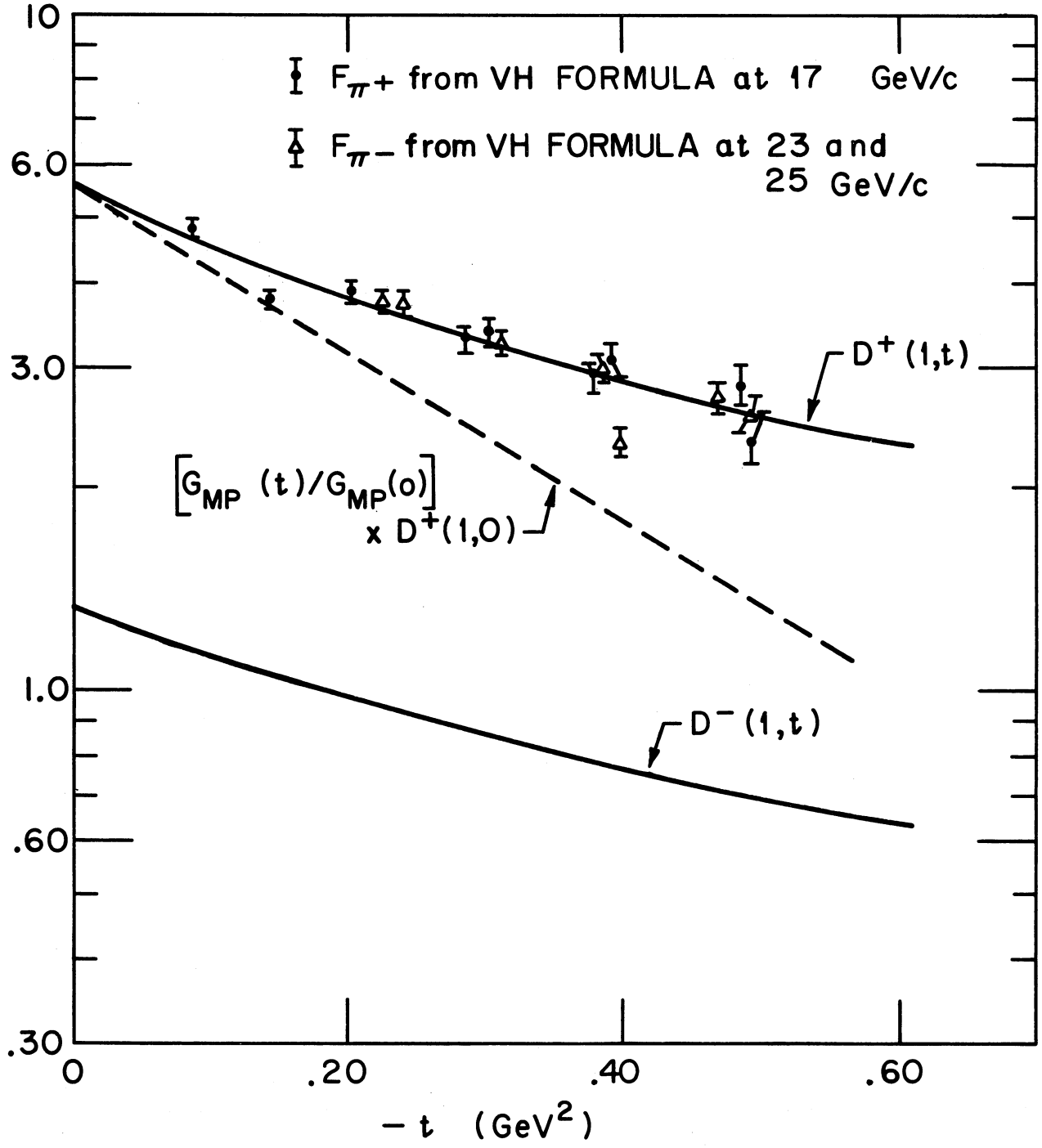

Figure 2.

Results of calculation for structure factors $D^{\pm}$ of mesons, using zero-range approximation with M = 425 MeV and μ = 800 MeV, evaluated at ℓ = 1. For comparison, the pion electromagnetic form factors F_{π^+} and F_{π^-} are shown as deduced from small-angle high-energy $\pi^{\pm}p$ scattering using the Van Hove formula. Data sources are given in reference 3. Also shown (dotted line) is proton form factor.

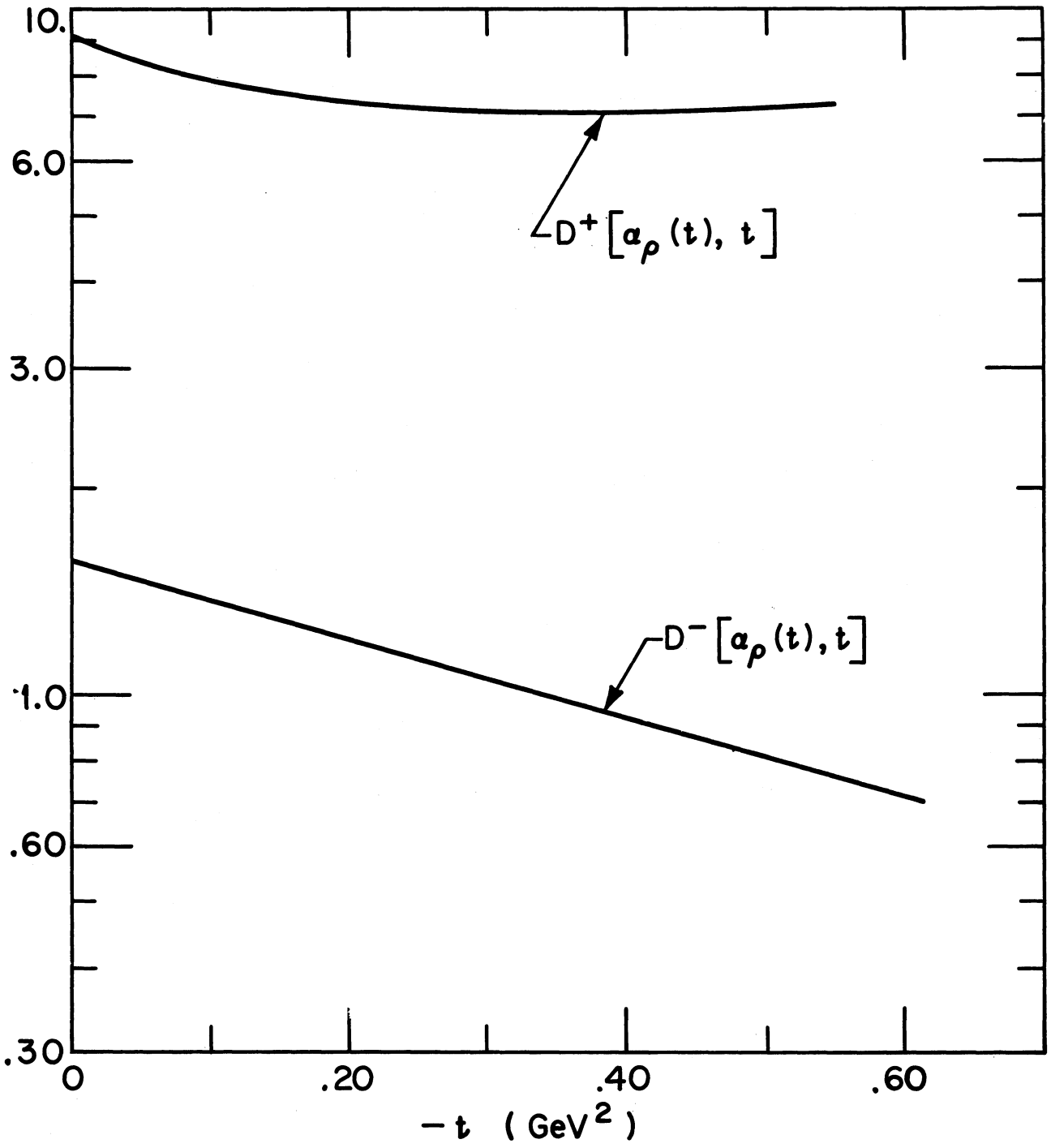

Figure 3.

Calculated residue structure factors $D^{\pm}$ for the ρ trajectory, $\alpha_\rho(t) = .5 + 1.0\ t(\text{GeV}^2)$, with same masses as in Figure 2.

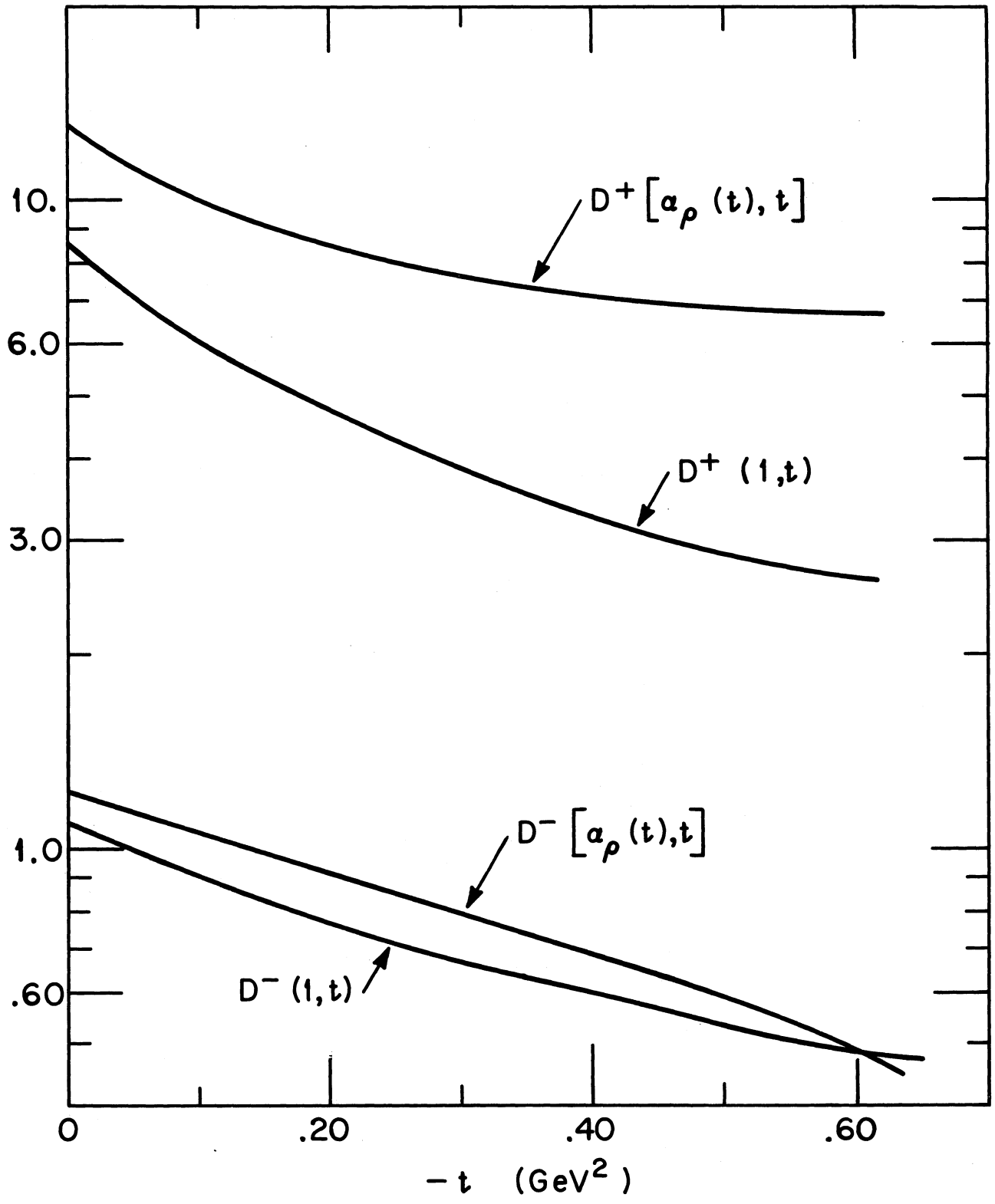

Figure 4.

Structure factors $D^{\pm}$ for M = 410 MeV and μ = 800 MeV, both with $\ell = 1$ and $\ell = \alpha_\rho(t)$.

COMPARISON OF REGGE POLE MODEL TO EXPERIMENT FOR $\pi N \rightarrow \rho N$

by

Gerald E. Hite

Physics Department
University of Illinois
Urbana, Illinois

and

Institute of Theoretical Science
University of Oregon
Eugene, Oregon*

ABSTRACT

Special attention is given to the Reggeized helicity amplitudes used to describe vector meson production. Sets of amplitudes are presented which describe all trajectories with natural parity and all trajectories with unnatural parity whose G-parity restricts the $\bar{N}N$ channel spin to be zero (e.g. Reggeized π exchange). These amplitudes have the proper kinematic singularity structure and satisfy certain threshold constraint conditions. Using these amplitudes a comparison of Regge pole theory is made to experiment for ρ production at 4.0 GeV/c and 8.0 GeV/c. A short discussion is given concerning the information on the number and types of Regge exchanges that can be obtained from experiments using polarized targets. Predictions are made of the effect of polarized targets on the decay angular distribution of the ρ meson.

*Research supported in part by the Office of Naval Research and in part by the Atomic Energy Commission.

I INTRODUCTION

Recently there has been a great deal of theoretical work done in the area of Regge pole theory. The advancement of the basic theory to particles with non-zero spins has enabled one to write helicity amplitudes in a way which permits the angular momentum to be continued to give Regge poles[1,2]. Detailed expressions for the kinematic singularities of the residue functions and threshold constraint relations between amplitudes have been derived[3,4,5]. As the previous paper presented by J. D. Jackson[3] has shown, these singularities and constraint relations can easily be interpreted in terms of angular momentum coupling rules. The threshold constraint conditions for amplitudes remove the undesirable, apparent kinematic singularities that appear in expressions for cross sections and helicity density matrices if no constraints are imposed. It has been found also that the remaining functions that parameterize the amplitudes can be identified with form factors and that for values of momentum transfer corresponding to the exchange of a physical particle the form factors are given by products of coupling constants[4].

This paper is primarily interested in comparing Regge pole theory to experiment for ρ production in πN scattering. Though experiments have not been done with polarized targets we discuss the information about the types and numbers of Regge pole trajectories contributing to a reaction that can be obtained from such experiments and describe some experimental effects on the decay distribution of the ρ meson at 8.0 Gev/c that would result from using polarized targets. Definitions of various symbols used in the calculations can be found in the appendix.

II ASSUMPTIONS AND EXPRESSIONS USED IN CALCULATION

Though the calculation is made for ρ production the material in this section can be applied as well to ω production. The following sets of Reggeized helicity amplitudes where obtained by assuming that the trajectories couple to sense-sense channels and after inserting the proper kinematic singularities demanding that the unnormalized helicity density matrix of the vector meson be free of apparent kinematic singularities in the physical region of the s-channel[4]. The resulting amplitudes can be shown to describe all trajectories with natural parity and for all trajectories with unnatural parity whose G-parity restricts the $\bar{N}N$ channel spin to be zero (e.g. Reggeized π and B mesons)[4].

For natural parity exchange the independent amplitudes are:

$$f^{t+}_{10++} = s^j\left[a_+\alpha + b_+(t/4m_N^2-1)\right]\frac{m_N\tau'}{2s_o}\left(\frac{s-u}{2s_o}\right)^{\alpha-1}\sin\theta_t\,\alpha/\alpha!$$

$$f^{t+}_{10+-} = s^j\, a_+\, t^{\frac{1}{2}}(1+\cos\theta_t)\frac{\tau'}{2s_o}\left(\frac{s-u}{2s_o}\right)^{\alpha-1}\frac{\alpha^2}{2\alpha!} \qquad (1a)$$

$$f^{t+}_{10-+} = s^j\, a_+\, t^{\frac{1}{2}}(1-\cos\theta_t)\frac{\tau'}{2s_o}\left(\frac{s-u}{2s_o}\right)^{\alpha-1}\frac{\alpha^2}{2\alpha!}$$

For unnatural parity exchange, the independent amplitudes are:

$$f^{t-}_{10++} = s^j\, a_-\left(\frac{\tau}{2s_o}\right)\left(\frac{s-u}{2s_o}\right)^{\alpha-1}\frac{\alpha}{2\sqrt{2}\,\alpha!}\sin\theta_t \qquad (1b)$$

$$f^{t-}_{00++} = s^j\left(\alpha a_-(t+m_v^2-m_p^2)/2m_v + b_-\tau'^2\right)\frac{\tau t^{-\frac{1}{2}}}{4s_o\,\alpha!}\left(\frac{s-u}{2s_o}\right)^{\alpha-1}\cos\theta_t$$

where $b_- = b_1\alpha + b_o(1-\alpha)$,

$a_\pm$ and $b_\pm$ are analytic functions and s^j is a signature factor given by

$$s^j = \frac{\pi\alpha'}{2}\left|\frac{e^{i\pi(j-\alpha)}-1}{\sin\pi(j-\alpha)}\right| = \frac{\pi\alpha'}{2}\left(\operatorname{ctn}\pi(j-\alpha)/2 + i\right)$$

where j is the spin of any physical particle on the trajectory being considered, and α' is taken to be the value of the derivative of $\alpha(t)$ at the lowest physical state of the trajectory. α' is included so that near $t=m_E^2$, $s^j \sim (m_E^2-t)^{-1}$ where m_E is the mass of the physical particle. Though there are no subscripts on j, α, or

α' in general they will be different each trajectory contributing to the reaction. The other amplitudes can be obtained by using

$$f_{-c-d;ab} = -(-1)^{\lambda-\mu} f_{cd;ab} \qquad (2)$$

Using Eq. (1) and (2) the cross section for physical values of s and t can be easily calculated for the s-channel reaction $PN \rightarrow VN$. By construction the cross section and the helicity density matrix for physical s and t will not contain any inverse powers of $(t-4\ m_N^2)^{1/2}$, $(t-(m_v \pm m_p)^2)^{1/2}$ or t. Such terms are in general present in the cross sections and helicity density matrix elements calculated from the expressions presently found in the literature.[5,6,7] In the latter two references it is suggested that the reduced residue functions can be taken to be the corresponding functions in the Born amplitudes. If this is done, cancellation of the coefficients of singular threshold factors will not take place, since the factors of α for each amplitude will differ in the physical region from their value at $t=m_E^2$. The latter two references also retain the function $(\alpha+1/2)!$ in their expressions, which, according to the arguments of Gell-Mann et al.[2] and Wang[8] should not be present. For sufficiently large s and for a trajectory with a reasonable slope, it is possible for the poles of $(\alpha+1/2)!$ to be in the physical region.

As pointed out by Jackson[9] the use of polarized targets can be a very useful tool in studying particle reactions. For example, by studying the effects of the polarization of the target nucleon on the decay distribution of the vector meson in the s-channel reaction $PN \to VN$, information can be obtained about the contribution from various single particle exchanges in the t- or u-channels. Consequently it is useful to compare the effects predicted by the Regge pole model for a polarized target to experiment.

To describe the decay distribution of the vector meson we need to define in addition to the canonical density matrix, which can be written in the physical region of the s-channel as

$$\rho^{c}_{mm'} = N \sum_{\bar{\lambda}\lambda'} f^{t}_{mo;\bar{\lambda}\lambda} f^{t*}_{m'o;\bar{\lambda}\lambda} \quad , \tag{3}$$

the matrix ρ'_{mm} by

$$\rho'_{mm'} = \mathrm{Im}\left[N \sum_{\bar{\lambda}\lambda\lambda'} d_{+\lambda}^{\frac{1}{2}}(\chi_b)\, d_{-\lambda'}^{\frac{1}{2}}(\chi_b)\, f^{t}_{mo;\bar{\lambda}\lambda}\, f^{t*}_{m'o;\bar{\lambda}\lambda} \right] \tag{4}$$

where N is such that $\sum_{m} \rho^{c}_{mm} = 1$, χ_b is the crossing angle for particle b given in the appendix and the t-channel amplitudes, $f^{t}_{mo;\bar{\lambda}\lambda}$, describing the reaction $\bar{N}N \to VP$ are listed in Eq. (1). Since all amplitudes for a given Regge trajectory have the same phase, ρ'_{mm}, will be identically zero if only one trajectory is present.

In terms of $\rho^{c}_{mm'}$ and $\rho'_{mm'}$ the decay distribution for the vector meson can be written as

$$W_1(\alpha,\beta) = W_1^o(\alpha,\beta) - \frac{3}{4\pi} P \sin\omega\left[(\rho'_{1-1}-\rho'_{-11})\sin^2\alpha \sin 2\beta + \sqrt{2}(\rho'_{10}-\rho'_{01})\sin 2\alpha \sin\beta\right] \quad (5)$$

$$+ \frac{3}{4\pi} P \cos\omega\left[2\rho'_{00}\cos^2\alpha + 2\rho'_{11}\sin^2\alpha - (\rho'_{1-1}+\rho'_{-11})\sin^2\alpha\cos 2\beta - \sqrt{2}(\rho'_{10}+\rho'_{01})\sin 2\alpha\cos\beta\right]$$

where $W_1^o(\alpha,\beta)$ and the decay angles, α and β are defined in the paper by Gottfried and Jackson[10] and ω is the angle between the normal to the production plane and the target polarization $\vec{P}$ which is assumed for simplicity to be perpendicular to the incident beam.[9]

If one averages over the Treiman Yang angle, β, the angular distribution is given by

$$\frac{1}{2\pi}\int_0^{2\pi} W_1(\alpha,\beta)\,d\beta = \frac{3}{4\pi}\left[\rho^c_{00}\left(\frac{3\cos^2\alpha-1}{2}\right)+P\cos\omega(\rho'_{00}\cos^2\alpha+\rho'_{11}\sin^2\alpha)\right] . \quad (6)$$

Since all amplitudes for natural parity exchanges in the reaction $\bar{N}N \to VP$ are zero for $\lambda_V = 0$, ρ'_{00} will be zero unless there is interference between two trajectories with unnatural parity. This means that if only one unnatural parity exchange is present the contribution to the decay distribution averaged over β will be $(3/4\pi) P \cos\omega\, \rho'_{11} \sin^2\alpha$. This provides a simple experimental way to determine if

more than one trajectory of unnatural parity contributes to the reaction.

If one averages the decay angular distribution over cos α, the distribution in the Treiman Yang angle, β, is

$$\tfrac{1}{2}\int_{-1}^{1} W(\alpha,\beta)\,d(\cos\alpha) = \frac{1}{4\pi}\Big[1-2\rho^{c}_{1-1}\cos2\beta - 2P\sin\omega(\rho'_{1-1}-\rho'_{-11})\sin2\beta + 2P\cos\omega(\rho'_{00}+2\rho'_{11}-(\rho'_{1-1}+\rho'_{-11})\cos2\beta\Big] \tag{7}$$

$$= \frac{1}{4\pi}\Big[1 + 2P\cos\omega(\rho'_{00}+2\rho'_{11}) - 2P\sin\omega(\rho'_{1-1}-\rho'_{-11})\sin2\beta - 2(\rho^{c}_{1-1}+P\cos\omega(\rho'_{1-1}+\rho'_{-11}))\cos2\beta\Big].$$

If the polarization of the target is in the production plane, $\omega=\pi/2$, this expression reduces to

$$\frac{1}{4\pi}\Big[1 - 2P(\rho'_{1-1}-\rho'_{-11})\sin2\beta - 2\rho^{c}_{1-1}\cos2\beta\Big] \tag{8}$$

$$= \frac{1}{4\pi}\Big[1 - 2A\cos2(\beta-\varphi)\Big]$$

where

$$A^2 = \rho^{c\,2}_{1-1} + P^2(\rho'_{1-1}-\rho'_{-11})^2$$

and

$$\varphi = \tfrac{1}{2}\tan^{-1}\left[P(\rho'_{1-1} - \rho'_{-11})/\rho^{c}_{1-1}\right] .$$

This shows that the decay angular distribution for P = +1 and -1 will have the same shape but since Φ changes sign they will be shifted by 2Φ from each other.

To reduce the numbers of parameters in the calculation we assumed that all trajectories could be described by

$$\alpha = j + \alpha'(t - m_E^2)$$

where j and m_E are the spin and mass of the lower physical state of the trajectory. We assumed $\alpha' = 1.0(\text{BeV/c})^{-2}$ for all trajectories, since the effects of using different values of α' were not important enough to warrant the use of separate values. For convenience we set

$$s_o = 2\sqrt{m_N m_N m_p m_v} .$$

By setting $\alpha = j$ and comparing the amplitudes given by Eq. (1) to the known Born amplitudes, the functions $a_{\pm}$, b_+, b_1 and b_o can be identified with coupling constants. In the calculation we assume them to be constants and identify them with known coupling constants whenever possible. This assumption is equivalent to assuming the vertex form factors are constants.

III ρ-Production at 4.0 and 8.0 GeV/c

For the s-channel reaction $\pi^{\pm}P \rightarrow \rho^{\pm}P$ the important t-channel exchanges should be the two Regge trajectories passing through the π and ω mesons. For the natural parity exchange we took

$$j = 1 \ , \ m_E = m_\omega \ , \ \alpha'_\omega = 1.0 \ (\text{BeV/c})^{-2}$$

and

$$a_+ = 2s_o(f_{\pi\omega\rho}/m_\omega)(G^V_{NN\omega} + G^T_{NN\omega})/\sqrt{2}$$

$$b_+ = 2s_o(f_{\pi\omega\rho}/m_\omega)\ G^T_{NN\omega}/\sqrt{2} \ .$$

While it is known that $f^2_{\pi\omega\rho}/4\pi \sim 10.5$, the values of $G^V_{NN\omega}$ and $G^T_{NN\omega}$ are not very well known. We took

$$a_+/4\pi = 38.$$

$$b_+/4\pi = 50.$$

which corresponds to

$$G^{V\ 2}_{NN\omega}/4\pi = 11.6$$

$$G^T_{NN\omega}/G^V_{NN\omega} = -4.2.$$

For the unnatural parity exchange, since we only consider the π trajectory we took $j = 0$, $m_E = m_\pi$, $\alpha'_\pi = 1.0(\text{GeV/c})^{-2}$

$$a_-/4\pi = 45.$$

and

$$b_o = 2\ G_{NN\pi}\ g_{\pi\pi\rho}/m_\omega$$

where

$$G_{NN\pi}{}^2/4\pi = 14.5$$

and

$$g_{\pi\pi\rho}{}^2/4\pi = 2.5 \ .$$

Figures 1 and 2 show the cross section and density matrix elements as a function of t for incident π momentum of 4.2 and 8.0 GeV/c respectively. The data for both ρ^+ and ρ^- at 8.0 GeV/c are shown in Figure 2. There are no known effects in the Regge pole model which can explain the differences in differential cross sections for ρ^+ and ρ^- production. There is a possible uncertainty of about 40% in the values of the ρ^+ data.

The calculated curves indicate that the vector contribution is more important at 8 GeV/c than at 4.2 GeV/c. This is essentially due to the fact that the trajectory of the ω meson is higher than that of the π and consequently the energy dependence of the amplitudes, s^{α}, will favor ω exchange for large values of s.

In the forward direction, where $\cos\theta_t = -1$, the only non-vanishing natural parity exchange amplitude varies as $\tau'(1-\cos\theta_t)s^{\alpha' t+\alpha_\omega(0)}t^{1/2}$ whereas the unnatural parity exchange amplitude f_{00++} varies as $(t-4m^2)^{1/2}\ s^{\alpha' t+\alpha_\pi(0)}\cos\theta_t$. Consequently the π exchange contribution will be greatest for t near its minimum physical value. Since the

value of t_{min} for inelastic reactions decreases as s^{-1} for large s, the relative contribution of the π exchange will fall off as $s^{\alpha_\pi(0)-\alpha_\omega(0)+1/2}$ in the forward direction. Consequently the values of ρ^c_{00} should be closer to unity for t near t_{min} than for larger t. This effect can be seen in the data where ρ^c_{00} decreases rapidly from unity as -t increases from t_{min}.

Though the exchange of the π trajectory is necessary for non-zero values of ρ^c_{00}, it is not necessary to have vector exchange to obtain a value of ρ^c_{00} different from unity. The amplitude f^{t-}_{10++} is not zero for Reggeized π exchange and permits ρ^c_{00} to deviate from unity. Since f^{t-}_{10++} is proportional to $\alpha_\pi \sin\theta_t$, the predicted values of $|\rho^c_{10}|, |\rho^c_{1-1}|$ and ρ^c_{11} should all be zero in the forward direction and increase as $|t|$ increases. One way to determine the presence of natural exchanges is to look at the sign of ρ^c_{1-1}. By using the parity properties of amplitudes one obtains $\rho^c_{1-1} = N \sum_{\lambda\bar{\lambda}} f^t_{10;\bar{\lambda}\lambda} \cdot f^{t\,*}_{-10;\bar{\lambda}\lambda}$

$= N \sum_{\lambda\bar{\lambda}} (-1)^{\lambda-\bar{\lambda}} \left[|f^{t+}_{10;\bar{\lambda}\lambda}|^2 - |f^{t-}_{-10;\bar{\lambda}\lambda}|^2 \right]$ where $f^{t+}_{10;\bar{\lambda}\lambda}$ and $f^{t-}_{10;\bar{\lambda}\lambda}$ are t-channel amplitudes for natural and unnatural parity exchanges respectively given by Eq. (1), the sign of ρ_{1-1} is negative if only unnatural parity trajectories with G-parity such that $\bar{\lambda}=\lambda$ (e.g. Reggeized π and B mesons) are present. Consequently the experimental data implies the

presence of at least one trajectory with natural parity or one with unnatural parity and G-parity for which the $\bar{N}N$ channel spin is unity.

Another check on the presence of more than one trajectory could be provided by polarization experiments to measure $\rho'_{mm'}$. The calculated values of $\rho'_{mm'}$ were found to be slowly varying functions of t. The average values for ρ-production at 8.0 GeV/c were found to be:

$$\langle \rho'_{mm'} \rangle = \begin{pmatrix} \sim 0 & .11 & .08 \\ -.11 & 0 & -.11 \\ -.08 & .11 & \sim 0 \end{pmatrix}$$

This implies that the significant contribution to the decay distribution resulting from a polarized target will be from the term proportional to $\sin\omega$. Thus the effect will be greatest if the polarization of the target is in the production plane. Figure 3 shows the effect on the decay distribution averaged over $\cos\alpha$ as given in Eq. (8) for polarization, P, equal to +1 and -1. The curves have been calculated for $\rho^c_{1-1} = .25$ which is consistent with $-t \geq .05$ $(\text{GeV/c})^2$. The values of A and Φ are .30 and 16° respectively.

IV CONCLUSIONS

The basic assumptions made for the calculation were: 1) the trajectories couple to sense-sense channels; 2) the amplitudes contain kinematic singularities and should satisfy threshold kinematic constraints; 3) the functions, that parameterized the solutions of the constraint equa-

tions, could be taken to be constants and identified when possible with products of coupling constants; 4) the amplitudes satisfied constraints at t=0 by evasion and thus no conspiring trajectories were needed; 5) the trajectory, α, for any Regge exchange could be taken to be a straight line of slope 1.0 $(\text{Gev/c})^{-2}$ passing through the lowest physical state; 6) for ρ production it was further assumed that only π and ω trajectories were important. With these assumptions reasonable fits were obtained to the data for ρ production at 4.2 Gev/c and 8.0 Gev/c. Since the experimental value of ρ^{c}_{oo} was non-zero, it was concluded that π exchange was necessary. Similarly from the sign of ρ^{c}_{1-1} it was concluded that Reggeized π exchange was not sufficient and that an ω exchange must be included. It was observed that ρ'_{oo} would be zero unless at least two trajectories of unnatural parity contributed. With the parameters used in fitting the data the values of ρ'_{mm}, were calculated and the experimental consequences were discussed. It was pointed out that there were no known effects in the Regge pole theory that could explain a difference in differential cross sections for ρ^{+} and ρ^{-} productions. It was noted that even though f_{10++} for Reggeized π exchange vanished at $\alpha=0$ and in the forward direction, that in general, for non-forward scattering it would yield non-zero values of ρ^{c}_{10}, ρ^{c}_{1-1} and ρ^{c}_{11}. This is particularly important since the value of ρ^{c}_{10} is identically zero for natural parity exchanges such as ω exchange.

ACKNOWLEDGEMENTS

I am grateful to J. D. Jackson for suggesting this problem, and to M. J. Moravcsik for reading the manuscript and for his helpful suggestions.

NOTE

During the conference at which this paper was presented, D.R.O. Morrison reported that the cross sections have been recalculated and now show a peak instead of dip at small t. Whereas the previous data, being less than the theoretical curves, implied conspiracy was not present, the newer results imply that either conspiracy or other effects such as absorption are present.

APPENDIX

$f_{cd;ab}$ helicity amplitude describing the t-channel reaction $ab \to cd$ which when crossed to the s channel is $\bar{d}b \to c\bar{a}$ (e.g. t-channel reaction $\bar{N}N \to \rho\pi$ and s-channel reaction $\pi N \to \rho N$). The subscribes are the helicities of the respective particles.

γ the reduced residue function which is the analytic part of the residue function after the kinematic singularities have been factored off.

$\lambda = a-b$

$\mu = c-d$

η_i, s_i the intrinsic parity and spin of the i^{th} particle.

m_N mass of nucleon

m_p mass of pseudo-scalar meson (e.g. π)

m_V mass of vector meson (e.g. ρ)

s_o scaling factor with dimensions of energy squared.

$$\tilde{\tau}^2 = (t-(m_a+m_b)^2)(t-(m_a-m_b)^2) = (t-4m_N^2)t$$

$$\tilde{\tau}'^2 = (t-(m_c+m_a)^2(t-(m_c-m_d)^2) = (t-(m_p+m_v)^2)(t-(m_p-m_v)^2)$$

$\cos\theta_t$, $\sin\theta_t$ trigometric functions of th t-channel scattering angle given by

$$\cos\theta_t = \frac{t(s-u)+(m_a^2 - m_b^2)(m_c^2 - m_d^2)}{\tilde{\tau}\cdot\tilde{\tau}'}$$

$$\sin\theta_t = 2[t\Phi(s,t)]^{1/2}/\tilde{\tau}\cdot\tilde{\tau}'$$

where

$$\Phi = stu - s(m_a m_b + m_c m_d) - t(m_a m_c + m_b m_d)$$

$$-u(m_a m_d + m_b m_c) + 2m_a m_b m_c m_d\left(\frac{1}{m_a} + \frac{1}{m_b} + \frac{1}{m_c} + \frac{1}{m_d}\right)$$

and

$$s + t + u = \Sigma m^2.$$

$$\sin\chi_b = 2m_b\,[\Phi(s,t)]^{1/2}/S_{bd}\,\tilde{\tau}$$

where $S_{bd}^2 = (s-(m_b+m_d)^2)(s-(m_b-m_d)^2)$

1) Calogero, F., J. M. Charop, and R. J. Squires, Ann. Phys. 25, 325 (1963).

2) Gell-Mann, M., M. L. Goldberger, F. E. Low, E. Marx, and F. Zachariasen, Phys. Rev. 133, B145 (1964).

3) Jackson, J. D., G. E. Hite, "Kinematic Singularities and Threshold Relations for Helicity Amplitudes", presented at the Topical Conference on High Energy Collisions of Hadrons at CERN, (1967).

4) Hite, G. E., Dissertation, University of Illinois (1967).

5) Wang, L. L., Phys. Rev. 153. 1664 (1967).

6) Frautschi, S. and L. Jones, "The Reggeization of Pion Exchange in Production Processes," Phys. Rev., to be published (1967).

7) Barmawi, M., Phys. Rev. 142, 1088 (1966); Phys. Rev. Letters 16, 595 (1966).

8) Wang, L. L., Phys. Rev. Letters 16, 756 (1966).

9) Jackson, J. D., "Polarized Targets: Why?", presented at the Saclay Conference on Polarized Targets and Ion Sources, Saclay, France (1966).

10) Gottfried, K. and J. D. Jackson, Nuovo Cimento 33, 309 (1964).

11) Yen, W. L., R. L. Eisner, L. Gutay, P. B. Johnson, P. R. Klein, R. E. Peters, R. J. Sahni, and G. W. Tautfest, Phys. Rev. Letters 18, 1091 (1967).

12) Derado, I., J. A. Poirier, N. N. Biswas, N. M. Cason, V. P. Kenney, and W. D. Shephard, Phys. Letters 24B, 112 (1967).

13) Deutschmann, M., D. Kropp, R. Schulte, H. Weber, W. Woischnig, C. Grote, J. Klugow, H. W. Meier, A. Pose, S. Brandt, V. T. Cocconi, O. Czyzewski, P. F. Dalpiaz, E. Flaminio, H. Hromadnik, G. Kellner, D.R.O. Morrison, and S. Nowak, Phys. Letters 19, 608 (1965).

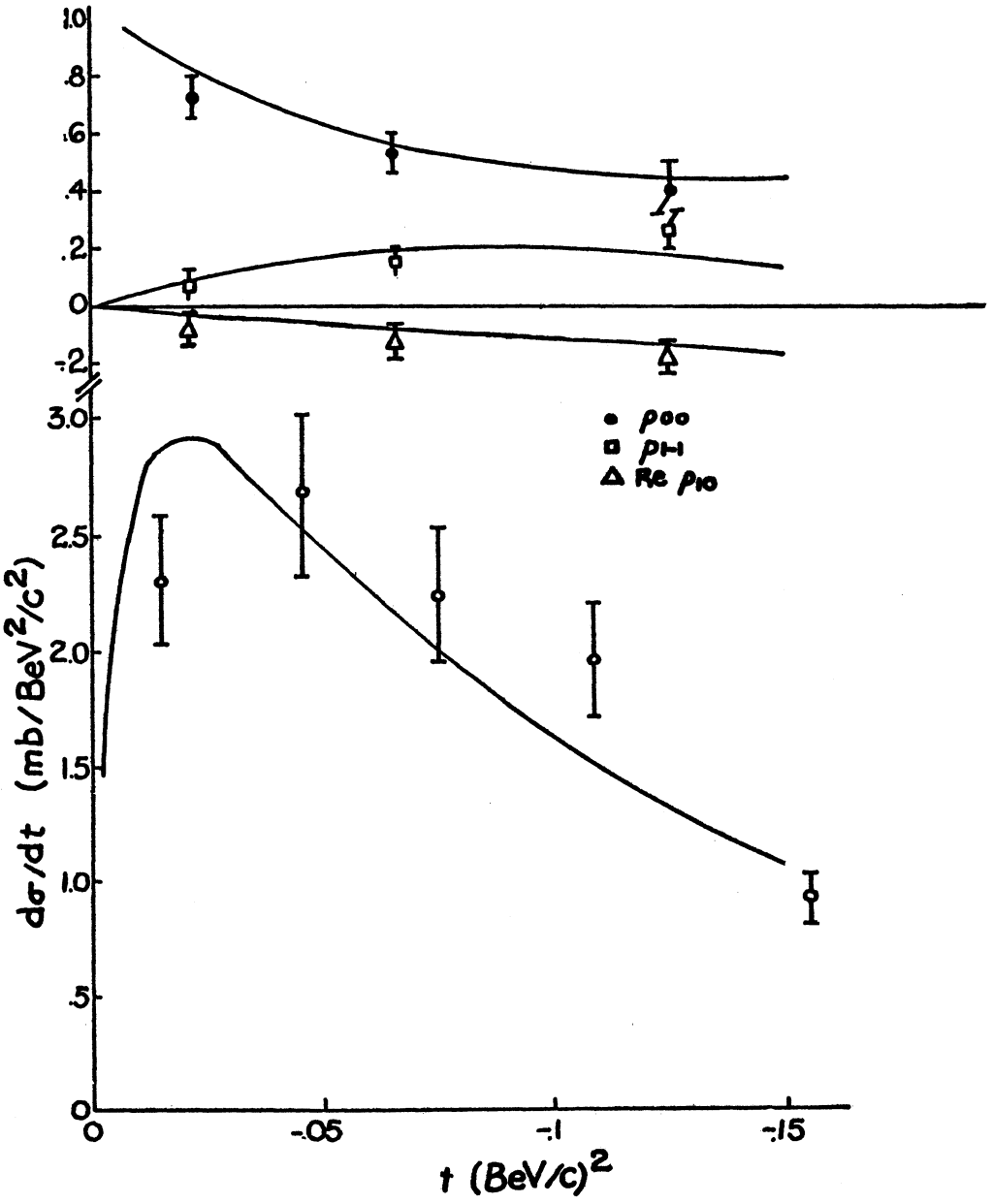

Figure 1. Differential cross section and density matrix elements for ρ-production at 4.2 GeV/c. The data are those of reference 12.

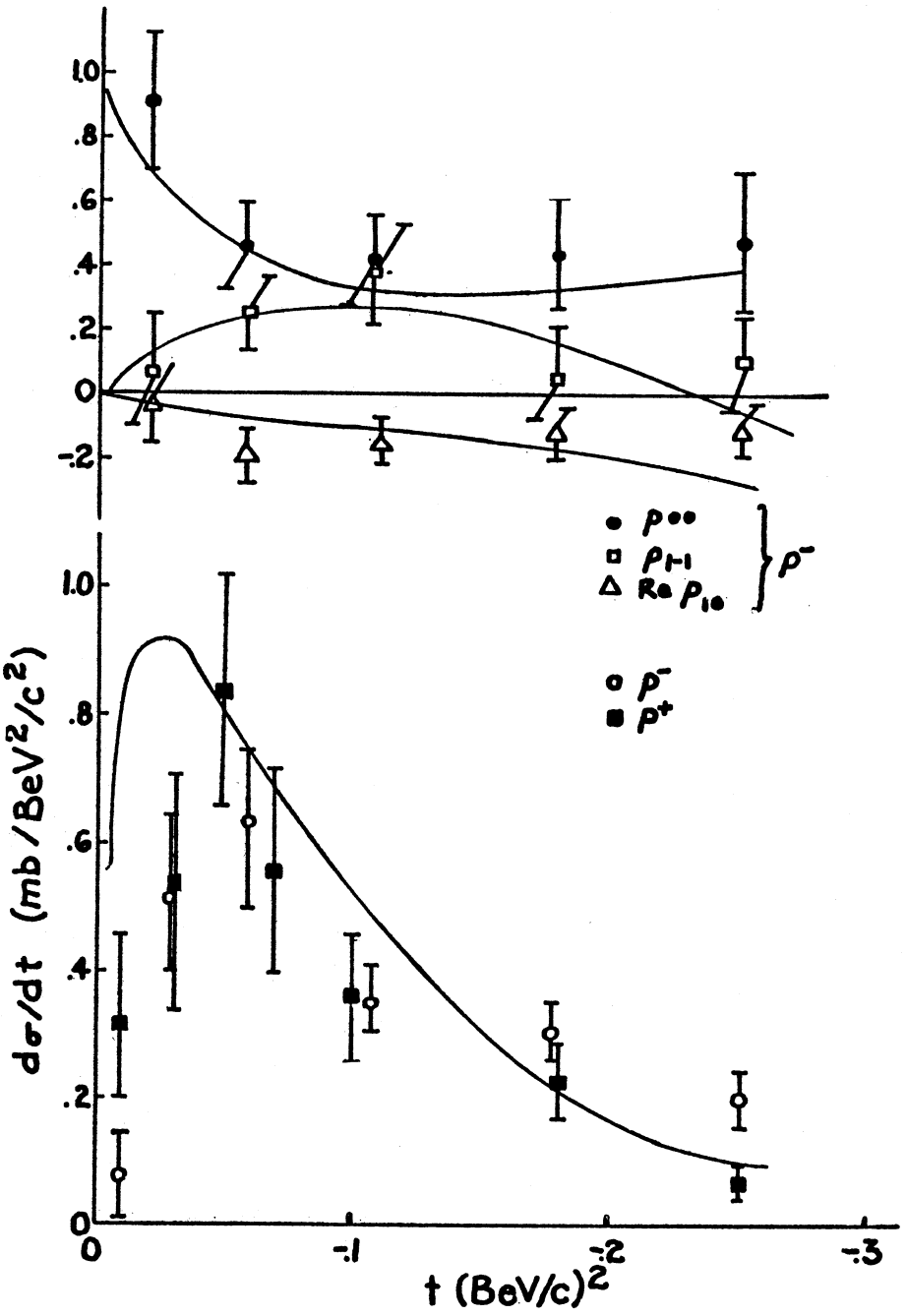

Figure 2. Differential cross section and density matrix elements for ρ-production at 8.0 GeV/c. The data for the ρ^- production are those of reference 12. The data for the ρ^+ production are those of reference 13.

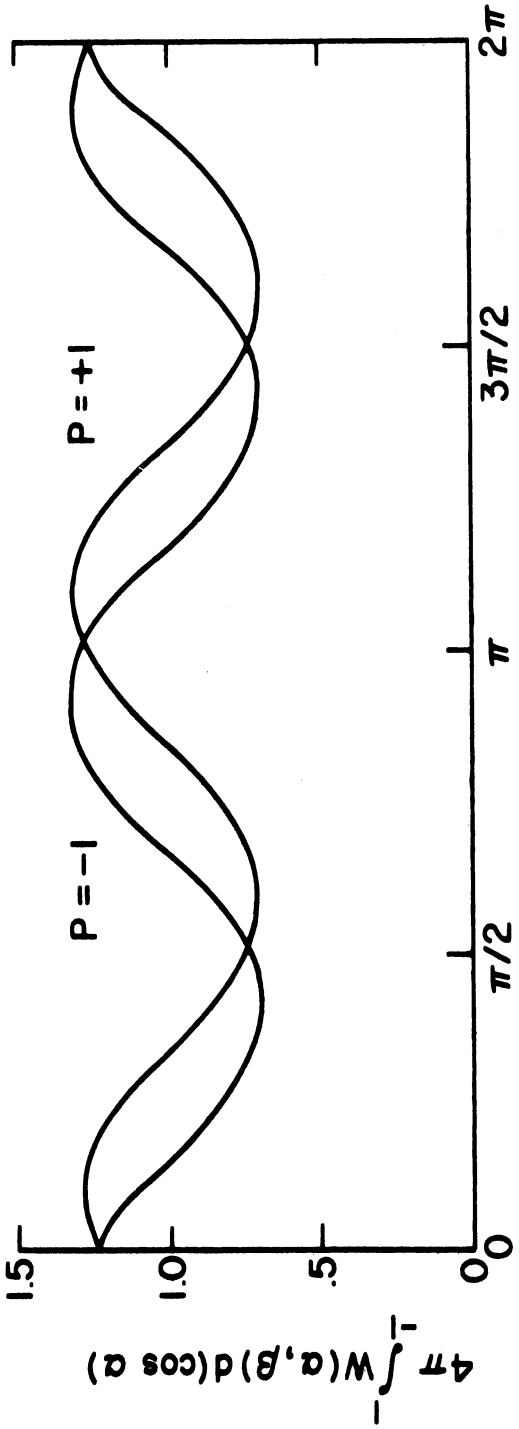

Figure 3. Comparison of decay angular distribution averaged over cosα for target polarization +1 and -1.

ON THE GROUP THEORETICAL APPROACH TO THE CONSPIRACY PROBLEM FOR ARBITRARY MASSES

G. Cosenza

Istituto di Fisica dell'Università, Napoli, Italy
and Istituto di Fisica dell'Università, Roma, Italy.

A. Sciarrino *)

Istituto di Fisica dell'Università e Scuola di Perfezionamento, Roma, Italy.

M. Toller

CERN, Geneva, Switzerland.

1. INTRODUCTION

In the phenomenological analysis of the high energy scattering amplitudes in terms of Regge poles, the following problem has recently assumed a primary importance: given a set of two particle reactions, to find all the sets of Regge trajectories such that their total contribution satisfies, above a certain energy, all the conditions required by analyticity and Lorentz invariance [1),2)]. We assume that all the Regge trajectories have factorized residues and well-defined quantum numbers. This problem is very difficult for the following two reasons :

a) it is not possible to treat the various reactions separately because they are connected by the factorization property of the residues;

b) it is not possible to treat the various trajectories separately because it often happens that the sum of their contributions satisfies the analyticity conditions, but the contributions of the single trajectories are singular. This is the phenomenon called "conspiracy".

---

*) Present address : International Centre for Theoretical Physics, Trieste, Italy.

Here, we shall consider only the problems which arise in a small interval around $t = 0$. A partial solution of these problems can be found by means of the expansion of the amplitude in terms of the matrix elements of the irreducible representations of the Lorentz group $O(3,1)$ [3] or of the group $O(4)$ [4),5]. This formalism takes automatically into account the factorization condition and some kinematic constraints. However, it has two strong limitations :

i) in its original form, it can be applied only to equal mass scattering (EE case), i.e., if we consider the reaction

$$(3)+(4)\rightarrow(1)+(2), \tag{1}$$

where

$$Q = P_1 - P_3 = P_4 - P_2 ,$$
$$t = Q^2 , \quad s = (P_1 + P_2)^2, \tag{2}$$

we have to assume

$$M_1 = M_3 , \quad M_2 = M_4 ; \tag{3}$$

ii) only amplitudes at exactly $t = 0$ can be treated. Therefore, if a Regge pole residue vanishes at $t = 0$, one cannot determine, by means of this method, the power of t that it contains.

Various modifications to the formalism have been proposed in order to avoid these limitations [4),6),7)]. Here we shall summarize a formalism which, in some respects, is similar to a formalism proposed by Domokos and Tindle [8]. The main difference is that we treat explicitly the analytic properties of the amplitude, while these authors emphasize the algebraic aspects of the problem. Moreover, we discuss the connection, due to factorization, between equal mass and unequal mass reactions. A more complete and detailed description of the method will be given elsewhere [9].

2. AN AMPLITUDE FREE OF KINEMATIC SINGULARITIES

We start from the usual M function [10] continued to complex values of the four momenta, which satisfies the following covariance condition

$$\sum_{m_1' m_2' m_3' m_4'} \Lambda^{(1)}_{m_1 m_1'}(a^{-1})\,\Lambda^{(2)}_{m_2 m_2'}(a^{-1})\,\Lambda^{(3)}_{m_3 m_3'}(a^{-1})\cdot$$

$$\cdot\Lambda^{(4)}_{m_4 m_4'}(a^{-1})\,M_{m_1' m_2' m_3' m_4'}(L(a)P_1, L(a)P_2, \tag{4}$$

$$L(a)P_3, L(a)P_4) = M_{m_1 m_2 m_3 m_4}(P_1, P_2, P_3, P_4),$$

where a is an element of the complex Lorentz group $\tilde{A}^c$, $L(a)$ is the corresponding 4×4 matrix and the matrices $\Lambda^{(i)}_{mm'}(a)$ are analytic representations of the group $\tilde{A}^c$.

Then, for every value of t, we choose a four-vector Q_t with the property

$$Q_t^2 = t\,, \tag{5}$$

and four elements b_{it} of $\tilde{A}^c$ with the properties

$$\begin{cases} L(b_{1t})P_1^0 - L(b_{3t})P_3^0 = Q_t\,, \\ L(b_{4t})P_4^0 - L(b_{2t})P_2^0 = Q_t\,, \end{cases} \tag{6}$$

where

$$P_i^0 = (Mi, 0, 0, 0)\,. \tag{7}$$

Then we define the following subgroups of the complex Lorentz group

$$H_t^c = \{h : h \in \tilde{A}^c,\ L(h)Q_t = Q_t\}\,, \tag{8}$$

$$K_t^{(A)c} = \{h : h \in \tilde{A}^c,\ L(h b_{1t}) P_1^0 = L(b_{1t}) P_1^0,\ L(h b_{3t}) P_3^0 = L(b_{3t}) P_3^0\}, \tag{9}$$

$$K_t^{(B)c} = \{h : h \in \tilde{A}^c,\ L(h b_{4t}) P_4^0 = L(b_{4t}) P_4^0,\ L(h b_{2t}) P_2^0 = L(b_{2t}) P_2^0\}. \tag{10}$$

H_t^c is called the complex little group and the groups $K_t^{(A)c}$ and $K_t^{(B)c}$ are called the right and left complex covariance group, respectively.

Now we define the function

$$T^t_{m_1 m_2 m_3 m_4}(h) = \sum_{m'_1 m'_2 m'_3 m'_4} \Lambda^{(1)}_{m_1 m'_1}\left[(h b_{1t})^{-1}\right] \cdot \Lambda^{(2)}_{m_2 m'_2}(b_{2t}^{-1}) \Lambda^{(3)}_{m_3 m'_3}\left[(h b_{3t})^{-1}\right] \Lambda^{(4)}_{m_4 m'_4}(b_{4t}^{-1}) \cdot M_{m'_1 m'_2 m'_3 m'_4}\left(L(h b_{1t}) P_1^0, L(b_{2t}) P_2^0, L(h b_{3t}) P_3^0, L(b_{4t}) P_4^0\right). \tag{11}$$

From Eq. (6) and four-momentum conservation, we have that $h \in H_t^c$. From this definition and from condition (4), we see that this T function has to satisfy the following two covariance conditions

$$T^t_{m_1 m_2 m_3 m_4}(h k) = \sum_{m'_1 m'_3} \Lambda^{(1)}_{m_1 m'_1}(b_{1t}^{-1} k^{-1} b_{1t}) \cdot \Lambda^{(3)}_{m_3 m'_3}(b_{3t}^{-1} k^{-1} b_{3t})\, T^t_{m'_1 m_2 m'_3 m_4}(h), \quad k \in K_t^{(A)c}, \tag{12}$$

$$T^{t}_{m_1 m_2 m_3 m_4}(k h) = \sum_{m_2' m_4'} \Lambda^{(2)}_{m_2 m_2'}(b^{-1}_{2t} k b_{2t}) \cdot$$

$$\cdot \Lambda^{(4)}_{m_4 m_4'}(b^{-1}_{4t} k b_{4t}) T^{t}_{m_1 m_2' m_3 m_4'}(h), \quad k \in K^{(B)c}_{t} . \tag{13}$$

It is clear that if the elements b_{it} are analytic functions of t, the T function contains only the singularities already contained in the M function. It can also be shown [9] that if the T function satisfies the covariance conditions (12), (13), it is possible to invert Eq. (11) and to reconstruct the M function. If the elements b_{it} are analytic, the M function contains only the singularities already present in the T function. This means that the T function is free of kinematic singularities and of kinematic constraints, besides the covariance conditions.

3. THE LORENTZ POLE CONTRIBUTIONS

It has been shown [11),12)], that the Regge expansion of the amplitude is equivalent to the expansion of the above defined T function in terms of the irreducible representations of the real little group H_t. In order to take easily into account the analyticity conditions, it seems natural to choose the elements b_{it} analytic at least in a neighbourhood of $t = 0$. It follows from Eq. (6) that also Q_t must be analytic. However, the usual choice

$$\begin{cases} Q_t = (\sqrt{t}, 0, 0, 0) , & t > 0 , \\ Q_t = (0, 0, 0, \sqrt{-t}) , & t < 0 , \end{cases} \tag{14}$$

has not this property, and we have to use another choice, for instance,

$$Q_t = \left(\mu + \frac{t}{4\mu}, 0, 0, \mu - \frac{t}{4\mu}\right), \tag{15}$$

where p is an arbitrary positive constant. It follows that the group H_t^c depends oontinuously on t and it can be shown that when $t \to 0$, the structure of this group changes. This phenomenon is known as "contraction". Also the real little groups H_t are subject to contraction and the problem is now to expand a function in terms of the representations of a group which depends on t and changes its structure at $t = 0$, without introducing unwanted singularities.

A trick which permits to avoid this difficulty is to consider a function defined on the whole complex Lorentz group $\tilde{A}^c$, which coincides with the above defined T function when the argument belongs to the complex little group H_t^c. Then we expand this function in terms of the irreducible representations of the real Lorentz group $\tilde{A} = O(3,1)$. It can be shown [9] that the matrix elements of these representations can be continued analytically in the complex Lorentz group and that their singularities correspond to finite values of the energy, which are not relevant for our investigation. Then we may proceed as in the equal mass case [3] and define "Lorentz pole contributions" to the extended T function.

We have said that these Lorentz pole contributions are analytic above a certain energy, but we have also to require that they satisfy the covariance conditions (12) and (13). If none of the equalities (3) is satisfied (UU case), it is possible to choose the elements b_{it} in such a way that :

a) they are analytic in a neighbourhood of $t = 0$ and they are real if t is real;

b) the covariance groups $K_t^{(A)c}$ and $K_t^{(B)c}$ do not depend on t.

In this case we can extend the T function in such a way that the covariance conditions hold in general, for $h \in \tilde{A}^c$. Then it is easy to write the $O(3,1)$ expansion in such a way that the covariance conditions are automatically satisfied.

If one or both the equalities (3) hold, (cases EU, UE, EE), it is not possible anymore to choose the elements b_{it} with the properties a) and b). This is due to the fact that in this case the

point $t=0$ coincides with a "pseudo-threshold" [1),2)]. In particular, if the elements b_{it} are analytic at $t=0$, one or both covariance groups depend on t and change their structure at $t=0$. As a consequence, it is very difficult to write the $O(3,1)$ expansion taking automatically into account the covariance conditions. We overcome this difficulty assuming that the extended T function satisfies extended covariance conditions, where the element k belongs to a subgroup of $\tilde{A}^c$, which does not depend on t and contains all the groups $K_t^{(A)c}$ [or $K_t^{(B)c}$] corresponding to the values of t belonging to a neighbourhood of $t=0$. It can be shown that in the cases UE and EU this assumption does not imply unphysical restrictions on the scattering amplitude. In the EE case, this assumption is too strong and this is the origin of some defects of the formalism, that we shall discuss in the following.

In conclusion, we have been able to build "Lorentz pole contributions", which satisfy all the requirements of analyticity and Lorentz invariance, in a neighbourhood of $t=0$.

4. THE DECOMPOSITION INTO REGGE POLES

The above defined Lorentz pole contributions can be decomposed into a family of Regge pole contributions, using the same technique introduced in Ref. 3) for equal mass forward scattering. The details of this procedure are rather complicated and will be discussed elsewhere [9)]; here we give only a summary of the results.

The Lorentz poles, as in the case treated in Ref. 3), are described by :

a) a complex parameter $\lambda(t)$, similar to the complex angular momentum;

b) a quantum number M, which is integral non-negative if the sum of the spins of the particles (1) and (3) is integral and is positive half-integral in the other case;

c) a quantum number τ which can assume two values and is called the Lorentz signature;

d) if $M=0$, there is another quantum number $\sigma = \pm 1$, called the Lorentz natural parity.

The Regge trajectories generated by a Lorentz pole are parallel and displaced by integral numbers, that is, we have

$$l_n(t) = \lambda(t) - n - 1 \,, \quad n = 0, 1, 2, \ldots \tag{16}$$

Their signatures τ_n are given by

$$\tau_n = \tau\,(-1)^n \,. \tag{17}$$

If $M=0$, there is only one trajectory for every value of n and all the trajectories have the same natural parity σ. If it is $M > 0$, for every value of n there are two superposed trajectories with the same signature but with opposite natural parity. This is the phenomenon called "parity doubling".

The fact that the trajectories are superposed or displaced by integers also for $t \neq 0$, has to be considered as a defect of our solution, which is not sufficiently general. We hope that, using more refined techniques, it is possible to modify the families described above in such a way that the kinematic constraints are still satisfied, but the trajectories are not anymore superposed or parallel.

If the Lorentz pole residues are factorized, the Regge pole residues have the factorized form

$$\beta^{(A)\,n\sigma}_{\lambda_1\lambda_3}(t)\;\beta^{(B)\,n\sigma}_{\lambda_2\lambda_4}(t) \,, \tag{18}$$

where the subscripts λ_i are the t channel helicities and σ is the natural parity of the Regge pole. The behaviour of the Regge residues at $t=0$ for $M_1 \neq M_3$ is given by

$$\beta^{(A)\,n\sigma}_{\lambda_1\lambda_3}(t) \sim t^{\frac{1}{2}[-\lambda(t)+1+|M-|\lambda_1-\lambda_3||]} \,, \tag{19}$$

and for $M_1 = M_3$ it is given by

$$\begin{cases} \beta^{(A)\,n\sigma}_{\lambda_1\lambda_3}(t) = 0 \ , \ \text{if} \ \begin{cases} \sigma = -(-1)^{M+n+\lambda_1-\lambda_3} \ , \\ \text{or if} \quad M > j_1 + j_3 \ , \end{cases} \\ \beta^{(A)\,n\sigma}_{\lambda_1\lambda_3}(t) \sim \text{constant in the other cases.} \end{cases} \tag{20}$$

The symbol j_i represents the spin of the particle (i). Similar formulae hold for the functions $\beta^{(B)n\,\sigma}_{\lambda_2\lambda_4}(t)$. We see that if two masses are equal, some residues vanish identically in t, also if this is not required by Regge pole theory. In particular, if $M_1 = M_3$, a Lorentz pole with $M > j_1+j_3$ cannot give any contribution even at $t \neq 0$. We consider this as another defect of our solution, which should disappear in a more general formalism.

Another interesting property of the generalized Lorentz pole contributions is the high energy behaviour of the s channel helicity amplitudes in the forward direction ($\theta_s = 0$). The result is the same for all the values of the masses, that is

$$f^{s}_{\lambda_1\lambda_2\lambda_3\lambda_4}(s, \theta_s = 0) \sim \delta_{\lambda_1-\lambda_3,\lambda_2-\lambda_4}\, s^{\lambda - 1 - |M - |\lambda_1-\lambda_3||} \ . \tag{21}$$

In conclusion, we have built families of Regge trajectories, with well-defined quantum numbers and factorized residues, whose contribution to an arbitrary number of reactions, with arbitrary masses and spins, satisfies all the constraints of analyticity and Lorentz invariance in a neighbourhood of $t = 0$. This is a solution of the problem stated at the beginning of the Introduction. It is not the most general one, but we believe that it represents a useful step towards the general solution of this problem.

ACKNOWLEDGEMENTS

We would like to thank Professor D. Amati, Dr. G. Cohen-Tannoudji, Dr. H. Epstein and Dr. Ph. Salin for very helpful discussions.

REFERENCES

1) L.L. Wang, Phys.Rev. 142, 1187 (1966).

2) G. Cohen-Tannoudji, A. Morel and H. Navalet, CEN preprint, Saclay, April (1967).

3) M. Toller, CERN preprint TH.780 (1967). References to previous work can be found in this paper.

4) G. Domokos, Phys.Rev. 159, 1387 (1967).

5) D.Z. Freedman and J.M. Wang, Phys.Rev. 160, 1560 (1967).

6) R. Delbourgo, A. Salam and J. Strathdee, Phys.Letters 25B, 230 (1967).

7) R.F. Sawyer, Phys.Rev.Letters 18, 1212 (1967); and University of California preprint, Santa Barbara (1967).

8) G. Domokos and G.L. Tindle, University of California preprints, Berkeley (1967).

9) G. Cosenza, A. Sciarrino and M. Toller, to be published.

10) H.P. Stapp, Phys.Rev. 125, 2139 (1962).

11) M. Toller, Nuovo Cimento 37, 631 (1965); and CERN preprint TH.770. References to previous work can be found in this paper.

12) J.F. Boyce, J.Math.Phys. 8, 675 (1967).

PHASE CONTOURS OF SCATTERING AMPLITUDES*

UCRL-17921

Charles B. Chiu

CERN, Geneva, Switzerland,

Richard J. Eden**† and Chung-I Tan

Lawrence Radiation Laboratory
University of California
Berkeley, California, U.S.A.

1. INTRODUCTION

We will describe the method of phase contours and its application to some problems in the study of strong interactions. Phase contours are curves along which the phase of a scattering amplitude is constant. They are sections of complex surfaces in the space of the invariants s, t and u. We will give a brief discussion of the following topics:

(i) Properties of phase contours.

(ii) Phase contours for pion-nucleon scattering.

(iii) Phase contours in a Regge model for pion-nucleon scattering.

(iv) Resonance poles, and zeros, in a crossing symmetric model.

(v) Fixed angle scattering at high energy.

A more detailed discussion of these topics will be given in forthcoming papers[1),2),3)].

---

* This work was supported by the U. S. Atomic Energy Commission.

** At the Cavendish Laboratory, Cambridge, England, after 1st January 1968.

† To read the paper.

2. PROPERTIES OF PHASE CONTOURS

We limit our discussion to the scattering of spinless bosons of mass m, except when considering pion-nucleon scattering.[1] The phase $\phi(s,t)$ of a scattering amplitude $F(s,t)$ is defined by

$$\phi(s,t) = \mathrm{Im}[\log \{F(s,t)\}]. \qquad (2.1)$$

It is also necessary to define the phase at an initial point (s_0,t_0). When the amplitude has zeros or poles, the phase depends on the route chosen from the initial point to the point (s,t), so we must always specify the route taken.

A phase contour is defined by

$$\phi(s,t) = C, \qquad (2.2)$$

where C is a real constant. It is useful to study their properties both for real s and t, and for complex s and fixed t. These properties include:

a) Phase contours, for different values of C, do not meet each other, except at zeros or poles of the scattering amplitude, and at certain other singularities.

b) The phase change clockwise round a zero is -2π, and round a pole is 2π.

c) For fixed t and complex s, the phase is an harmonic function, and the phase contours are orthogonal to the modulus contours.

d) The asymptotic phase in a Regge model for a symmetric amplitude, for $t < 4m^2$, assuming a non-zero residue is given by

$$\phi(s,t) \sim \pi[1 - \tfrac{1}{2}\alpha(t)] , \qquad (2.3)$$

as $s \to +\infty$ along $s + i0$ (above the real branch cut). In complex directions, as $|s| \to \infty$

$$\phi(|s|e^{i\theta},t) \sim \pi[1 - \tfrac{1}{2}\alpha(t)] + \alpha\theta . \qquad (2.4)$$

The simple relation of the phase to the power $s^{\alpha(t)}$ should be noted.

e) Phase contours contain information about the oscillations of Im $F(s,t)$ as s moves along the real axis. These oscillations, together with information about poles and zeros, can be used to set bounds on the high energy behavior of F.

f) From the optical theorem, we have

$$\text{Im } F(s,0) > 0 , \quad \text{for} \quad s > 4m^2. \qquad (2.5)$$

We define the phase $\phi(s,t)$ at an initial point along $t = 0$, namely along $s + i0$ (above the branch cut),

$$\phi(s \to +\infty, 0) = \tfrac{1}{2}\pi . \qquad (2.6)$$

g) The phase contours

$$\phi(s,t) = 0 , \quad \text{or} \quad \pi, \qquad (2.7)$$

cannot enter the region

$$0 \leqslant t < 4m^2, \quad s > 4m^2. \qquad (2.8)$$

For a symmetric amplitude, they also cannot enter the region,

$$0 \leqslant u < 4m^2, \quad s > 4m^2. \qquad (2.9)$$

Except when considering low and medium energy pion-nucleon phase contours, we work with a Regge model in which there is dominance by a single, continuously rising, Regge trajectory, as $s \to \infty$ for fixed t, and there is symmetry between all three channels, s, t and u. The method of phase contours can equally well be applied to other models, or it can be used to generalize existing models.

3. PHASE CONTOURS FOR PION-NUCLEON SCATTERING AMPLITUDES

We have used the results of the phase shift analysis of pion-nucleon scattering to obtain phase contours for invariant amplitudes in the energy range

$$0 < T_\pi < 1.4 \text{ GeV}, \tag{3.1}$$

where T_π denotes the pion kinetic energy. The amplitudes that we have studied,[1] are the symmetric and antisymmetric combinations of $\pi^+ p$ and $\pi^- p$, namely,

$$A'^{(+)}, \quad B^{(+)}, \quad A'^{(-)}, \quad B^{(-)} . \tag{3.2}$$

We have used the 1966 phase shifts of Lovelace[4] in the range (3.1), and some preliminary results of Johnson[5] in the range $0 < T_\pi < 1.6$ GeV. Our purpose is to show that phase contours provide:

(a) A useful visual aid for comparing different phase shift solutions and for indicating regions where the resulting scattering amplitudes are complicated. In these regions one might conclude that the continuation of the phase shift solutions is doubtful and more experiments

are desirable.

(b) They determine the location of real zeros of the amplitudes from the crossover points of phase contours and indicate complex zeros.

(c) They may help to give an indication of how to match high energy models for scattering, onto low energy models. For this purpose we have obtained phase contours for the extrapolated Regge model described in Section 4.

Phase contours for $A'^{(+)}$ derived from the Lovelace (1966) phase shifts[4] are shown in Fig. 1. There are several points of special interest.

(i) The phase, in an energy range from 0.2 to 1.2 GeV at angles from 0° to 90°, lies in the range

$$90^\circ < \phi(s,t) < 150^\circ. \qquad (3.3)$$

Above 1.2 GeV, there is a wider range of phases which suggests the onset of high energy effects, possibly of Regge type.

(ii) There are two real zeros indicated by the crossing of phase contours. There are probably also some nearby complex zeros indicated by the bunching of phase contours, especially along a scattering angle of about 120°.

The corresponding modulus contours are shown in Fig. 2. This shows the minima in the modulus near the crossover points of the phase contours, and also in regions where there was a bunching of phase contours in Fig. 1.

The phase contours for $A'^{(+)}$, based on the Johnson phase shifts,[5] are shown in Fig. 3. They resemble those of Fig. 1 in their general features. However the zero at 1.27 GeV in Fig. 1 has disappeared. It appears to be replaced by a complex zero near the physical region, which would be one of a pair of complex zeros.

All the other amplitudes indicate considerable complexity around $T_\pi = 0.85$ GeV, which is just below the 1688 resonance. As an example the phase contours for $B^{(+)}$ are shown in Fig. 4. Rapid phase changes like those near 0.85 GeV indicate rapid changes in polarization. They also suggest that more experimental information would be valuable.

4. PHASE CONTOURS IN A REGGE MODEL FOR PION-NUCLEON SCATTERING

We have calculated the phase contours for the pion-nucleon amplitudes (3.2) using extrapolation from a Regge model for high energy scattering.[1] Our extrapolation is not meant to be realistic at this stage, but it is hoped that it gives some orientation on what might be attributed to Regge effects from the few poles that dominate near-forward and near-backward scattering at high energies. We have done this simply by adding the Regge solutions based on P, P' and ρ, exchange in the t channel,[6] and N, N^*, exchange in the u channel.[7] We have also assumed that the trajectories fall linearly as t decreases (or u).

The results are illustrated in Fig. 5 for the invariant amplitude $A'^{(+)}$. It is interesting to find that real zeros arise from the interference of different Regge terms. The contours in

$0 < (-t) < 1\ (\mathrm{GeV})^2$ illustrate the behavior of the phase near the dip and peak of the differential cross section near the forward direction, which is attributed to the zero in the residue of the Regge term from ρ exchange. The shape of the contours at large angles is characteristic of our Regge model with rising Regge trajectories.

5. RESONANCE POLES AND ZEROS IN A CROSSING SYMMETRIC MODEL

Phase contours provide a method for studying part of the consistency problem in strong interactions, and may help towards formulating approximations in which the bootstrap problem is meaningful. However at this stage we do not introduce unitarity, but consider only the consistency that is required by crossing symmetry for a given high energy behavior, taking into account the associated resonance poles (Regge poles).

We consider a symmetric scattering amplitude for equal mass spinless bosons.[2] Our aim is to construct a model, or a class of models, that satisfies the crossing conditions and has given high energy behavior. The latter is based on Regge terms of the type,

$$\frac{b(t)\ s^{\alpha(t)}\ \exp[i\pi\{1 - \frac{1}{2}\alpha(t)\}]}{\sin[\frac{1}{2}\pi\alpha(t)]\ \Gamma(\alpha)}\ , \qquad (5.1)$$

where $\mathrm{Re}\{\alpha(t)\}$ is a rising function of t.

We assume that there are no real poles on the physical sheet, and we neglect the local distortions of phase contours that are

introduced at low energies in the physical regions. This leads to the Regge dominance model for phase contours in the physical regions that is illustrated for the s channel in Fig. 6.

The phases in regions of crossed branch cuts are obtained from (5.1). In these regions it is important to specify whether the real values of s, t and u, lie above or below their respective branch cuts, on the physical sheet. The formula (5.1) applies along $s + i0$, and $\alpha(t)$ is real for $t < 4m^2$. For $t > 4m^2$, $\text{Im}\,\alpha > 0$ for $t + i0$ (t above the cut), and $\text{Im}\,\alpha < 0$ for $t - i0$ (below the cut but still on the physical sheet).

The form of the solution depends on how many real zeros of the scattering amplitude lie on the boundary of the physical sheet. The location of the first of these zeros (the one nearest the symmetry point $(4m^2/3,\ 4m^2/3,\ 4m^2/3)$, is directly related to the scattering length. There is an infinite sequence of other zeros, but not all of them need be on the physical sheet. They are associated with interference between resonance poles, or between a resonance pole and a background term.

One of our solutions for the phase contours is illustrated in Fig. 7. This solution corresponds to an infinite sequence of zeros on the physical sheet $(s + i0,\ t - i0,\ u - i0)$. A complex section is given in Fig. 8, with t real and $t > 4m^2$. This shows how these zeros are associated with phase contours and resonance poles in the complex s plane including part of the unphysical sheet.

6. FIXED ANGLE SCATTERING AT HIGH ENERGY

We have considered[3] the problem of fixed angle scattering at high energy within the general framework of the crossing symmetric amplitude described in Section 5. The method of phase contours is used to discuss the relation between high energy behavior at fixed momentum transfer and at fixed angle. The former is given by our assumption of dominance by Regge poles with rising trajectories in each channel.

As an example we will consider the phase contours shown in Fig. 7. These correspond to the limit appropriate for fixed angle scattering with $\text{Im } s > 0$. We reduce the scattering amplitude to a Herglotz function by factoring out zeros and oscillations. In this example there are no zeros of F in $\text{Im } s > 0$, and no zeros of $\text{Im } F$ along real $s < 0$.

With certain simplifying assumptions we can write,

$$F(s, \cos\theta) = \frac{H(s, \cos\theta)}{R(s, \cos\theta)}, \tag{6.1}$$

where H is a Herglotz function and R is an entire function in the variable s. The order $p(\theta)$ of the entire function is related to the phase by means of Jensen's theorem, which gives

$$\phi(s, \cos\theta) \sim C\, s^{p(\theta)}. \tag{6.2}$$

Using Polya's inequality, one can obtain bounds on the scattering amplitude in the upper half s plane,

$$\exp[-A\, s^{p(\theta)}] \;<\; |F(s,\cos\theta)| \;<\; \exp[-A(\cos\pi p - \epsilon)s^{p(\theta)}]. \tag{6.3}$$

If we generalize (6.1) to allow a sequence of zeros in $\mathrm{Im}\, s > 0$ for fixed $\cos\theta$, we obtain

$$F(s,\cos\theta) = \frac{E(s,\cos\theta)\, H(s,\cos\theta)}{R(s,\cos\theta)}\,, \tag{6.4}$$

where E is an entire function of order $q(\theta)$. Then, if $q > p$, we obtain the bounds for large $|s|$,

$$\exp\left[B(\cos q\pi - \epsilon)s^{q}\right] \;<\; F(s,\cos\theta) \;<\; \exp[Bs^{q}]\,, \tag{6.5}$$

except near the zeros of E. This gives

$$q(\theta) \geqslant \tfrac{1}{2}\,, \qquad \text{for all } \theta. \tag{6.6}$$

No such condition is required if $p(\theta) > q(\theta)$ for all θ.

We are indebted for hospitality and for helpful discussions to Professor G. F. Chew at the Lawrence Radiation Laboratory, Berkeley, and to Dr. L. Van Hove at CERN, Geneva.

REFERENCES

1. C. B. Chiu, R. J. Eden and C-I. Tan, Phase Contours of Scattering Amplitudes I, Phase Contours, Zeros, and High Energy Behavior, Lawrence Radiation Laboratory Report No. UCRL-17899 (1967).

2. R. J. Eden and C-I. Tan, Phase Contours of Scattering Amplitudes II, Crossing Symmetry, Resonance Poles and High Energy Behavior, Lawrence Radiation Laboratory Report No. UCRL-17922 (1967).

3. R. J. Eden and C-I. Tan, Phase Contours of Scattering Amplitudes III, High Energy Behavior at Fixed Angles, Lawrence Radiation Laboratory Report No. UCRL-17923 (1967).

4. C. Lovelace, Proceedings of the Berkeley Conference on High Energy Physics (1966).

5. C. H. Johnson, Ph.D. Thesis, University of California, Berkeley (1967).

6. W. Rarita, R. J. Riddell, Jr., C. B. Chiu, R. J. N. Phillips, Regge Pole Model for πp, pp, and $\bar{p}p$ Scattering, Lawrence Radiation Laboratory Report No. UCRL-17523 (1967).

7. C. B. Chiu and J. Stack, Phys. Rev. 153, 1575 (1967).

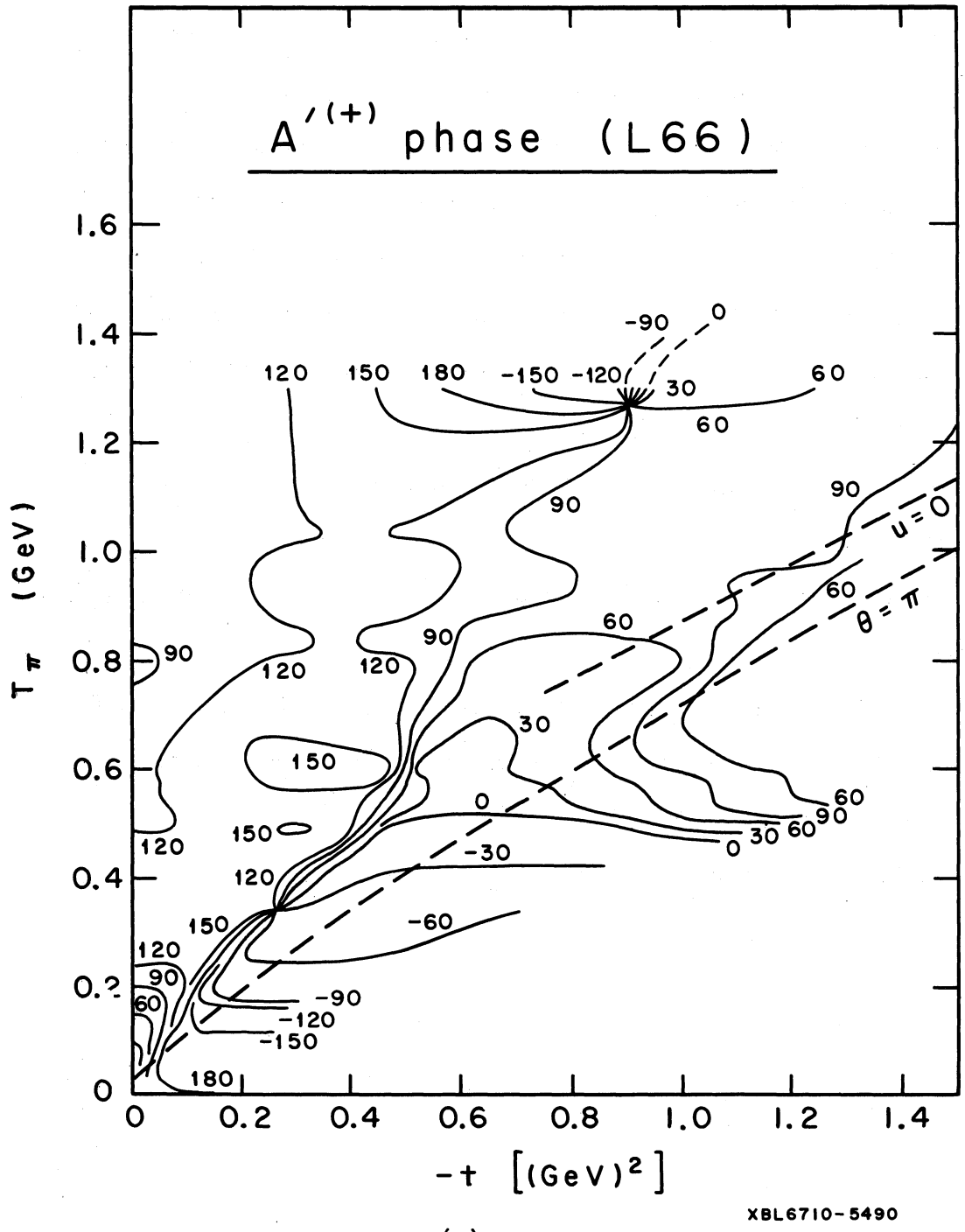

Fig. 1. Phase contours for $A'^{(+)}$ as functions of the pion kinetic energy T_π and the momentum transfer variable (-t). Derived from the Lovelace (1966) phase shifts for πN scattering.

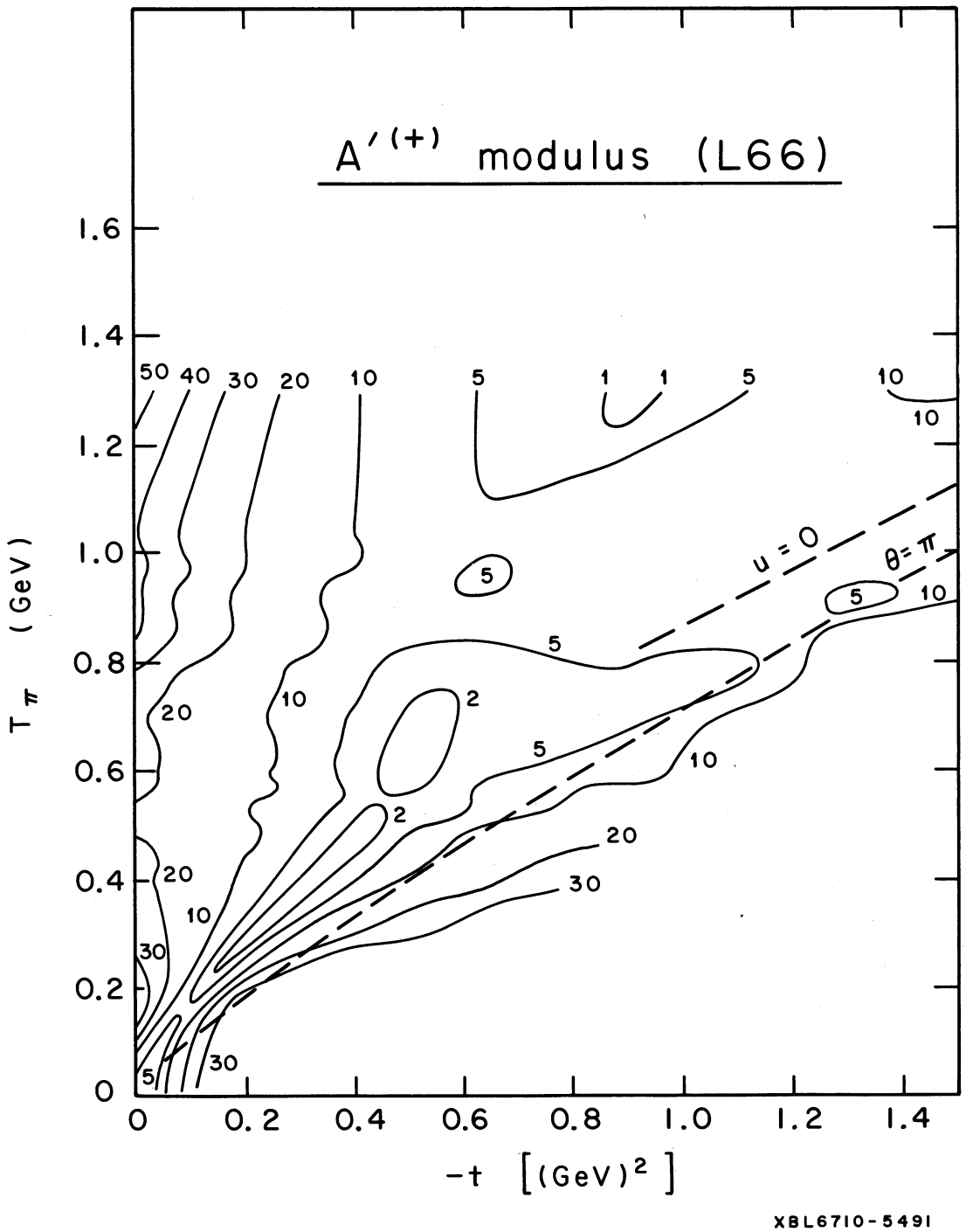

Fig. 2. Modulus contours for $A'^{(+)}$, derived from the Lovelace (1966) phase shifts for πN scattering.

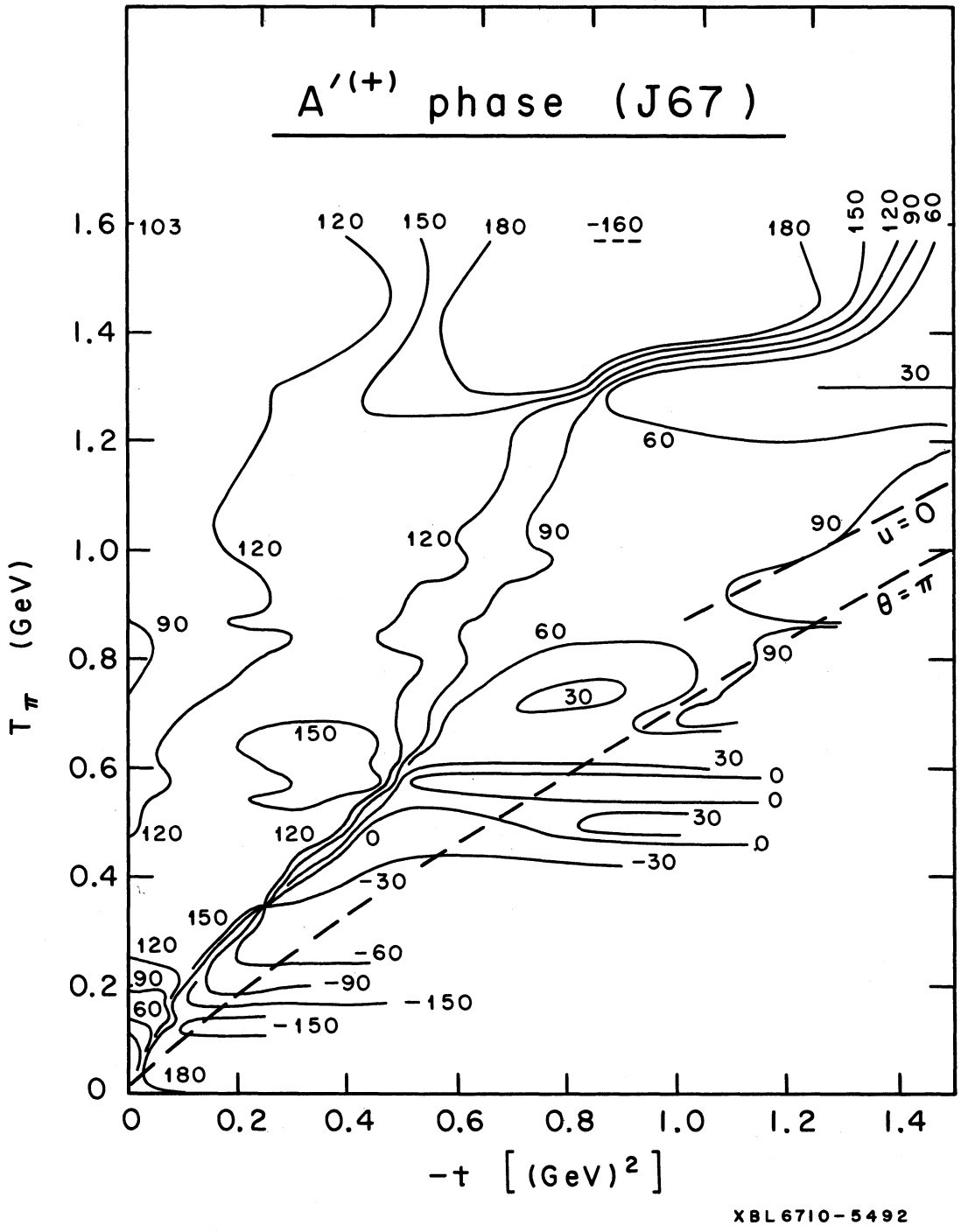

Fig. 3. Phase contours for $A'^{(+)}$ derived from the Johnson (1967) phase shifts for πN scattering.

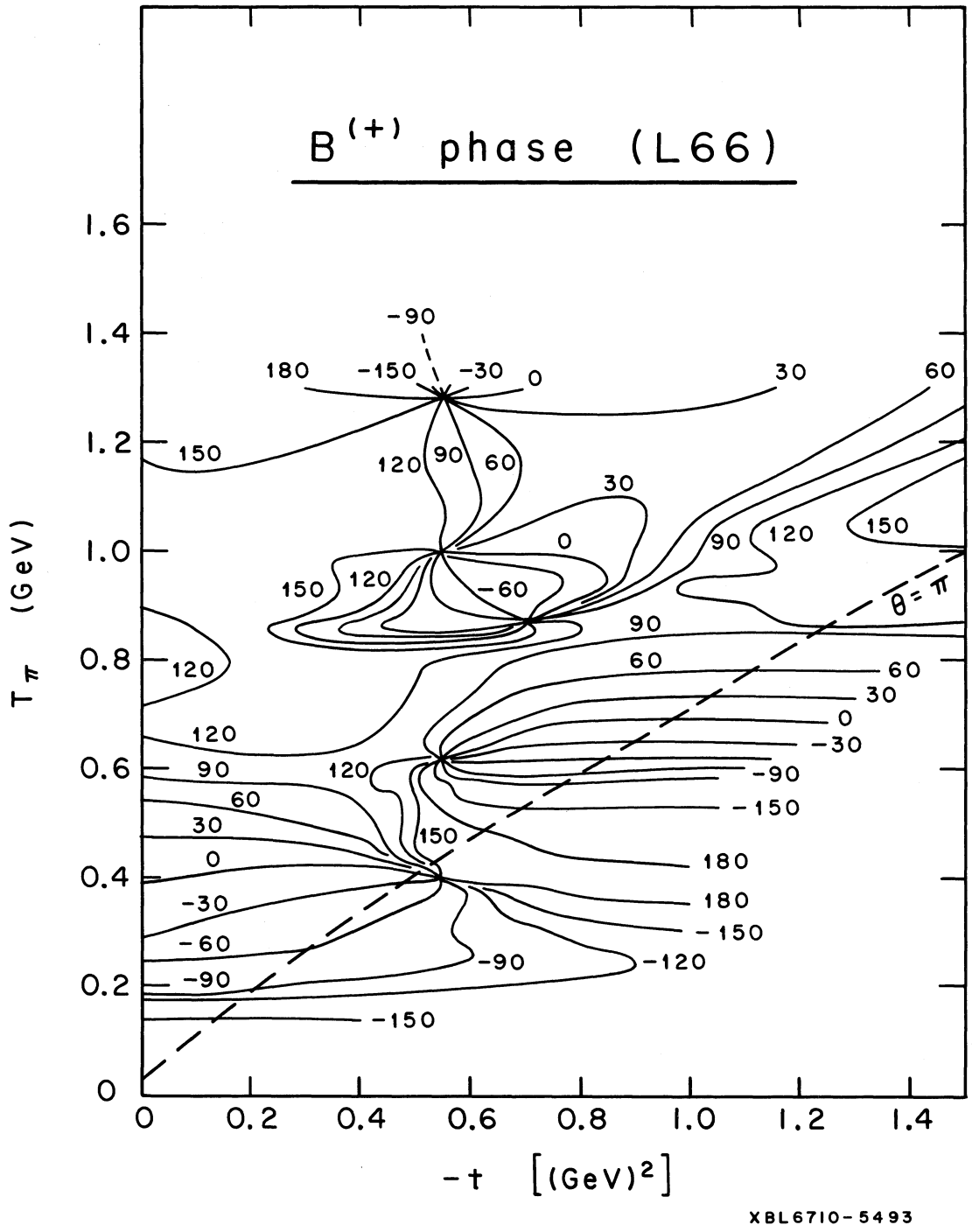

Fig. 4. Phase contours for $B^{(+)}$, derived from the Lovelace (1966) phase shifts for πN scattering.

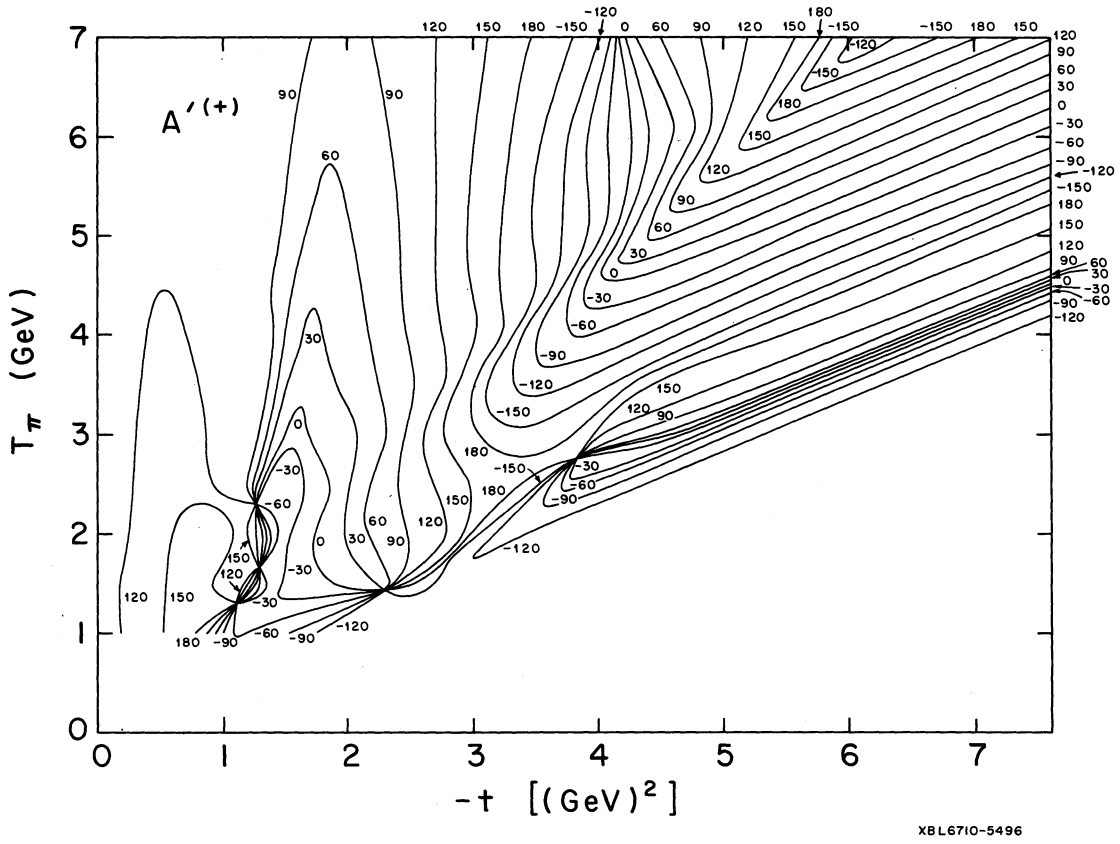

Fig. 5. Phase contours for $A'^{(+)}$, derived by extrapolating from the high energy Regge solutions for πN scattering.

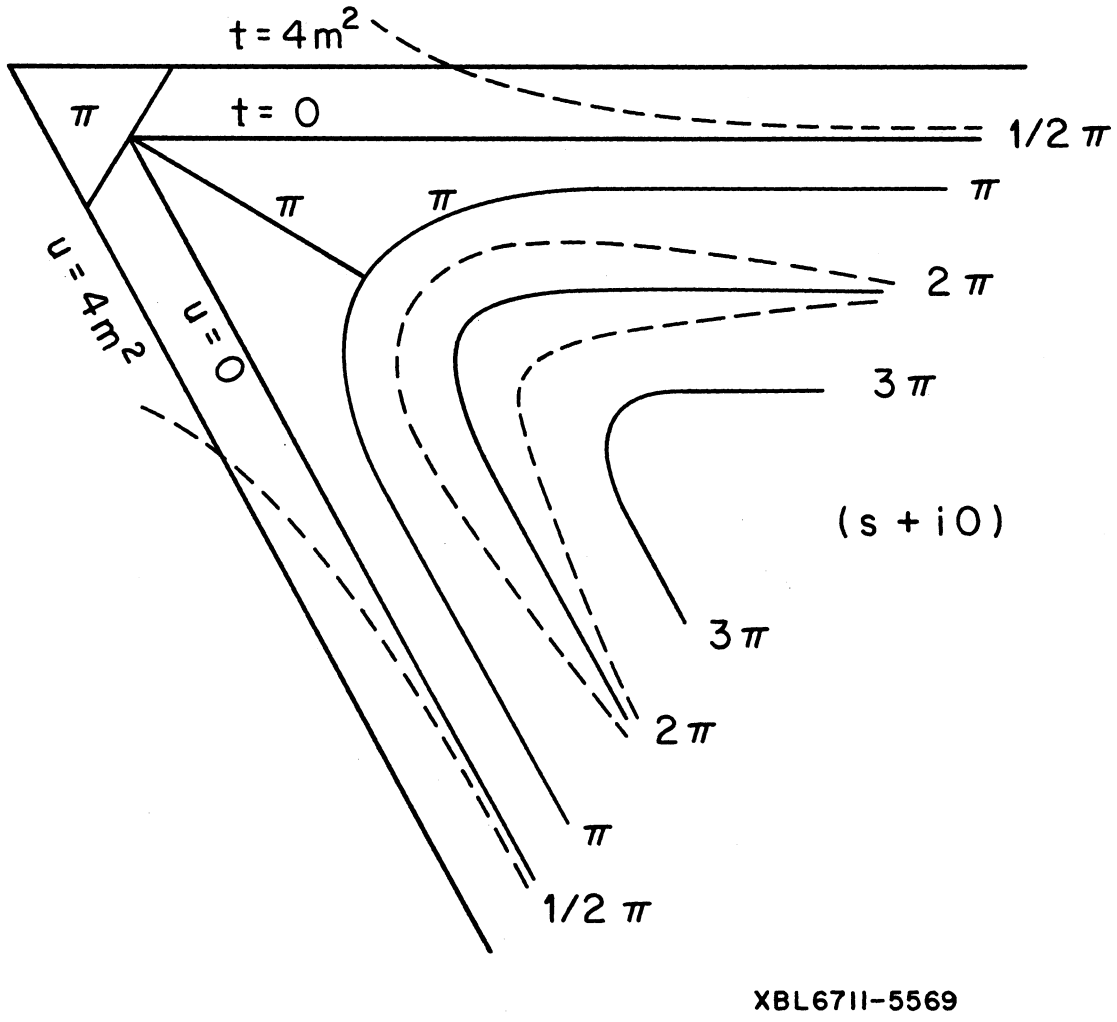

Fig. 6. Phase contours in the s channel for a Regge model. Broken lines correspond to half integer multiples of π.

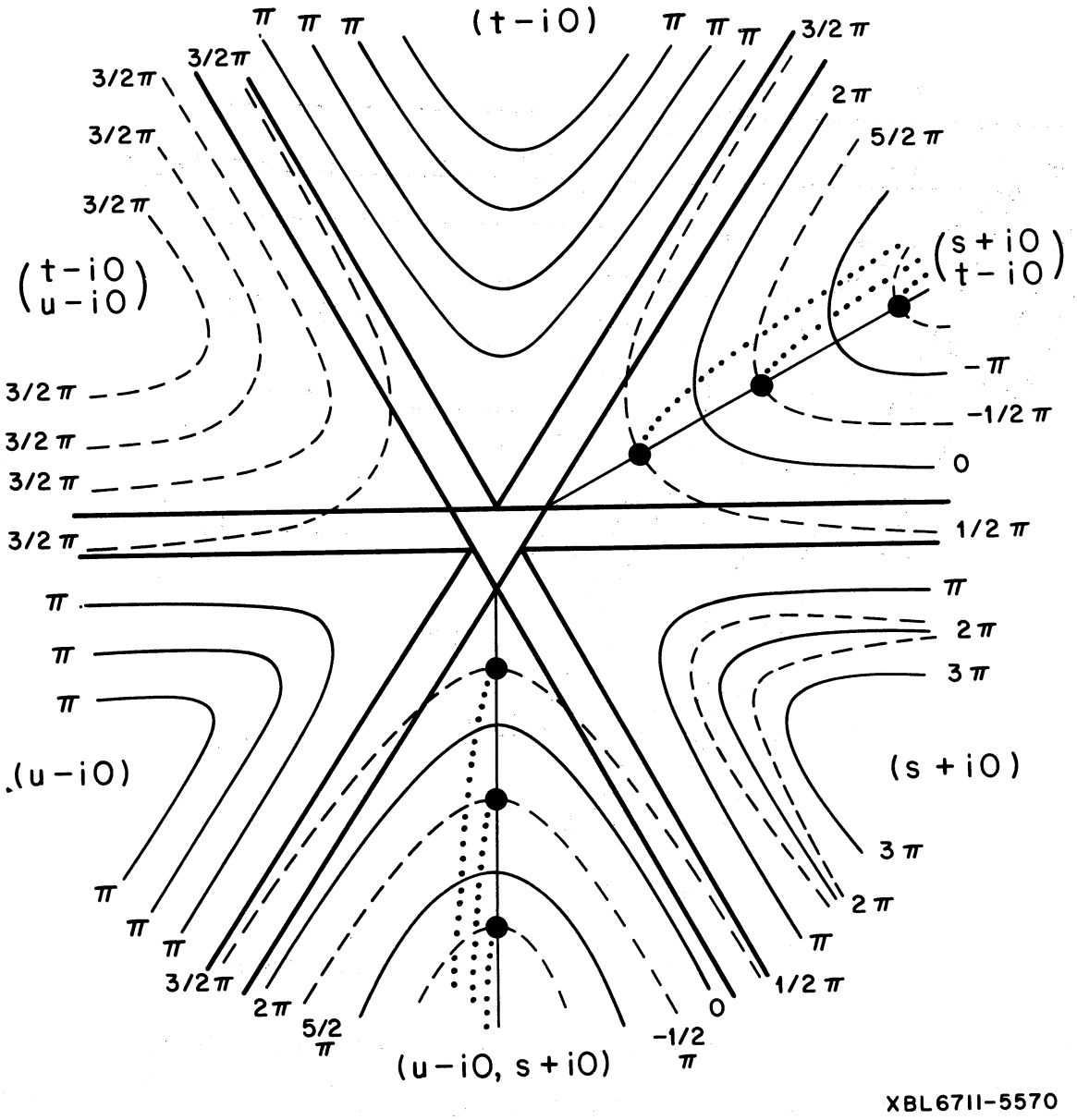

Fig. 7. Phase contours for a crossing symmetric amplitude in the limit (s + i0, t - i0, u - i0). The apparent lack of symmetry is due to the existence of complex zeros, some of which are indicated by the dotted lines. The black circles indicate real zeros.

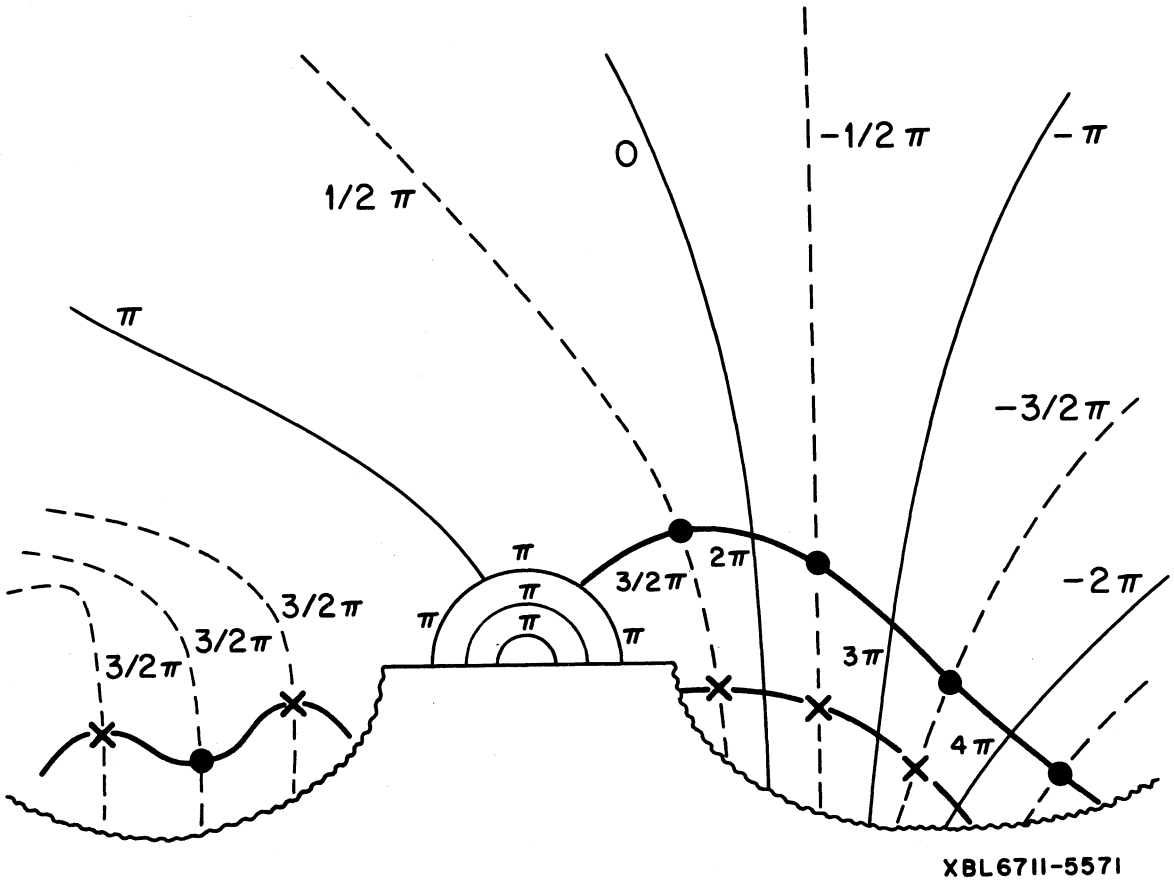

Fig. 8. Phase contours in the complex s plane, for fixed $t > 4m^2$, that correspond to the real section shown in Fig. 7. Poles are denoted by crosses and zeros by circles.

ON SOME CONSEQUENCES OF ANALYTICITY AND UNITARITY

A.A.Logunov
Institute of High Energy Physics, Serpukhov, USSR

Nguyen van Hieu
Joint Institute for Nuclear Research, Dubna, USSR

A b s t r a c t

In this paper we present the results concerning the asymptotic behaviour of the cross sections of elastic and inelastic processes. Some of these results were obtained together with M.A.Mestvirishvili and Nguyen ngoc Thuan. For the sake of simplicity we assume all particles to be spinless.

1. Upper bounds for the cross-sections of binary processes

First we consider some process of elastic scattering

$$a + b \longrightarrow a + b \tag{1}$$

We assume the amplitude of this process $F(s,z)$ to be analytical in $z = \cos\theta$, θ being the scattering angle in the centre of mass system, inside the Mandelstam ellipse E_c with foci at ± 1 and with the major semi-axis $c \sim 1 + \frac{\gamma}{s}$, $\gamma > 0$, at $s \to \infty$. For a number of processes such analytic properties were proved on the basis of the fundamental postulates of the local quantum field theory [1]. Let us expand $F(s,z)$ in partial waves

$$F(s,z) = 8\pi \frac{\sqrt{s}}{p} \sum_{l=0}^{\infty} (2l+1)\, a_l(s)\, P_l(z). \tag{1}$$

As is well known, from the analyticity in z and from the polynomial boundedness at $s \to \infty$ it follows that $a_l(s)$ decreases exponentially when l increases [2]

$$\cdot \left| a_l(s) \right| \leq R(s) \left[c + \sqrt{c^2 - 1} \right]^{-l}, \tag{2}$$

where $R(s)$ is a polynomial in s. Let L be that value of l at which the r.h.s. of the relation (2) equals 1, and L_0 be the smallest integer number still greater than L. Now we rewrite the sum in (1) as follows

$$F(s,z) = 8\pi \frac{\sqrt{s}}{p} \sum_{l=0}^{nL_0} (2l+1)\, a_l(s)\, P_l(z) + 8\pi \frac{\sqrt{s}}{p} \sum_{l=nL_0+1}^{\infty} (2l+1)\, a_l(s)\, P_l(z). \tag{3}$$

By using the inequality (2) we can prove that a finite integer number n can always be chosen to make the second term in the r.h.s. of (3) decrease faster than any power of s at $s \to \infty$.

We remember that if we substitute for $a_\ell(s)$ in the first sum their upper unitarity bound

$$|a_\ell(s)| \leq 1 \tag{4}$$

then, in virtue, of the relation

$$nL_0 \sim \text{const}\ \sqrt{s}\ \ln s \tag{5}$$

we obtain the Froissart bounds

$$|F(s,1)| \leq \text{const}\ s \ln^2 s, \tag{6}$$

$$|F(s,\cos\theta)| \leq \text{const}\ \frac{s^{3/4} \ln^{3/2} s}{\sqrt{\sin\theta}}, \quad \theta \neq 0,\pi. \tag{7}$$

It is possible to improve these results using in the first sum of (3) the Schwartz inequality instead of the substitution $|a_\ell(s)| \to 1$. Then we have

$$|F(s,z)|^2 \sim \left| \sum_{\ell=0}^{nL_0} (2\ell+1)\, a_\ell(s)\, P_\ell(z) \right|^2 \leq \tag{8}$$

$$\leq \sum_{\ell=0}^{nL_0} (2\ell+1)\, |P_\ell(z)|^2 \cdot \sum_{\ell=0}^{\infty} (2\ell+1)\, |a_\ell(s)|^2 .$$

We denote by $\frac{d\sigma_{e\ell}}{d\cos\theta}$ and $\sigma_{e\ell}$ the differential and the total cross-sections of the process (I). We obtain, as a consequence of the relation (8), the inequalities [3]

$$\left.\frac{d\sigma_{el}}{d\cos\theta}\right|_{\theta=0} \leq \text{const}\; s\ln^2 s\,\sigma_{el}\,, \tag{9}$$

$$\left.\frac{d\sigma_{el}}{d\cos\theta}\right|_{\theta\neq 0,\pi} \leq \text{const}\;\frac{\sqrt{s}\ln s}{\sin\theta}\,\sigma_{el}\,. \tag{10}$$

We consider now any binary process

$$a + b \longrightarrow c + d\,, \tag{11}$$

and we decompose its amplitude $T(s,z)$ in partial waves

$$T(s,z) = 8\pi\frac{\sqrt{s}}{p}\sum_{l=0}^{\infty}(2l+1)\,b_l(s)\,P_l(z)\,. \tag{11}$$

This always can be done in the interval $-1 \leq z \leq 1$. The contribution from the partial amplitude $b_l(s)$ in the imaginary part $\operatorname{Im} a_l(s)$ equals $|b_l(s)|^2$

$$\operatorname{Im} a_l(s) = |a_l(s)|^2 + |b_l(s)|^2 + \ldots\ldots \tag{12}$$

Since all the terms in the r.h.s. of (12) are positive, we can write

$$|b_l(s)| < \sqrt{\operatorname{Im} a_l(s)} \leq \sqrt{|a_l(s)|}\,. \tag{13}$$

We conclude thus on the basis of relations (2) and (13) that also $b_l(s)$ decreases exponentially when l increases and for the differential and total cross sections $\frac{d\sigma_{inel}}{d\cos\theta}$ and σ_{inel} we get the same inequalities as for the elastic processes

$$\left.\frac{d\sigma_{inel}}{d\cos\theta}\right|_{\theta=0} \leq \text{const}\; s\ln^2 s\,\sigma_{inel}\,, \tag{14}$$

$$\left.\frac{d\sigma_{inel}}{d\cos\theta}\right|_{\theta\neq 0,\pi} \leq const\ \frac{\sqrt{s}\ \ln s}{\sin\theta}\ \sigma_{inel}\ . \qquad (15)$$

If the differential cross sections are considered at fixed t instead of $\cos\theta$ then we have

$$\left.\frac{d\sigma_{el}}{dt}\right|_{t=0} \leq const\ \ln^2 s\ \sigma_{el}\ ,\quad \left.\frac{d\sigma_{el}}{dt}\right|_{t\neq 0} \leq const\ \frac{\ln s}{\sqrt{|t|}}\ \sigma_{el}\ , \qquad (16)$$

$$\left.\frac{d\sigma_{inel}}{dt}\right|_{t=0} \leq const\ \ln^2 s\ \sigma_{inel}\ ,\quad \left.\frac{d\sigma_{inel}}{dt}\right|_{t\neq 0} \leq const\ \frac{\ln s}{\sqrt{|t|}}\ \sigma_{inel}\ . \qquad (17)$$

The relations (16), in particular, shows that the width of the diffraction peak for elastic and inelastic processes

$$\Delta_{el} = \frac{\sigma_{el}}{d\sigma_{el}/dt\,|_{t=0}}\ ,\quad \Delta_{inel} = \frac{\sigma_{inel}}{d\sigma_{inel}/dt\,|_{t=0}} \qquad (18)$$

can not decrease at $s\to\infty$ faster than $1/\ln^2 s$. This result for elastic processes was obtained earlier in a paper of Bessis who used a different method [4].

2. Upper bounds for the cross-sections of inelastic processes of multiple production

Now we are intended to show that the results obtained before are true also for the processes of multiple production of the type

$$a + b \longrightarrow c + B_j\ , \qquad (III)$$

where B_j denotes a system of hadrons. We denote the angle between "a" and "c" particles momenta in the centre of mass system by θ. The amplitude of the process III $T^{jc}(s, \cos\theta, \dots)$ will be presented in the form of a function of s, $z = \cos\theta$ and other independent variables, which always can be chosen in such a way that the integration domains in these variables are independent of the angle θ. The amplitude $T^{jc}(s, z, \dots)$ can always be decomposed in the Legendre polynomials

$$T^{jc}(s,z,\dots) = 4\pi \frac{\sqrt{s}}{p} \sum_{l=0}^{\infty} (2l+1)\, f_l^{jc}(s,\dots)\, P_l(z). \quad (19)$$

The contribution from the process (III) to the imaginary part of the partial amplitude of the process (I) is equal to

$$\operatorname{Im} a_l(s)\Big|_{III} = \eta_l^{jc}(s) = \frac{1}{2\pi} \frac{\sqrt{s}}{p} \int (2\pi)^4 \delta^4(p_a + p_b - p_c - \Sigma p_i) \quad (20)$$
$$\frac{p_c^2 dp_c}{2\varepsilon_c} \prod_i \frac{d^3 p_i}{(2\pi)^3 2\varepsilon_i} \left| f_l^{jc}(s,\dots) \right|^2,$$

where p_a, p_b and p_c are the momenta of the corresponding particles, p_i are the momenta of the particles of the system B_j, and $\varepsilon_c, \varepsilon_i$ are the time components of p_c and p_i. The differential cross section of the process (III) at a given θ, integrated over all other variables, reads

$$\frac{d\sigma_{inel}^{jc}}{d\cos\theta} = \frac{2\pi}{p^2} \sum_{l,l'} (2l+1)(2l'+1)\, P_l(\cos\theta) P_{l'}(\cos\theta)\, C_{ll'}^{jc}(s), \quad (21)$$

where

$$C^{jc}_{\ell\ell'}(s) = \frac{1}{2\pi}\,\frac{\sqrt{s}}{p}\int (2\pi)^4\delta^4(\;)\,\frac{p_c^2\,dp_c}{2\varepsilon_c}\prod_i\frac{d^3p_i}{(2\pi)^3 2\varepsilon_i}\;b^{jc}_{\ell}(s,\dots)\,b^{jc}_{\ell'}(s,\dots)^{*} \tag{22}$$

Due to the Schwartz inequality we can write

$$\left|C^{jc}_{\ell\ell'}(s)\right|^2 \le \eta^{jc}_{\ell}(s)\,\eta^{jc}_{\ell'}(s) \le \left|a_{\ell}(s)\right|\left|a_{\ell'}(s)\right| . \tag{23}$$

As a consequence of this inequality we have, on the basis of the relation (2), the exponential decrease of $C^{jc}_{\ell\ell'}$ in ℓ and ℓ'. By means of the arguments used above it is easy to derive inequality of the type (14) and (15) for $\frac{d\sigma^{jc}_{inel}}{d\cos\theta}$ (see [5])

$$\left.\frac{d\sigma^{jc}_{inel}}{d\cos\theta}\right|_{\theta=0} \le \text{const}\; s\ln^2 s\;\sigma^{jc}_{inel} , \tag{24}$$

$$\left.\frac{d\sigma^{jc}_{inel}}{d\cos\theta}\right|_{\theta\neq 0,\pi} \le \text{const}\,\frac{\sqrt{s}\ln s}{\sin\theta}\cdot\sigma^{jc}_{inel} . \tag{25}$$

Performing summation on the cross sections $\frac{d\sigma^{jc}_{inel}}{d\cos\theta}$ over all the possible system B_j we obtain the expression for the total cross section for the production of a particles "c" at a given angle θ

$$\frac{d\sigma^{c}_{inel}}{d\cos\theta} = \sum_j \frac{d\sigma^{jc}_{inel}}{d\cos\theta} .$$

Similar relations can be established also for these quantities

$$\left.\frac{d\sigma^{c}_{inel}}{d\omega\theta}\right|_{\theta=0} \leq \text{const}\; s\ln^2 s\;\sigma^{c}_{inel}\,, \tag{26}$$

$$\left.\frac{d\sigma^{c}_{inel}}{d\omega\theta}\right|_{\theta\neq 0,\pi} \leq \text{const}\;\frac{\sqrt{s}\ln s}{\sin\theta}\;\sigma^{c}_{inel}\,. \tag{27}$$

Similarly to (18) we introduce the notion of the width of the diffraction peak for the inelastic processes

$$\Delta^{jc}_{inel} = \frac{s\sigma^{jc}_{inel}}{d\sigma^{jc}_{inel}/d\omega\theta\big|_{\theta=0}}\,,\qquad \Delta^{c}_{inel} = \frac{s\sigma^{c}_{inel}}{d\sigma^{c}_{inel}/d\omega\theta\big|_{\theta=0}}\,. \tag{28}$$

Then, due to the relations (24) and (26), it follows that these widths can not decrease faster than $1/\ln^2 s$.

3. The exponential increase of the imaginary part of the amplitude of the elastic scattering at real $z > 1$.

We have in the foregoing sections established a number of relations assuming polynomial boundedness of the elastic scattering amplitude $F(s,z)$ for all finite z inside the ellipse E_c. Using the unitarity condiionwe can replace this assumption by a weaker one, the polynomial boundedness of $\mathrm{Im}\,F(s,z)$. If, at least, one of these inequalities is not fulfilled, it could mean that either $\mathrm{Im}\,F(s,z)$ is not analytical in z or it increases faster than any polynomial in this ellipse. We denote by $N(s)$ the maximum of the modulus of $\mathrm{Im}\,F(s,z)$ for any z inside E_c. It can easely be proved that $\mathrm{Im}\,F(s,z)$ reaches this maximum at $z=c$:

$$\mathrm{Im}\, F(s,c) = N(s) \,. \tag{29}$$

Again we assume $\mathrm{Im}\, F(s,z)$ to be analytical in E_c. Then, even in the case when only one of the established inequalities is broken this would mean that $N(s)$ at $s \to \infty$ increases faster then any polynomial. We show now that the study of the behaviour of the corresponding quantities (the cross-section or the width of the diffraction peak) enables us to guess the character of the increase of this function.

Indeed, by means of calculations used above we can, instead of the inequality (6), for example, derive relation

$$F(s,1) \leq \mathrm{const}\; s \ln^2 N(s) \tag{30}$$

where $N(s)$ is determined by (29). This gives

$$N(s) \geqslant \exp\left[\mathrm{const}\;\frac{|F(s,1)|}{s}\right]^{1/2} \sim \exp\left[\mathrm{const}\;\frac{1}{s}\;\frac{d\sigma_{el}}{d\cos\theta}\Big|_{\theta=0}\right]^{1/4} \tag{31}$$

which is a generalization of the inequality

$$N(s) \geqslant \exp\left[\mathrm{const}\;\sigma_{tot}\right]^{1/2}$$

obtained by Martin in a different way [2]. The following formulae can be derived analogously

$$N(s) \geqslant \exp\left[\mathrm{const}\;\frac{\sin\theta}{\sqrt{s}}\;\frac{d\sigma_{el}}{d\cos\theta}\Big|_{\theta\neq 0,\pi}\right]^{1/3}, \tag{32}$$

$$N(s) \geqslant \exp\left[\mathrm{const}\;\frac{1}{s\sigma_{el}}\;\frac{d\sigma_{el}}{d\cos\theta}\Big|_{\theta=0}\right]^{1/2}, \tag{33}$$

$$N(s) \geq \exp\left[\text{const}\ \frac{\sin\theta}{\sqrt{s}\,\sigma_{el}}\ \frac{d\sigma_{el}}{d\cos\theta}\Big|_{\theta\neq 0,\pi}\right], \tag{34}$$

$$N(s) \geq \exp\left[\text{const}\ \frac{1}{s}\ \frac{d\sigma_{inel}}{d\cos\theta}\Big|_{\theta=0}\right]^{1/4}, \tag{35}$$

$$N(s) \geq \exp\left[\text{const}\ \frac{\sin\theta}{\sqrt{s}}\ \frac{d\sigma_{inel}}{d\cos\theta}\Big|_{\theta\neq 0,\pi}\right]^{1/3}, \tag{36}$$

$$N(s) \geq \exp\left[\text{const}\ \frac{1}{s\sigma_{inel}}\ \frac{d\sigma_{inel}}{d\cos\theta}\Big|_{\theta=0}\right]^{1/2}, \tag{37}$$

$$N(s) \geq \exp\left[\text{const}\ \frac{\sin\theta}{\sqrt{s}\,\sigma_{inel}}\ \frac{d\sigma_{inel}}{d\cos\theta}\Big|_{\theta\neq 0,\pi}\right], \tag{38}$$

where σ_{inel} means either the cross section of a binary inelastic process, or the cross section of an inelastic process of multipole production.

4. Lower bound for the cross sections of inelastic processes

In this section we estiblish some lower bounds for the cross sections of inelastic processes of the type (III).

We write the differential cross section in the form

$$\frac{d\sigma^{jc}_{incl}}{d\cos\theta} \doteq \frac{\pi^2}{p\sqrt{s}}\, G^{jc}(s,\cos\theta) \tag{39}$$

where

$$G^{jc}(s,\cos\theta) = \int \delta^4\Big(p_a + p_b - p_c - \sum_i p_i\Big) \frac{p_c^2 dp_c}{2\varepsilon_c} \prod_i \frac{d^3p_i}{(2\pi)^3 2\varepsilon_i} \Big| T^{jc}(s,\cos\theta\ldots)\Big|^2. \tag{40}$$

We denote by $I_m F(s,\cos\theta)\Big|_{jc}$ the contribution to the imaginary part of the amplitude of the corresponding elastic process (1). Then we can write

$$I_m F(s,\cos\theta)\Big|_{jc} = \pi \int d\Omega_{p_c}\, H^{jc}(s,\cos\theta_1,\cos\theta_2), \tag{41}$$

where

$$H^{jc}(s,\cos\theta_1,\cos\theta_2) = \int \delta^4\Big(p_a + p_b - p_c - \sum p_i\Big) \frac{p_c^2 dp_c}{2\varepsilon_c} \prod \frac{d^3p_i}{(2\pi)^3 2\varepsilon_i} \tag{42}$$

$$T^{jc}(s,\cos\theta_1,\ldots)\, T^{jc}(s,\cos\theta_2,\ldots)^*.$$

θ_1 and θ_2 denote here the angles between the momenta of initial and final particles "a" and that of the intermediate particles "c". The total cross section is

$$\sigma^{jc}_{incl} = \int \frac{d\sigma^{jc}_{incl}}{d\cos\theta}\, d\cos\theta = \frac{1}{2p\sqrt{s}}\, I_m F(s,1)\Big|_{jc} \tag{43}$$

We remind that Martin has proved the analyticity in z of the imaginary part of the amplitude of the elastic scattering $F(s,z)$ inside the Mandelstam ellipse [1]. By the arguments similar to those in the preceeding section, it can be shown that $Im\, F(s,z)\Big|_{jc}$ is also an analytical function in this domain. The study of the analytic properties of the Feynman diagrams shows, however, that the contribution from some simplest diagrams of the perturbation theory to the amplitude $F(s,z)$ satisfies a dispersion relation in z for the values of s in the physical domain of the s-channel. This was the motivation for the assumption that $F(s,z)$ is analytic in the complex z plane with the cuts and poles on the real axis. It is quite natural to assume that $Im\, F(s,z)\Big|_{jc}$ for the values of s in the physical domain of the $s-$channel is also an analytic function in z in the complex plane with singularitites on the real axis. Let us assume that $Im\, F(s,z)\Big|_{jc}$ is polynomially bounded, i.e, an $n>0$ exists, such that

$$\left| Im\, F(s,z)\Big|_{jc} \right| \leq const\, s^n, \quad s \to \infty$$

for all z from any finite domain. Then a certain relation between the behaviour of this function at $z=1$ and their behaviour at $s \to \infty$ in the interval $-1 < z < 1$ can be established. Let us assume that the total cross section σ_{inel}^{jc} does not decrease faster than some power of $1/s$ at $s \to \infty$:

$$\left| Im\, F(s,1)\Big|_{jc} \right| > \frac{const}{s^m}, \quad s \to \infty$$

where m is some positive constant (see relation (43)).Then the following lower bound can be written[6]

$$\left| \mathrm{Im}\, F(s, \cos\theta) \right|_{jc} \geq \text{const}\; e^{-c(\theta)\sqrt{s}\ln s}, \quad s \to \infty, \quad (44)$$
$$c(\theta) > 0, \quad -1 < \cos\theta < 1 .$$

We show now that the inequality (44) will be broken at $\pi - 2\theta_0 < \theta < 2\theta_0$ if the following inequality holds for all θ in the interval $\pi - \theta_0 \leq \theta \leq \theta_0$ for some θ_0 satisfying $\frac{\pi}{4} > \theta_0 > 0$:

$$\left[G^{jc}(s, \cos\theta) \right]^{1/2} < \text{const}\; e^{-b(\theta)\sqrt{s}\ln s}, \quad s \to \infty, \quad (45)$$
$$b(\theta) > 0 .$$

Hence we conclude that there exists a certain interval of angles in which we have

$$\frac{d\sigma^{jc}_{inel}}{d\cos\theta} \geq \text{const}\; e^{-2b(\theta)\sqrt{s}\ln s}, \quad s \to \infty \quad (46)$$

To this end we consider the function $\Phi^{jc}(s, \cos\theta_1, \cos\theta_2)$. Comparing the expression (42) of this function with the expression (40) of $G^{jc}(s,\cos\theta)$ and using the Schwartz inequality we get

$$\left| \Phi^{jc}(s, \cos\theta_1, \cos\theta_2) \right| \leq \left[G^{jc}(s, \cos\theta_1)\, G^{jc}(s, \cos\theta_2) \right]^{1/2} .$$

Thus

$$\left| \mathrm{Im}\, F(s, \cos\theta) \right|_{jc} \leq \pi \int d\Omega_{pc} \left[G^{jc}(s, \cos\theta_1)\, G^{jc}(s, \cos\theta_2) \right]^{1/2} .$$

Now, assuming (45) it is easy to derive on the basis of the last relation an inequality reciprocal to (44). We have thus proved the lower bound (46).

We have introduced the notion of the total cross section $\frac{d\sigma^{c}_{inel}}{d\omega\theta}$ with the production of a particle "c" at a given angle θ. It is possible to write a similar inequality also for this quantity

$$\frac{d\sigma^{c}_{inel}}{d\omega\theta} \geq \text{const}\, e^{-2b(\theta)\sqrt{s}\ln s}, \quad s \to \infty, \quad (47)$$

$$b(\theta) > 0,$$

for the values of θ in a certain interval.

We point out that our assumption that the cross sections σ^{jc}_{inel} and σ^{c}_{inel} do not decrease faster than a certain power of 1/s can be also proved experimentally. In the framework of the Regge theory such a behaviour of the cross sections for zero angles is valid for the majority of processes.

5. Asymptotic equality of the cross sections of crossing processes of multipole production

We consider now the inelastic crossing processes

$$a + b \to a_1 + a_2 + \cdots + a_n + b', \qquad (IV_1)$$

$$\tilde{a} + b' \to \tilde{a}_1 + \tilde{a}_2 + \cdots + \tilde{a}_n + b. \qquad (IV_2)$$

We denote the momenta of particles "b" and "b'" in (IV_1) and those of particles "b'" and "b" in (IY_2) by p and p', the momenta of particles "a" and "a_i" (or those of their antiparticles by q and q_i . We put $k_i = \sum_{j=i}^{n} q_j$.

We can chose

$$s = -(p+q)^2, \quad t = -(p-p')^2, \tag{48}$$

$$W_i^2 = -k_i^2, \quad t_i = -(q-k_{i+1})^2, \quad \eta_i \equiv e^{2\xi_i} = \frac{q_i(p+p')}{k_{i+1}(p+p')}$$

as suitable independent invariant variables.

Let $T^{1,2}(s, t, W_i^2, t_i, \xi_i)$ be the amplitudes of the processes under consideration. These amplitudes for fixed values of the variables t, t_i, W_i^2, η_i, generally speaking, do not satisfy the dispersion relation in s . At $s \to \infty$, however, they tend to certain asymptotic amplitudes $T_\infty^{1,2}(s, t, W_i^2, t_i, \xi_i)$ analytic in s in the complex plane with cuts on the real axis [3]. The crossing-symmetry relation holds for these asymptotic amplitudes

$$T_\infty^1(u, t, W_i^2, t_i, \eta_i) = T_\infty^2(s, t, W_i^2, t_i, \eta_i)^* \tag{49}$$

where $s + u + t = m_a^2 + m_b^2 + m_{b'}^2 + W_1^2$.

From this relation, we can prove [7] that for non-oscillating amplitudes $T^{1,2}$ at $s \to \infty$ we have the asymptotic equality of the differential cross sections of the processes (IY_1) and (IY_2)

for the finite values of the variables t, W_i^2, t_i, η_i .

Let us consider the processes (IY_1) and (IY_2) at fixed values of t and W_1^2 . The physical domains of the variables W_i^2, $i \geq 2$ and t_i, η_i, $i \geq 1$ depend on s,t and W_1^2. However, these domains remain finite at $s \to \infty$. It means that at very high energies the domains of integration over the variables W_i^2, $i \geq 2$ and t_i, η_i, $i \geq 1$ are practically independent of s and the values of these variables are finite Both sides of the asymptotic equality for the differential cross sections of the processes (IY_1) and (IY_2) can therefore be integrated over all possible values of W_i^2, $i \geq 2$ and t_i, η_i, $i \geq 1$. As a result we have

$$\frac{\partial^2 \sigma_1}{\partial t \partial W_1^2} \sim \frac{\partial^2 \sigma_2}{\partial t \partial W_1^2} \quad , \tag{50}$$

where σ_1 and σ_2 are the cross sections of the processes (IY_1) and (IY_2). For fixed values of W_1^2 the number of possible systems $a_1 + \cdots + a_N$ is finite. We can therefore perform a summation in both sides of the relation (50) over all possible channels. As a result we obtain

$$\frac{\partial^2 \sigma (a + b \to \cdots + b')}{\partial t \partial W_1^2} \sim \frac{\partial^2 \sigma (\tilde{a} + b' \to \cdots + b)}{\partial t \partial W_1^2}, \tag{51}$$

$$s \to \infty .$$

The dots in the brackets denote the particle systems with the effective mass W_1 . We note that for the determination of the cross-sections appearing in the relation (41) it is sufficient to measure the momentum of one of the particles (particle "b" or particle "$\tilde{b}'$") since this allows the definition of t and W_1^2 (the mixing mass method). Because of the C-invariance the cross section of the process (IY_2) is equal to that of the process

$$a + \tilde{b}' \to q_1 + q_2 + \cdots + q_n + \tilde{b} \qquad (IY_3)$$

So we have besides the relation (51) another equation

$$\frac{\partial^2\sigma(a+b \to \cdots + b')}{\partial t\, \partial W_1^2} \sim \frac{\partial^2\sigma(a+\tilde{b}' \to \cdots + \tilde{b})}{\partial t\, \partial W_1^2} . \qquad (52)$$

Concluding this section, we present some concrete relations (see also ref. [8])

$$\frac{\partial^2\sigma(\pi^+ + p \to \cdots + p)}{\partial t\, \partial W_1^2} \sim \frac{\partial^2\sigma(\pi^- + p \to \cdots + p)}{\partial t\, \partial W_1^2}$$

$$\frac{\partial^2\sigma(\pi^+ + p \to \pi^+ + \cdots)}{\partial t\,\partial w_1^2} \sim \frac{\partial^2\sigma(\pi^- + p \to \pi^- + \cdots)}{\partial t\,\partial w_1^2},$$

$$\frac{\partial^2\sigma(\pi^+ + p \to K^+ + \cdots)}{\partial t\,\partial w_1^2} \sim \frac{\partial^2\sigma(K^- + p \to \pi^- + \cdots)}{\partial t\,\partial w_1^2},$$

$$\frac{\partial^2\sigma(p + p \to p + \cdots)}{\partial t\,\partial w_1^2} \sim \frac{\partial^2\sigma(\tilde{p} + p \to \tilde{p} + \cdots)}{\partial t\,\partial w_1^2},$$

$$\frac{\partial^2\sigma(p + p \to \cdots + p)}{\partial t\,\partial w_1^2} \sim \frac{\partial^2\sigma(\tilde{p} + p \to \cdots + p)}{\partial t\,\partial w_1^2}.$$

References:

1.A.Martin, Nuovo Cim. 42A, 930 (1966); 44A, 1219 (1966)
J.D.Bessis and V.Glaser, Nuovo Cim. 50A, 568 (1967).
G.Sommer, Nuovo Cim. 48, 92 (1967), 52A, 373 (1967).

2.M.Froissart, Phys.Rev. 123, 1053 (1961).
O.W.Greenberg, and F.E.Low, Phys.Rev. 124, 2047 (1961).
A.Martin, Phys.Rev. 129, 1432 (1961).

3.A.A.Logunov, Nguyen van Hieu, Lectures given at the international School on High Energy Physics, Tchekoslovakia,1967.
Preprint IFVE STF 67-62, 1967.

4.J.D.Besis, Nuovo Cim. 45, 974 (1966).

5.A.A.Logunov, M.A.Mestvirishvili, and Nguyen van Hieu,
Phys.Lett. 25B, 611 (1967).

6.F.Cerulus and A.Martin, Phys.Rev. 8, 80 (1964).

7.L.Van Hove, Phys.Lett. 5, 252 (1963).
A.A.Logunov, Nguyen van Hieu, and I.T.Todorov, Ann.Phys.
31, 203 (1965).

8.A.A.Logunov, Nguyen van Hieu, and I.T.Todorov,
Nucl.Phys. 67, 666 (1965).
Nguyen van Hieu, K.V.Rerich and A.A.Khelashvili, Nucl.Phys.
76, 551 (1966).

ON HIGH-ENERGY AND HIGH-MOMENTUM TRANSFER COLLISIONS OF HADRONS

Hans A. Kastrup

Sektion Physik
Universität München
München, Germany

1. INTRODUCTION

Hadron collisions with very large momentum transfers ($-t,-u \gg M^2_{nucleon}$) are generally considered to be of principal importance for two main reasons:

1.1. They are supposed to give information about the short-range properties of the various types of interactions, in contrast to reactions with small momentum transfers which test the long-range properties of the different forces.

1.2. Since unitary symmetries like SU_3 or $SU_3 \otimes SU_3$ etc. assume mass differences or even masses themselves to be negligible, there is a general belief that large momentum transfer collisions should provide an appropriate testing ground for unitary symmetries.

It is the purpose of the following remarks to give a short critical analysis of these two basic assumptions in the framework of a specific picture which implies a number of interesting experimental predictions.

2. THE MAIN ASSUMPTIONS

2.1. We consider energies (say $E_{lab} > 10$ GeV) where many collision channels are open so that a single channel, in particular the elastic one, is in general dominated by what is going on in all the other channels. This essential property is expressed by the unitarity of the S-matrix. It means that not only the elastic but also the inelastic collisions can give important in-

formation concerning our two basic interests in large momentum transfer reactions mentioned above.

2.2. In large momentum transfer reactions at very high energies there is a considerable rearrangement of the long-range parts of the hadronic fields (we neglect the electromagnetic field in the following) of the incoming primary particles (we always mean the c.m. system if not stated otherwise). This strong rearrangement is very probably accompanied by the emission of secondaries. Our second assumption then is that the main bulk of secondaries is a consequence of the rearrangement of the long-range parts of the hadronic fields.[1] This hypothesis is supported by the observation[2] that most (about 80 %) of the secondaries are pions. However, we do not know how many of these pions are decay products of resonances (e.g. vector mesons) which were produced in the first place.

E.W. Anderson et al. found[3] the π+-and π- -spectra in inelastic proton-proton collisions at 30 GeV to be almost the same for large pion c.m. scattering angles. This is an indication that the resonance contributions are relatively small, but the indication is inconclusive in so far as we do not know whether these pion spectra are associated with large or small momentum transfers of the primary protons. An experiment which determines the identity of secondaries in multi-particle final states as a function of the momentum transfer of the primary hadrons is very desirable!

The main conclusion to be drawn from the second assumption is that we will not get much information about the short-range properties of the hadronic fields if we are not able to subtract the dominant long-range effects. This was first pointed out by Wu and Yang[4].

2.3. In order to separate the long-range properties from the short-range ones we make the further assumption that all secondaries are "soft",i.e. their 4-momentum is

negligible. This hypothesis is supported by cosmic ray experiments[2], where the secondary pions seem to be soft in the c.m. system and where the existence of the "leading" particles which carry about 60 to 70 % of the initial energy seems to be well established.

However, one has to face the problem that most of the inelastic cosmic ray events very likely are not associated with large momentum transfers of the primary particles. This follows clearly from the proton spectra measured by E.W. Anderson et al.[3]. These experiments show that large momentum transfers of the primary protons are strongly suppressed and that the cross sections decrease with increasing momenta of the cutgoing protons for a fixed initial energy and for fixed large scattering angles.

There are at least two ways of bypassing these difficulties for our "softness"-assumption:

a) The large momentum transfer nucleon-nucleon collisions do not seem to be sensitive towards losses of longitudinal momentum of the primary particles, because the cross sections depend predominantly on the transverse momentum[3)5)]. For this reason it would already be enough for our approach if the collisions are quasielastic with respect to the transverse momentum of the primary particles alone[6]. This suggestion is supported by the results of L.G. Ratner et al. who observed[7] that the transverse momenta of the secondary pions spectra in inelastic proton-proton collisions at 12,5 GeV initial laboratory energy have a Gaussian distribution centered around $p_\perp = 0$.

The same does not seem to apply to the c.m. longitudinal momenta $p_{||}$ of the pions,[7] but the maximum of the $p_{||}$ -spectrum is around 0.5 GeV/c and the spectrum drops approximately exponentially with increasing $p_{||}$[3].

b) The second way out consists in dropping the "softness"-assumption for the phase space factor of the

secondaries but keeping it for the amplitude. Much of the structure of the inelastic spectra which conflicts with the softness-assumption seems to be accounted for by phase space corrections[8)-10)].

In the following we shall adopt the soft meson approximation in the sense of a), because it has simple but important consequences which can be tested by experiments. A comparison of its predictions with available data is quite encouraging. Since the details of this comparison have been discussed recently[11)], we shall emphasize the predictions for future experiments.

Neglecting momentum- spin- and unitary spin recoil, the cross section for the quasielastic scattering of the two primary hadrons accompanied by the emission of n soft mesons of the same type is given by[1)]

$$d\sigma^{(n)}/d\Omega = \bar{\sigma}(E,\theta)\, w_n(E,\theta), \qquad (1)$$

where E is the c. m. energy and $\theta \neq 0, \pi$ the c. m. scattering angle of the primary hadrons. The "potential" cross section $\bar{\sigma}$ (E, θ) is supposed to describe the short range interaction of the primary hadrons, independent of the long range properties of the hadronic fields which are supposed to account for the soft meson emission and which are characterized by the statistical Poisson factor

$$w_n = \exp[-\bar{n}(E,\theta)]\cdot[\bar{n}(E,\theta)]^n/n!\,,$$

where $\bar{n}$ (E, θ) is the average number of soft mesons as a function of E and θ.

The factorization of Eq. (1) into two factors is one of its most characteristic features which allows for a theoretical and experimental separation of long-and short-range effects.
We make the following hypothesis about the short-range interactions:

2.4. We assume the short-range interactions of the "bare" hadrons - i. e. without their long-range meson cloud - te be pointlike (no hard core, negligible rest masses and dimensionless coupling constants!) for large momentum transfers ($s, -t, -u \gg M^2_{nucleon}$). From this it follows that

$$\sigma(E,\theta) = E^{-2} A(\theta), \qquad (2)$$

because E is the only quantity left which can provide us with a dimension of length. In other words, we assume the short-range interactions of the nucleons to become invariant under dilatations at very high energies and large momentum transfers.[1)]

3. SOME EXPERIMENTAL PREDICTIONS

As I already mentioned before, a comparison of the model with available data of large angle elastic and inelastic nucleon-nucleon scattering is quite encouraging. In the following I want to make some remarks about predictions for future experiments.

3.1. Since the model assumes the inelastic reactions to be quasielastic, one should see whether there is a well-defined relation between the momenta $\vec{p}'_1$ and $\vec{p}'_2$ of the two outgoing primary particles in inelastic reactions. The best one can hope for is that these momenta are opposite equal in the c. m. system, even for large multiplicities. If this does not prove to be the case - which is likely - the model would still work (for the reasons given above) if only the transverse momenta (or some corresponding components of the momenta) of the outgoing primary particles are approximately opposite.

3.2. A very important new quantity associated with the model is the <u>differential multiplicity</u> $\bar{n}(E, \vec{p}'_1, \vec{p}'_2)$. According to the model this quantity should be a function of the energy and the scattering angle of the primary

nucleons, and this function should be approximately equal to the exponent appearing in the exponential of the empirical fits for elastic and inelastic large-angle scattering (s. Eq. (1))!
A measurement of $\bar{n}$ (E, $\vec{p}_1'$, $\vec{p}_2'$) is very desirable!

3.3. The recently discovered discontinuity[12) 13)] of the constant a in the exponent of Orear's fit implies a discontinuity of $d\bar{n}/dp_\perp$ (or $d\bar{n}/d$ ($E^2 \sin\theta$), depending on the variable one uses) in our picture. This means that there is a discontinuity in the rate of increase of $\bar{n}$. Exactly this happens when new channels become available as supposed by Allaby et al.[13)]. An experimental investigation of the inelastic channels in p-p collisions around 8-12 GeV lab. energies for θ between 60° and 90° would be very interesting.

3.4. In order to test whether the pions obey Poisson statistics one should analyse the r. m. s. fluctuations which are $\bar{n}^{1/2}$ for a Poisson distribution.

3.5. Summing Eq. (1) over n gives

$$(d\sigma^{tot}/d\Omega)(E,\theta) = E^{-2} A(\theta) \,. \qquad (3)$$

This is a definite prediction for the asymptotic energy dependence of the differential total cross section outside the diffraction peak in an energy region where all rest masses are negligible. The prediction (3) may be valid independent of the soft meson assumption, because all the special features of this hypothesis have dropped out after the summation.

The available experimental data in order to test Eq. (3) are scarce. E.W. Anderson et al. measured the quantity $d^2\sigma/d\Omega\, dp$ for $\theta = 29^\circ$ and $p \gg 1$ GeV/c at lab. energies of 10 and 30 GeV. A graphical numerical integration by hand of the corresponding curves in Fig. 1. of Ref.[8)] gives the values

$$d\sigma^{tot}(10\,GeV)/d\Omega = \int \frac{d^2\sigma}{d\Omega\, dp}\, dp \approx 3.0 \pm 0.5\ mb/sr$$

and

$$d\sigma^{tot}(30\,GeV)/d\Omega \approx 2.2 \pm 0.4\ mb/sr.$$

The errors are estimates.
From Eq. (3) we get the ratio 3:1 instead of 3:2.2. Although the data indeed indicate a slow decrease of $d\sigma^{tot}/d\Omega$ with increasing energy, a serious comparison of the data with Eq. (3) cannot be claimed for the following reasons:

a) At 10 GeV lab. energies we definitely cannot neglect rest masses of baryons in the c. m. system, but this has been assumed in Eq. (3).

b) The quantities $d^2\sigma/d\Omega\, dp$ have been measured only for $p \gtrsim 1$ GeV/c, although the maxima of the curves lie at this lower limit.

c) The angle $\theta = 29^\circ$ is rather small and leads to small momentum transfers, at least at 10 GeV.

The importance of Eq. (3) consists in its providing the possibility of probing the short-range properties of the interactions directly without dominating side effects which occur for large momentum transfer <u>elastic</u> scattering.

It is obvious that experiments which measure $d\sigma^{tot}/d\Omega$ in many collisions are very desirable!

3.6. Because of the assumption that $d\sigma^{tot}/d\Omega$ and not $d\sigma^{elast.}/d\Omega$ becomes mass independent for high energies and large momentum transfers, the differential <u>total</u> cross section seems to be the appropriate candidate for testing unitary symmetries[6]. In a soft meson model which neglects unitary spin recoil, too, the dominating factor $\exp[-\bar{n}(E,\theta)]$ of the two-body reactions becomes

a unitary spin invariant[6]. This implies a universal behaviour of large energy, large momentum transfer 2-body cross sections for all members of a unitary spin multiplet.

Again, the different unitary spin channels could be seen better by looking at the differential total cross sections. Details of this approach to the application of unitary symmetries to large momentum transfer collisions have been discussed in Ref.[6].

One last word concerning the drastical assumption of neglecting the unitary spin recoil associated with the meson emission: This approximation is probably quite bad for the emission of a single meson, but it might become better for high multiplicities, when statistical effects play a major role and when the recoil effects of a single emission may be averaged out.

I am indebted to Dr. G. Mack for many stimulating discussions.

FOOTNOTES AND REFERENCES

1) H.A. Kastrup, Phys. Rev. 147, 1130 (1966); references to earlier papers can be found here.

2) See, for instance, V.S. Barashenkov, V.M. Maltsev, I. Patera and V.D. Toneef, Fortschr. Physik 14, 357 (1966); V.S. Barashenkov and V.M. Maltsev, Fortschr. Physik 15, 435 (1967).

3) E.W. Anderson et al., Phys. Rev. Letters 19, 198 (1967).

4) T.T. Wu and C.N. Yang, Phys. Rev. 137, B 708 (1965).

5) J. Orear, Phys. Letters 13, 190 (1964).

6) H.A. Kastrup, Nuclear Phys. B1, 309 (1967).

7) L.G. Ratner et al., Phys. Rev. Letters 18, 1218 (1967).

8) E.W. Anderson and G.B. Collins, Phys. Rev. Letters 19, 198 (1967).

9) G. Bialkowski and R. Sosnowski, Phys. Letters 25 B, 519 (1967).

10) G. Mack, A Bremsstrahlung Model with Phase Space Corrections for Inelastic Proton-Proton Collisions, to be publ.

11) H.A. Kastrup, A Bremsstrahlung Model for High Energy Large Angle Scattering of Nucleons, paper presented at The Heidelberg International Conference on Elementary Particles 1967.

12) C.W. Akerlof et al., Phys. Rev. Letters 17, 1105 (1966).

13) J.V. Allaby et al., Phys. Letters 25 B, 156 (1967); see also J.J.J. Kokkedee and L. van Hove, Phys. Letters 25 B, 228 (1967).

MULTIPARTICLE PRODUCTION IN A SOFT PARTICLE EMISSION MODEL.

A.Giovannini and E.Predazzi,

Istituto di Fisica dell'Università and
Istituto Nazionale di Fisica Nucleare,
Torino, Italy .

In this paper, the main results obtained in the framework of a multi-soft-particle emission model [1] based on group-theoretical arguments are reviewed and extended . The limitations of the model are shortly discussed together with its possible generalizations currently under investigation.

The basic idea which is used in the approach of Ref. 1 is that in the scattering of high energy particles, in the limit when the masses and momenta of the emitted particles can be neglected, an arbitrary number of soft particles can be produced provided the total charge of the system be an invariant . It is assumed that only one kind of soft scalar particles exist (in the two possible states of charge + and -) with creation and destruction operators a_1^+, a_1 (charge +) and a_2^+ , a_2 (charge -). These operators obey the usual commutation rules of the boson calculus

$$(1) \qquad \left[a_i \ , \ a_j^+ \right] = \delta_{ij}$$

$$\left[a_i \ , \ a_j \right] = \left[a_i^+ \ , \ a_j^+ \right] = 0$$

and, using previous results [2,3], it has been shown that the imposition of charge invariance is sufficient to select the set of states which characterize the production of soft particles . By defining

$$(2) \qquad \left| k_1 \ , \ k_2 \ ; \ Q \ , \ N \right\rangle \equiv \left| k_1 \ , \ k_2 \right\rangle \otimes \left| Q \ , \ N \right\rangle$$

where $|k_1,k_2\rangle$ is the state describing the "elastic" transition (about which nothing can be said within the present formalism), and Q,N represent respectively the charge and number of soft particles produced , one easily proves [1] that the requirement that Q be invariant, singles out among all possible states, the set $|Q,N\rangle$ which forms the basis of the unitary irreducible representation of the discrete positive series of SU(1,1) . The charge Q is given in terms of the Casimir operator of SU(1,1) as

$$Q = 2\varkappa - 1 \qquad \varkappa = \tfrac{1}{2} , 1 , \ldots \tag{3}$$

whereas the number of particles is given in terms of the magnetic component m by

$$N = 2m - 1 \qquad m = \varkappa , \varkappa+1 , \ldots \tag{4}$$

As a consequence of the range of variation of $\varkappa$ and m, we find the following possible number of soft particles created

$$N_{fin} - N_{in} = 2 , 4 , \ldots . \tag{5}$$

corresponding to the obvious fact that whenever a soft particle of charge + (-) is created, another soft particle of charge - (+) must also be created to compensate its charge.

In terms of the creation operators previously introduced, we have the following explicit expression for the states Q,N

$$|Q,N\rangle = \left[\left(\frac{N+Q}{2} \right)! \left(\frac{N-Q}{2} \right)! \right]^{-\frac{1}{2}} (a_1^+)^{(N+Q)/2} (a_2^+)^{(N-Q)/2} |0\rangle \tag{6}$$

where $|0\rangle$ is the vacuum of soft particles .

Due to the particularly simple mathematical situation encountered here, one can also explicitely calculate the matrix elements for the transition from a given initial state to any permissible final state. This is so because of the explicit knowledge of the matrix elements of SU(1,1) as fun-

ctions of the generalized Euler angles[4]. The form of these transition matrix elements becomes particularly simple if we further assume that

$$(7) \qquad T(k,\theta) = \langle k_1' , k_2' \mid T \mid k_1 , k_2 \rangle$$

which is still an operator in the Q,N space (and whose vacuum expectation value in this space describes the elastic scattering), transforms like an element[5] of SU(1,1) . In this case , there exists a mapping of the form

$$(8) \qquad T(k,\theta) \longrightarrow T_g(\gamma)$$

where $T_g(\gamma)$ is the unitary irreducible representatio $D^{+\varkappa}$ of an element g of SU(1,1) . In so doing , an "a priori" undetermined function $\gamma(k,\theta)$ is introduced .

An immediate consequence of the model is that all production processes of soft particles can be expressed in terms of the elastic amplitude and, in the case $N_{in}=Q=0, N_{fin}=N$, we have

$$(9) \quad \langle N|T(k,\theta)|0\rangle = \langle 0|T(k,\theta)|0\rangle\, e^{-iN\mu/2} \left(1-\frac{2}{\gamma+1}\right)^{N/2}, \qquad \begin{matrix}(-1\le\mu\le 1)\\ (N=0,2,..)\end{matrix}$$

Eq.(9) is the clue to correlate different processes and can be exploited to phenomenologically determine $\gamma(k,\theta)$.

In Ref. 1 arguments have been given to support the conclusion that

$$(10) \qquad \begin{matrix}\gamma(k,\theta) \underset{k\to 0}{\longrightarrow} 1\\ \gamma(k,\theta) \underset{k\to\infty}{\longrightarrow} \infty\end{matrix}$$

From Eqs.(9,10b) it then follows

$$(11) \qquad \lim_{N\to\infty} \left| \frac{\langle N \mid T(k,\theta) \mid 0\rangle}{\langle 0 \mid T(k,\theta) \mid 0\rangle} \right| = \exp -\left(\frac{N}{\gamma(k,\theta)+1}\right) \longrightarrow 0 \ .$$

The above result is very reasonable in that it shows that inelastic processes are depressed compared to the elastic one . The knowledge of the rate at which inelastic processes are depressed,would in principle be useful to fix $\gamma(k,\theta)$. In Ref.1 this problem has been considered in the simplified case in which the angular dependence is supposed factorizable in the high energy limit and integrated over in order to calculate the multeplicity of soft particles produced . The result in the general case is given by

$$(12) \qquad \bar{N}(n,Q;\gamma) = 2 \sum_{n=1}^{\infty} n\, P^{Q}_{N'N}(\gamma) \Big/ \sum_{n=0}^{\infty} P^{Q}_{N'N}(\gamma)$$

where

$$(13) \qquad n = (N'-N)/2 \qquad\qquad n=0,1,2,\ldots$$

and $P^{Q}_{N'N}(\gamma)$ are the emission probabilities for a transition $(Q,N) \rightarrow (Q,N')$ which turn out to be given in general by

$$P^{Q}_{N'N}(\gamma) = (\sinh\xi \cosh\xi)^{-(N+1)} \; (\tanh\xi)^{N'+1}$$

$$(14) \qquad \frac{\Gamma(1+\frac{N'-Q}{2})\;\Gamma(1+\frac{N'+Q}{2})}{\Gamma(1+\frac{N-Q}{2})\;\Gamma(1+\frac{N+Q}{2})} \; \frac{1}{\Gamma^{2}(1+\frac{N'-N}{2})}$$

$$\cdot\; {}_2F_1^2\left(-\frac{N-Q}{2}, -\frac{N+Q}{2}; 1+\frac{N'-N}{2}; -\sinh^2\xi\right),$$

where,without any restriction we have assumed N' N and

$$\sinh^2\xi = \tfrac{1}{2}(\gamma - 1)$$
$$\cosh^2\xi = \tfrac{1}{2}(\gamma + 1) .$$

In the case N=Q=0 , Eq.(12) gives

$$(15) \qquad \bar{N}(\gamma) = \gamma(k) - 1$$

which implies that

$$(16) \qquad \gamma(k) \underset{k\to\infty}{\longrightarrow} \infty .$$

We can now show that under the same hypothesis of factorizability , the use of the optical theorem enables us to conjecture that the maximum growth of $\gamma(k)$ with k is of a logarithmic nature and that this is consistent with a Regge like behavior for the elastic scattering amplitude at high energies . We define

$$(17) \qquad \left(\frac{d\sigma}{dt}\right)_{el} = \left|\langle 0 \mid T(k,\theta) \mid 0\rangle\right|^2 .$$

The optical theorem

$$(18) \qquad \sigma_{tot} = \frac{4\pi}{k} \operatorname{Im} f(k,0)$$

together with

$$(19) \qquad \sigma_{tot} = \frac{k^2}{\pi} \sum_{n=0}^{\infty} \int d\Omega \left|\langle n \mid T(k,\theta) \mid 0\rangle\right|^2$$

and using Eq.(9) (in which we set N=2n) becomes

$$(20) \qquad \operatorname{Im}\langle 0|T(k,0)|0\rangle = \frac{1}{4\sqrt{\pi}} \int_{t_<}^{t_>} dt \left|\langle 0|T(k,\theta)|0\rangle\right|^2 (\gamma(k,\theta)+1)$$

where $t=-2k^2(1-\cos\theta)$. We now assume that in the high energy limit

$$(21) \qquad \langle 0 \mid T(k,\theta) \mid 0\rangle \underset{\substack{k\to\infty \\ \theta\to 0}}{\sim} (i A + B)\, e^{bt}$$

where

$$(22) \qquad \begin{cases} \lim\limits_{k\to\infty} A = \text{constant} \\ \lim\limits_{k\to\infty} B = 0 \end{cases}$$

and

$$(23) \qquad \lim_{k\to\infty} \gamma(k,\theta) = \gamma(k) .$$

Notice that Eq.(22a) is the statement that total cross sections become asymptotically constant whereas Eq.(22b) takes account the predominantly imaginary character of elastic

scattering amplitudes at high energies . With the above assumptions , Eq.(20) gives

$$A \underset{k\to\infty}{\simeq} \frac{A^2+B^2}{4\sqrt{\pi}} (\gamma(k)+1) \int_{-4k^2}^{0} dt\ e^{2bt}$$

or

$$\lim_{k\to\infty} \frac{A^2+B^2}{4A\sqrt{\pi}} \frac{\gamma(k)+1}{2b} = 1 . \tag{24}$$

Eqs. (24) and (22) can be reconciled only if

$$\lim_{k\to\infty} b = \frac{A}{8\sqrt{\pi}} (\gamma(k)+1) \tag{25}$$

which implies that the slope b in Eq.(21) must increse like $\gamma(k)$ with energy . On the other hand the only permissible rate of growth for the slope of the forward elastic amplitude is, on phenomenological grounds , the one predicted by the Regge pole theory[6] which gives a logarithmic variation of b with energy and since we already know from Eq.(15) that $\gamma(k)$ must grow with energy , we finally conclude that a Regge-like behavior for the elastic amplitude is the only high energy behavior compatible with the present model and that

$$\lim_{k\to\infty} \gamma(k) = \ln(k/k_o) \qquad (k_o = \text{const.}). \tag{26}$$

It is amusing to note that if Eq.(26) holds , the law of multiple production (15) in the present model is the same as predicted by the multiperipheral model of Amati et al.[7] .

Having thus quickly summarized the main lines of the present approach together with some of the results , a few comments are now in order .

The major limitations of the model are :

i) The soft nature of the emitted particles ;

ii) The limited number of species of particles allowed in the game.

As far as point ii) is concerned,we are trying to generalize the above considerations to include more kinds of different particles. The only problem,in this context,appears to be of mathematical nature,namely,the matrix elements of SU(n,1) are presently not available,at our knowledge , as functions of the generalized Euler angles . Point i) ,on the other hand,seems to really be the crucial assumption which allows us the complete analytical solution of the problem at hand and we are therefore inclined to believe that the soft nature limitation will not be easily removed. Work is presently in progress to extend the model (along the line in ii)) as well as to investigate in detail its implications on the various quantities that can be calculated in its present form.

To conclude,we wish to emphasize that the present approach represents an attempt to apply group-theoretical methods to investigate elementary particle physics in a rather different spirit than it is usually done.It differs from the various SU(n) models in that it attempts a direct classification of amplitudes rather than of particles.It differs on the other hand from the various expansions in partial waves or à la Toller[8] in that instead of using invariance properties specific of a given amplitude,we try to enforce general conservation laws and this allows us to connect among themselves several processes.Finally,we should like to mention that non-compact groups have been applied recently to the exploration of the dynamics of strongly interacting systems in a number of other interesting ways [9,10,11] and their use in this context is certainly worth further investigation .

REFERENCES AND FOOTNOTES.

(1) A.Giovannini and E.Predazzi : Nuovo Cimento 52A 255 (1967) .

(2) J.Schwinger in "Quantum Theory of Angular Momentum" edited by L.C.Biedenharn and H.Van Dam - Academic Press New York 1965 , p. 229 .

(3) L.C.Biedenharn and W.J.Holman:Ann.of Phys. 39 1 (1966).

(4) V.Bargmann : Ann. of Math. 48 568 (1947) .

(5) This assumption is probably too restrictive , although $T(k,\Theta)$ can certainly be represented as a superposition of elements of SU(1,1) . Great simplification is , however , obtained under the above assumption.

(6) The only other alternative being a constant slope as in an optical model approach .

(7) D.Amati,S.Fubini and A.Stanghellini : Nuovo Cimento 26 896 (1962) .

(8) See for instance M.Toller , CERN report Th. 780 (1967), to be published in the Nuovo Cimento.

(9) Y.Nambu : Phys.Rev. 160 1171 (1967) .

(10) A.O.Barut : Phys.Rev. 156 1538 (1967) ; A.O.Barut and H.Kleinert : Phys.Rev. 156 1546 (1967) .

(11) G.Cocho, C.Fronsdal , I.T.Grodsky and R.White : Phys.Rev. 162 1662 (1967) .

ON TOTAL CROSS-SECTIONS IN THE MULTI REGGE MODEL

J. Finkelstein *) and K. Kajantie **)
CERN
Geneva, Switzerland

In this note we report some results on integrated cross-sections in the multi Regge model (MRM) [1)-6)]. Details and proofs will be presented elsewhere [7)].

1. The matrix element for the process $p_a+p_b \to p_1+\ldots+p_n$ is given, in the MRM in our parametrization, by

$$|M_n|^2 = g^2 \prod_{i=1}^{n-1} e^{2(a_i+\alpha_i' \ln s_i/s_0)t_i} \left(\frac{s_i}{s_0}\right)^{2\alpha_i} \qquad (1)$$

where g is a product of coupling constants, the a_i's are diffractive parameters, the α_i's and α_i''s are the intercepts and slopes of trajectories exchanged, and $s_i = (p_i+p_{i+1})^2$, $t_i = (p_a-p_1-\ldots-p_i)^2$. This matrix element is valid in the region of the phase space where the s_i's are large and the t_i's small. The condition that the t_i's be small implies that $s_1 \ldots s_{n-1} \approx \mu^{n-2} s$ where μ is a new parameter. Using the variables introduced by Bali, Chew and Pignotti [4)], we can write, taking $\alpha_i = \alpha$, $\alpha_i' = \alpha'$, $a_i = a$,

---

*) NATO Postdoctoral Fellow.

**) On leave from the Department of Nuclear Physics, University of Helsinki, Finland.

$$\sigma_n(s) = \frac{1}{s^2}\int_0^\infty dx_1 \cdots dx_{n-1} \int_{-\infty}^{0} dt_1 \cdots dt_{n-1} \int_0^{2\pi} d\omega_2 \cdots d\omega_{n-1}\, \delta\left(x_1 + \cdots + x_{n-1} - \ln \frac{s\mu^{n-2}}{s_0}\right) |M_n|^2$$

$$= A B^{n-2} \left(\frac{s}{s_0}\right)^{2\alpha-2} I_n\left(\frac{\alpha'}{a} \ln \frac{s\mu^{n-2}}{s_0}\right) , \tag{2}$$

where A and B are parameters, $x_i = \ln(s_i/s_0)$,

$$I_n\left(\frac{\alpha'}{a} \ln \frac{s\mu^{n-2}}{s_0}\right) = \int_0^\infty du_1 \cdots du_{n-1} \frac{1}{1+u_1} \cdots \frac{1}{1+u_{n-1}}\, \delta\left(u_1 + \cdots + u_{n-1} - \frac{\alpha'}{a} \ln \frac{s\mu^{n-2}}{s_0}\right) . \tag{3}$$

2. From Eq. (2) one finds the following lower bound for $\sigma_n(s)$:

$$\sigma_n(s) \geq \frac{A}{a} \left(\frac{s}{s_0}\right)^{2\alpha-2} \frac{1}{1+\frac{\alpha'}{a}\ln\frac{s}{s_0}} \left[\frac{B}{\alpha'} \ln\left(1 + \frac{\alpha'}{(n-2)a} \ln \frac{s\mu^{n-2}}{s_0}\right)\right]^{n-2} \tag{4}$$

Letting n and $\ln(s/s_0)$ go to infinity together but staying always within the limits of validity of the model, this lower bound is sufficient to show that, if $\alpha = 1$, the contribution of the MRM to the total cross-section, i.e., to $\sigma_n(s)$ summed over all appropriate n, increases like some power of s as $s \to \infty$. This means that repeated Pomeranchuk exchange will, for sufficiently large s, violate unitarity. On the other hand, if $\alpha < 1$, then for sufficiently small values of B, this trouble does not arise. A possible explanation for this is that the effects of the cuts must be included together with the Pomeranchuk trajectory, while they can be neglected for trajectories with $\alpha < 1$.

3. Although the integrals I_n cannot be done in closed form, a very good approximation to them can be obtained by using the methods of Ref. [8]. One finds

$$I_{n+1}(c) = \frac{e^{\beta c}}{\left[\beta\left(1+\frac{c}{n}\right)\right]^n} \cdot \frac{1}{\sqrt{2\pi(c+n)\left(\frac{1}{\beta}-\frac{c}{n}\right)}} \tag{5}$$

where $\beta = \beta(c/n)$ is the unique solution of

$$\beta \int_0^\infty du \frac{e^{-\beta u}}{1+u} = \frac{n}{c+n} \tag{6}$$

Eq. (5) becomes correct for large n; however, even for $n = 3$ it is correct to within a few per cent.

4. From Eqs. (5) and (6), one can see that I_n as a function of n has a maximum at about $n = (\alpha'/a)\ln(s/s_0)$. Physically, the reason is as follows : the average value of the subenergies is roughly $\langle \ln(s_i/s_0) \rangle \approx \ln(s/s_0)/n$. Hence, for fixed large s and small n the subenergies are large and I_n small since the peaks in t_i are shrunk. As n increases, shrinkage becomes less important, but eventually one runs out of phase space. The maximum value of I_n occurs at the boundary between the shrinkage and phase space regions; since the peak in t_i is given by $\exp\left[(a+\alpha'\ln(s_i/s_0))t_i\right]$ this boundary is roughly at $n \approx (\alpha'/a)\ln(s/s_0)$.

5. The simplest cases to which these results could be applied are those for which, as n increases, one just adds more vertices of the type already present. An example of this is $K^- p \to (n\pi)Y$, where

Y is a Λ or a Σ^0 or a Σ^+, constrained to emerge from the proton vertex; then in the limit of exchange degeneracy only the K^* trajectory can be exchanged. Some other examples are $\pi^+ p \to K^+ Y(n\pi)$, $p\bar{p} \to (n\pi)$, $p\bar{p} \to Y\bar{Y}(n\pi)$, and $K^- p \to (n\rho^0)Y$.

REFERENCES

1) K.A. Ter-Martirosyan, Soviet Phys. - JETP 17, 233 (1963), Nuclear Phys. 68, 591 (1965).

2) Chan Hong-Mo, K. Kajantie and G. Ranft, Nuovo Cimento 49, 157 (1967).

3) F. Zachariasen and G. Zweig, Phys.Rev. 160, 1322, 1326 (1967).

4) N.F. Bali, G.F. Chew and A. Pignotti, Phys.Rev. 163, 1572 (1967).

5) N.F. Bali, G.F. Chew and A. Pignotti, Phys.Rev.Letters 19, 614 (1967).

6) K. Kajantie, Nuovo Cimento 53, 424 (1968).

7) J. Finkelstein and K. Kajantie, CERN preprint TH.857, to be published in Nuovo Cimento; and, Phys.Letters 26B, 305 (1968).

8) A.I. Khinchin, Mathematical Foundations of Statistical Mechanics, Dover (1949);
F. Lurçat and P. Mazur, Nuovo Cimento 31, 140 (1964).

EXPERIMENTAL EVIDENCE FOR MULTIPERIPHERALISM

G. Zweig *)

Department of Physics
University of Wisconsin
MADISON, Wisconsin
U.S.A.

We would like to present preliminary experimental evidence for the existence of multiperipheral processes [1]. The reaction to be considered is $\pi^- + p \to \pi^- + \pi^- + \pi^+ + p$ at incident π^- momentum of 25 GeV/c. The data was obtained at the 80" BNL chamber by the University of Wisconsin. The analysis to be presented was performed by William Robertson and the author.

Although there are four particles in the final state, we will try to pick a class of event which may be analyzed as if there were only three. That is, we select events where the invariant mass of the π^+ and the slow π^- (slow in the laboratory) is small :

$$(\pi^+ + \pi_s^-)^2 \equiv S_{\pi^+\pi_s^-} < 2\ GeV^2$$

We then consider the $\pi^+\pi_s^-$ system as a single object or cluster called X and look for the existence of the multiperipheral production process

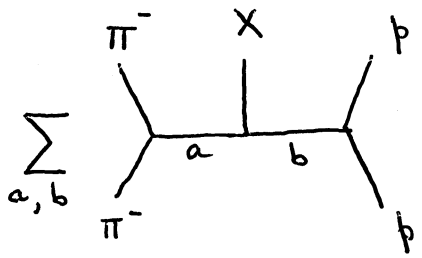

*) Sloan Foundation Fellow, on leave of absence from Caltech, Pasadena, California, U.S.A.

where a and b represent possible exchanges. Note that at fixed incident π^- energy, the reaction depends on four variables; the momentum transfers to the π^- and p, t_π and t_p; and the invariant masses $S_{\pi X}$ and S_{Xp}.

The most characteristic feature to be expected of this sum of multiperipheral diagrams is a strong peaking at <u>simultaneously</u> small values of the two momentum transfers. To isolate this effect, we remove the resonance background by selecting events which satisfy

$$S_{\pi x} > 2\ GeV^2, \quad S_{xp} > 4\ GeV^2, \quad S_{\pi p} > 4\ GeV^2$$

i.e., we work in the triangular region of the Dalitz plot as shown in Fig. 1 :

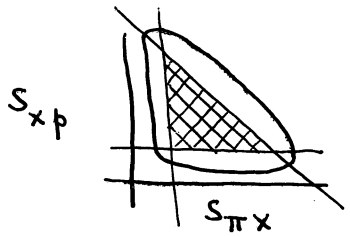

Fig. 1

We further require that the π^+ contained in X and the fast π^- do not form a ρ or f and that the π^+ and p do not form a $\Delta(1238)$. Finally, since we demand identification of the proton by ionization in the bubble chamber, we consider only events with $t_p < 0.8\ GeV^2$.

The events which remain are now exhibited on a $t_\pi - t_p$ scatterplot (Fig.2)[2]. In spite of the fact that phase space inhibits the appearance of events in the corner of this plot, a strong peaking ($\sim$ 70 events) is observed there. To our knowledge, this is the first time that simultaneous peaking in two momentum transfers has been observed, a result which indicates the existence of multiperipheral processes.

In order to investigate the form of the amplitude in the multiperipheral region, we have divided the number of events in each square of the $t_\pi - t_p$ plot by phase space and projected the result on the

t_{π} and t_p axes. The generated curves are shown in Figs. 3 and 4 and indicate that the multiperipheral amplitude may be crudely represented in the form $e^{t_p/\tau_p + t_{\pi}/\tau_{\pi}}$ where τ_p and τ_{π} have values characteristic of ordinary two-body peripheral processes.

We are now in the process of analyzing the complete functional dependence of the multiperipheral events on the t_p, t_{π}, $S_{\pi X}$ and S_{Xp} variables.

REFERENCES

1) D. Amati, A. Stanghellini and S. Fubini, Nuovo Cimento 26, 896 (1962);

S.C. Frautschi, Nuovo Cimento 28, 409 (1963);

F. Zachariasen and G. Zweig, Phys.Rev. 160, 1322 and 1326 (1967).

2) The numbers shown in Fig. 2 indicate the number of events observed in the corresponding region of the $t_{\pi}-t_p$ plot.

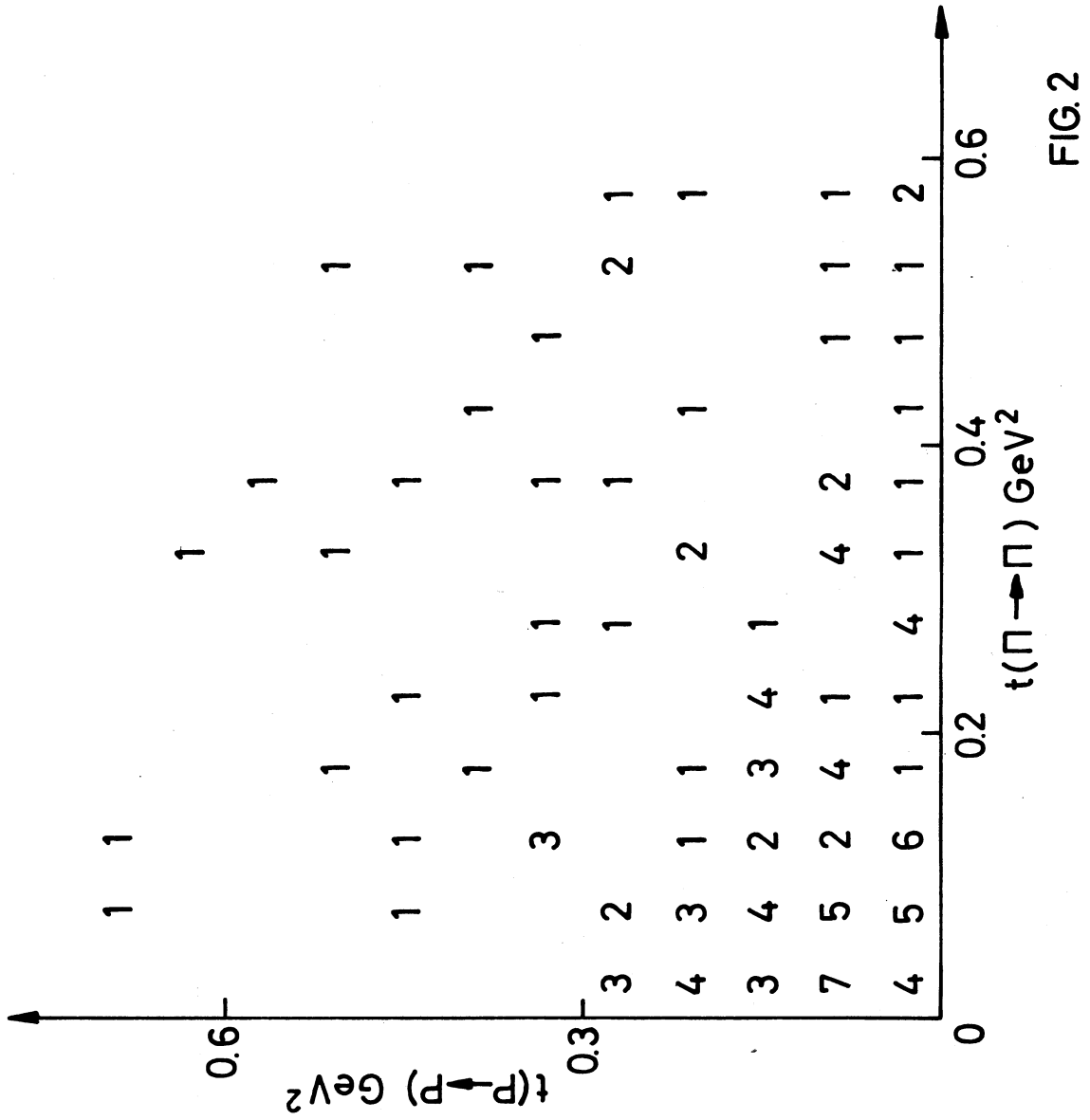

FIG. 2

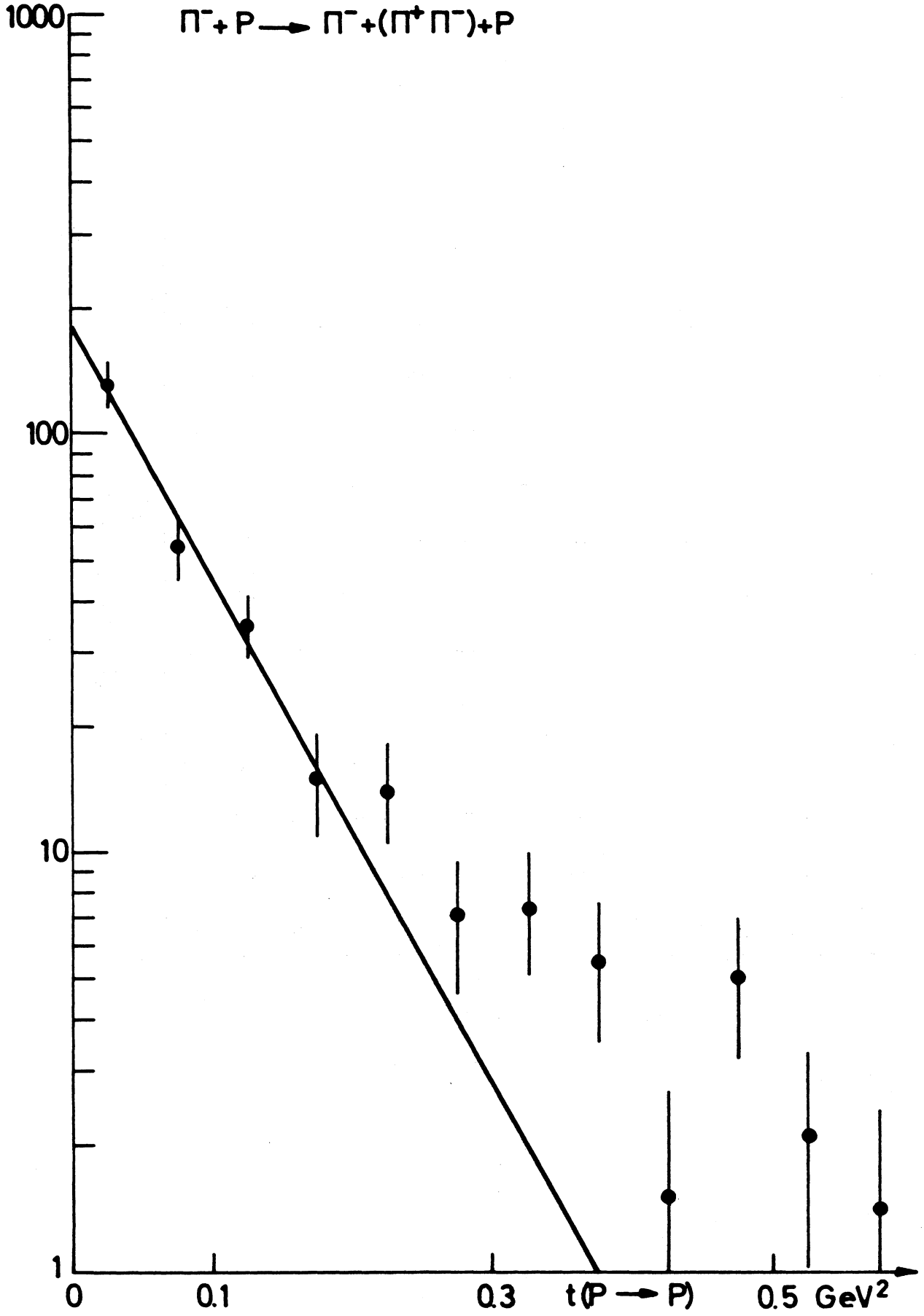

FIG. 3

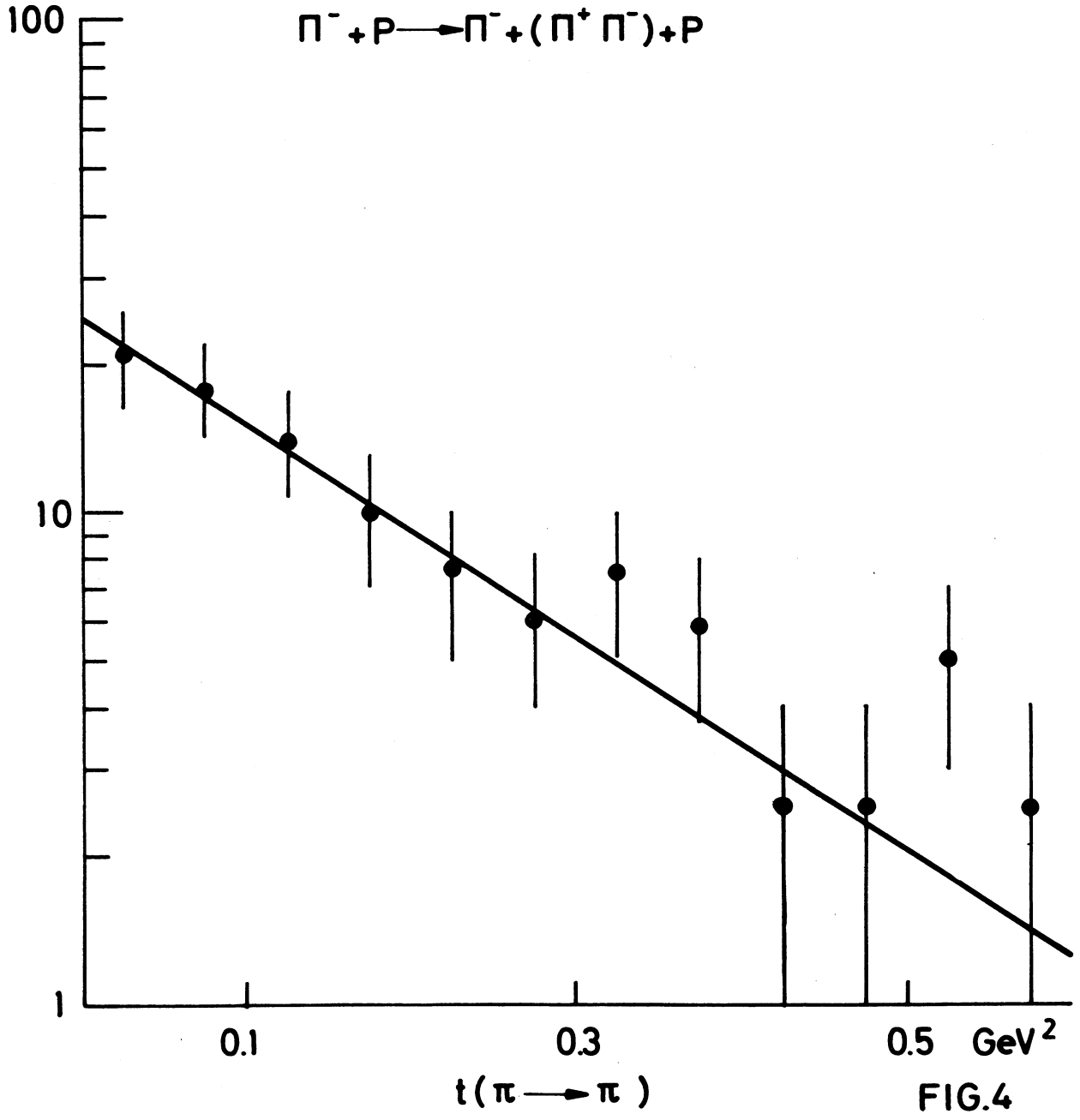
100
10
1
$\pi^- + P \longrightarrow \pi^- + (\pi^+ \pi^-) + P$
0.1
0.3
0.5 GeV^2
$t(\pi \longrightarrow \pi)$

FIG.4

TWO-BODY FINAL STATES PRODUCED IN K^+-PROTON INTERACTIONS AT 10 GeV/c

Birmingham-Glasgow-Oxford Collaboration.

1. INTRODUCTION

The two-body reactions

$$K^+ p \rightarrow p K^{*+} \quad \text{1a}$$

$$K^+ p \rightarrow p K^{*+}(1420) \quad \text{1b}$$

$$K^+ p \rightarrow K^0 N^{*++} \quad \text{1c}$$

and

$$K^+ p \rightarrow K^{*0} N^{*++} \quad \text{1d}$$

have been studied at an incident momentum of 10 GeV/C using 200,000 pictures from the CERN 2-metre hydrogen bubble chamber exposed to a radio-frequency separated beam. (Here K^* refers to the $K^*(890)$ and N^{*++} to the $N^{*++}(1238)$). Previous work on reactions 1a, 1c and 1d at 3.0, 3.5 and 5 GeV/C incident K^+ momenta [1] has shown that the total cross-sections for these reactions fall sharply with increasing beam momentum and provided some evidence that the differential cross sections shrink as the energy increases. The K^* and N^* decay correlations observed are consistent with those expected for vector meson exchange in 1a and 1c and for pseudoscalar exchange in 1d. [2] This note extends the results for these reactions to 10 GeV/C and also gives results for reaction 1b at this beam momentum.

2. SELECTION OF EVENTS

The quasi-two-body final states 1a, 1b and 1c were selected from events fitting the hypothesis

$$K^+ p \rightarrow K^0 \pi^+ p \qquad \text{(278 events)} \quad \text{2.}$$

The Dalitz plot for this channel is shown in Figure 1 and the distributions in M ($K^o\pi^+$) and M(π^+p) in Figure 2. These distributions show that the two-body final states pK^* and K^oN^{*++} occur with negligible background and represent respectively (40 $\pm$ 5)% and (20 $\pm$ 4)% of channel 2. In addition the $K^o\pi^+$ effective mass plot shows a clear $K^*(1420)$† signal, again with a very low background, amounting to (18 $\pm$ 4)% of the total number of events.

Reaction 1d was studied using events fitting

$$K^+p \rightarrow K^o\pi^+p\pi^o \qquad \text{(1189 events)} \qquad \text{3.}$$

Evidence for the presence of this reaction is given in Figure 3 which shows a triangle plot of M($K^o\pi^o$) versus M(π^+p) for the channel. There are well-defined K^{*o} and N^{*++} bands with an excess of 22 $\pm$ 10 events in the overlap region above the number expected by comparison with adjacent areas of the bands. The analysis of this channel is complicated by the presence of enhancements in effective mass distributions other than those contributing to the $K^{*o}N^{*++}$ final states (e.g. in M($K^o\pi^+$), M($\pi^+\pi^o$), M(π^op) and M($K^o\pi^o\pi^+$)). In view of this complexity and the small number of genuine $K^{*o}N^{*++}$ events it has not been possible to do anything more than quote a cross-section for this reaction.

3. Cross-sections

Preliminary values of the cross-sections for the two-body reactions considered are given in Table 1 together with the

† The fitted mass is (1424 $\pm$ 10) MeV/c^2 and the width is (110 $\pm$ 30) MeV/c^2.

overall channel cross sections. These cross-sections were determined both by a τ count and by normalising the the total number of events found in a portion of the film to a total K^+p cross-section of (17.3 ± 0.1) mb at 10 GeV/c.[3] The uncertainties quoted in Table 3 include estimates for possible systematic effects in the selection of events and in the normalisation. The variation of the cross-sections with energy is shown in Figure 4 where ln.σ is plotted versus ln. p for each of the reactions in question. In each case the straight line shown was obtained from a least squares fit to the data of the expression

Table 1 - Reaction Cross-sections

Final State	σ
$K^o\pi^+p$	$215 \pm 40\,\mu b$
(1a) pK^{*+}	85 ± 20
(1b) $pK^{*+}(1420)$	39 ± 15
(1c) K^oN^{*++}	43 ± 15
$K^o\pi^+p\pi^o$	860 ± 160
(1d) $K^{*o}N^{*++}$	16 ± 9

$K^{*+} \to K^o\pi^+$; $K^{*o} \to K^o\pi^o$

$$\sigma = K\, p^{-n} \qquad (4),$$

previously used by Morrison,[4] where p is the beam momentum and K is a constant. The reactions $K^+p \to pK^*$ and $K^+p \to K^oN^{*++}$ give good fits, but the cross sections for $K^+p \to K^{*o}N^{*++}$ are widely scattered about the straight line. The values of n obtained are given in Table 2. For reactions 1a and 1c $n = 1.9 \pm .2$ and $n = 2.3 \pm 0.3$, respectively, in disagreement with the value $n = 1$ expected from simple Regge-pole models based on ρ-exchange[5] and on ρ and A_2 exchange for reaction 1c.[6] For 1d, n is 1.6 ± 0.2 indicating a very much steeper fall off with increasing energy than found for the analogous reaction $\pi^+p \to \rho^oN^{*++}$, where $n \simeq 0.5$.[7] The only

Table 2 Values of n in $\sigma = Kp^{-n}$

Final State	n
(1a) pK^{*+}	1.9 ± 0.2
(1c) K^oN^{*++}	2.3 ± 0.3
(1d) $K^{*o}N^{*++}$	1.6 ± 0.2

published result for reaction 1b at lower energies is at 3.5 GeV/c [2] but the value found is uncertain because of interference between $K^o N^{*++}$ and $p K^{*+}$ (1420) final states.

4. t distributions

Figure 5 shows the distributions of $\ln d\sigma/d|t|$ versus -t, the four-momentum transfer squared, for 1a, 1b and 1c with fitted lines of the form

$$d\sigma/d|t| = Ae^{bt} \qquad 5,$$

where A and b are constants. In reaction 1a the point at the smallest $|t|$ value has not been used in the fit. The low value observed here cannot be due to experimental biases since recoil protons with lab momenta as low as 0.1 GeV/c, corresponding to $-t = 0.01(GeV/c)^2$ can be detected with certainty for the two prong plus V^o events studied. The values of b obtained from the fits are given in Table 3 for the -t intervals specified together with the results from [1].

Table 3 Values of b for $d\sigma/d|t| = Ae^{bt}$

Reaction	Momentum	-t interval	b
(1a) $K^+ p \to p K^{*+}$	3.0	0.05-1.00	3.6 ± 0.4
	3.5	"	3.2 ± 0.3
	5.0	"	4.2 ± 1.1
	10.0	0.10-1.00	3.7 ± 0.5
(1b) $K^+ p \to p K^{*+}$ (1420)	10.0	0-1.00	1.5 ± 0.4
(1c) $K^+ p \to K^o N^{*++}$	3.0	0.05-1.00	3.2 ± 0.6
	3.5	"	3.5 ± 0.5
	5.0	"	4.1 ± 0.7
	10.0	"	4.6 ± 1.1

There is no evidence for shrinkage in $K^+ p \to p K^{*+}$ but the differential cross-section does appear to shrink for the reaction $K^+ p \to K^o N^{*++}$. $d\sigma/d|t|$ for $K^*(1420)$ production is considerably less forward peaked than for either of the other reactions, having $b = 1.5 \pm 0.4$. At 3.5 GeV/c a value of $2.88 \pm .33$

is quoted but the situation here is complicated by the interference already mentioned, and at 5 GeV/$_c$ a study based on the K$\pi\pi$ decay of the K^* (1420) gives $b = 4.5 \pm 1.6$ [8] for $0.02 < -t < 0.6$ (GeV/$_c$)^2. There is clearly no systematic trend.

A characteristic of all three reactions listed in Table 3 is that the differential cross-section is less sharply peaked forward than in the corresponding $\pi^+ p$ reactions† at 8 GeV/c. This effect occurs also at lower energies and probably arises because some exchanges allowed in $K^+ p$ interactions are forbidden by G-parity conservation in the $\pi^+ p$ case. Thews [9] has noted this for $K^+ p \to K^o N^{*++}$ and has obtained good fits to the lower energy data using ρ and A_2 exchange in this reaction but ρ exchange only in $\pi^+ p \to \pi^o N^{*++}$.

5. Decay Angular Distributions

The Gottfreid-Jackson angles [10] for the K^{*+} in 1a and the N^{*++} in 1c are shown in Figure 6 and values for the density matrix elements are given in Table 4.

Table 4 K^{*+} and N^{*++} Density Matrix Elements

Reaction	ρ_{00}	ρ_{1-1}	Re ρ_{10}	ρ_{33}	Re ρ_{3-1}	Re ρ_{31}
(1a) $K^+ p \to p K^*$ (1c) $K^+ p \to K^o N^{*++}$	$0.01 \pm .07$	$0.39 \pm .05$	$-0.03 \pm .03$	$0.30 \pm .08$	$0.22 \pm .07$	$0.01 \pm .07$

The decays were fitted by the method of maximum likelihood to distributions W (cosθ, ϕ) of the form given in reference 10. The curves shown

† (i.e. $\pi^+ p \to \rho^+ p$ cf 1a, $\pi^+ p \to p A_2^+$ cf 1b and $\pi^+ p \to \pi^o N^{*++}$ cf 1c).

in Figure 6 correspond to the density matrix elements shown in Table 4.

In reaction 1a the K^* alignment is similar to that found at lower momenta and agrees with production via vector meson exchange. For reaction 1c, $K^+p \rightarrow K^oN^{*++}$, the density matrix elements again have similar values to those at lower energies, and are consistent with production via vector meson exchange and M1 coupling at the baryon vertex[11]. No spin analysis has been performed for the $K^*(1420)$ because of the small number of events.

Acknowledgements

The members of the collaboration wish to express their thanks to the operating crews of the CERN P.S. and 2-metre LHBC and to those concerned with the R.F. beam, especially P.Lazeyras and H. Lengeler. Thanks are also due to members of the scanning and computing groups at the collaborating laboratories. The work was supported in part by the U.K. Science Research Council.

References

1) Y. Goldschmidt-Clermont et al., CERN-Bruxelles collaboration CERN 66-17.

2) 3.0 GeV/c P. Sällström, G. Otter and G. Ekspong, Stockholm Nuovo Cimento 49A 348, (1967)
3.5 GeV/c W. De Baere et al CERN-Bruxelles Nuovo Cimento 51A 401, (1967)
3.5 and 5 GeV/c R. George et al CERN-Bruxelles Nuovo Cimento 49A, 9, (1967)

3) W. Galbraith et al Phys. Rev. 158 B913 (1965)

4) D.R.O Morrison Physics Letters 22 528 (1967)

5) H. M. Chan CERN 67-16

6) M. Krammer and U. Maor CERN/D Ph 11/Physics 67-22.

7) D. Brown et al. PRL 19 644 (1967)

8) G. Bassompierre et al CERN-Bruxelles-Birmingham CERN 67-25

9) R.L. Thews Phys. Rev. 155, 1624, (1967).

10) K. Gottfried and J.D. Jackson Nuovo Cimento 33, 309 (1964)

11) L. Stodolsley and J. J. Sakurai Phys. Rev. Lett. 11, 90, (1963)

Figure Captions

Fig. 1 The Dalitz plot for $K^+p \to K^o p\pi^+$, $M^2(\pi^+p)$ vs $M^2(\pi^+K^o)$.

Fig. 2 Distributions in (a) $M(\pi^+K^o)$ and (b) $M(\pi^+p)$ for the reaction $K^+p \to K^o\pi^+p$.

Fig. 3 The scatter plot of $M(\pi^+p)$ versus $M(\pi^+K^o)$ for events fitting $K^+p \to K^o\pi^+\pi^o p$.

Fig. 4 Ln σ versus Ln. p, where σ is the cross-section at an incident K^+ beam momentum p, (a) for the reaction $K^+p \to pK^{*+}$, (b) for $K^+p \to K^oN^{*++}$ and (c) for $K^+p \to K^{*o}N^{*++}$; $K^{*+} \to K^o\pi^+$, $K^{*o} \to K^o\pi^o$.

Fig. 5 Ln $d\sigma/dt$ versus -t where t is the square of the four-momentum transfer from the target proton to the recoil proton (a) for $K^+p \to pK^{*+}$ and (b) for $K^+p \to pK^{*+}(1420)$. (c) shows Ln $d\sigma/dt$ versus -t for $K^+p \to K^oN^{*++}$ where in this case t is the four momentum transfer squared between target proton and recoil N^{*++}.

Fig. 6 Decay angular distributions for the K^* produced in the reaction $K^+p \to pK^{*+}$, (a) W (cos θ) and (b) W(ϕ) as defined by Gottfried and Jackson[10], and for the N^{*++} in the reaction $K^+p \to K^oN^{*++}$ (c) W(cos Θ) and (d) W (Φ). The curves shown are drawn for the density matrix elements given in Table 4.

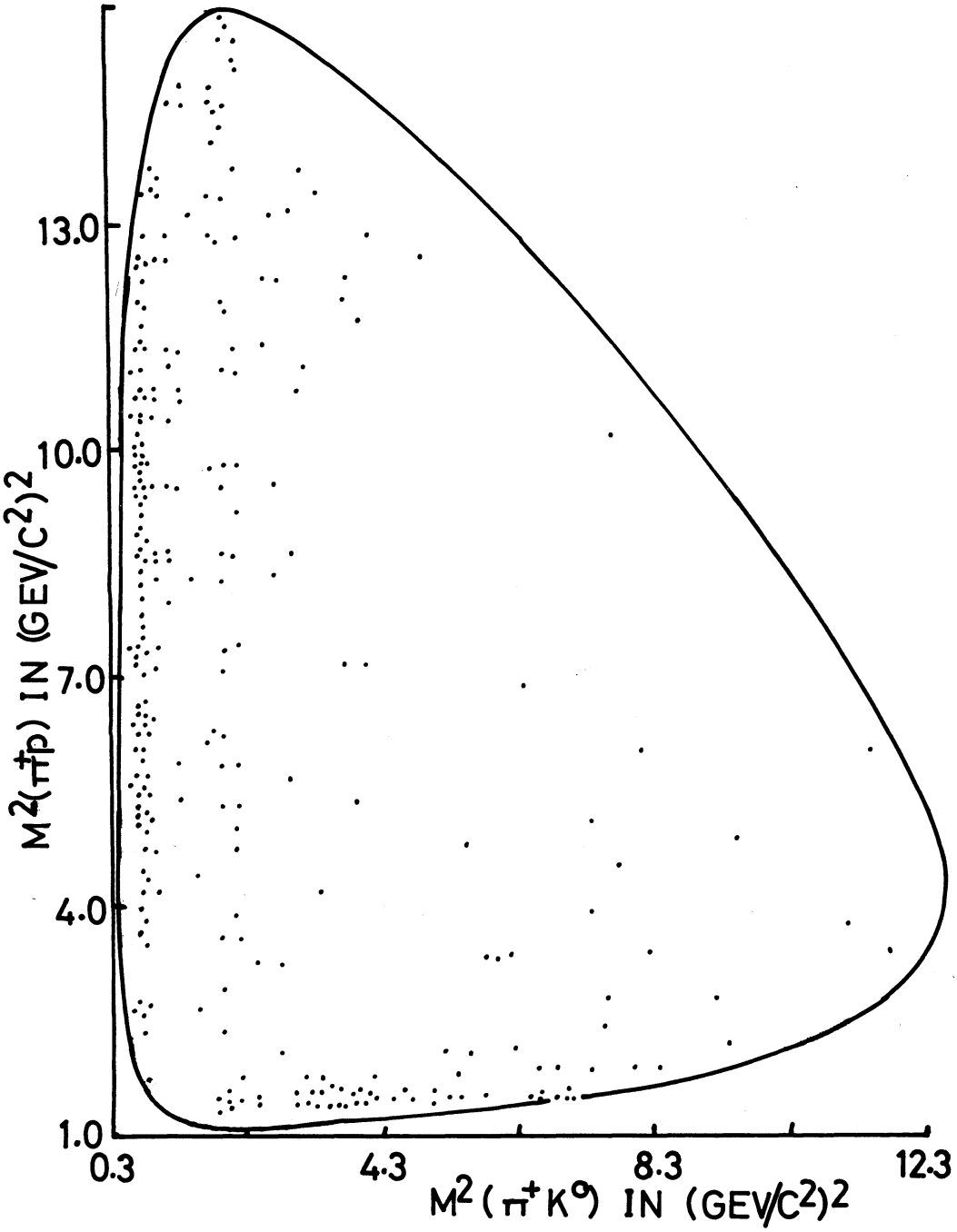
13.0
10.0
7.0
4.0
1.0
$M^2(\pi^{\pm}p)$ IN $(GEV/C^2)^2$
0.3
4.3
8.3
12.3
$M^2(\pi^+K^0)$ IN $(GEV/C^2)^2$

FIGURE 1

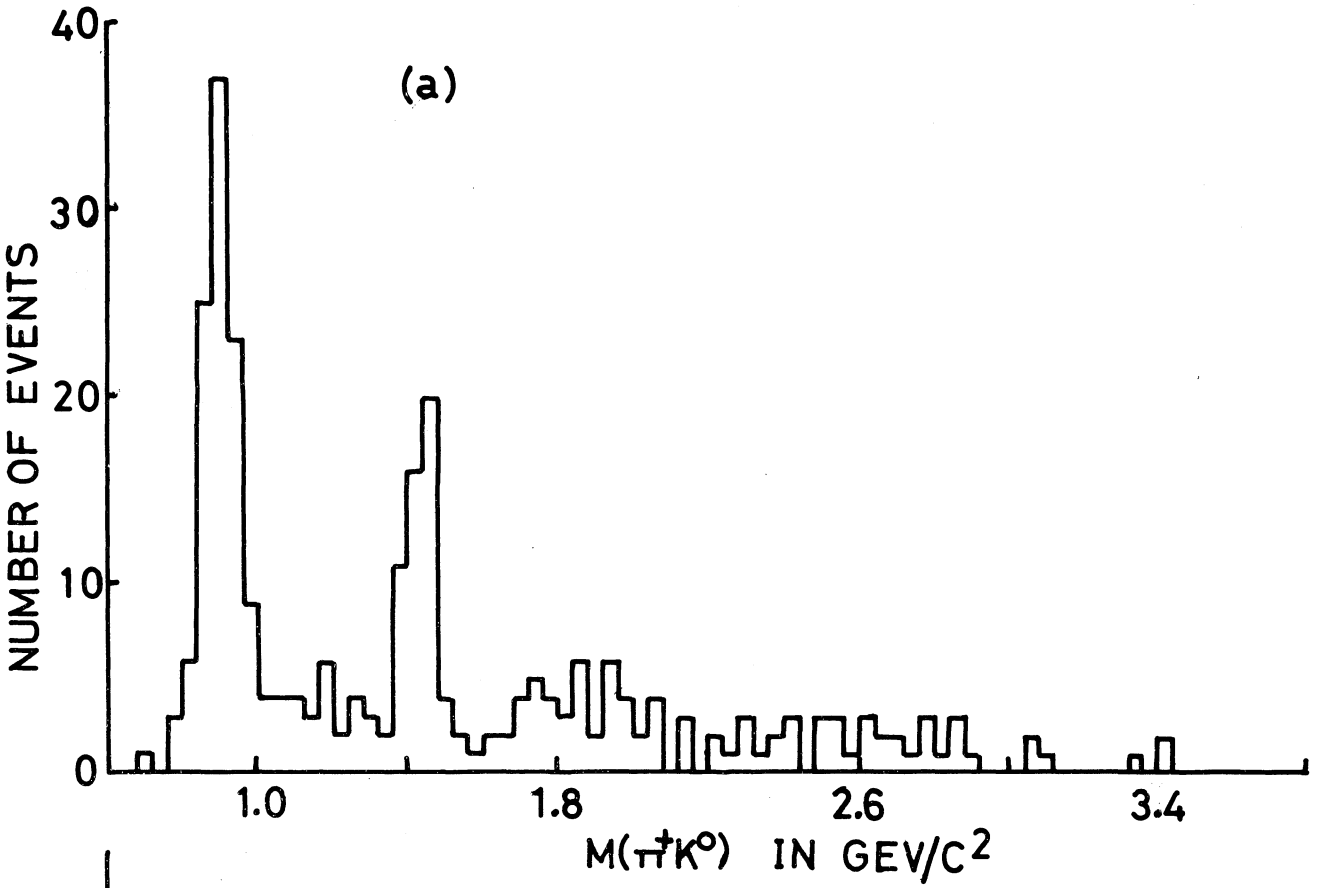
(a)
NUMBER OF EVENTS
40
30
20
10
0
1.0
1.8
2.6
3.4
M(π⁺K°) IN GEV/C²

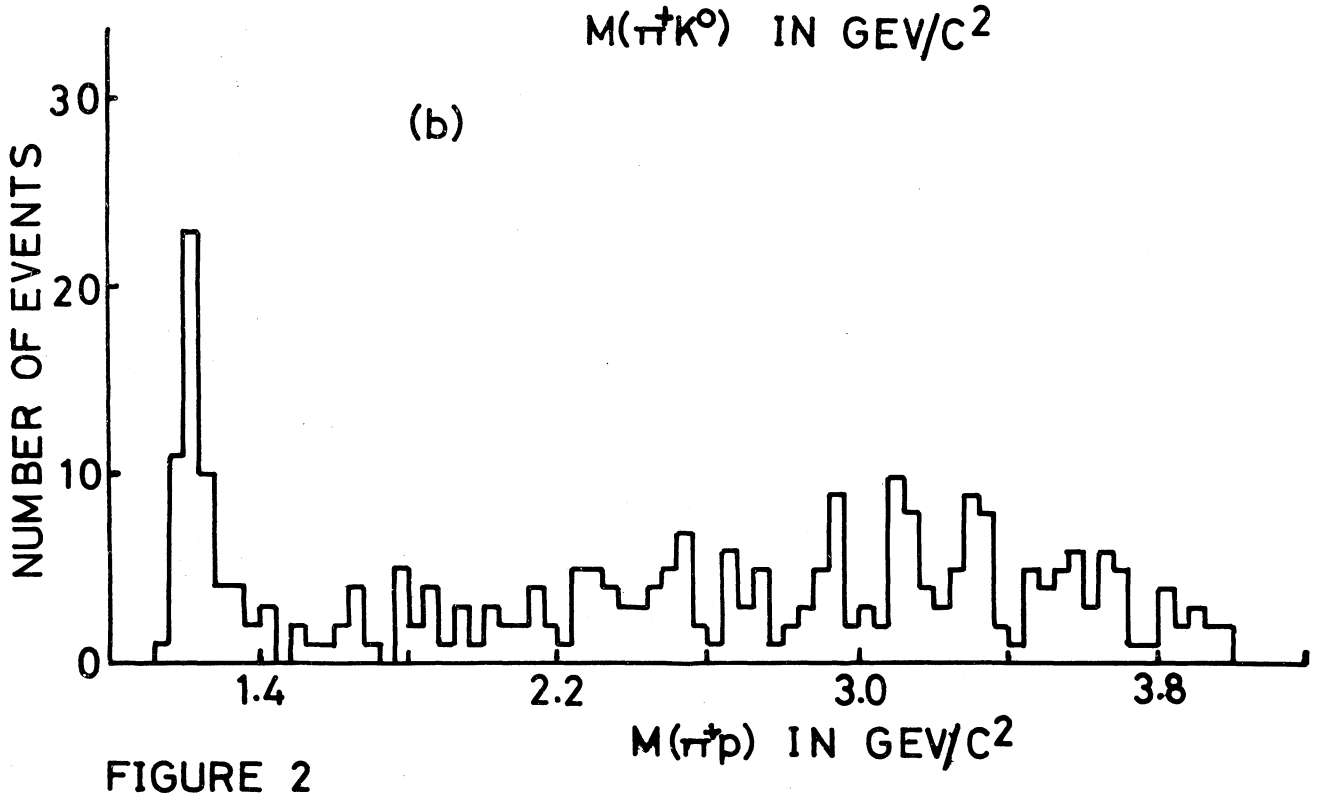
(b)
NUMBER OF EVENTS
30
20
10
0
1.4
2.2
3.0
3.8
M(π⁺p) IN GEV/C²

FIGURE 2

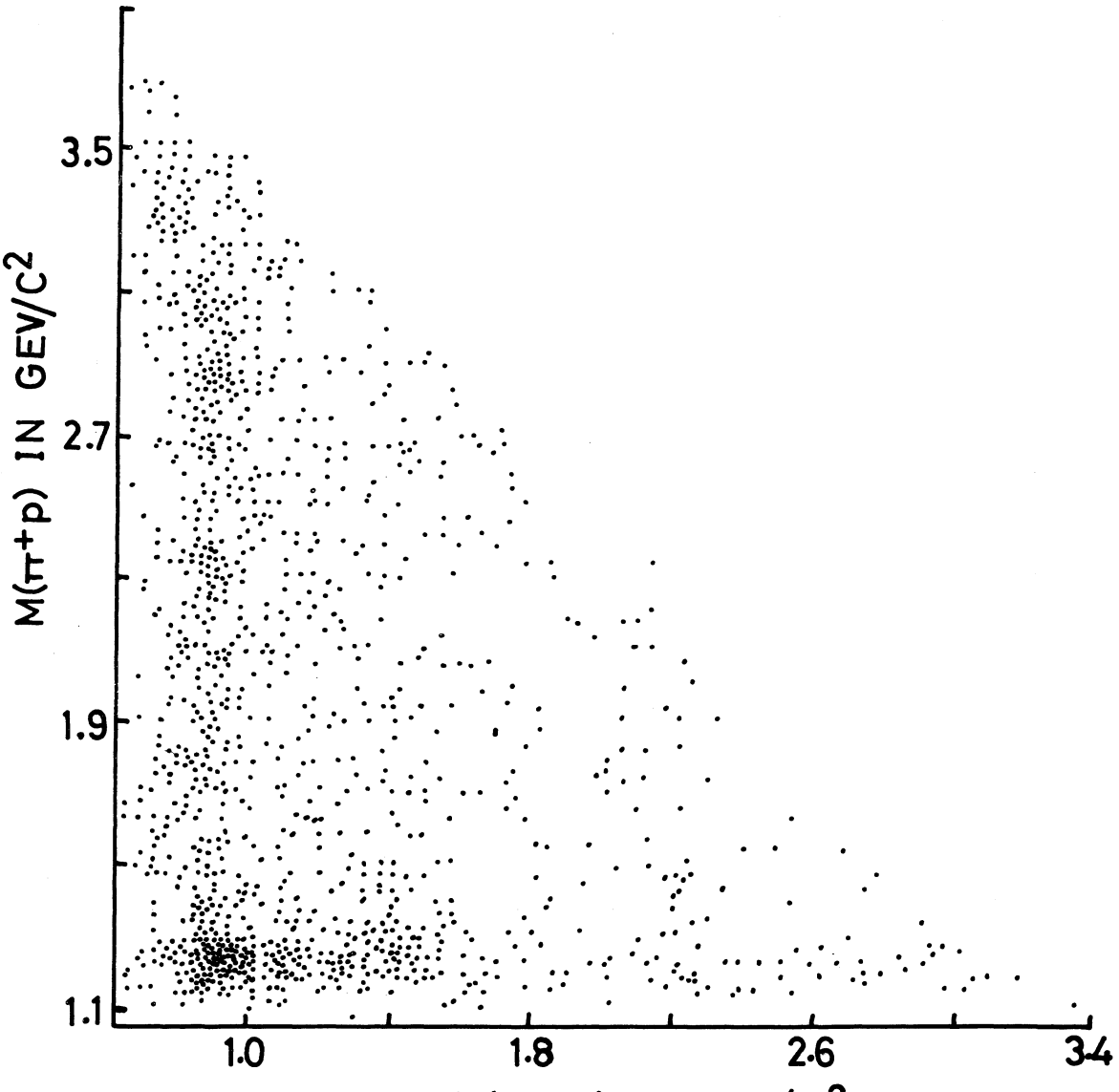

FIGURE 3

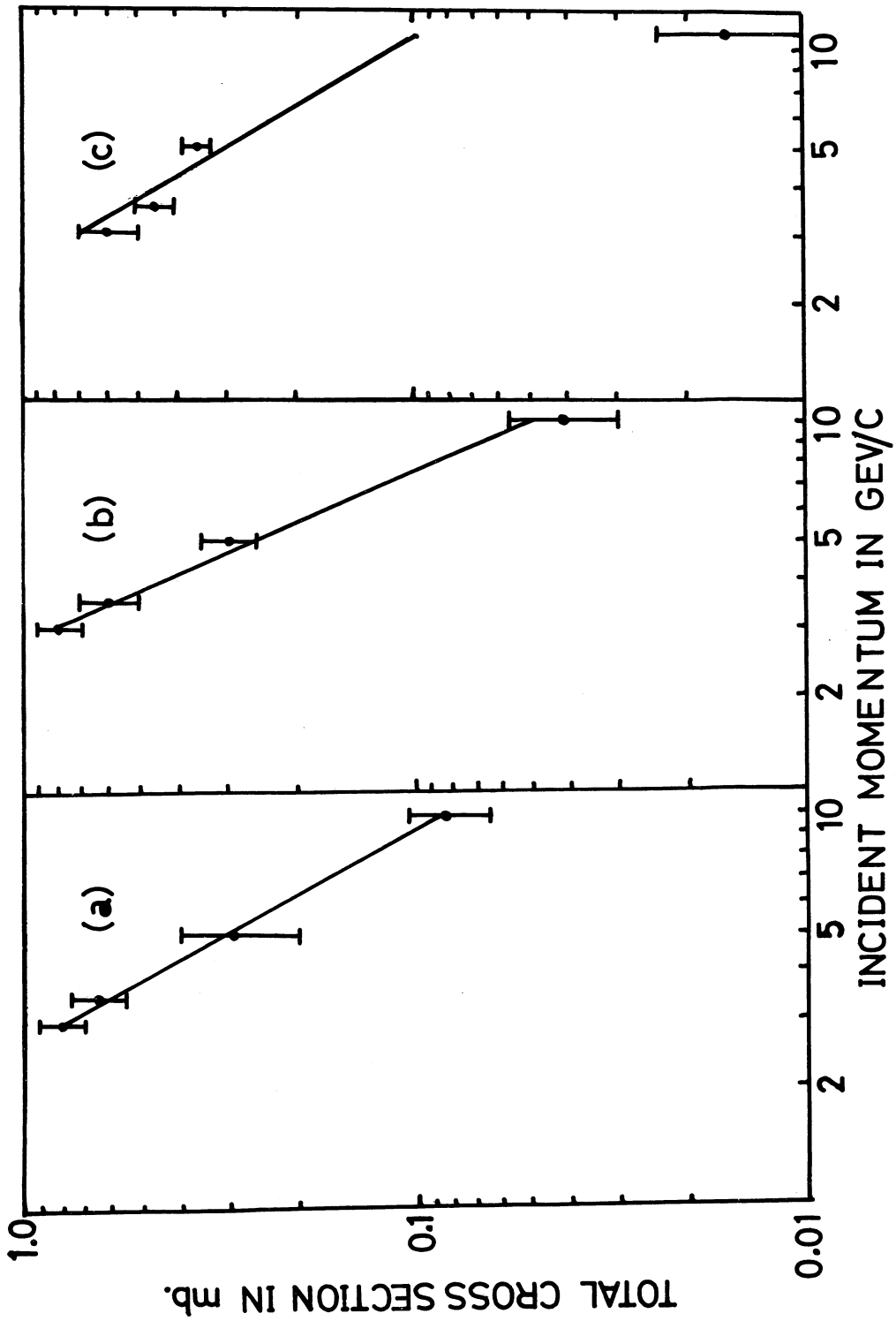
TOTAL CROSS SECTION IN mb.
1.0
0.1
0.01
(a)
(b)
(c)
2
5
10
INCIDENT MOMENTUM IN GEV/C

FIGURE 4

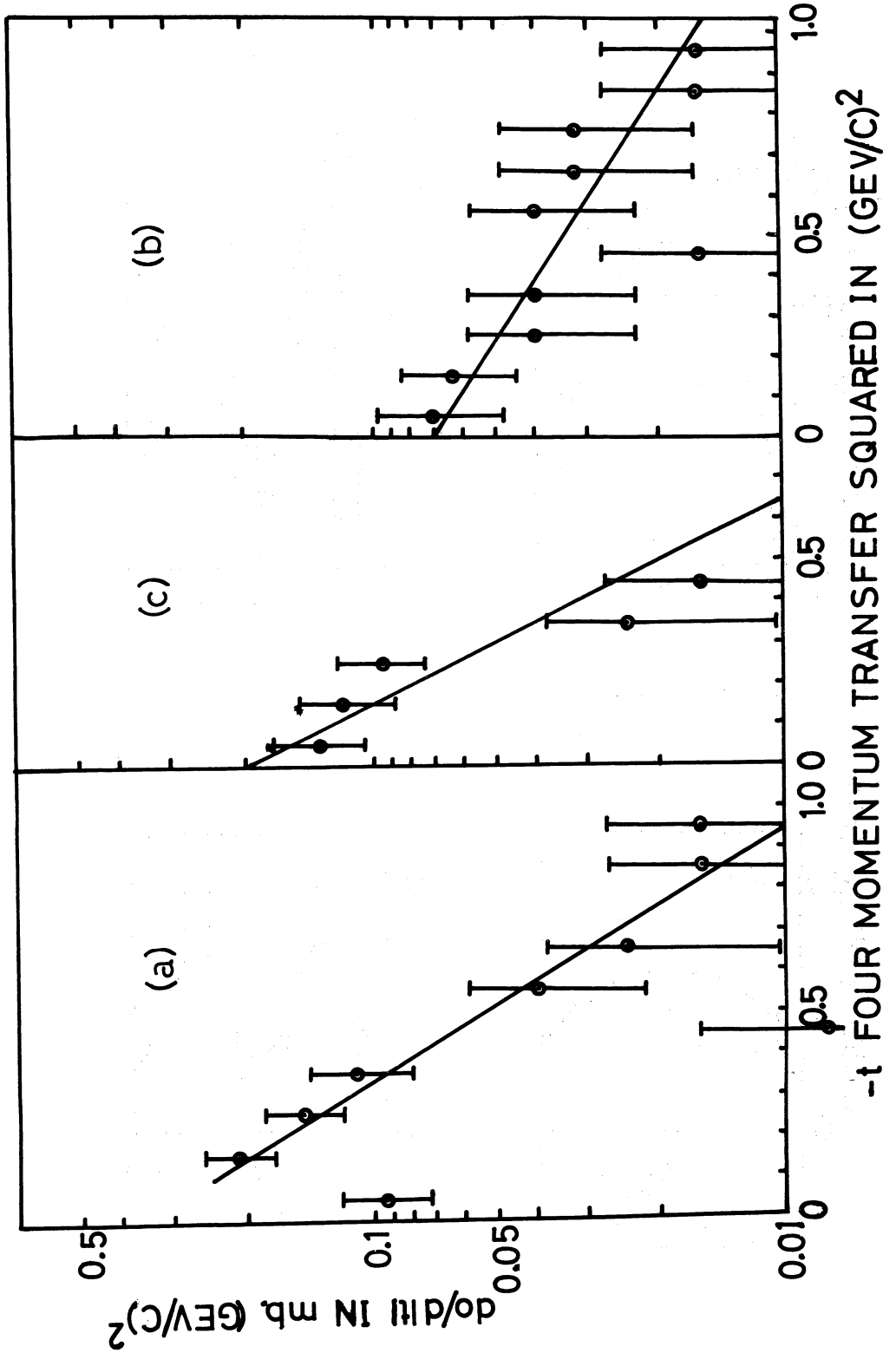
(a)
(b)
(c)
0.5
0.1
0.05
0.01
0
0.5
1.0
0
0.5
1.0
0
0.5
1.0
dσ/dt IN mb (GEV/C)²
-t FOUR MOMENTUM TRANSFER SQUARED IN (GEV/C)²

FIGURE 5

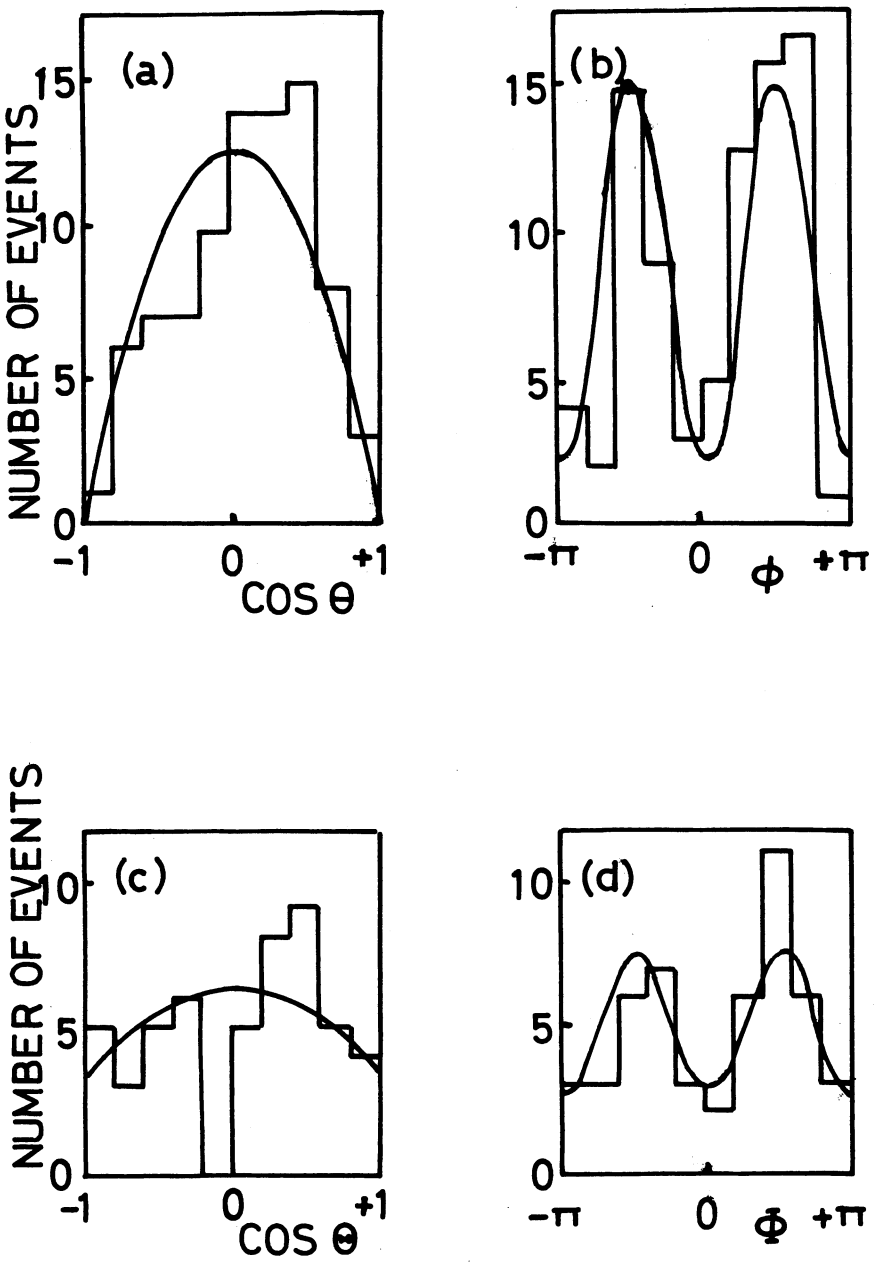
(a)
NUMBER OF EVENTS
15
10
5
0
-1
0
+1
COS θ
(b)
15
10
5
0
-π
0
Φ
+π
(c)
NUMBER OF EVENTS
10
5
0
-1
0
+1
COS θ
(d)
10
5
0
-π
0
Φ
+π

FIGURE 6

QUASI TWO BODY REACTIONS IN $\pi^+ d$ INTERACTIONS AT 5,1 GeV/c

Orsay (I.P.N.$_1$) Bari, Bologne, Florence collaboration

presented by J. LABERRIGUE I.P.N.$_1$

INTRODUCTION :

Analysing $\pi^+ d$ interactions at 5,1 GeV/c in 400.000 pictures of the 81 cm Saclay deuterium bubble chamber exposed at CERN PS, we obtained results concerning reactions :

$$\pi^+ d \rightarrow p_s p + \text{neutrals} \qquad (1)$$

$$\pi^+ d \rightarrow p_s p\, \pi^+ \pi^- \qquad (2)$$

$$\pi^+ d \rightarrow p_s p\, \pi^+ \pi^- \pi^\circ \qquad (3)$$

Experimental conditions and details on analysis of these reactions were already reported in previous papers [1]. The spectator proton and the faster proton have momenta less than .28 GeV/c and 1.3 GeV/c respectively.

Here we present results concerning quasi two body

List of Authors

M. Barrier, J. Laberrigue-Frolow, D. Mettel, J. Quinquard, M. Sené, Institut de Physique Nucléaire - Orsay-Paris.
N. Armenise, B. Ghidini, V. Picciarelli, A. Romano, A. Silvestri. Istituto di Fisica dell'Universita di Bari I.N.F.N. Sottosezina di Bari.
A. Forino, R. Gessarolli, L. Lendinara, G. Quareni, A. Quarenc-Vignudelli. Istituto di Fisica dell'Universita di Bologna. I.N.F.N. Sezione di Bologna.

—/..

reactions :

1 a $\quad \pi^+ n \rightarrow p\, f^\circ \hookrightarrow \pi^\circ\pi^\circ$

2 a $\quad \pi^+ n \rightarrow p\, \rho^\circ$

b $\quad \pi^+ n \rightarrow p\, f^\circ$

c $\quad \pi^+ n \rightarrow p\, g^\circ$

3 a $\quad \pi^+ n \rightarrow p\, \eta$

b $\quad \pi^+ n \rightarrow p\, \omega$

c $\quad \pi^+ n \rightarrow p\, A_2^\circ$

d $\quad \pi^+ n \rightarrow p\, (\rho\pi)^\circ_{1650}$

Associated $N^{*\circ}\,\rho^+$ and $N^{*+}\,\rho^\circ$ being present in reaction 3, we exclude for analysis of reaction 3(a, b, c, and d) peripheral isobars (events with $Mp\pi < 1.3$ GeV and $\Delta^2_{(p\pi)} < 0.3\ GeV^2$.

CROSS SECTIONS

Fig. 1 shows the invariant $\pi^+\pi^-$ mass spectrum. The best fit obtained adding to a statistical background three Breit-Wigner's for ρ° f° and g° resonances (positions, widths and intensities being all free parameters) give the results reported Table 1.

	Positions (GeV)	Widths (GeV)	Percentage	barns
$\rho^\circ \rightarrow \pi^+\pi^-$	.775 ± .002	.168 ± .006	47, 02	596 ± 95.
$f^\circ \rightarrow \pi^+\pi^-$	1.261 ± .004	.216 ± . 013	33,49	421 ± 76.
$g^\circ \rightarrow \pi^+\pi^-$	1.683 ± .013	.189 ± .049	6, 03	76 ± 11
background			13, 06	158.

TABLE 1.

/ A. Cartacci, M.G. DAGLIANA, G. Di Caporiacco, G. Parrini. Istituto di Fisica dell'Universita di Firenze. I.N.F.N. Sottosezione di Firenze.

The rather small background, specially in the low mass region is particularly interesting for the analysis of $p\rho^\circ$ and pf° two body reactions.

ρ_o, f°, and g° production cross sections values obtained in our experiment : $(596 \pm 95)\mu b$, $(421 \pm 76)\mu b$ and $(76 \pm 11)\mu b$ respectively are quite compatible with values obtained at other energies [2]. At 4 GeV/c [3] cross sections for $\pi^- \rightarrow n\rho$ and nf° are (0.75 ± 0.13) mbarns and $(0.42 \pm 0,06$ mb) respectively, and those obtained for reactions 2(a, b, c) in a $\pi^+ d$ experiment at 6 GeV/c (4) are $(400 \pm 13)\mu b$, $(180 \pm 13)\mu b$ and $(56 \pm 14)\mu b$.

Fig. 2 shows the tripion mass spectrum ; η and ω are produced above a negligible background. Analysis of $\rho\pi$ structures [1] indicate, A_2° and $(\rho\pi)_{1640}$ productions (see ref. 1c).

The best fit obtained for the low mass region gives for η and ω position, width the values :

	M_{gev}	Width
$\eta \rightarrow \pi^+\pi^-\pi^\circ$	537,6 ± 2,5	28,4 ± 4,9
$\omega \rightarrow \pi^+\pi^-\pi^\circ$	781,9 ± 1,1	33,9 ± 1,8

To avoid biases due to cuts in protons momenta in our experiment we evaluate all cross sections by normalizing the cross section $\sigma(\pi^+ d \rightarrow p_s p \eta)$, with $\eta \rightarrow \pi^+\pi^-\pi^\circ$, to the cross section from reaction $\pi^- p \rightarrow \eta n$ at the same energy [5]: (56 μb)

Then $\sigma_{\pi^+ n \rightarrow p\, \omega^\circ_{\hookrightarrow \pi^+\pi^-\pi^\circ}} = 128 \pm 3$ μbarns

Analysis of $\rho\pi$ structure is rather difficult due to the intrinsec properties of the A_2° and to the important background. The best fit obtained eliminating ω and η production, with a 20% confidence level is given table 2.

TABLE 2

	Positions gev	Widths gev	Percentages	σ_μ barns
A_2°	1.311 ± 0.006	0.096 ± 0.016	16,7 ± 27	147 ± 30
$2^{nd}(\rho\pi)$ peak	1.636 ± 0.020	0.112 ± 0.060	6 ± 2	53 ± 20
Background	-	-	58 % ± 10	515 ± 50
Deck effect	-	-	19 % ± 2	168 ± 25

DIFFERENTIAL CROSS SECTIONS. SLOPES

Δ^2 distributions for events corresponding to ρ°, f°, g° production (fig. 3) show clearly a forward peak suggesting a peripheral contribution.

However, it has to be noticed that for $\Delta^2 > .3 GeV^2$, while f° and g° vanish, a clear peak is still present in the dipion mass spectrum at the same mass and with the same width than the ρ°. The corresponding cos Θ distribution, (Θ = first angle defined by Jackson) does not exhibit the well known forward - backward assymetry ($\frac{F-B}{F+B} = 0.35 \pm 0,04$) observed for events with $\Delta^2 < .3\ GeV^2$.

The three Δ^2 distributions for ρ° f° and g° production are well fitted (fig. 4) for low Δ^2 values by exponential lows $\frac{\Delta\sigma}{\Delta\Delta^2} \sim e^{\alpha t}$, with α sumarized in table 3.

	Mass band. GeV	Δ^2 GeV^2	Slope
$\rho^\circ \to \pi^+\pi^-$	$.675 < M\pi\pi < .875$	$.06 < \Delta^2 < .28$	9.63 ± 0.59
$f^\circ \to \pi^+\pi^-$	$1.16 < M\pi\pi < 1.36$	$.04 < \Delta^2 < .28$	8.75 ± 0.48
$g^\circ \to \pi^+\pi^-$	$1.58 < M\pi\pi < 1.78$	$0.16 < \Delta^2 < .56$	5.57 ± 0.56

TABLE 3

For $f^\circ \to \pi^\circ\pi^\circ$ observed in reaction 1a, the value of the slope is 8.8 ± 1.7 Values of the slopes for ρ° and f° are compatible with these obtained at other energies in $\pi^- p$ interactions [2,3]. For ω production fig. 5(a) the fit gives a value of $3,08 \pm 07$ GeV^{-2}. There is a back of events in the region of $\Delta^2 = 0,6$ GeV^2 but the statistic involved does not allow to speak of a minimum.

For A_2° and $(\rho\pi)^\circ_{1640}$ production the analysis of the differential cross section is much more complicated due to the important background; moreover it depens of the cut made to eliminate the competitive isobar production. Values obtained with the cuts described above are summarized table 4.

TABLE 4.

	Mass band GeV	Δ^2 GeV^2	Slope
$\omega^\circ \to \pi^+\pi^-\pi^\circ$	$.74 < M_{\pi^+\pi^-\pi^\circ} < .84$	$.12 \leqslant \Delta^2 < .54$	3.08 ± 0.7
$A_2^\circ \to \rho\pi$	$1.22 < M_{\pi^+\pi^-\pi^\circ} < 1.42$	$.04 \leqslant \Delta^2 \leqslant .4$	2.83 ± 0.8
$(\rho\pi)^\circ_{1640}$	$1.550 < M_{\pi^+\pi^-\pi^\circ} < 1.750$	$0.12 \leqslant \Delta^2 \leqslant 1.0$	3.3 ± 0.8

Value obtained for the slope of $N^*\rho$ production $\alpha = 11,3 \pm 3$ GeV^{-2} is in good agreement with values obtained at 4 GeV/c and 8 GeV/c.

Spin density matrix elements

They were calculated for ρ° and f° production. The high statistic obtained for ρ° production allowed us to calculate the spin density matrix elements relative to the amplitude

$$W(\theta,\varphi) = \frac{1}{4\pi} + \frac{3}{4\pi}\left[(\rho_{oo} - \rho_{11})(\cos^2\theta - \frac{1}{3}) - \sqrt{2}\,\mathrm{Re}\,\rho_{10}\sin 2\theta\cos\varphi - \right.$$

$$\left. - \rho_{1,-1}\sin^2\theta\cos 2\varphi\right) + \frac{\sqrt{3}}{4\pi}\left(-2\sqrt{2}\,\mathrm{Re}\,\rho^{int}_{10}\sin\theta\cos\varphi + 2\mathrm{Re}\,\rho^{int}_{oo}\cos\theta\right)$$

as a function of Δ^2. The results summarized table 5 are rather compatible with theoretical values predicted by the S-P model, the deviation of $\rho_{oo} - \rho_{11}$ from the theoretical prediction reproduces the strang depolarization observed for the ρ° at $\Delta^2 > .3$ GeV^2.

Δ^2 GeV^2	$\rho_{oo} - \rho_{11}$	$\mathrm{Re}\,\rho^{int}_{oo}$	N^b ev.
$\Delta^2 < .05$	0,56 ± 0,04	0,29 ± 0,02	526
$.05 < \Delta^2 < .1$	0,55 ± 0,03	0,25 ± 0,01	415
$.1 < \Delta^2 < .25$	0,54 ± 0,04	0,21 ± 0,02	463
$\Delta^2 > .25$	0,09 ± 0,07	0,03 ± 0,03	274
$\Delta^2 > .3$	-0,05 ± 0,08	-0,009 ± 0,03	217

TABLE 5

For f_o production, the calculated values of the spin density matrix elements for a $J^P = 2^+$ state for $\Delta^2 < .3$ GeV^2 are the following.

$$\rho_{oo} = 1,02 \pm .15$$
$$\rho_{11} = .20 \pm .07$$
$$\rho_{22} = -.21 \pm .07$$
$$\rho_{1,-1} + \frac{\sqrt{6}}{3}\,\mathrm{Re}\,\rho_{20} = .02 \pm .02$$

$$\rho_{2,-2} = -.01 \pm .02$$

$$\frac{5}{64}\pi\,(3\,\mathrm{Re}\,\rho_{21} + \sqrt{6}\,\mathrm{Re}\,\rho_{10} = .10 \pm .01)$$

ρ_{00} and ρ_{11} values are not incompatible with theoretical values. The negative value of ρ_{22} reflects the absence of the bump in cos $\theta = 0$ region, which is certainly not due to an experimental bias.

The decay angular distribution of g° resonance is strongly peaked forward. It does not reflect a pure resonant wave. Furthermore the assymetry parameter $\frac{F-B}{F+B}$ does not show any anomalous behaviour in the g mass region. There is no significative structures in the coefficients $a_1, a_2 \ldots a_{10}$ of the Legendre polynomial coefficients calculated with the momenta method. So it is impossible here to determine ρ_{ij} values for g° resonance.

CONCLUSION

In conclusion results obtained in $\pi^+ d$ interactions at 5,1 GeV/c show that the quasi two body process is dominant. $p\rho^\circ$, pf°, pg°, $p\omega^\circ$, $p A_2^\circ$, $p(\rho\pi)^\circ_{1640}$ reactions are rather well represented by theoretical predictions in t chanel. The presence of depolarized ρ° for t values higher. 3 GeV^2 beyand diffraction peak is evident and has to be understood.

References

1) a) A_2° production in $\pi^+ d$ interaction (collaboration Orsay-Bari-Bologne - FLorence)
Physics letters 24 juillet 67

b) Communications at Heidelberg Conference (same collaboration) Sept. 1967
- ρ° f° g° resonances produced in $\pi^+ d$ Interactions at 5,1 GeV/c
- expérimental results on the A_2° resonance
- charged ρ production in Association with N^*_{33} in $\pi^+ d$ interactions at 5 GeV/c.

c) - Expérimental results on the $(\rho\pi)^\circ$ resonances in $\pi^+ d$ interactions at 5,1 GeV/c (same collaboration) to be published.

2) D.R.O. Morrisson (Physics letters 22, 528, 1966)

3) A.B.B.H.L.M. Collaboration Nuovo Cimento XXXI 729 1964.

4) G. de Rosny Thèse Faculté des Sciences Paris 1966.

5) O. Guisan, J. Kirz, P. Sondereger, A.V. Stirling, P. Borgeaud, G. Bruneton, P. Falk-Vairant, B. Amblard, C. Caverzasio, J.P. Guillaud, M. Yvert. Physics Letters 18, 200 (1965).

FIGURE CAPTION

Fig. 1 Invariant $\pi^+\pi^-$ mass spectrum

Fig. 2 a) Invariant $\pi^+\pi^-\pi^\circ$ mass spectrum

b) Analysis of this spectrum in $(\rho\pi)$ structure

Fig. 3 $\Delta^2(\pi^+\pi^-)$ distributions for $\pi^+\pi \to p\rho^\circ$, pf°, pg° reaction

Fig. 4 $\Delta^2(\pi^+\pi^-)$ distributions for ρ°, f° and g° for small Δ^2 region. Straight lines are fitted results.

Fig. 5 $\Delta^2_{(\pi^+\pi^-\pi^\circ)}$ distributions in reaction $(\pi^+ d \to p_s p\pi^+\pi^-\pi^\circ)$

a) for $\pi^+ n \to p\,\omega^\circ$ $(.74 < M_{\pi^+\pi^-\pi^\circ} < .84$ GeV)

b) for $\pi^+ n \to p\,A_2^\circ$ $(1.22 < M_{\pi^+\pi^-\pi^\circ} < 1.42$ GeV).

Fig. 6 Δ^2 distribution in reaction $\pi^+ d \to p_s p\pi^+\pi^-\pi^\circ$ for $\pi^+ n \to p\,(\rho\pi)_{1640}$ $(1.550 < M_{\pi^+\pi^-\pi^\circ} < 1750$ GeV).

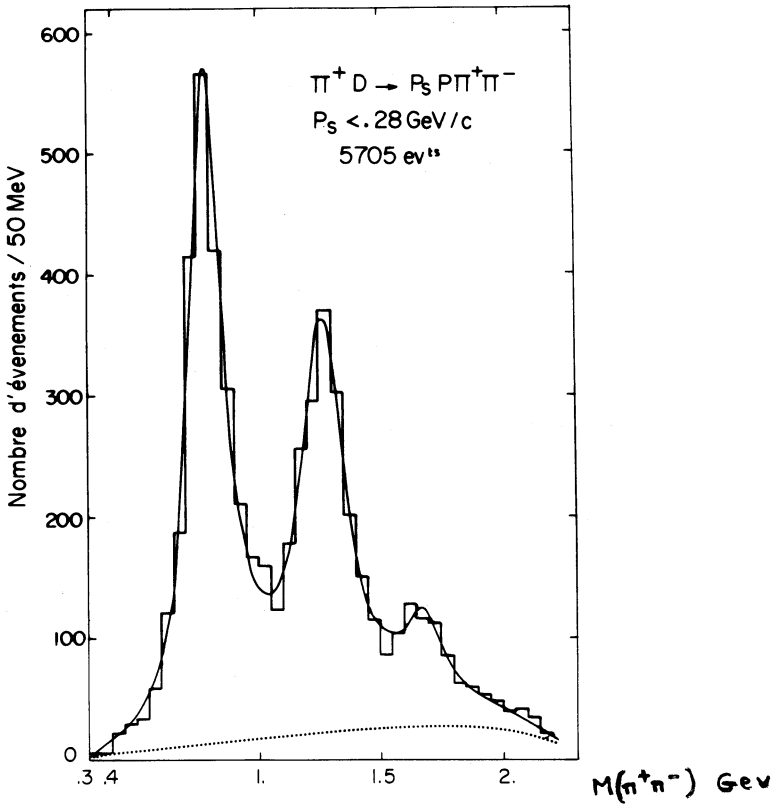
$\pi^+ D \rightarrow P_S P\pi^+\pi^-$
$P_S < .28$ GeV/c
5705 evts
Nombre d'évenements / 50 MeV
600
500
400
300
200
100
0
.3
.4
1.
1.5
2.
M(π⁺π⁻) Gev

Fig. 1

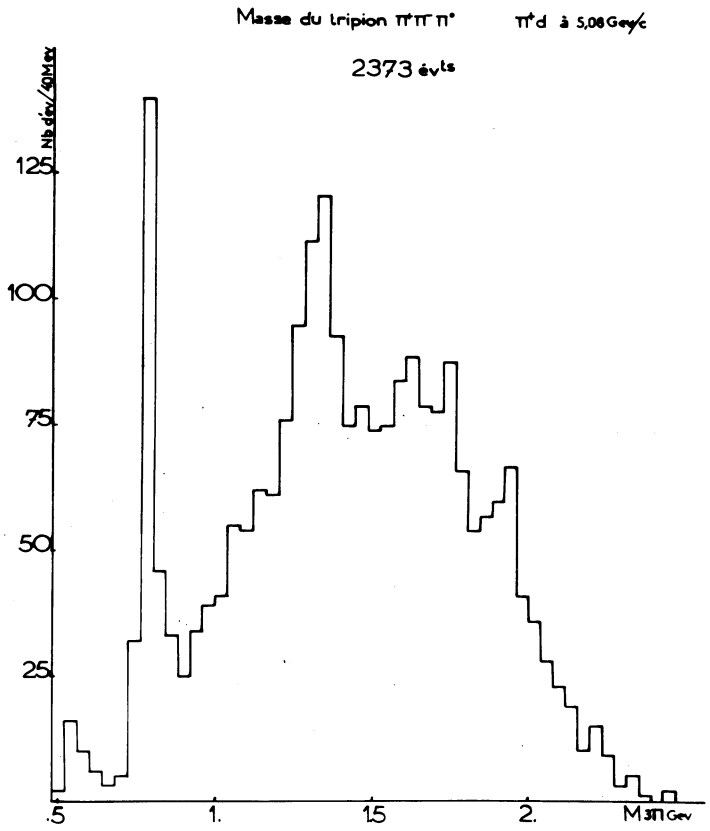
Masse du tripion π⁺π⁻π° π⁺d à 5,08 Gev/c
2373 évts
Nb d'év./40 Mev
125
100
75
50
25
.5
1.
1.5
2.
M 3π Gev

Fig. 2a

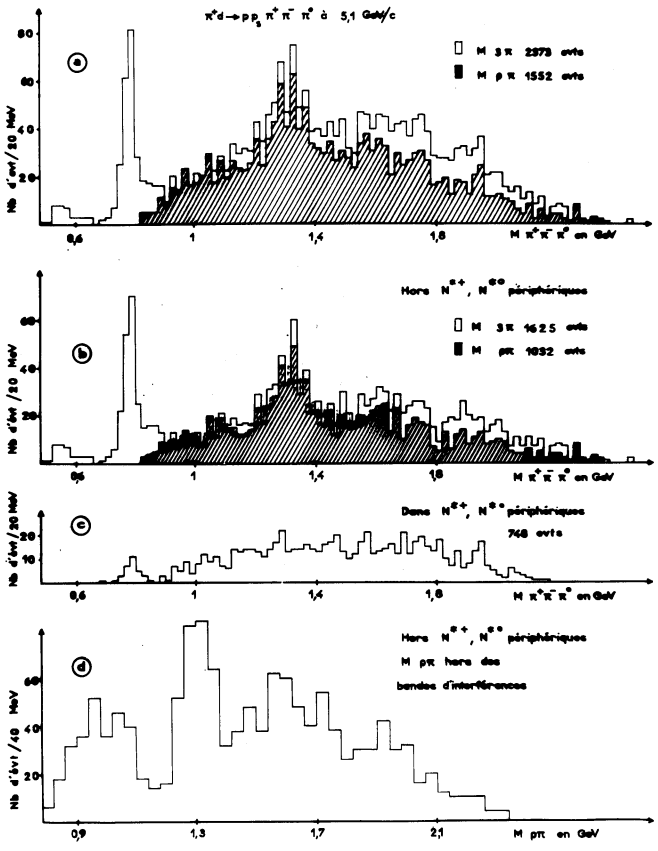
π⁺d → p p_s π⁺ π⁻ π° à 5,1 Gev/c
M 3π 2373 evts
M ρ π 1552 evts
Nb d'evt / 20 MeV
M π⁺π⁻π° en GeV
Hors N⁺⁺, N⁰⁰ périphériques
M 3π 1625 evts
M ρπ 1032 evts
Dans N⁺⁺, N⁰⁰ périphériques
748 evts
Hors N⁺⁺, N⁰⁰ périphériques
M ρπ hors des
bandes d'interférences
Nb d'evt / 40 MeV
M ρπ en GeV

Fig. 2b

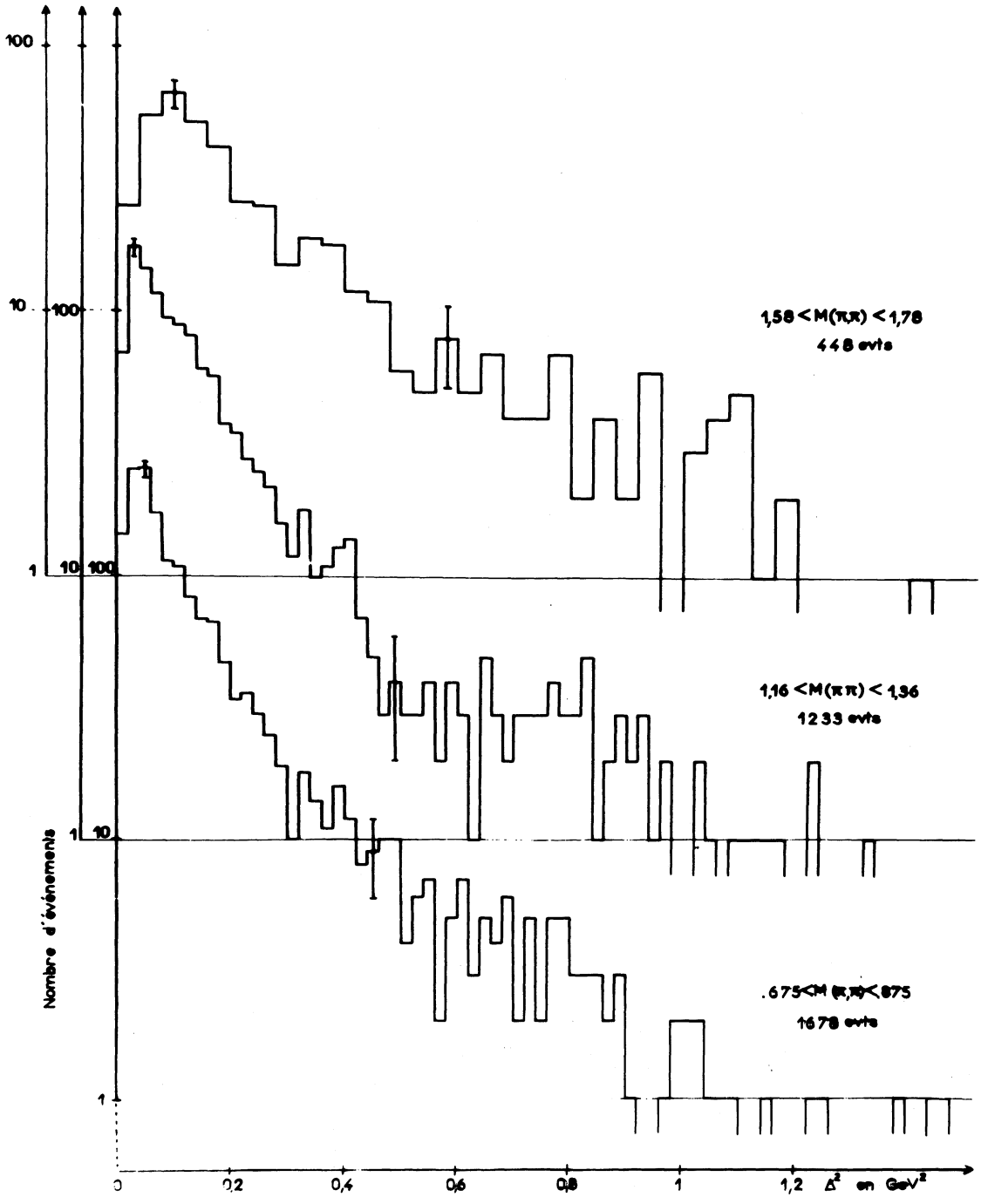
100
10
100
1
10
100
1,58 < M(ππ) < 1,78
448 evts
1,16 < M(ππ) < 1,36
1233 evts
.675 < M(ππ) < .875
1678 evts
Nombre d'événements
1
10
1
0
0,2
0,4
0,6
0,8
1
1,2
Δ² en GeV²

Fig. 3

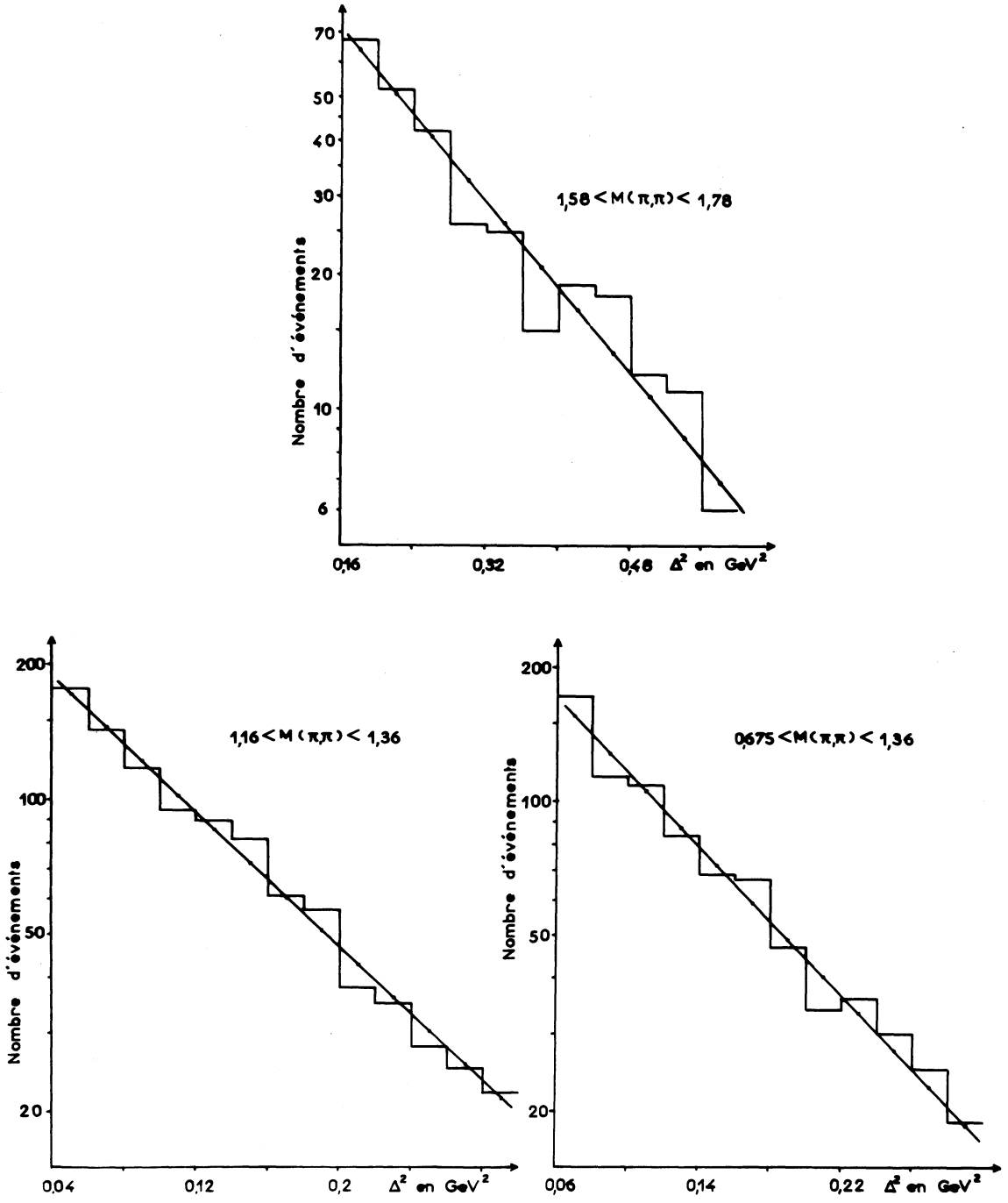
70
50
40
30
20
10
6
Nombre d'événements
1,58 < M(π,π) < 1,78
0,16
0,32
0,48 Δ² en GeV²
200
100
50
20
1,16 < M(π,π) < 1,36
0,04
0,12
0,2 Δ² en GeV²
0,675 < M(π,π) < 1,36
0,06
0,14
0,22 Δ² en GeV²

Fig. 4

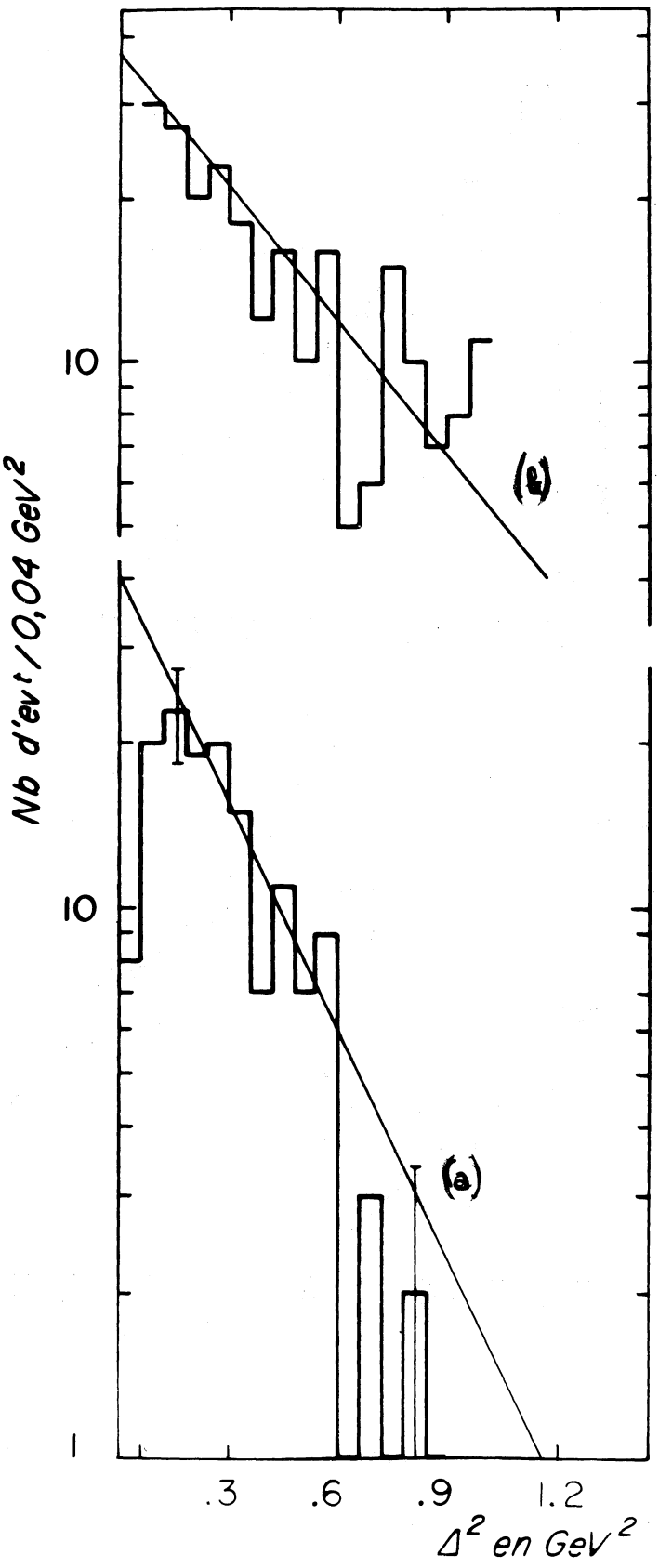

Fig. 5

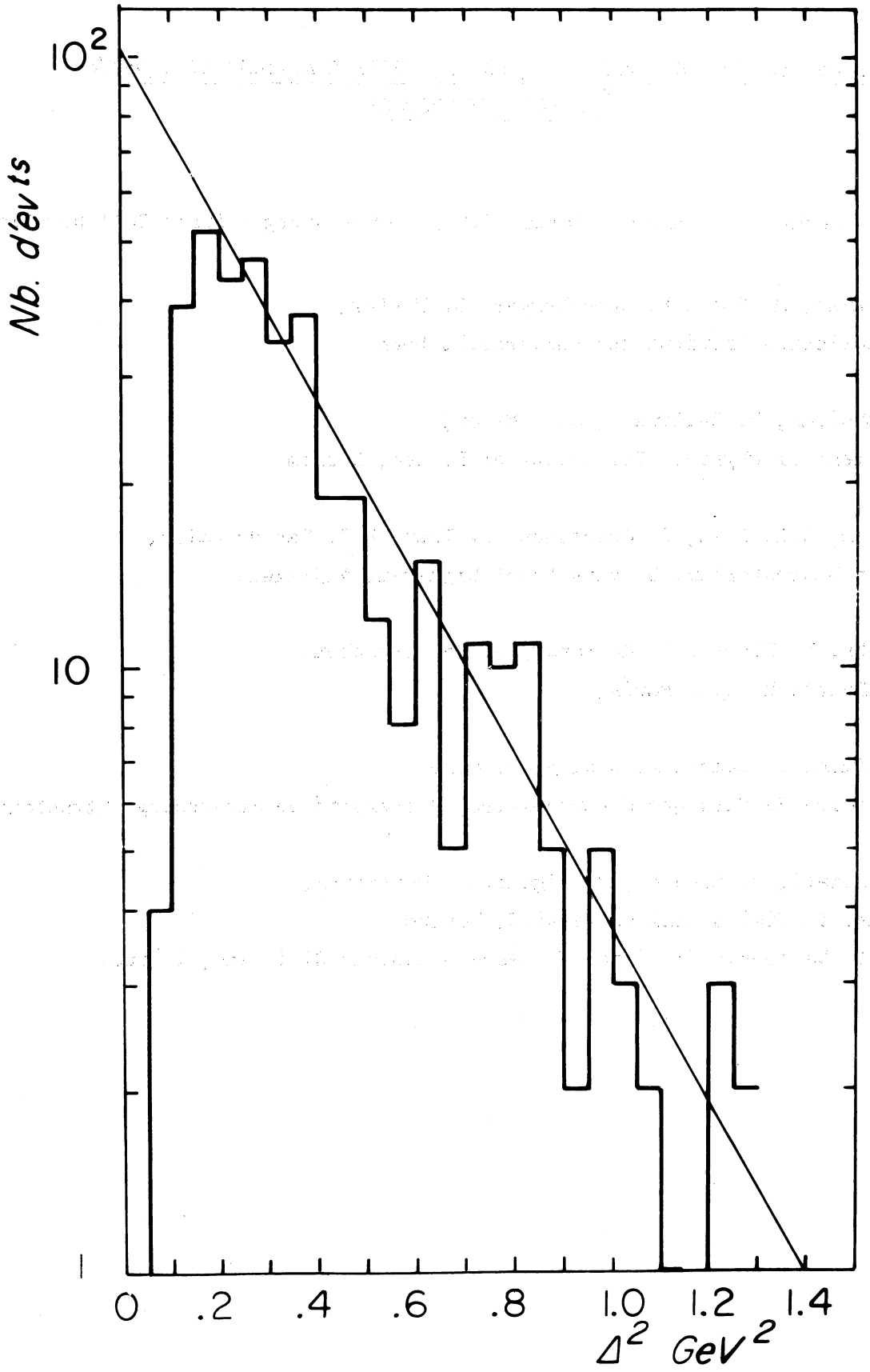

Fig. 6

FURTHER ANALYSIS OF $N^*\rho$ AND $N^*\omega$ QUASI-TWO-BODY REACTIONS BY 5 GeV/c π^+ MESONS ON PROTONS

(Bonn - Durham - Nijmegen - Paris (E.P.) - Strasbourg - Turin Collaboration)

K. Böckman, M. Rost, K. Sternberger, G. Winter,
Physikalisches Institut der Universität Bonn.

Z.I. Bhuiyan, H. Halliwell, J.V. Major,
Department of Physics, University of Durham, Durham.

T.G. Lim, C.L. Pols, D. Schotanus, D. Toet, R.T. Van de Walle,
Fysisch Laboratorium, University of Nijmegen, Nijmegen.

E. Cirba, P. Fleury, G. de Rosny, R. Vanderhaghen,
Ecole Polytechnique, Paris.

A. Fridman, J. Oudet, B. Schiby, R. Strub,
Laboratoire de Physique Corpusculaire, Université de Strasbourg, Strasbourg.

B. Quassiati, G. Rinaudo, M. Vigone, A. Werbrouck,
Istituto di Fisica dell'Università, Torino.
Istituto Nazionale di Fisica Nucleare - Sezione di Torino, Torino.

INTRODUCTION

An analysis of double resonance production by 5 GeV/c π^+ mesons on protons has been presented at the Heidelberg Conference ([1]). The analysis was based on a sample of approximately 6000 events of the type:

$$\pi^+ p \rightarrow \pi^+ p \pi^+ \pi^- \tag{1}$$

and approximately 6500 events of the type:

$$\pi^+ p \rightarrow \pi^+ p \pi^+ \pi^- \pi^o \tag{2}$$

For both the reactions:

$$\pi^+ p \rightarrow N^{*++}_{3/2,3/2} \rho^o \tag{3}$$

and

$$\pi^+ p \rightarrow N^{*++}_{3/2,3/2} \omega^o \tag{4}$$

we presented results for $d\sigma/d|t|$ and the (single-vertex) density matrix elements as a function of $|t|$.

Comparisons with the absorption model predictions were made. For the $N^*\rho$-channel a satisfactory over-all agreement with the predictions of the one-pion-exchange absorption (OPEA-)model was found. Our $N^*\omega$-results however, differed appreciable from the predictions of the absorption model with ρ-meson exchange.

For both channels we looked for a possible correlation between the polar angles of the vector meson- and the isobar-decay ($\Theta_{\rho(\omega)}$ and Θ_{N^*}) using the method originally employed by G. Goldhaber et al. at 3.65 GeV/c. Ref. ([2]). For the $N^*\rho$-channel the existence of such a correlation was established; its magnitude was found to be in rough agreement with the expectations from the OPEA-model. For the $N^*\omega$-channel no statistically significant correlation of the above type could be detected.

The present paper deals with preliminary results of a further and more detailed analysis of the reactions (3) and (4).

Five topics will be (briefly) discussed:

I. The differential cross-section as a function of $|t - t_{min}|$ ($|t_{min}|$ being the minimum value of $|t|$ allowed by the masses at both vertices).

II. The constraints implied on the single-vertex density matrix-elements by the positivity of spin density matrix (in function of $|t|$).

III. Preliminary results of an attempt to evaluate the effect of background on the spin-density matrix-elements.

IV. The results of an evaluation of the average value of <u>all</u> joint-decay density matrix-elements (including those expressing correlations between the two vertices) and a study of the variation of these elements as a function of $|t - t_{min}|$.

V. A test of the relations between the spin-density matrix elements obtained by the quark-model and the so-called additivity assumption (Bialas & Zalewski).

We refer to the Heidelberg-paper for all notations and conventions used in this paper and not explicitely redefined here ([1]).

I. DIFFERENTIAL CROSS-SECTIONS $d\sigma/d|t - t_{min}|$.

The differential cross-section for reactions (3) and (4) as a function of $|t - t_{min}|$ is shown in figs. 1 and 2 ([4]).

For the $N^*\rho$-channel the "round-off" of the $d\sigma/d|t|$-distribution at small $|t|$-values has completely disappeared and the $d\sigma/d|t - t_{min}|$-curve remains a pure exponential in $|t - t_{min}|$ up to the lowest transfer allowed. For the $N^*\omega$-channel we observe a plateau extending from zero to about 0.2 $(GeV/c)^2$; above 0.2 $(GeV/c)^2$ the $d\sigma/d|t - t_{min}|$-distribution shows a smooth exponential decrease.

In table I we compare the slopes of the $d\sigma/d|t|$- and $d\sigma/d|t - t_{min}|$-distributions for both the $N^*\rho$ and $N^*\omega$-channel.

II. POSITIVITY CONDITIONS ON THE SPIN-DENSITY MATRIX-ELEMENTS.

P. Minnaert has stressed that the (single-vertex) spin-density matrix-elements must satisfy certain conditions due to the fact that this (hermitian) matrix has positive eigenvalues and unit trace ([5]).

For a spin 1 particle, and for any frame of reference which has the quantization axis in the (2-body) production plane (i.e. the Jackson reference-frame), these conditions are:

$$|\rho^{1,-1}| \leqslant \frac{1 - \rho^{00}}{2} \tag{5}$$

$$|\mathrm{Re}\ \rho^{10}| \leqslant \frac{1}{2}\sqrt{\rho^{00}(1 - \rho^{00} - 2\rho^{1,-1})} \tag{6}$$

For a spin 3/2 particle we find:

$$0 \leqslant \rho_{33} \leqslant \frac{1}{2} \tag{7}$$

$$(\mathrm{Re}\ \rho_{3,-1})^2 + (\mathrm{Re}\ \rho_{31})^2 + (\rho_{33} - \tfrac{1}{4})^2 \leqslant \frac{1}{16} \tag{8}$$

Fig. 3 shows a plot for the $N^*\rho$-channel of $\rho^{1,-1}$ and $\mathrm{Re}\ \rho^{10}$ ($\mathrm{Re}\ \rho_{3,-1}$ and $\mathrm{Re}\ \rho_{31}$) in function of ρ^{00} (ρ_{33}). The projection of

the positivity domain on the 2 dimensional space of the parameters considered, is shown by dashed lines. Positivity requires the points to lie inside this domain. The points with error-flags correspond to the values obtained for the 3 different regions of momentum transfer considered. (See fig. 4 - Ref. ([1])). The black dots correspond to the values of the density matrix elements averaged over a $|t|$-interval from 0-0.3 $(GeV/c)^2$.

Fig. 4 shows a similar plot for the $N^*\omega$-channel. In this case 4 different $|t|$ regions were considered (See fig. 8 - Ref. ([1])) and the black dots now correspond to averages over a $|t|$ range from 0-0.6 $(GeV/c)^2$.

The conclusion is that for both the $N^*\rho$ and $N^*\omega$ channel, the density matrix elements at each vertex are in excellent agreement with the positivity requirements.

III. BACKGROUND EFFECTS.

We have tried to obtain a feeling for the importance of the background-effects on the (single-vertex) density-matrix-elements by the following very simple-minded procedure:

a) evaluation of the density-matrix-element expressions for events lying resp. above, below, to the left and to the right of the double resonance mass-region considered ([6]);

b) averaging of the values obtained under a) (ρ_{BG});

c) estimation of the number of background events in the double resonance region by 2 dimensional interpolation (N_{BG});

d) calculation of a corrected density-element value ρ_c by means of the expression:

$$\rho_c = \frac{\rho \cdot N - \rho_{BG} \cdot N_{BG}}{N - N_{BG}} \qquad (9)$$

where N is the total number of events in the double resonance region and ρ the uncorrected density-matrix-element.

The results are shown in table II. No significant effects are observed. In view of the uncertainties connected with the procedure

sketched above (especially in the case of $N^*\rho$-production) we prefer to look upon the results of table II as an indication that no dramatic background effects are distorting our data and we will continue to use the uncorrected values in our analysis.

IV. JOINT SPIN-DENSITY MATRIX-ELEMENTS.

The general joint-decay angular distribution for a spin 1 and spin 3/2 resonance in terms of the orthogonal functions of the two polar and two azimuthal (Jackson) angles and the joint-decay matrix-elements involved, was given by Pilkuhn and Svensson ([7]) to be of the form:

$$W(\Omega_1, \Omega_{3/2}) = 1 + W_1(\Omega_1) + W_2(\Omega_{3/2}) + W_3(\Omega_1, \Omega_{3/2}) \qquad (10)$$

where the index 1 stands for the vector-meson and the index 3/2 for the N^*.

Inspection shows that $1 + W_1(\Omega_1)$ and $1 + W_2(\Omega_{3/2})$ are the expressions used in the separate spin-density matrix-analyses of the corresponding vertices. $W_1(\Omega_1)$ is a linear expression of the density elements labeled 1 to 3 in table III. Similarly $W_2(\Omega_{3/2})$ is a linear expression of the left-hand side quantities labeled 4 to 6 in table III.

Without any physical angular correlation between the two vertices the overall distribution would read:

$$W'(\Omega_1, \Omega_{3/2}) = 1 + W_1(\Omega_1) + W_2(\Omega_{3/2}) + W_1(\Omega_1)\, W_2(\Omega_{3/2}) \qquad (11)$$

This implies that the presence of correlations between the two vertices will manifest itself by the non-vanishing of:

$$W'' = W_3(\Omega_1, \Omega_{3/2}) - W_1(\Omega_1)\, W_2(\Omega_{3/2}) \qquad (12)$$

The expression W'' can be written as a linear sum of the quantities labeled 7 to 19 in table III ([7]).

For the case of $N^*\rho$ we have introduced two additional angular terms in the expansion of Pilkuhn & Svensson in order to parameterize the observed ρ^o-decay asymmetry in terms of an S-wave background

interference ([8]). The corresponding elements are labeled 20 and 21.

In table III we present our experimental results (derived by means of the so-called method of moments) for the quantities defined in terms of the joint-decay matrix-elements as shown on the L.H.S. The results represent averages over $|t - t_{min}|$ between 0 and 0.2 $(GeV/c)^2$ for $N^*\rho$ and between 0 and 0.6 $(GeV/c)^2$ for $N^*\omega$ (*).

From table III we conclude that there exist three significant correlation terms in the $N^*\rho$-channel, labeled {7}, {12} and {18}, and three in the $N^*\omega$-channel, labeled {12}, {16} and {18} resp. (Significant here means more than 2 standard deviations away from zero). The following is a list of the angular functions which have the above correlation-terms as a co-factor in the Pilkuhn & Svensson-expansion:

$$\{7\} \rightarrow (1 - 3\cos^2\Theta_{\rho(\omega)})(1 - 3\cos^2\Theta_{N^*})$$

$$\{12\} \rightarrow \sin 2\Theta_{\rho(\omega)} \cdot \sin 2\Theta_{N^*} \cos(\phi_{\rho(\omega)} + \phi_{N^*}) \qquad (13)$$

$$\{16\} \rightarrow \sin 2\Theta_{\rho(\omega)} \sin^2\Theta_{N^*} \cos(\phi_{\rho(\omega)} + 2\phi_{N^*})$$

$$\{18\} \rightarrow \sin^2\Theta_{\rho(\omega)} \sin^2\Theta_{N^*} \cos(2\phi_{\rho(\omega)} + 2\phi_{N^*})$$

The correlation implied by the non-vanishing of {7} for $N^*\rho$ is nothing but the Θ_ρ, Θ_{N^*} correlation first noted by Goldhaber et al. at 3.65 GeV/c ([2]) and already reported in our previous paper ([1]).

From the remaining correlations especially the coefficient {12} in the case of $N^*\rho$, and coefficient {18} in the case of $N^*\omega$ are very significant. The genuineness of these correlations has been checked directly by plotting appropiate projections of the W-distributions.

In figs. 5 and 6 we show the $|t - t_{min}|$ dependence of the most significant correlation terms.

Donohue has pointed out that, for simple kinematical reasons, only the $\Theta_{\rho(\omega)} - \Theta_{N^*}$ correlation term and those depending on the

(*) Differences with the results obtained when averaging in terms of |t| are as required negligible. The reader can see this for himself by comparing the first six density elements of table III with those presented in the Heidelberg paper ([1]) and repeated in table II.

azimuthal angles ϕ_1 and ϕ_2 through the sum $(\phi_1 + \phi_2)$ can have non-vanishing values in the forward direction ([10]). From the Pilkuhn-Svensson expansion ([7]) one can see that only the expressions labeled {7}, {12} and {18} contain terms satisfying this requirement. It is reassuring (and to some extend an internal-consistency check on our data and our analysis procedure) that the expressions {7}, {12} and {18} correspond exactly to correlation coefficients which we found to be significant. The fourth one, i.e. {16}, actually the least significant one, is furthermore compatible with becoming zero in the forward direction (see fig. 6). We also stress that our strongest correlation elements, i.e. $\mathrm{Re}(\rho_{31}^{10} - \rho_{31}^{0,-1})$ in the case of $N^*\rho$, and $N^*\omega$ and $\mathrm{Re}(\rho_{3,-1}^{1,-1})$ in the case of $N^*\omega$, obey, within the error-limits, the forward-direction kinematic limits given by Donohue ([10]):

$$|\mathrm{Re}(\rho_{31}^{10} - \rho_{31}^{0,-1})| \leq \sqrt{\tfrac{1}{2}\rho^{00}\rho_{33}} \qquad (14)$$

$$|\mathrm{Re}(\rho_{3,-1}^{1,-1})| \leq \sqrt{\tfrac{1}{2}(1 - \rho^{00} - 2\rho_{33})\rho_{33}} \qquad (15)$$

V. BIALAS & ZALEWSKI QUARK-MODEL PREDICTIONS.

From the quark-model and using only the so-called additivity assumption Bialas & Zalewski derived a set of predictions for the joint-decay density matrix-elements in double resonance production shown in table IV ([3]). In table V we have compared our results of section IV with these predictions. For both the $N^*\rho$ and the $N^*\omega$ channel, the agreement is very satisfactory.

The first Bialas-Zalewski prediction is a relation between single-vertex density matrix-elements. From relation (2) to (6) the L.H.S. contains but correlation terms, the R.H.S. but single-vertex elements. It is trivial to note that each time a single-vertex R.H.S. term (or any combination of R.H.S. terms) has a value significantly different from zero (at a certain momentum transfer), the relations (2) to (6) imply that a certain sum of correlation-elements should also differ significantly from zero (at the same momentum transfer). A particularly interesting example, in which the sum of correlation-terms

can be reduced to a single one, is obtained by looking, for collinear production (i.e. for $|t - t_{min}| \to 0$), at the relation derived by adding the Bialas-Zalewski relations (3) and (4). From the Donohue-argument mentioned above, we know that in this situation, all but one of the L.H.S. coefficients vanish and that therefore, at $|t - t_{min}| = 0$, we should have the equality:

$$4\sqrt{3}\mathrm{Re}(\rho^{1,-1}_{3,-1}) = 1 + 2(\rho_{33} - \rho_{11}) + 4/\sqrt{3}\mathrm{Re}(\rho_{3,-1}) \qquad (16)$$

In fig. 7 we show the dependence on $|t - t_{min}|$ of both sides of Eq.(16) for the reaction $\pi^+ p \to N^*\omega$. The hatched boundary represents the upper limit imposed on the L.H.S. by the second Donohue Eq.(15). The agreement required by Eq.(16) is indeed present. The significance of the test illustrated in fig. 7 resides in the fact that we are looking at a prediction of the quark-model, which is clearly satisfied, and which requires a correlation-element to be equal to a combination of single-vertex quantities (used as "input"), in a situation where this equality does not seem to be imposed by kinematics.

Table I: Comparison of $d\sigma/d|t|$ and $d\sigma/d|t - t_{min}|$-Slopes.

Reaction	$\pi^+ p \to N^* \rho$	$\pi^+ p \to N^* \omega$
$d\sigma/d\|t\|$-Slopes $(GeV/c)^{-2}$	(11.8 ± 0.5)	(3.4 ± 0.3)
$d\sigma/d\|t - t_{min}\|$-Slopes $(GeV/c)^{-2}$	(15.5 ± 1.0)	(3.9 ± 0.3)
$\|t\|$-band $(GeV/c)^2$	$0.05 \to 0.35$	$0.1 \to 0.8$
$\|t - t_{min}\|$-band $(GeV/c)^2$	$0.0 \to 0.25$	$0.2 \to 0.6$

Remark: The mass-bands used are:

1.14 - 1.30 GeV for the N^*

.66 - .86 GeV for the ρ

.74 - .82 GeV for the ω

Table II: Density-Matrix-Elements in $\pi^+ p$-collisions at 5 GeV/c corrected for background as described in section III.

Reaction	$\pi^+ p \to N^* \rho$		$\pi^+ p \to N^* \omega$	
	Before Correct.	After Correct.	Before Correct.	After Correct.
Vector Meson (ρ^0 or ω^0)				
ρ^{00}	0.781 ± 0.024	0.791	0.388 ± 0.039	0.404
Re ρ^{10}	-0.087 ± 0.016	-0.090	-0.126 ± 0.021	-0.135
$\rho^{1,-1}$	-0.058 ± 0.015	-0.069	0.077 ± 0.031	0.085
Baryon (N^{*++})				
ρ_{33}	0.127 ± 0.018	0.129	0.210 ± 0.028	0.215
Re ρ_{31}	-0.059 ± 0.018	-0.070	-0.042 ± 0.028	-0.035
Re $\rho_{3,-1}$	-0.016 ± 0.016	-0.019	0.004 ± 0.026	-0.003
$\|t\|$-range $(GeV/c)^2$	≤ 0.30		≤ 0.60	

Table III: Joint Density Matrix Elements of Resonances in $\pi^+ p$ collisions at 5 GeV/c.

Reaction	$N^*\rho$ $\lvert t-t_{min}\rvert < .2$ GeV^2	$N^*\omega$ $\lvert t-t_{min}\rvert < .6$ GeV^2
{1} ρ^{00}	0.79 ± 0.02	0.39 ± 0.04
{2} $Re(\rho^{10})$	-0.06 ± 0.02	-0.13 ± 0.02
{3} $\rho^{1,-1}$	-0.05 ± 0.02	0.07 ± 0.03
{4} ρ_{33}	0.13 ± 0.02	0.23 ± 0.03
{5} $Re(\rho_{31})$	-0.05 ± 0.02	-0.05 ± 0.03
{6} $Re(\rho_{3,-1})$	-0.02 ± 0.02	0.01 ± 0.03
{7} $(\rho_{33} - \rho_{11}) - 2(\rho^{11} - \rho^{00})(\rho_{33} - \rho_{11})$	0.19 ± 0.08	0.10 ± 0.14
{8} $Re(\rho^{10}) - 2(\rho_{33} - \rho_{11})Re(\rho^{10})$	0.01 ± 0.04	0.02 ± 0.05
{9} $\rho^{1,-1} - 2(\rho_{33} - \rho_{11})\rho^{1,-1}$	-0.00 ± 0.04	-0.05 ± 0.07
{10} $Re(\rho_{31}) - 2(\rho^{11} - \rho^{00})Re(\rho_{31})$	0.07 ± 0.04	0.04 ± 0.07
{11} $Re(\rho_{3,-1}) - 2(\rho^{11} - \rho^{00})Re(\rho_{3,-1})$	0.00 ± 0.04	0.07 ± 0.07
{12} $Re(\rho_{31}^{10} - \rho_{31}^{0,-1}) - 2Re(\rho^{10})Re(\rho_{31})$	-0.14 ± 0.03	-0.09 ± 0.04
{13} $Re(\rho_{31}^{01} - \rho_{31}^{-1,0}) - 2Re(\rho^{10})Re(\rho_{31})$	-0.02 ± 0.03	0.03 ± 0.03
{14} $Re(\rho_{31}^{1,-1}) - \rho^{1,-1}Re(\rho_{31})$	-0.01 ± 0.01	0.03 ± 0.03
{15} $Re(\rho_{31}^{-1,1}) - \rho^{1,-1}Re(\rho_{31})$	-0.01 ± 0.01	0.00 ± 0.03
{16} $Re(\rho_{3,-1}^{10} - \rho_{3,-1}^{0,-1}) - 2Re(\rho^{10})Re(\rho_{3,-1})$	-0.04 ± 0.02	0.10 ± 0.03
{17} $Re(\rho_{3,-1}^{01} - \rho_{3,-1}^{-1,0}) - 2Re(\rho^{10})Re(\rho_{3,-1})$	-0.03 ± 0.02	-0.02 ± 0.03
{18} $Re(\rho_{3,-1}^{1,-1}) - \rho^{1,-1}Re(\rho_{3,-1})$	0.03 ± 0.01	0.14 ± 0.02
{19} $Re(\rho_{3,-1}^{-1,1}) - \rho^{1,-1}Re(\rho_{3,-1})$	-0.02 ± 0.01	-0.02 ± 0.03
{20} $\rho^{0\varepsilon}$	0.215± 0.02	———
{21} $\rho^{1\varepsilon}$	-0.029± 0.01	———

Table IV.

Bialas & Zalewski Quark-Model Predictions.

(Based on the Additivity-Assumption only)

$$\frac{1}{3}\left(\rho^{11}-\rho^{00}\right)+\rho^{1,-1} = \frac{2}{3}\left(\rho_{33}-\rho_{11}\right)+\frac{4}{\sqrt{3}}\,\mathrm{Re}\,\rho_{3,-1} \qquad (1)$$

$$\sqrt{3}\left(\mathrm{Re}\,\rho^{1,-1}_{3,-1}+\mathrm{Re}\,\rho^{-1,1}_{3,-1}\right)+\frac{1}{2}\rho^{1,-1}-\sqrt{3}\,\mathrm{Re}\,\rho_{3,-1}-\frac{1}{2}\left(\rho_{33}-\rho_{11}\right) = \frac{1}{2}\left(\rho^{11}-\rho^{00}\right)-\frac{1}{2}\rho^{1,-1} \qquad (2)$$

$$\sqrt{3}\left(\mathrm{Re}\,\rho^{1,-1}_{3,-1}+\mathrm{Re}\,\rho^{-1,1}_{3,-1}\right)+\frac{1}{\sqrt{3}}\,\mathrm{Re}\,\rho_{3,-1}-\frac{3}{2}\rho^{1,-1}-\frac{1}{2}\left(\rho_{33}-\rho_{11}\right) = \left(\rho_{33}-\rho_{11}\right)-\frac{2}{\sqrt{3}}\,\mathrm{Re}\,\rho_{3,-1} \qquad (3)$$

$$3\sqrt{3}\left(\mathrm{Re}\,\rho^{1,-1}_{3,-1}+\mathrm{Re}\,\rho^{-1,1}_{3,-1}\right)+\frac{3}{2}\rho^{1,-1}+\sqrt{3}\,\mathrm{Re}\,\rho_{3,-1}+\frac{1}{2}\left(\rho_{33}-\rho_{11}\right) = 1+\left(\rho_{33}-\rho_{11}\right)+2\sqrt{3}\,\mathrm{Re}\,\rho_{3,-1} \qquad (4)$$

$$-\sqrt{3}\,\mathrm{Re}\,\rho^{10}-3\left[\mathrm{Re}\left(\rho^{10}_{3,-1}-\rho^{0,-1}_{3,-1}\right)+\mathrm{Re}\left(\rho^{01}_{3,-1}-\rho^{-1,0}_{3,-1}\right)\right] = \sqrt{3}\,\mathrm{Re}\,\rho^{10} \qquad (5)$$

$$-\sqrt{2}\,\mathrm{Re}\,\rho_{31}-3\sqrt{2}\left(\mathrm{Re}\,\rho^{1,-1}_{31}+\mathrm{Re}\,\rho^{-1,1}_{31}\right) = 2\sqrt{2}\,\mathrm{Re}\,\rho_{31} \qquad (6)$$

Table V.

Bialas-Zalewski Quark Model Predictions

Experimental Test for 5 GeV/c π^+ on Protons.

$\pi^+ p \to N^* \rho$			
Relation	L.H.S.	R.H.S.	L.H.S.-R.H.S.
(1)	$-.28 \pm .02$	$-.21 \pm .05$	$-.07 \pm .05$
(2)	$-.29 \pm .10$	$-.32 \pm .02$	$.03 \pm .10$
(3)	$-.26 \pm .12$	$-.22 \pm .04$	$-.04 \pm .12$
(4)	$.40 \pm .14$	$.69 \pm .07$	$-.29 \pm .16$
(5)	$.11 \pm .12$	$-.15 \pm .03$	$.26 \pm .13$
(6)	$-.17 \pm .11$	$-.15 \pm .05$	$-.02 \pm .11$

$\pi^+ p \to N^* \omega$			
Relation	L.H.S.	R.H.S.	L.H.S.-R.H.S.
(1)	$.04 \pm .04$	$-.03 \pm .07$	$.07 \pm .08$
(2)	$.00 \pm .15$	$-.08 \pm .04$	$.08 \pm .15$
(3)	$.28 \pm .15$	$-.08 \pm .06$	$.36 \pm .16$
(4)	$.70 \pm .20$	$.95 \pm .11$	$-.25 \pm .22$
(5)	$-.32 \pm .17$	$-.22 \pm .03$	$-.10 \pm .17$
(6)	$-.18 \pm .18$	$-.14 \pm .08$	$-.04 \pm .20$

REFERENCES

(1) Double Resonance Production by 5 GeV/c π^+ mesons on protons.
(Bonn-Durham-Nijmegen-Paris-Strasbourg-Turin Collaboration).
Paper presented at Heidelberg Conference on Elementary Particles;
September 1967. (Copies available upon request by writing to
Prof. R.T. Van de Walle - Fysisch Laboratorium, 200,
Driehuizerweg, NIJMEGEN - Netherlands).

(2) G. Goldhaber, J.L. Brown, I. Butterworth, S. Goldhaber, A. Hirata,
J.A. Kadyk, B.C. Shen and G.H. Trilling;
Physics Letters, 18, 76 (1965).

(3) A. Bialas and K. Zalewski;
Jagellonian University Preprint TPJU - 18/67. (November 1967).

(4) J.T. Donohue;
CERN Preprint - Ref. Th. 884. (October 1967).

(5) P. Minnaert;
Phys. Rev. Letters 16, 672 (1966) and Phys. Rev. 151, 1306 (1966).

(6) The 9 mass-regions included are defined by the following mass-bands (in GeV):

for the ρ^0 : 0.56 → 0.66 and 0.86 → 0.96
for the ω^0 : 0.60 → 0.70 and 0.85 → 0.95
for the N^{*++}: 1.06 → 1.14 and 1.30 → 1.38

(7) H. Pilkuhn and B.E. Svensson;
Nuovo Cimento 38, 518 (1965).

(8) I. Derado et al.;
Phys. Rev. Letters 14, 872 (1965); See also Ref.(7) in Ref.(1).

(10) J.T. Donohue;
CERN Preprint - Ref. Th. 749 (February 1967).

Fig. 1

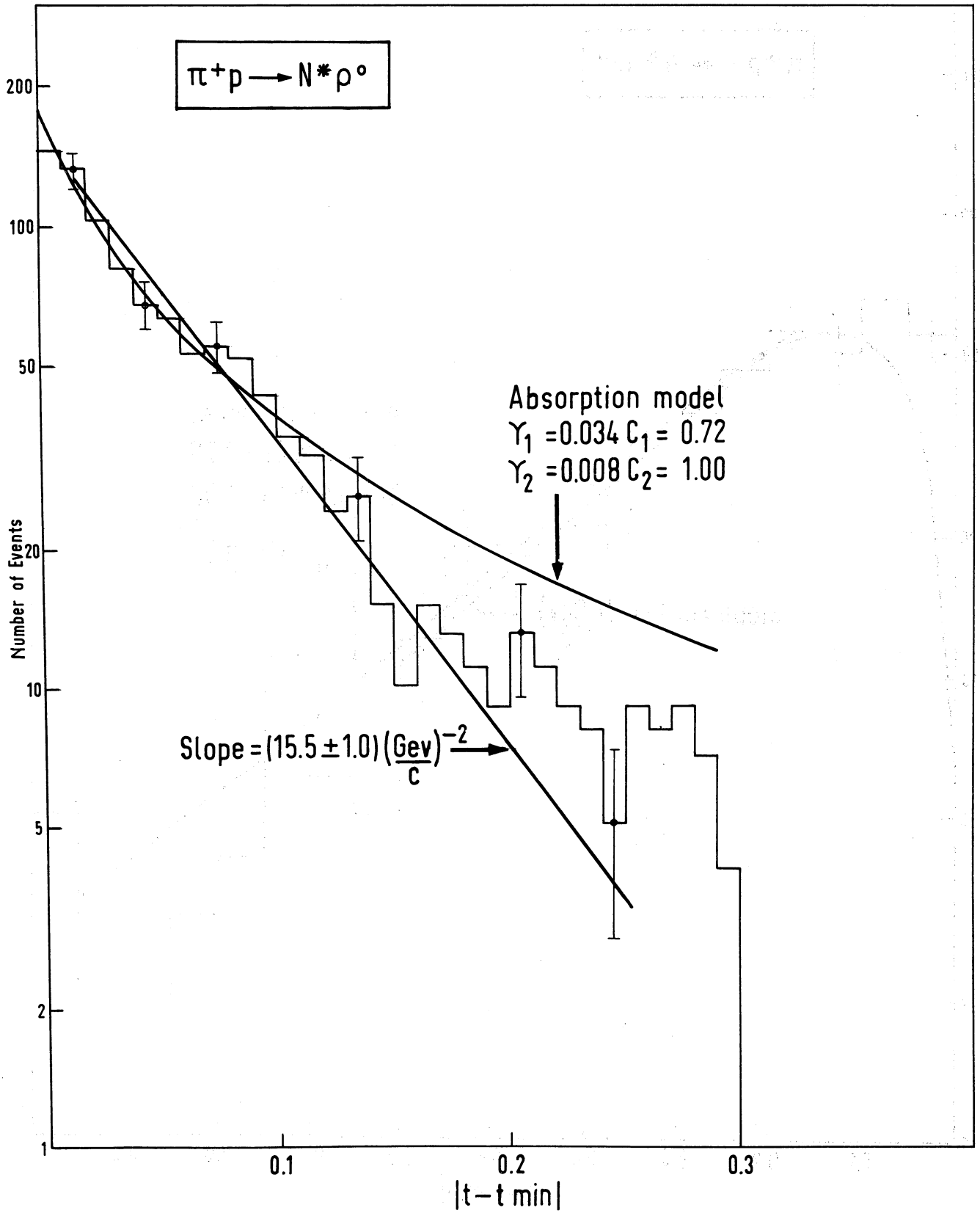
$\pi^+ p \rightarrow N^* \rho^\circ$
Absorption model
$\gamma_1 = 0.034$ $C_1 = 0.72$
$\gamma_2 = 0.008$ $C_2 = 1.00$
Slope = $(15.5 \pm 1.0) \left(\frac{Gev}{c}\right)^{-2}$
Number of Events
200
100
50
20
10
5
2
1
0.1
0.2
0.3
$|t - t\ min|$

Fig. 2

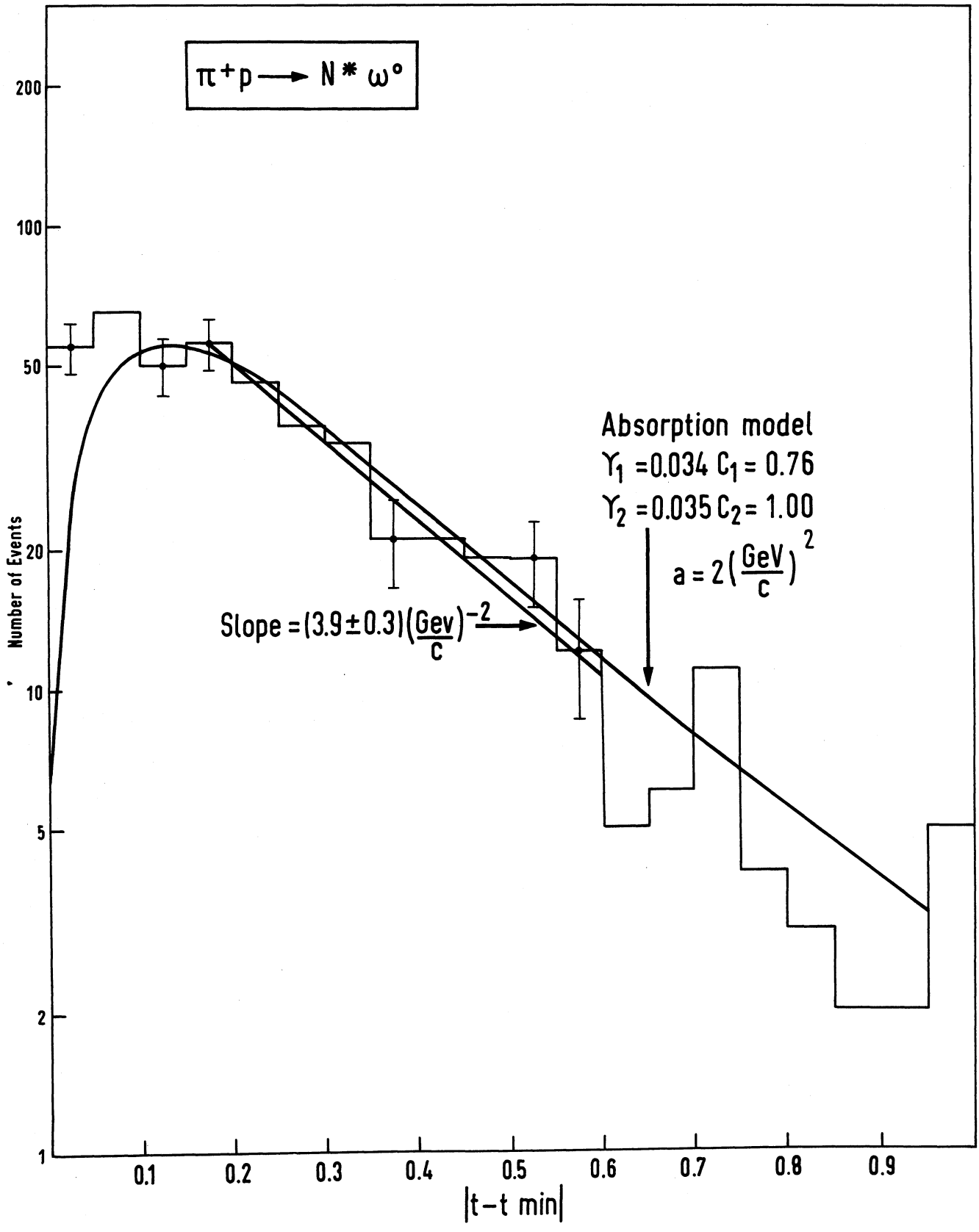
$\pi^+ p \longrightarrow N^* \omega^\circ$
Absorption model
$\gamma_1 = 0.034$ $C_1 = 0.76$
$\gamma_2 = 0.035$ $C_2 = 1.00$
$a = 2\left(\frac{GeV}{c}\right)^2$
Slope $= (3.9 \pm 0.3)\left(\frac{Gev}{c}\right)^{-2}$
Number of Events
200
100
50
20
10
5
2
1
0.1
0.2
0.3
0.4
0.5
0.6
0.7
0.8
0.9
$|t - t\ min|$

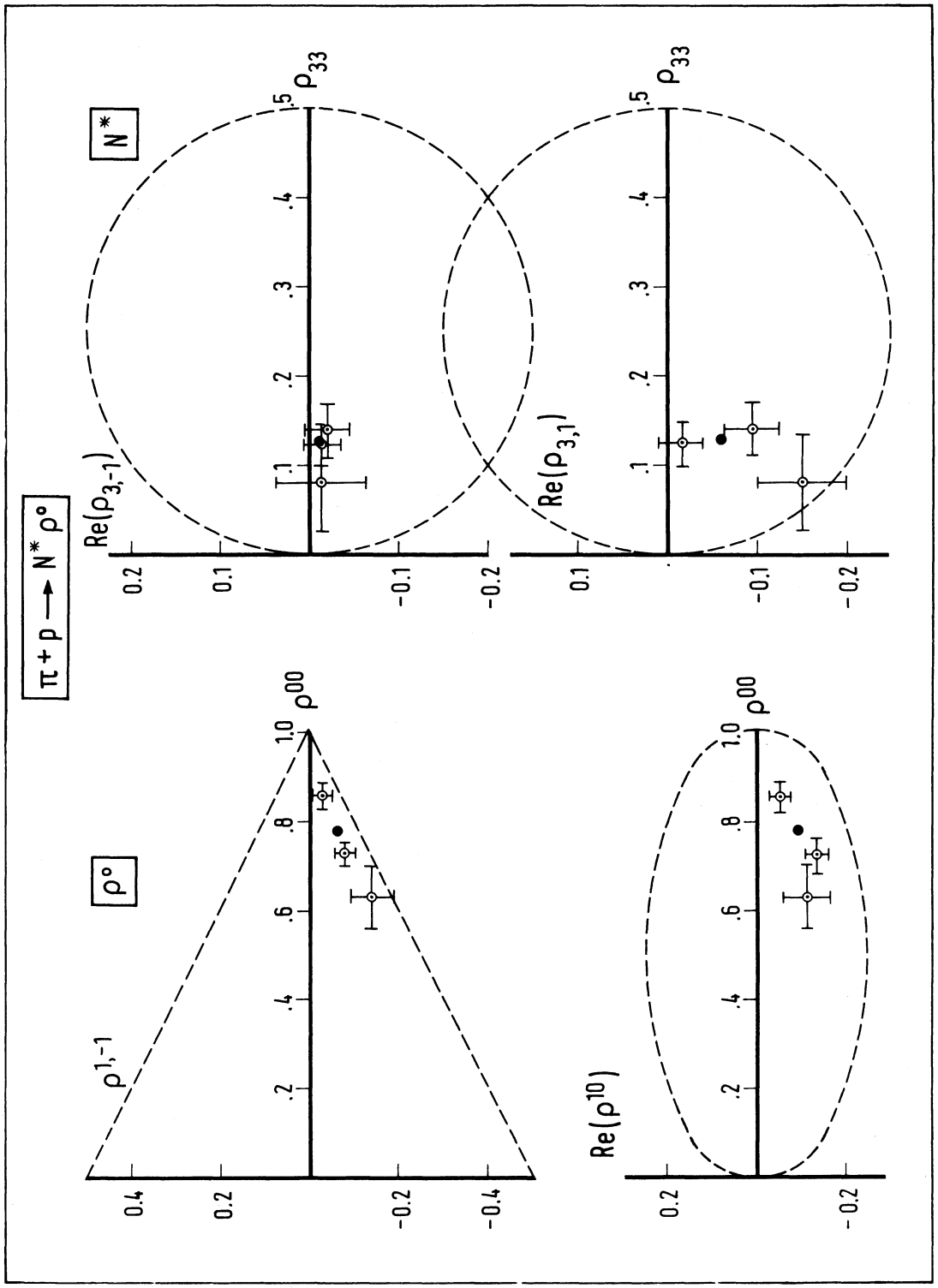
π + p → N* ρ°
N*
ρ°
ρ33
ρ00
Re(ρ3,-1)
Re(ρ3,1)
ρ1,-1
Re(ρ10)
0.2
0.1
-0.1
-0.2
0.4
-0.4
.1
.2
.3
.4
.5
.6
.8
1.0

Fig. 3

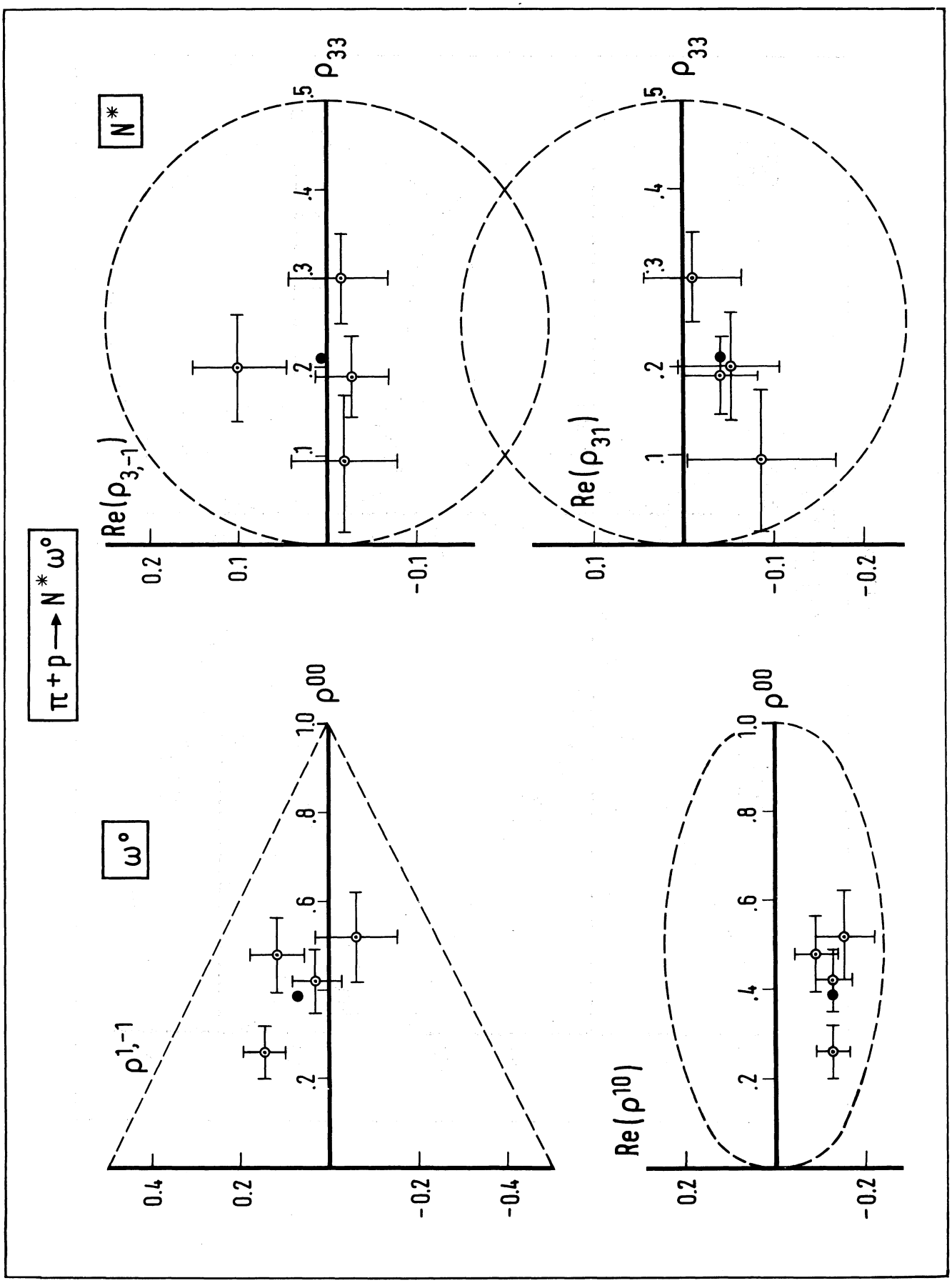
π⁺p → N*ω°
N*
ω°
ρ33
ρ00
Re(ρ3,-1)
Re(ρ31)
ρ1,-1
Re(ρ10)
0.2
0.1
-0.1
-0.2
0.4
-0.4
.1
.2
.3
.4
.5
.6
.8
1.0

Fig. 4

Fig. 5

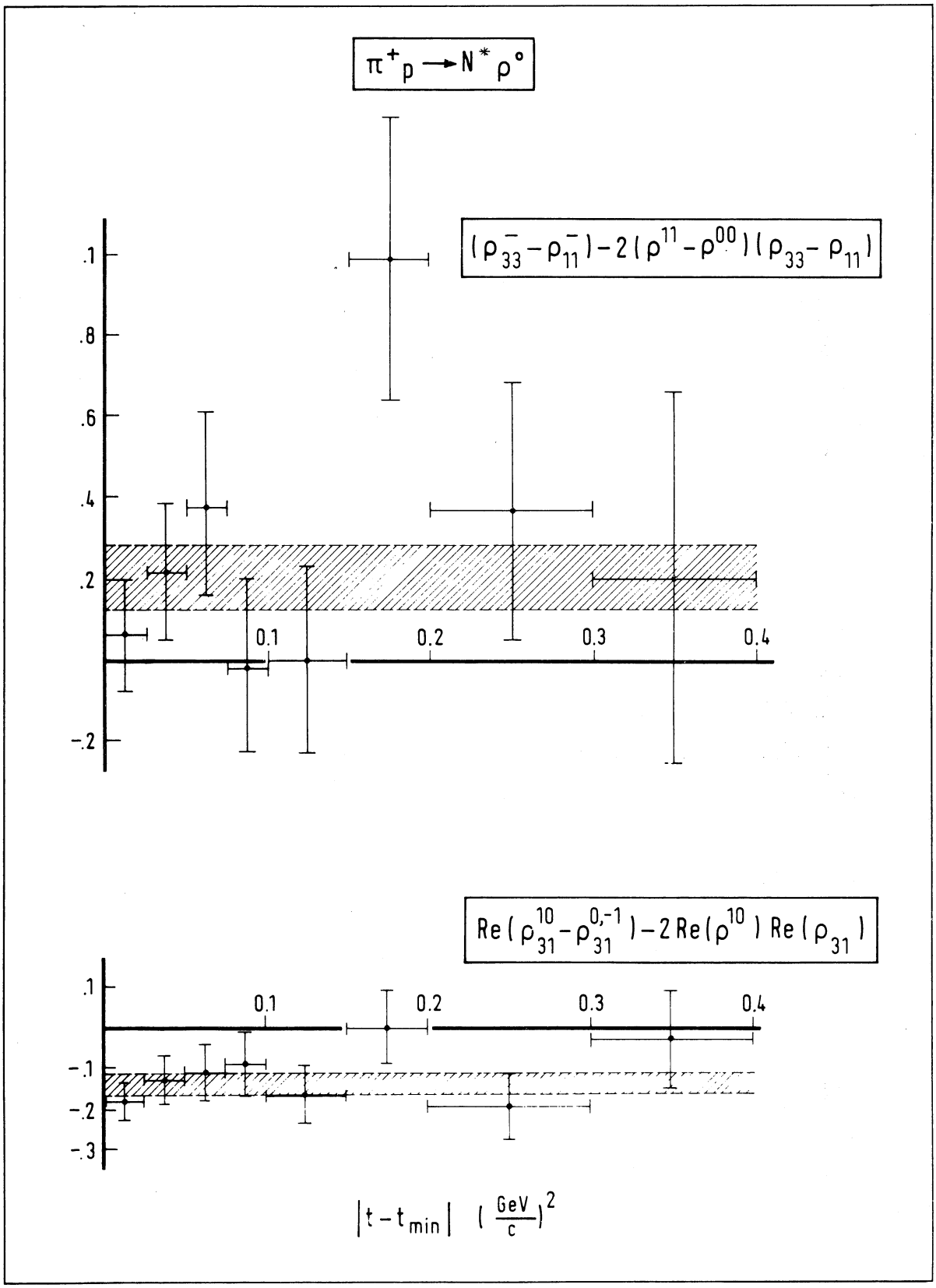
$\pi^+ p \rightarrow N^* \rho^\circ$
$(\rho_{33}^- - \rho_{11}^-) - 2(\rho^{11} - \rho^{00})(\rho_{33} - \rho_{11})$
.1
.8
.6
.4
.2
-.2
0.1
0.2
0.3
0.4
$\mathrm{Re}(\rho_{31}^{10} - \rho_{31}^{0,-1}) - 2\,\mathrm{Re}(\rho^{10})\,\mathrm{Re}(\rho_{31})$
.1
-.1
-.2
-.3
0.1
0.2
0.3
0.4
$|t - t_{min}|$ $(\frac{GeV}{c})^2$

Fig. 6

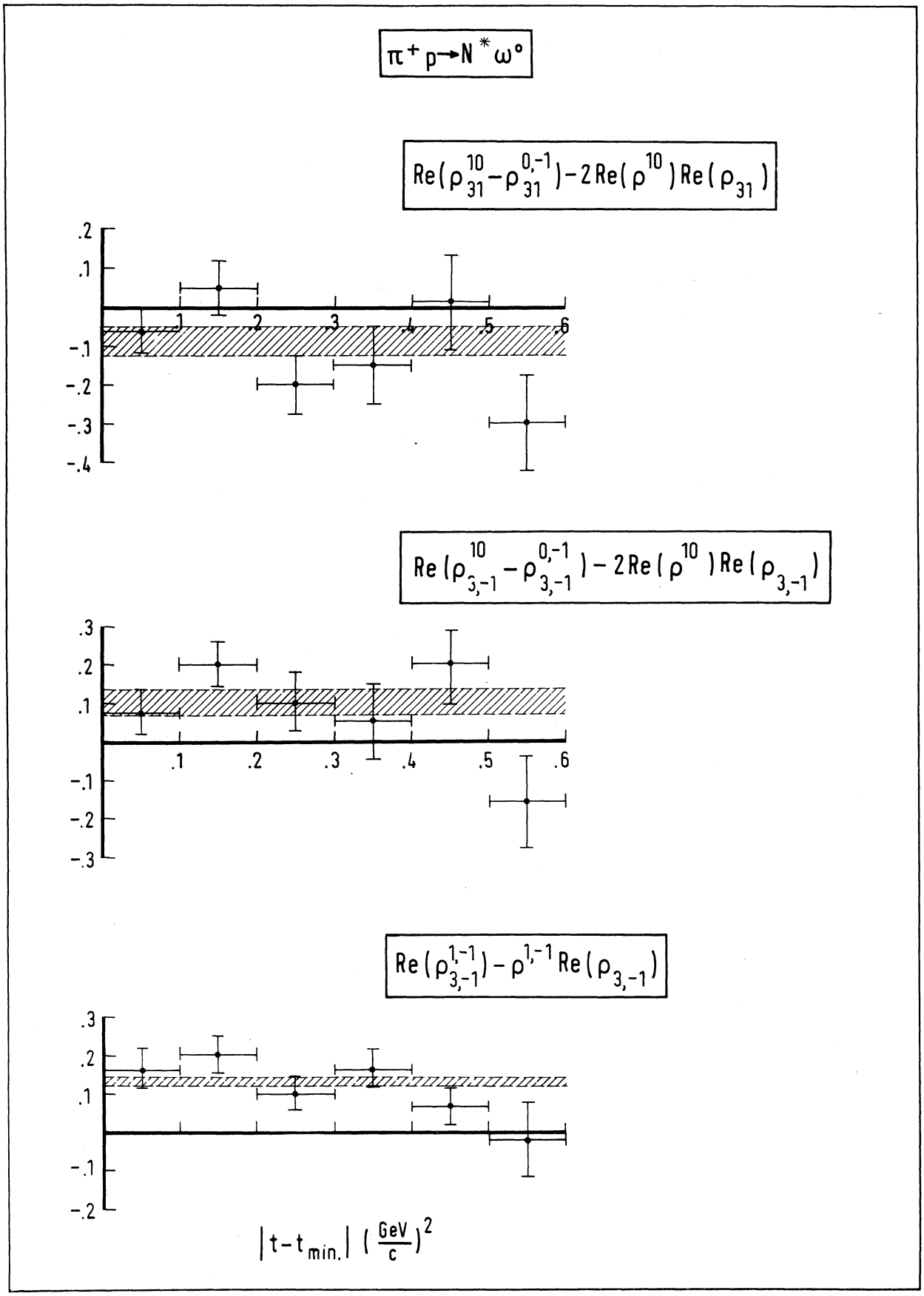
$\pi^+ p \to N^* \omega^\circ$
$Re(\rho_{31}^{10} - \rho_{31}^{0,-1}) - 2Re(\rho^{10})Re(\rho_{31})$
.2
.1
-.1
-.2
-.3
-.4
1
2
3
4
5
6
$Re(\rho_{3,-1}^{10} - \rho_{3,-1}^{0,-1}) - 2Re(\rho^{10})Re(\rho_{3,-1})$
.3
.2
.1
-.1
-.2
-.3
.1
.2
.3
.4
.5
.6
$Re(\rho_{3,-1}^{1,-1}) - \rho^{1,-1}Re(\rho_{3,-1})$
.3
.2
.1
-.1
-.2
$|t - t_{min.}|$ $(\frac{GeV}{c})^2$

Fig. 7

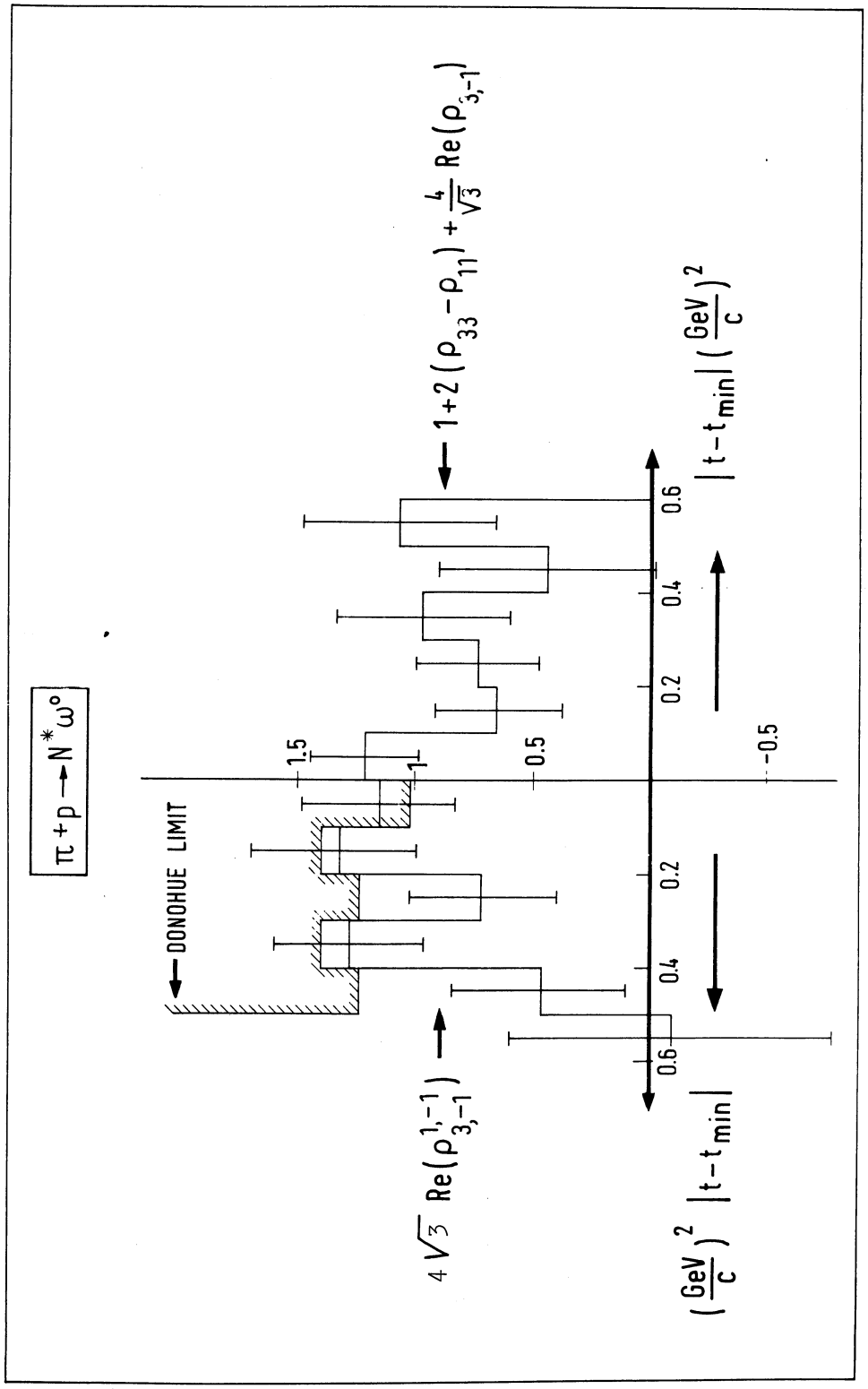
$\pi^+ p \rightarrow N^* \omega^\circ$
DONOHUE LIMIT
$1+2(\rho_{33}-\rho_{11})+\frac{4}{\sqrt{3}}\,\mathrm{Re}(\rho_{3,-1})$
$4\sqrt{3}\,\mathrm{Re}(\rho^{1,-1}_{3,-1})$
$|t-t_{min}|\,(\frac{GeV}{c})^2$
$(\frac{GeV}{c})^2\;|t-t_{min}|$
1.5
1
0.5
-0.5
0.2
0.4
0.6

K^+p INTERACTIONS AT 13 GEV/C*

J.C. Berlinghieri, M.S. Farber, T. Ferbel, B.E. Forman, A.C. Melissinos, P.F. Slattery, + T. Yamanouchi and H. Yuta

University of Rochester
Rochester, New York ++

We present a comparison of the characteristics of several relatively uncomplicated final states which we are studying in our 12.73 GeV/c K^+p experiment.[1] Table I enumerates the reactions of interest.[2]

Table I Reaction Cross Sections

	Final State	Cross Section (μb)
1.	$pK^{*+}(890)$ $\hookrightarrow K^0\pi^+$	57 ± 9
2.	$K^0N^*(1236)^{++}$	50 ± 9
3.	$K^+K^+\Lambda$	12 ± 3
4.	$p\ p\ \bar{\Lambda}$	6 ± 2
5.	$n\ \pi^+K^*(890)^+$ $\hookrightarrow K^0\pi^+$	75 ± 25
6.	$p\ Q^+$	440 ± 80(a)
	$\hookrightarrow K^+\pi^+\pi^-$	230 ± 60
	$\hookrightarrow K^0\pi^+\pi^0$	210 ± 50
7.	K^+B^+ $\hookrightarrow p\ \pi^+\pi^-$	250 ± 70(b)

(a) We refer to the enhancement at low $(K\pi\pi)^+$ mass as Q.

(b) We refer to the enhancement at low $(p\pi\pi)^+$ mass as B.

---

* Research supported by the United States Atomic Energy Commission

+ A.E.C. Post Doctoral Fellow

++ Authors hold guest appointments at Brookhaven National Laboratory

The quasi two-body reactions (1) and (2), which have been studied extensively at lower energies,[3] come from the $K^0p\pi^+$ final state. The Dalitz plot for these events is in Fig. 1, and it shows prominent $N^*(1236)^{++}$, $K^*(890)^+$ and $K^*(1420)^+$ signals. Figure 2 gives the momentum transfer spectra, and the resonance decay angular distributions for reactions (1) and (2).[4] The curves in Fig. 2 (a) are predictions of the absorption model.[5] Although the experimental momentum-transfer dependence is sharper than the model predicts it to be, the total cross section and the angular distributions predicted are nevertheless in excellent agreement with the data. In Fig. 2 (b) we show, for the decay of $N^*(1236)$, the predictions of the Stodolsky-Sakurai (ρ-photon analogy) model. This model does not agree as well with the data, and this is more clearly evident in the comparison of the density matrix elements we give in Table II.

Table II Density Matrix Elements[(a)]

Reaction (1)	$\rho_{0,\,0}$	$\rho_{1,\,-1}$	Re $\rho_{1,\,0}$
Data	0.00 ± 0.08	0.42 ± 0.08	-0.06 ± 0.04
Donohue	0.07	0.43	-0.03
Reaction (2)	$\rho_{3,\,3}$	Re $\rho_{3,\,-1}$	Re $\rho_{3,\,1}$
Data	0.23 ± 0.08	0.12 ± 0.09	0.08 ± 0.08
M-1 Model	0.38	0.22	0.0

(a) Calculated using method of moments. The K^* band used is 840 to 960 MeV, the N^* band used is 1120 to 1360 MeV. The momentum transfer region considered is $\Delta^2 < 0.7$ GeV^2.

Dalitz plots for the three-body reactions (3), (4) and (5) listed in Table I are given in Figs. 3, 4 and 5. The existence of two identical particles in both reactions (3) and (4) requires the Dalitz plots to be symmetric about the 45° line. However, in these reactions one of the two identical particles is usually produced forward (F) in the center of mass while the other one is emitted into the backward (B) hemisphere. We have therefore "unfolded" these Dalitz plots by labeling the identical particles as F or B depending on which of the two is produced more forward in the center of mass. For the events in reaction (4) the two protons were always found to go into opposite hemispheres. In reaction (3), on the other hand, approximately 30% of the time both of the K^+ mesons go forward.[6]

All three Dalitz plots show very similar enhancements in the low mass regions. The observed peaking at threshold in the π^+n, ΛK^+, and $p\bar{\Lambda}$ systems could simply be due to resonance formation.[7]

Production angular distributions of particles from reactions (3), (4) and (5) are shown in Fig. 6. The proton and π^+ angular distributions are symmetric and are peaked forward-backward in the center of mass system. The K^+ in the $K^+K^+\Lambda$ state has a strong forward peak but only a small backward enhancement. The Λ and the neutron are emitted strongly peaked in the direction of the incident proton, while the $\bar{\Lambda}$ follows the direction of the incident K^+. Of the 13 $\bar{\Lambda}$ two proceed in the backward direction.[8]

We have examined the Treiman-Yang azimuthal distributions (not shown) for the systems: $K_B^+\Lambda$, $p_F\bar{\Lambda}$, $\pi_F^+K^{*+}$, π_B^+n and for the K^{*+} decay. Although the statistics are poor the data for $K_B^+\Lambda$, $p_F\bar{\Lambda}$, $\pi_F^+K^{*+}$ and for K^* decay are consistent with isotropy (all at χ^2 probabilities higher than 0.15) while the results for the π_B^+n system show considerable anisotropy in φ_{TY}.[9]

The last two reactions we shall discuss involve the production of $K\pi\pi$ and $p\pi\pi$ systems with low effective mass. These reactions have their analogs in πp and pp interactions.[10] Lately there has been much interest in the characteristics of the $K\pi\pi$ (1300) mass region; we will not try here to resolve the problem of how many resonances (if any) exist at ~ 1300 MeV. We will assume that we can refer to the entire low mass enhancement as one unique object Q^+ (our data are consistent with this assumption). Similarly, for the $(p\pi\pi)^+$ system we will refer to the entire enhancement observed at low mass as B^+.

Figure 7(a) shows the sum of the two $(K\pi\pi)^+$ invariant mass spectra from the four-body states $K^+\pi^+\pi^-p$ (σ = 950 ± 100 μb) and $K^o\pi^+\pi^op$ (σ = 565 ± 70 μb). The distributions are highly consistent with each other and we have therefore added them to increase statistical accuracy. In the same graph, appearing cross-hatched, is the $K^o\pi^+\pi^+$ mass spectrum from the final state $K^on\pi^+\pi^+$ (σ = 130 ± 40 μb).

Figure 7(b) shows an effect similar to the Q; this is the large accumulation of events at low $p\pi^+\pi^-$ mass. Note that in analogy to the $K^o\pi^+\pi^+$ mass distribution the $p\pi^+\pi^o$ effective mass spectrum (shown cross-hatched) does not give this type of enhancement. In what follows we consider the Q mass region between 1.1 and 1.4 GeV,[11] and the B^+ $(p\pi\pi)^+$ mass region between 1.3 and 2.2 GeV. From the graphs in Fig. 7 it is clear that the background problem in the Q^+ data will not be as severe as in the B^+ events.

The next two figures show the momentum transfer distributions for the Q^+ and B^+ samples. We have superimposed on the data the shape of the elastic K^+p scattering cross section, and normalized it to the total number of events. The Q^+ spectrum falls off strongly in the forward direction while the B^+ does not show as strong a drop-off at $\Delta^2 = 0$.[12] At small values of Δ^2 ($\lesssim$ 0.1 GeV^2)

both distributions (but particularly the Q^+) have slopes in Δ^2 considerably steeper than that of the elastic K^+p distribution.

The Q^+ decays mainly into $\pi K^*(890)$ and into $K\rho$, the B^+ goes into $\pi N^*(1236)$. In Fig. 10 we show some of the decay properties of these low mass enhancements.[13] We see that the Treiman-Yang azimuthal angular dependences in the decay of the $Q \rightarrow \pi K^*$ ($B \rightarrow \pi N^*$) and the $K^* \rightarrow \pi K$ ($N^* \rightarrow \pi p$) appear consistent with isotropy. Also in contrast to the $\pi K^* \pi$ channel the distributions in the Jackson angle of the $K^* \rightarrow \pi K$ and $N^* \rightarrow \pi p$ decays indicate essentially complete alignment along the beam axis.[14]

As noted in Table I the total Q production cross section in the K^o and in the K^+ reactions is about the same as the cross section for the B enhancement (~ 250 μb). These processes thus account for a substantial part of the production cross section.[15]

References

1. The film is from 80,000 exposures of the 80-inch BNL liquid hydrogen chamber to the radio-frequency separated beam at the AGS. For information on the beam see H.W.J. Foelsche et al, Rev. Sci. Inst. 38, 879 (1967). For previous work on this experiment see J.C. Berlinghieri et al, Phys. Rev. Letters 18, 1087 (1967), University of Rochester Report UR-875-218, September 1967 (unpublished), and Proceedings of 1967 Athens Conference on Resonant Particles (to be published).

2. The cross sections which appear in the table have been corrected for neutral decays of the strange particles; also, cross sections for resonance production have been corrected for the Breit-Wigner tails of these resonances.

3. See, for example, Y. Goldschmidt-Clermont et al, CERN/TC/Physics Report 66-17; also, see J.H. Friedman and R.R. Ross, Phys Rev Letters 16, 485 (1966).

4. These are the conventionally defined decay angles - the azimuth φ_{TY} is the Treiman-Yang angle, θ_J is the Jackson or "scattering" angle. See for example N. Schmitz, CERN Report 65-24 Vol I, June 1965.

5. We thank Dr. J. Donohue for communicating his calculations to us. A mixture of π and vector exchange is used in the model; in extrapolating his calculations to our energy Dr. Donohue has assumed that the energy dependence of the vector meson couplings goes as the inverse of the incident laboratory momentum.

6. Comparing our results from reactions (3) and (4) to those at lower energies we find that at 13 GeV these events show more peripheral behavior in their angular distributions; also the invariant mass spectra

exhibit more clearly the characteristic enhancements near threshold. See C.Y. Chien et al, Physics Letters 25B, 426 (1967), also G. Bassompierre et al, Nuovo Cimento 48A, 589 (1967) for comparisons with lower energy data.

7. There also appears to be some broad enhancement in the π^+K^{*+} and in the K^+K^+ low mass regions.

8. These $\bar{\Lambda}$ are slow in the laboratory, their ionizations were checked and found to agree with the expected ionization predictions.

9. It is also interesting that the $K^{*+}(890)$ appears to be produced not aligned with respect to the beam direction, the decay distribution in the Jackson angle is isotropic in cos θ.

10. For a discussion of the A_1 characteristics see G. Goldhaber and S. Goldhaber UCRL-16744, March 1966 (Berkeley Report). Also see P. Slattery et al, Nuovo Cimento 50, 377 (1967) and references therein. For the low mass baryon systems see E.W. Anderson et al, Phys Rev Letters 16, 855 (1966), also P.L. Connolly et al, "Study of pp Interactions at 28.5 GeV/c", Proceedings of 1967 Athens Conference on Resonant Particles (to be published), and E. Gellert et al, Phys Rev Letters 17, 884 (1966).

11. We chose 1.4 GeV as the upper mass cut-off because of the possible confusion with $K^*(1420)$. The events in the $K^*(1420)$ region, as well as in the L-meson region exhibit momentum-transfer characteristics very similar to those of the Q events. We wish to point out that we do not expect to see much $K^*(1420)$ in these data due to its small production cross section ($\sigma = 25 \pm 8$ μb in the $K^0\pi^+p$ channel).

12. To avoid the problems of kinematic limits due to the spread in the effective masses of the Q and B we have examined the production angles in

the center of mass, the distributions in these variables give the same results as the Δ^2 spectra.

13. For the Q study we have restricted ourselves to the $K^+\pi^+\pi^-$ events. Here the $K^*(890)$ signal from the Q decay is much larger than the ρ^o signal, further, there is only one K^* possible. The $K^o\pi^+\pi^o$ Q events have a large amount of ρ^+ in the decay and in addition two K^* decay modes are possible. The interference effects can be very insidious and we have therefore chosen only the $K^+\pi^+\pi^-$ events for this study.

14. The small asymmetries observed in the B^+ data could be due to either the background events or to chosing the wrong N^* [we have ignored the possibility of $B^+ \rightarrow N^*(1236)^o\pi^+$]. It is interesting however that the asymmetry in the $N^*(1238)^{++}$ Jackson angle is the same as that observed in "off-shell" π^+p scattering analyses. See, for example, T. Ferbel et al, Phys Rev 138 B, 1528 (1965), and last paper in Reference 10.

15. An enhancement similar to the B^+ in the $\pi^+p \rightarrow \pi^+\pi^+\pi^-p$ reaction at 7 GeV/c is observed by the Rochester-Yale Collaboration, the estimated cross section for this B^+ analog is 320 ± 80 μb. We have also estimated the equivalent B^+ cross section from the state $pp\pi^+\pi^-$ in 6.6 GeV/c pp data of E. Gellert et al, and in the 28.5 GeV/c pp data of P.L. Connolly et al (Ref. 10), we find the cross sections for the B region in these data is approximately 450 μb. The B cross sections thus do not appear to be strong functions of the energy or of the nature of the interacting particles. Q production is also known to have a weak energy dependence (see second paper in Ref. 1). For a discussion of non-resonant diffractive processes see M. Ross and Y.Y. Yam, Phys Rev Letters 19, 546 (1967). Also with regard to $p \rightarrow \Lambda K^+$ and $K^+ \rightarrow \bar{\Lambda}p$ diffractive dissociation (which may be pertinent to our data) see M.L. Good and W.D. Walker, Phys Rev 120, 1857 (1960).

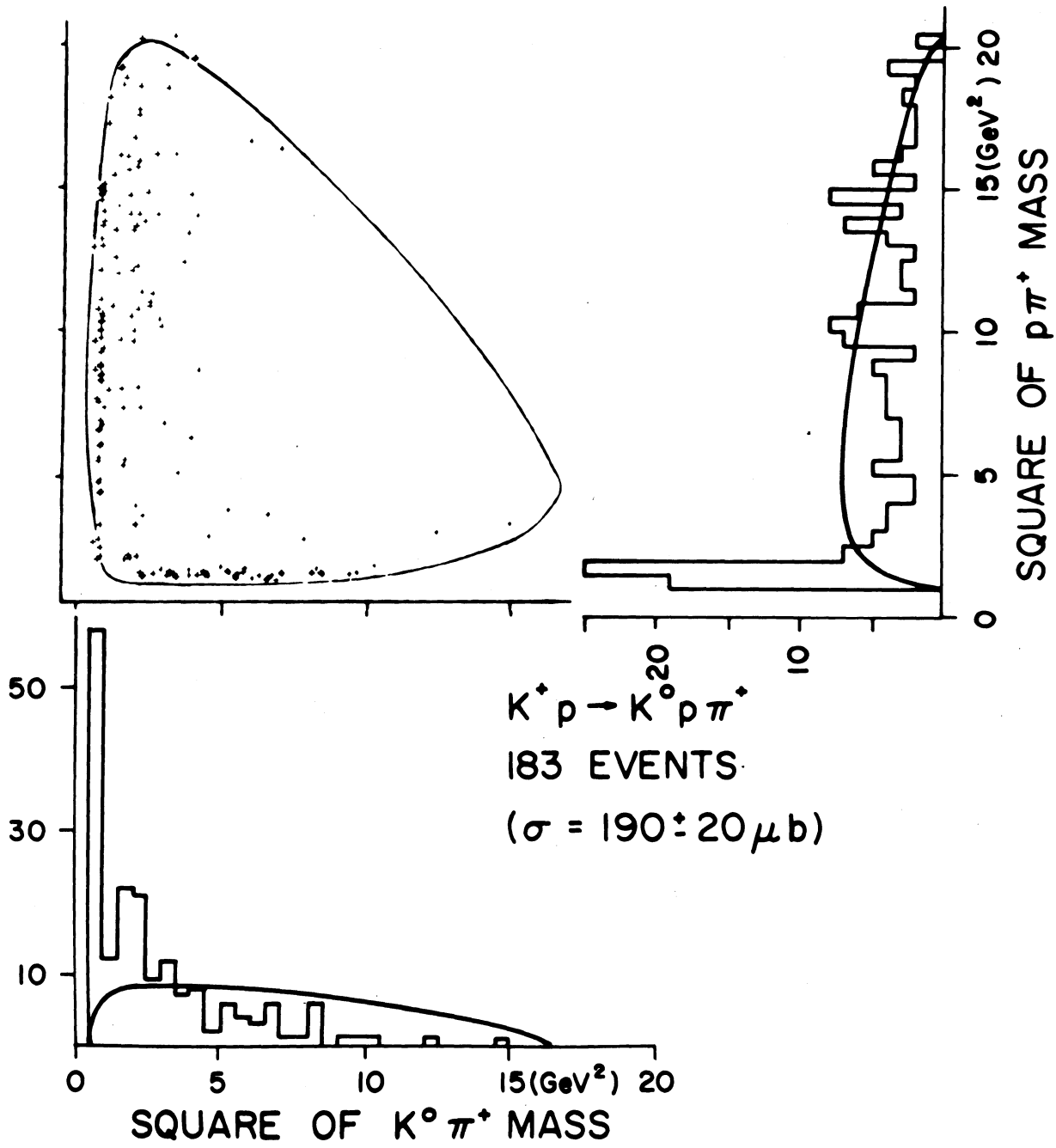

1. $K^0p\pi^+$ Dalitz plot. The predictions from the invariant phase space are drawn on the projected mass spectra.

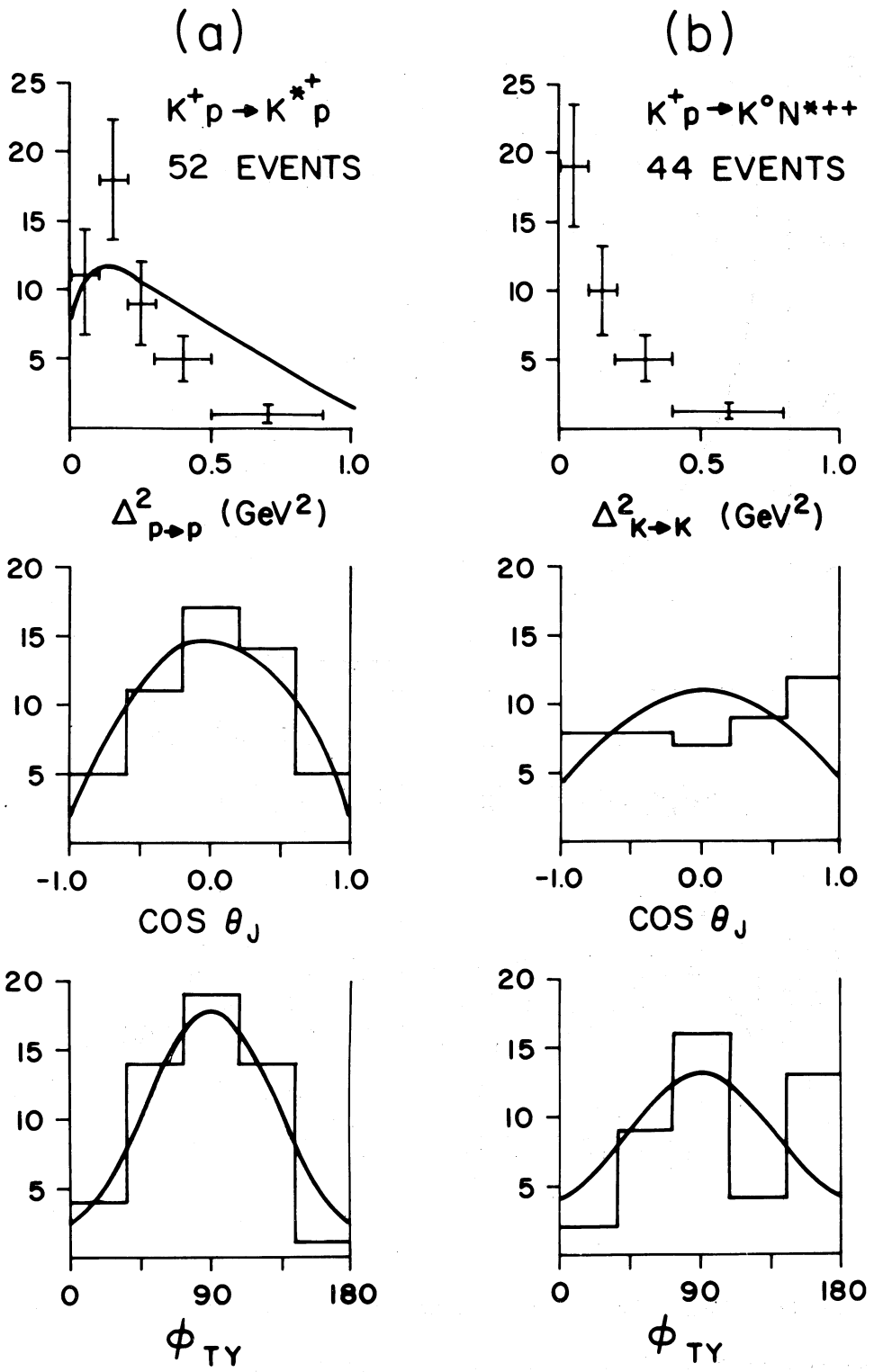

2. The square of the momentum transfer, the decay Jackson and Treiman-Yang angles are shown for reaction (1), and (2) in (a), and (b) respectively. See text for explanation of curves.

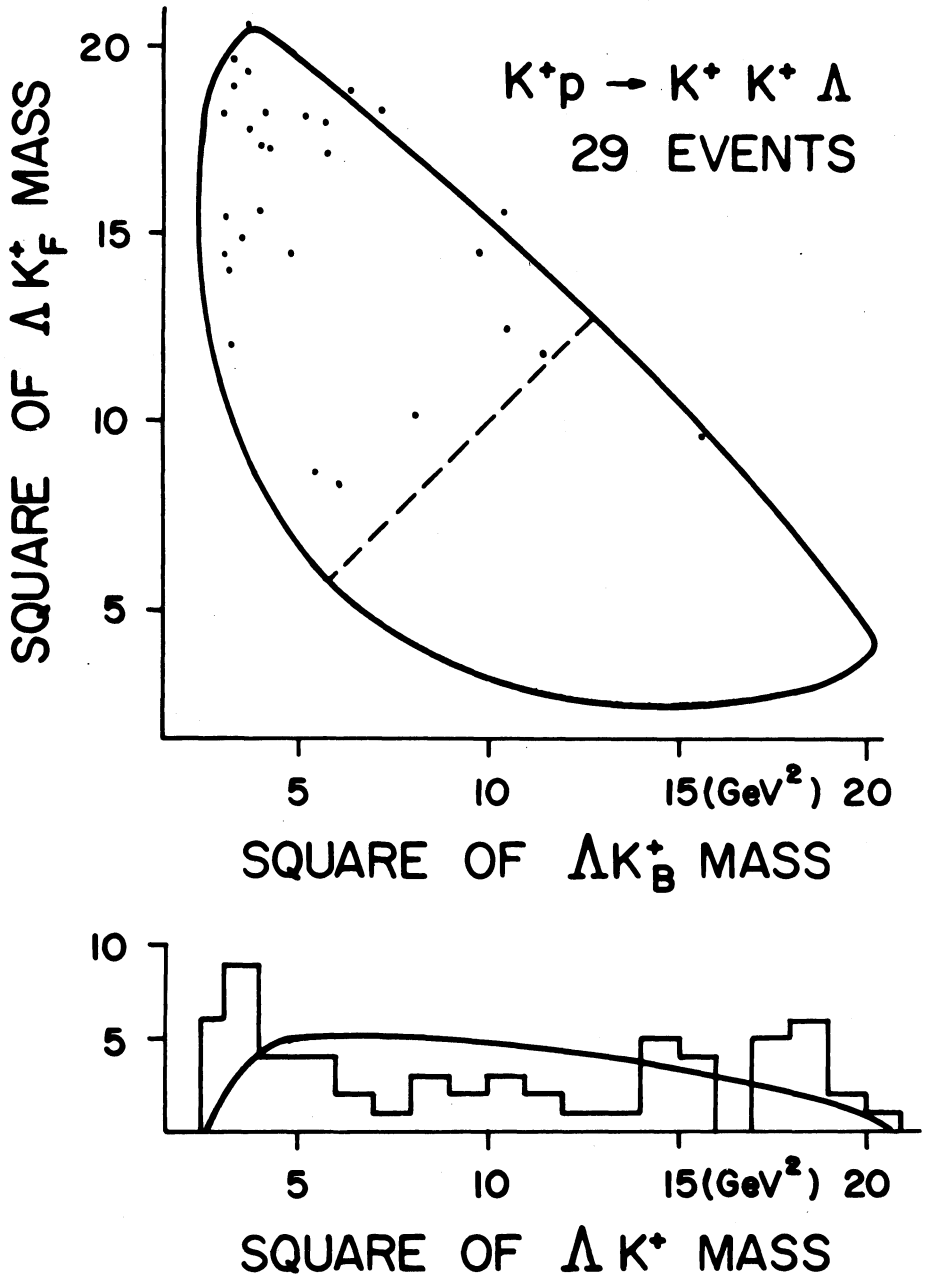

3. $K^+K^+\Lambda$ Dalitz Plot. Unfolded as described in the text. The smooth curve on the sum of the ΛK^+ mass projections is the phase space.

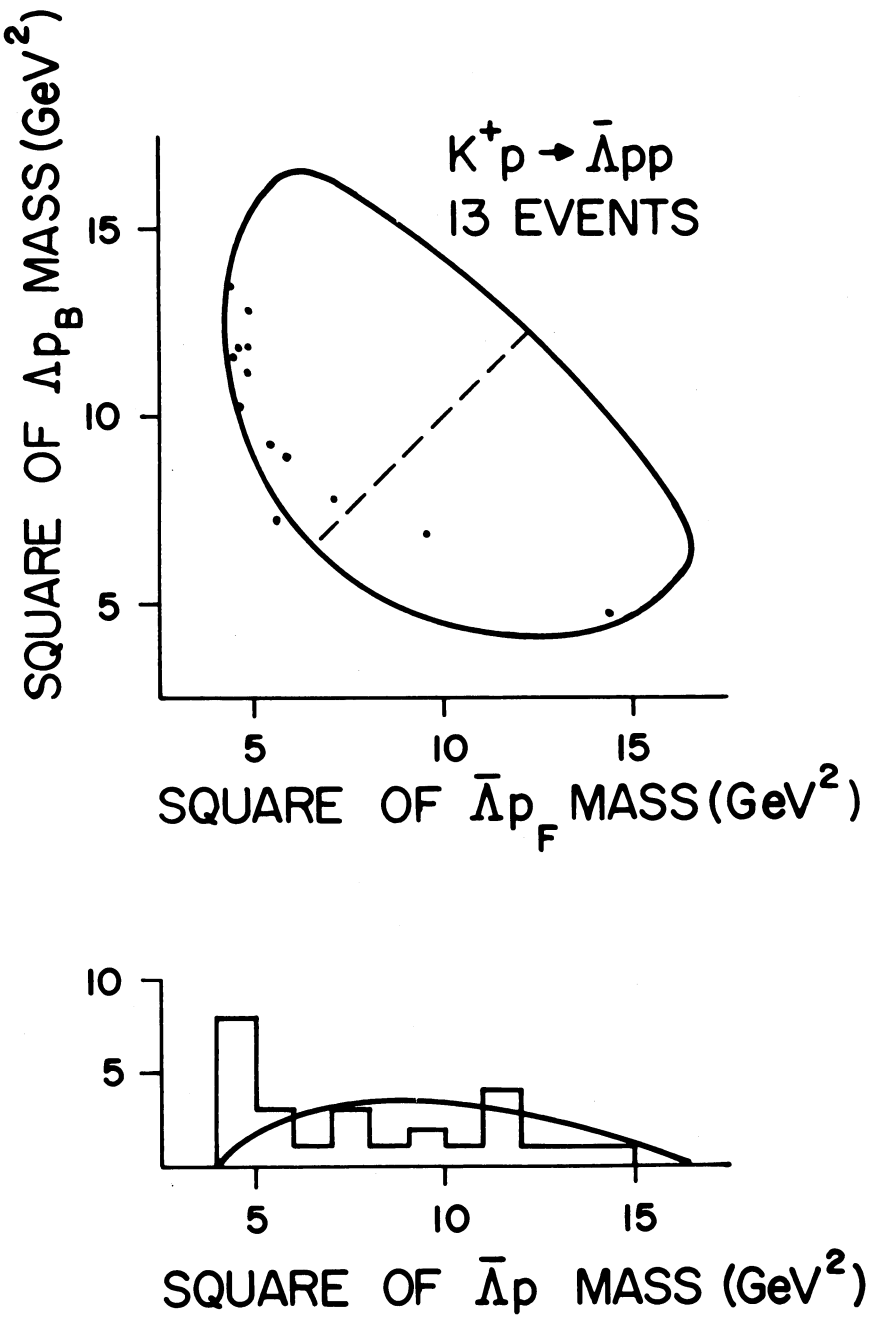

4. $pp\bar{\Lambda}$ Dalitz Plot. Unfolded as described in the text. The smooth curve on the sum of the $\bar{\Lambda}p$ mass projections is the phase space.

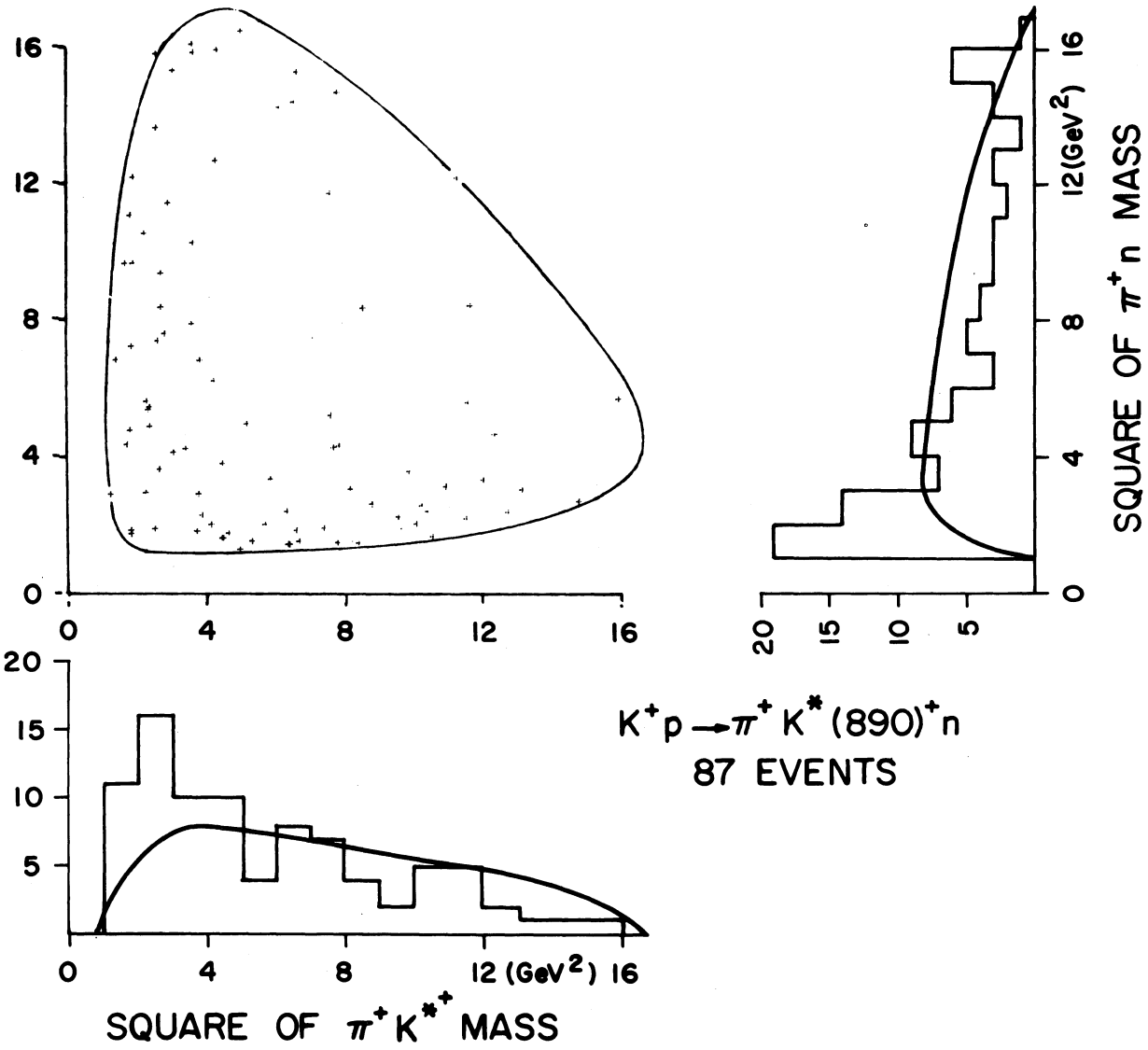

5. $K^*(890)^+ n\pi^+$ Dalitz Plot. The predictions from the invariant phase space are drawn on the projected mass spectra.

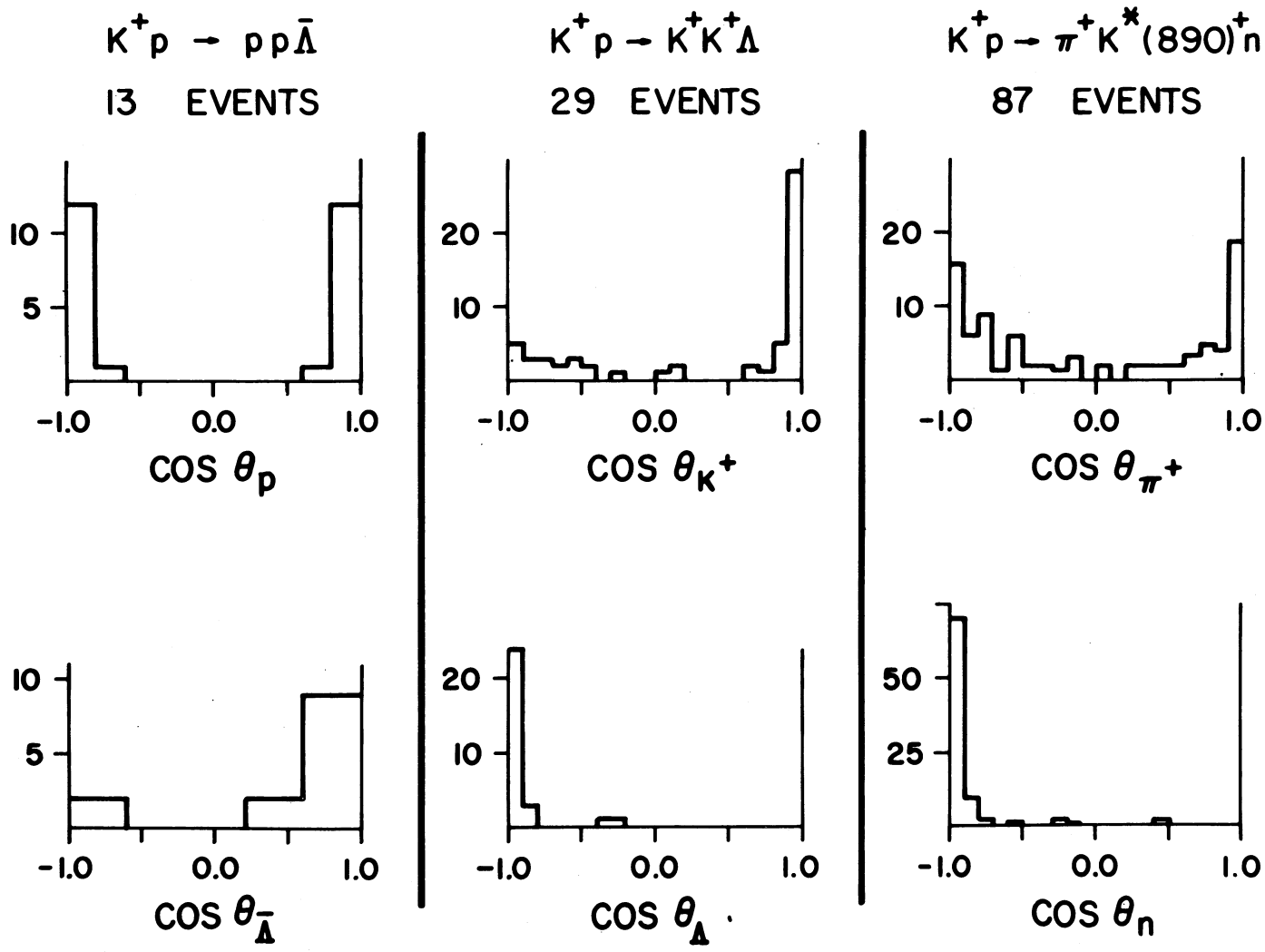

6. Production angular distribution in the center of mass system for reactions (3), (4) and (5).

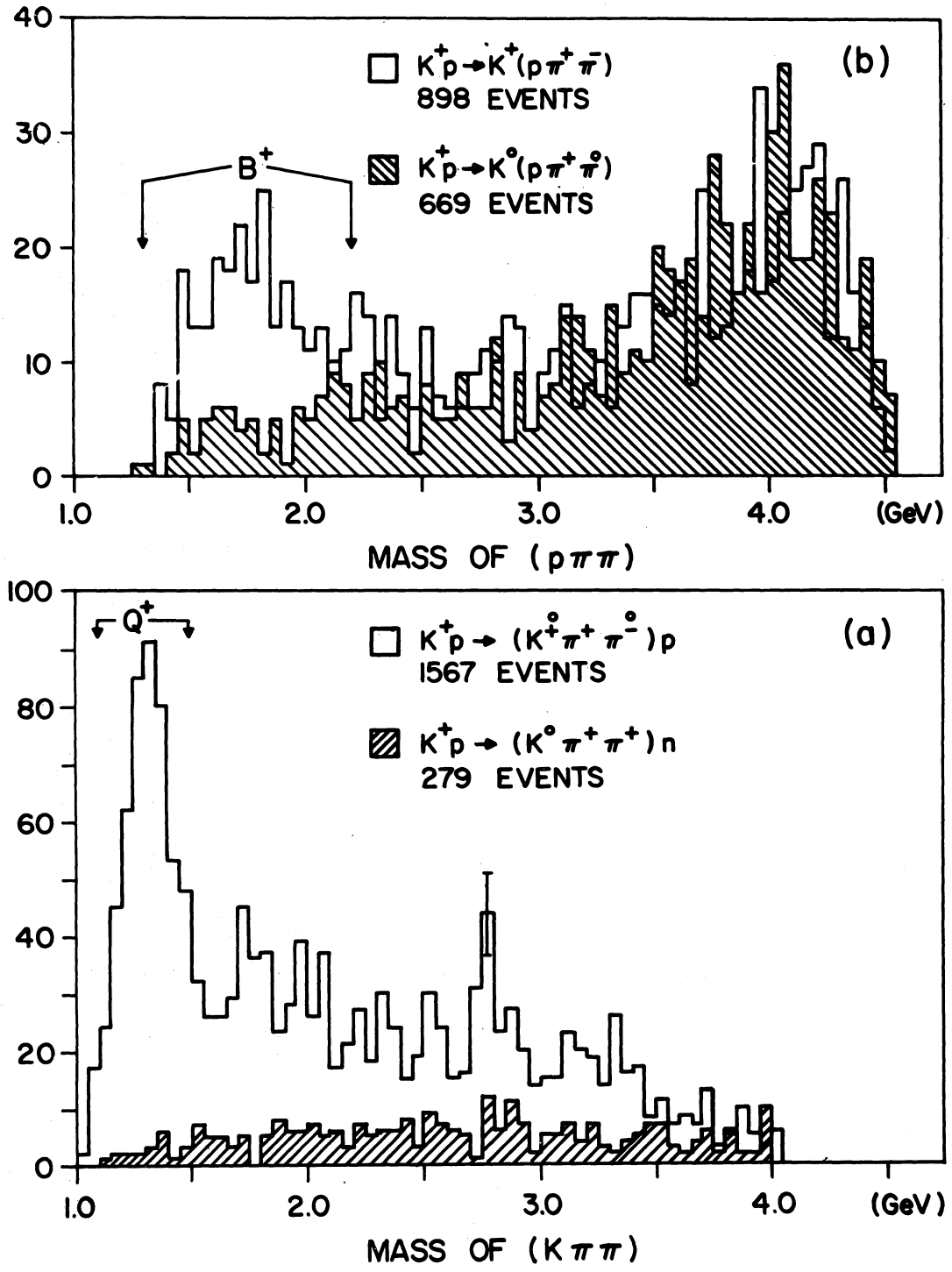

7. (a). Invariant mass distributions of the $(K\pi\pi)^+$, and $(K\pi\pi)^{++}$ systems from the final states $K^+\pi^+\pi^-p$, and $K^\circ\pi^+\pi^+n$ respectively.

(b). Invariant mass distributions of the $(p\pi\pi)^+$, and $(p\pi\pi)^{++}$ systems from the final states $K^+\pi^+\pi^-p$, and $K^\circ\pi^+\pi^\circ p$ respectively.

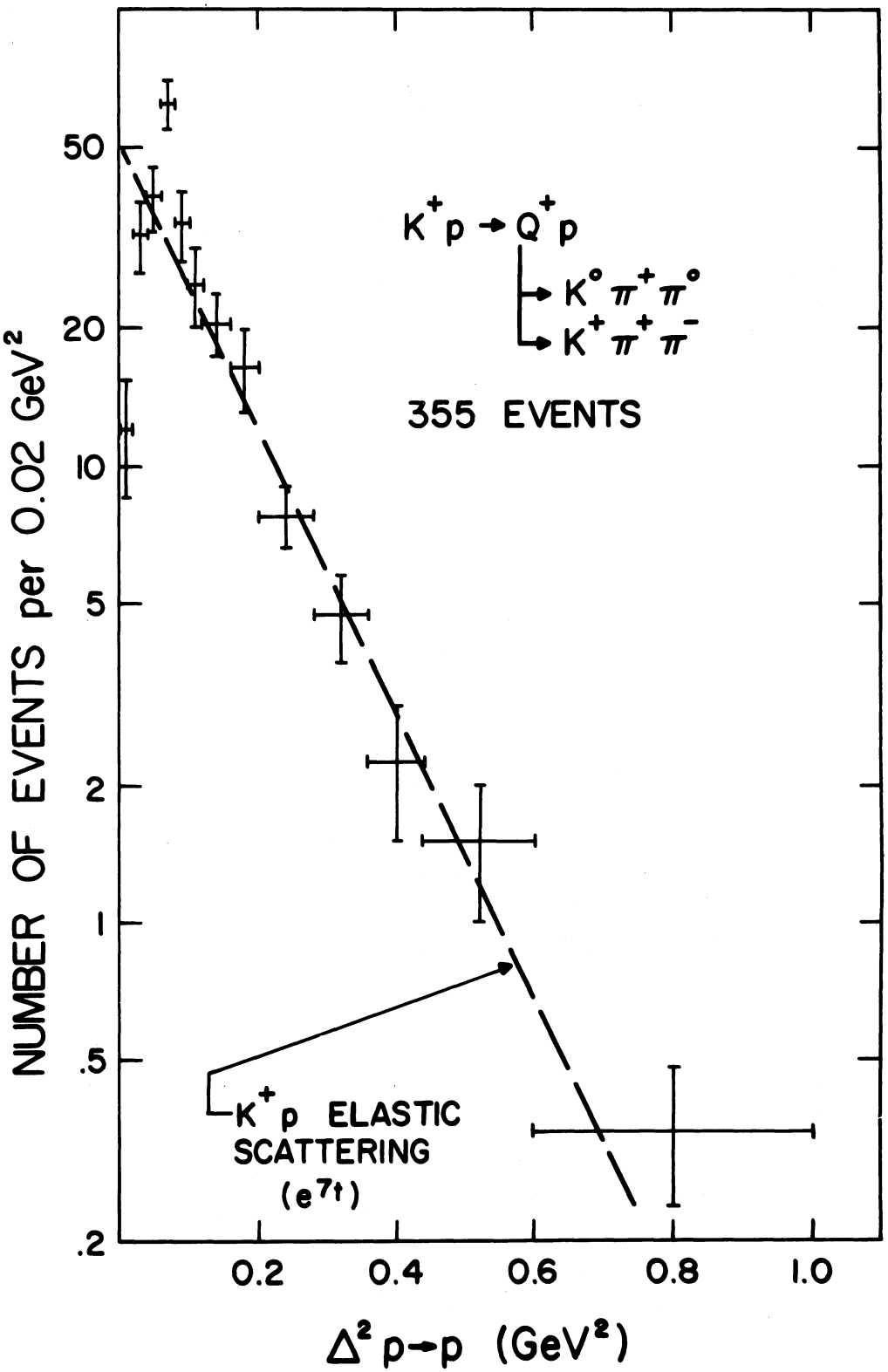

8. Square of the four-momentum transfer from target to final state proton for the Q^+ events.

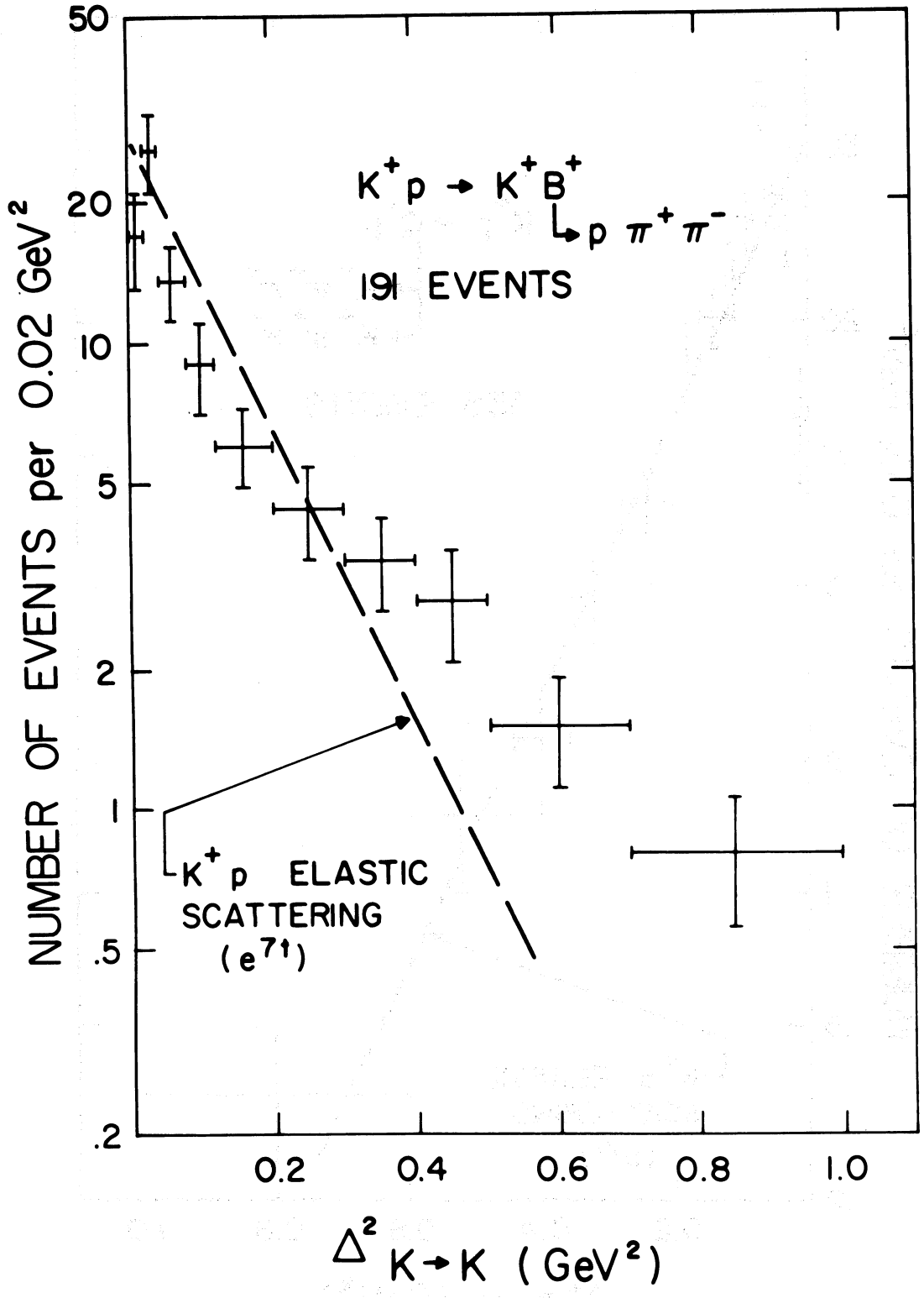

9. Square of the four-momentum transfer from the beam K^+ to the final state K^+ for B^+ events.

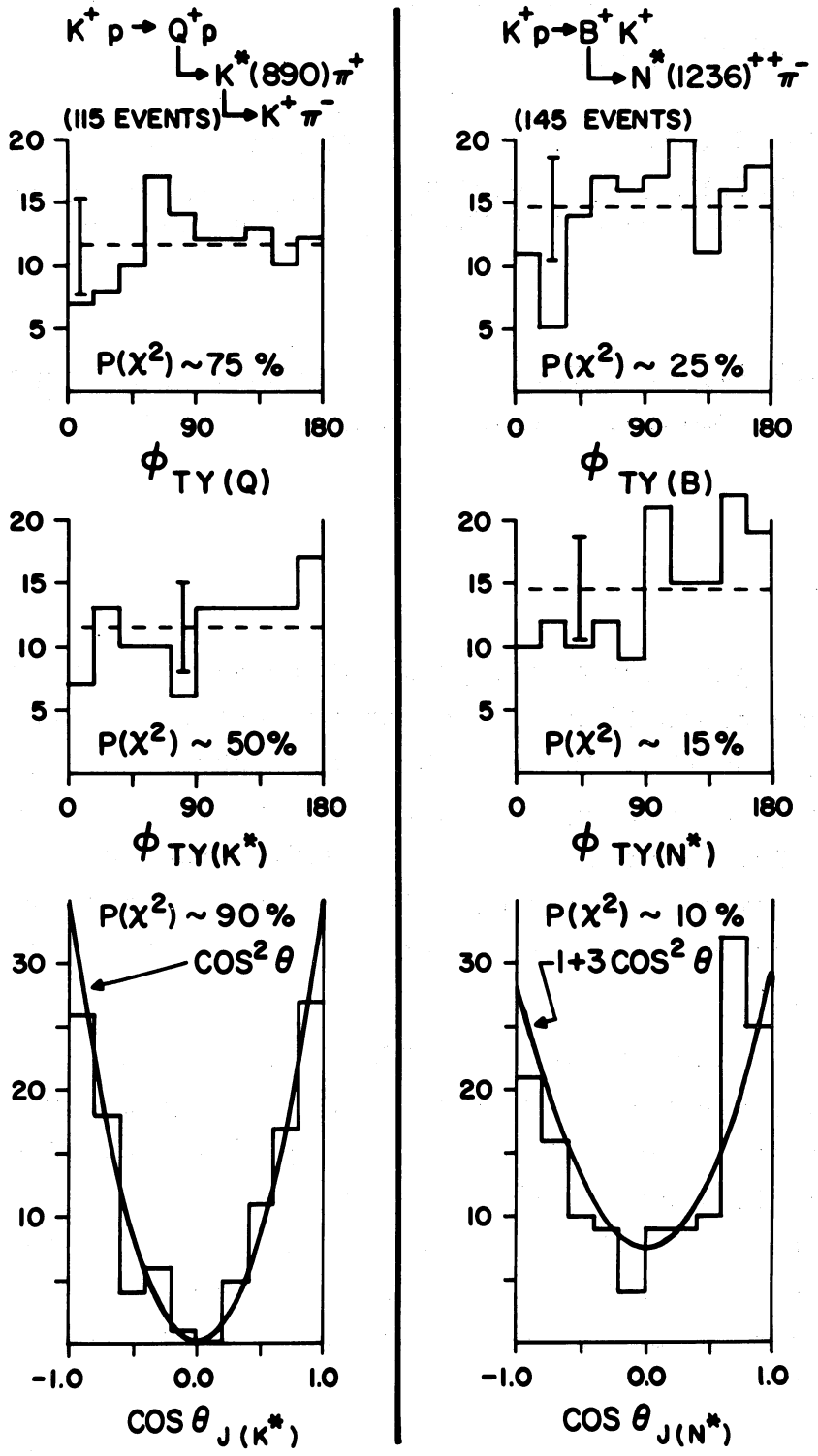

10. Decay characteristics of the Q^+ and B^+ events with $\Delta^2 < 1.0$ GeV^2. The $P(\chi^2)$ values indicate the degree of consistency in the hypothesis that the data are described by the smooth curves on the graphs.

FURTHER RESULTS ON $\pi^- p \rightarrow K^o Y^o$ IN THE FORWARD DIRECTION AT 6, 8 AND 11.2 GEV/C.

E. BERTOLUCCI, I. MANNELLI, G. PIERAZZINI, A. SCRIBANO, F. SERGIAMPIETRI, M.L. VINCELLI - Istituto di Fisica dell' Università di Pisa and I.N.F.N., Sezione di Pisa, Italy

and

C. CAVERZASIO, J.P. GUILLAUD[+], L. HOLLOWAY, M. YVERT - Institut du Radium, Orsay, France

ABSTRACT

A spark chamber experiment to measure the $\pi^- p \rightarrow K^o Y^o$ associated production at high energy has been recently completed at the CERN PS. Data has been taken at 6,8,10, 11.2 GeV/c for the incident π^- momentum. We present here further results (Ref.1) at 6, 8 and 11.2 GeV/c based on ~1100, 1300 and 3000 events (about 60%, 65% and 90% of the available statistics) respectively selected for the differential cross sections.

The sum of the $\pi^- p \rightarrow K^o \Lambda^o$ and $\pi^- p \rightarrow K^o \Sigma^o$ differential cross sections is strongly peaked in the forward direction and can be well fitted, for $|t_{min}| \leq |t| \leq 0.4$ $(GeV/c)^2$, by an exponential shape e^{at} with $a=8.0\pm0.5$ at 6, $a=7.7\pm0.5$ at 8 and $a=7.8\pm0.4$ $(GeV/c)^{-2}$ at 11.2 GeV/c. The integral over the interval $|t_{min}| \leq |t| \leq 1.01$ $(GeV/c)^2$ gives 40.5 ± 6 μb at 6, 25.3 ± 4 μb at 8 and 18 ± 3 μb at 11.2 GeV/c, including systematic errors.

A comparison is made with previous bubble and spark chamber results and Regge Poles fits.

[+] CERN Fellow.

1.- EXPERIMENTAL APPARATUS.

The experimental apparatus is shown schematically in Fig.1. The π^- beam, tipically 10^5 particles per burst, is focused on the 1.5 cm diameter, 10 cm long liquid hydrogen target(1), which is concentric with a cylindrical spark chamber containing both thin Al and Pb plates. The beam is defined electronically by four scintillation and two Cerenkov counters. Two hodoscopes, with 7×2 and 7×7 elements respectively, determine the incident π^- position with a ±.2 cm uncertainty at the target and ±.5 cm at the last spark chamber.

A picture is taken each time an incident π^- fails to give a pulse in the anticoincidence counter surrounding the target while at the same time a pulse is detected in the counter placed in front of the second spark chamber.

The hodoscope information is then BCD coded and displayed on the same film where the 90° stereo images(2) of the spark chambers are recorded. While the two thin Al foil S.C. are designed to detect the charged tracks with a minimum of multiple scattering, the last spark chamber(about 15 rad.lenghts of Pb) allows also the detection of forward emitted γ-rays. We have found that in about 1 out of 10 pictures a single V type event is present, while in the majority of the others there is at least one γ-ray.

2.- ANALYSIS AND SELECTION OF EVENTS.

The V type events selected by the scanners are measured on digitized tables. The coordinates of the sparks are reconstructed in true space with an accuracy of ±.06 cm. A plane is fitted through them and straight lines are fitted through the sparks which belong to the same track. The intersection of the best fit plane with the incident π^-, as defined by the two hodoscopes, is taken as the interaction point; the intersection of the two best fit lines as the neutral strange particle decay vertex. The line joining the interac-

tion with the decay vertex is assumed to coincide with the direction of emission of the strange particle. We then calculate the partial angle $\bar{\theta}$, formed by this direction and the nearest of the two charged prongs, and the total angle θ between them. On the assumption that the observed event is indeed a $K^0_S \to \pi^+\pi^-$ decay, the K° momentum is evaluated (Fig.2) together with the invariant mass of the associated recoil and the other kinematical quantities of interest.

Events are selected on the basis of coplanarity, collinearity, opening angle, recoil mass, position of decay and interactions points.

The effect of the cuts introduced by the acceptance criteria have been extensively studied by comparing the experimental distributions with the Montecarlo simulated ones for various hypothesis about the production processes. We have been able to fit satisfactorily every significant experimental distribution and this gives us confidence on the calculated efficiencies.

Fig.3a shows the reconstructed recoil mass distribution at 6 GeV/c for events, within the fiducial volume, which satisfy the coplanarity and collinearity requirements.

In Fig.3b the analogus, Montecarlo generated distributions for $\Lambda^\circ+\Sigma^\circ$, $Y^*(1385)$ and $Y^*(1519)$ are shown, normalized to the values which produce the best fit linear combination to the experimental data (dotted line in Fig.3a). It is possible to make a cut which selects events, produced in association with a Λ° or Σ° recoil, with about equal efficiencies, while only a small fraction of the events with an isobar as recoil enter in the cut.

The resolution in recoil mass, while it is independent of the momentum transfer and mass values, is however

a function of the incident momentum and of the spark chambers arrangement. For our running conditions we estimate half widths at half heights of 90, 140 and 200 MeV respectively at 6, 8, and 11.2 GeV/c. This fact, coupled with the rather copious production of all neutral final state isobars in our energy range, has made necessary a detailed study of the accuracy of the 'elastic' selection criteria and of the effects of contamination from isobar events on differential cross sections.

At each energy we have evaluated the contamination within various cuts in recoil mass and opening angle, by fitting the experimental mass distribution with a series of isobars contributions, as briefly mentioned above[3]. We have then subtracted from the momentum transfer distribution of the accepted events the weighted experimental $|t|$ distribution of the events in the recoil mass region from which the contamination is produced.

For each case the differential cross section (see ch.3) has been deduced and by comparing the shapes and absolute values obtained at the same incident momentum for different cuts we have reached the conclusion that the uncertainty due to the method of analysis is smaller than the statistical one.

The empty target contribution (typically 9% of the full target rate) has been subtracted bin by bin from the various distributions.

Fig.4 shows the resolution in the momentum transfer t for various t values at 6 and 11.2 GeV/c.

3.- NORMALIZATION.

The incoming flux has been monitored throughout the experiment. Contamination from e^- (0.4-0.2)% and μ^-(2-

1)% has been measured and subtracted at the different energies. Corrections have been made for δ-rays ((4±1)%. A δ-ray produced by the incoming particle before the occurrence of a $\pi^- p \to K^\circ Y^\circ$ interaction can reach the anticoincidence counter and veto the event), strong interactions of the incoming and outgoing particles (about 2.5%), scanning (98%) and measuring (about 95%) efficiencies. For the ratio $K^\circ_S \to \pi^+\pi^-/K^\circ$ we have used the value 0.33.

The effects connected with the lifetime (for which we used the Rosenfeld values) of the Λ° (supposed to decay as $\pi^- p$ in 67% of the cases) and K°_S have been incorporated in the Montecarlo program, which also take into account multiple scattering, measuring errors and the limitation of the fiducial volume.

The overall systematic uncertainty has been estimated to be ± 15%.

4.- RESULTS.

In Tab.I we list the results for differential and integrated cross sections. In Fig.5, where the differential cross sections are shown, we have also indicated the Montecarlo calculated relative detection efficiency as a function of t. Its variation (essentially independent of the incident momentum) is caused by the changing fraction of $\Lambda \to \pi^- p$ decays which, with a probability depending on the Λ production angle and momentum, trigger the anticoincidence. The values plotted are corrected for it and the errors indicated are statistical only (they include the statistical error for empty target and contamination subtraction).

For $|t|$ smaller than 0.40 $(GeV/c)^2$ the differential cross section can be well fitted by an exponential e^{at} with $a=8.0\pm0.5$ ($\chi^2=14$) at 6, $a=7.7\pm0.5$ ($\chi^2=6$) at 8 and $a=7.8\pm0.4$ $(GeV/c)^{-2}$ ($\chi^2=6$) at 11.2 GeV/c.

Crennel et al.(Ref.2) in a bubble chamber experiment at 6 GeV/c with 448 events obtained the value $a=7.8\pm.5$ $(GeV/c)^{-2}$ and a $\pi^-p \to K^\circ Y^\circ$ total cross section of 41 ± 4 μb.

Ehrlich et al.(Ref.3) with 101 events at 7.91 GeV/c obtained $a\simeq9.7$ $(GeV/c)^{-2}$ and a total cross section of about 32 μb. No other statistically significant data exist above this energy.

Recently Hoang et al.(Ref.4) have reported a spark chamber study of $\pi^-p \to K^\circ Y^\circ$ in the forward and backward direction at 4 GeV/c. They find $a=8.57\pm.38$ $(GeV/c)^{-2}$ for $|t|$ less than 0.4 $(GeV/c)^2$.

A systematic bubble chamber study of two body strange particles production from π^- between 1.9 and 4.2 GeV/c is reported by Dahl et al.(Ref.5). Some of the features found at our energies, as the magnitude of the slope and the change of slope at about $|t|\simeq 0.4$ $(GeV/c)^2$ are already present in this range of energy.

We have calculated the total cross section by integrating between $|t| = |t_{min}|$ and $|t|=1.01$ $(GeV/c)^2$. The values obtained are 40.5 ± 6 μb at 6, 25.3 ± 4 μb at 8 and 18 ± 3 μb at 11.2 GeV/c. In Fig.6 they are shown together with previous bubble chamber results. It appears that the trend already present in the 2 to 4 GeV/c region is not in contrast with the new results at higher energy. A good fit to the energy dependence can be obtained with the simple power law $E^{-3.6}$ where E is the CM total energy.

Recently a double Regge Pole exchange model, with exact SU_3 symmetry, has been proposed by Ph.Salin(Ref.8) and K.V.L.Sarma and D.D.Reeder (Ref.9) and applied in particular to the description of the associated production reactions. It consists in a rather straightforward extension to these strangeness-exchange processes of the model (Ref.10) successfully used for the π^-p and K^-p charge-exchange and for the $\pi^-p \to \eta n$ production.

A comparison of our results, with the calculation of the differential cross section based on the parametrization obtained at lower energies by Sarma and Reeder, shows qualitative agreement. A more detailed study of possible fits within this framework is presently being carried on.

5.- TEST MEASUREMENT OF $K^-p \to \overline{K}^0 n$.

During most of the running time we have triggered the spark chambers also on neutral final state K^- interactions. During a short period at 8 GeV/c we have taken data only on K^-. Using this sample (65% of the available statistics at 8 GeV/c) we have applied our method of analysis to $K^-p \to \overline{K}^0 n$ events.

The main difference is the flatness of the efficiency vs. t, since in this case there is not any more the partial suppression of events, which is caused by Λ decays within the anticoincidence counter.

We obtain with 169 events an integrated cross section of 80 ± 16 μb for $0 \leq |t| \leq 0.9$ $(GeV/c)^2$. This value and the shape of the differential cross section (Fig.7) are in good agreement with the interpolation of the data of Astbury et al.(Ref.11)at 7.1 and 9.5 GeV/c.

ACKNOWLEDGEMENTS

We would like to acknowledge the hospitality and support of CERN NP Division and the cooperation of the PS staff; the help received from CEN-Saclay; the collaboration of the Saclay group, who worked at the same time on $\pi^-p \to n\overleftarrow{\pi}^0$, and the dedicated help of our technicians and scanners.

Most of the computations have been performed with the IBM 7090 of the CNUCE-Pisa.

This experiment would not have been possible wi-

thout the special target built by Dr.P.Roubeau at Saclay. We like to thank him and also Mr.Derny, Dr.Borghini, Mr. Vermeulen, Mr.Uldry, Mr.Scherrer for the running of the target.

The enthusiastic support of Prof.P.Falk-Vairant and Prof.G.Stoppini throughout the experiment is gratefully acknowledged.

FOOTNOTES

(1) This special, He cooled, liquid H_2 target, designed by P.Roubeau and built at Saclay, has such geometry that it is possible to surround it with a 2.9 cm diameter anticoincidence counter, to place the last beam defi - ning counter at only 2 cm before the liquid H_2 and to insert the whole target-counters assembly in the center of the cylindrical spark chamber, without significantly obstructing its view.

(2) No stereo is provided for the cylindrical spark chamber.

(3) For the cuts considered, the contamination ranged between 3 and 12% at 6 GeV/c and between 15 and 30% at 8 and 11.2 GeV/c.

REFERENCES

1. INFN/AE-67/9 submitted to the Heidelberg Conference (1967).
2. D.J.Crennel, G.R.Kalbfleisch, K.Wu Lai, J.M.Scarr, Th. G.Schumann, I.O.Skillicorn, M.S.Webster - Phys.Rev.Lett. 18,86 (1967).
3. R.Ehrlich, W.Selove, H.Yuta - Phys.Rev. 152,1194 (1966).
4. T.F.Hoang, Y.S.Kim, S.Margulies, T.H.Groves - Phys.Lett. 25B,615 (1967).
5. O.I.Dahl, L.M.Hardy, R.J.Hess, J.Kirz, D.H.Miller, J.A. Schwartz - Phys.Rev. to be published and UCRL 17217.
6. T.P.Wangler, A.R.Erwin, W.D.Walker - Phys.Rev. 137,B414 (1965).
7. J.Bartsch, et al., Aachen, Hanburg, London, Munchen collaboration - Nuovo Cimento 43,A1010 (1966).
8. Ph. Salin - CERN preprint TH.762 (1967)
9. K.V.L.Sarma and D.D.Reeder - University of Winsconsin pre.
10. K.V.L.Sarma and D.D.Reeder - N.C. 51A,169 (1967).
11. P.Astbury, G.Brautti, G.Finocchiaro, A.Michelini, K.Terwilliger, D.Websdale, C.H.West, P.Zanella, W.Beusch, W. Fischer, B.Gobbi, M.Pepin, E.Polgar - Phys.Lett. 23,396 (1966).
    See also: A.Buffington - Ph.D. Thesis, MIT Cambridge
    $K^- p \to \bar{K}^0 n$ at 8 GeV/c (Dec.1966).

TABLE I

		6 GeV/c σ_T=40.5±6 μb	8 GeV/c σ_T=25.3±4 μb	11.2 GeV/c σ_T=18±3 μb
$\lvert t \rvert$ (GeV/c)^2	Δt	$d\sigma/dt$	$d\sigma/dt$ μb·GeV^{-2}·c^2	$d\sigma/dt$
.02	.02	289 ± 36	165 ± 22	125 ± 15
.04	"	274 ± 32	150 ± 19	99 ± 12
.06	"	156 ± 22	109 ± 16	93 ± 11
.08	"	177 ± 24	106 ± 15	70 ± 9.5
.10	"	131 ± 20	65 ± 12	56 ± 8.5
.12	"	131 ± 19	84 ± 13	44 ± 7.5
.14	"	97 ± 17	63 ± 11	52 ± 7.5
.16	"	104 ± 17	56 ± 11	40 ± 6.5
.18	"	64 ± 14	44 ± 10	40 ± 6
.20	"	52 ± 13	40.5 ± 9.5	27 ± 5.5
.23	.04	57 ± 8.5	32.5 ± 6	24.8 ± 3.3
.27	"	38 ± 7.5	20.8 ± 5	17 ± 3
.32	.06	18.5 ± 4.5	16.3 ± 3.7	9.6 ± 1.9
.38	"	21.8 ± 4.2	12.8 ± 3.1	7.5 ± 1.7
.44	"	17.6 ± 3.7	7.7 ± 2.5	4.9 ± 1.5
.50	"	15.4 ± 2.7	4.5 ± 1.9	4.9 ± 1.3
.58	.10	9.1 ± 1.9	6.6 ± 1.4	2.9 ± 0.6
.68	"	5.5 ± 1.5	5.8 ± 1.8	1.6 ± 0.6
.87	.28	3.5 ± 0.8	3.6 ± 0.5	1.9 ± 0.3

FIGURE CAPTIONS

Fig. 1 - Experimental apparatus. ≠ ≠ 2,3',3,4 are the beam defining counters; hod 1 and hod 2 the two hodoscopes, which determine the position of the incident π^-; ≠ 5 is the anticoincidence counter surrounding the H_2 liquid target. The cylindrical spark chamber, not so far used for the analysis, is meant to detect γ-rays produced at large angles, as in Σ° or Y° decays, in addition to the charged decay products of the Λ. Two threshold gas Cerenkov counters, used for π^- and K^- selection, are not shown. SC1 and SC2 are thin Al-foil spark chambers which detect the charged decay of the strange particles, while the Saclay spark chamber detects also the forward γ-rays. ≠6, in front of SC2, is a coincidence counter.
The figure shows also the triggering logic.

Fig. 2 - $K^\circ \to \pi^+\pi^-$ kinematics at high energy. As it can be seen from the figure a measurement of the total angle θ and partial angle $\bar{\theta}$ is sufficient to determine the K° momentum. For about 85% of the available phase space the lines of constant θ and $\bar{\theta}$ are almost perpendicular to each other and, since lines of constant θ are nearly parallel to lines of constant K° momentum, a good precision can be achieved even when θ (as it happens in our experiment) is rather poorly known in respect to θ.

Fig. 3a- Experimental distribution of the reconstructed recoil mass at 6 GeV/c (see text).

Fig. 3b- Montecarlo distribution of the recoil mass for $\Lambda^\circ+\Sigma^\circ$, $Y^*(1385)$, $Y^*(1519)$.

Fig. 4 - Momentum transfer resolution at 6 and 11.2 GeV/c, for various t values.

Fig. 5 - Differential cross section $d\sigma/dt$ for $\pi^-p \to K^\circ Y^\circ$ at 6, 8, 11.2 GeV/c and relative detection efficiency.
The curves superimposed on the experimental points represent the direct prediction, according to a calculation we performed, which follows from the Sarma and Reeder fit (Ref.9) to the associated production at lower energies.

Fig. 6 - Plot of the experimentally available values for $\sigma_{tot}(\pi^-p \to K^\circ Y^\circ)$, at incident π^- momenta above 2 GeV/c.

Fig. 7 - Differential cross section $d\sigma/dt$ for $K^-p \to \bar{K}^\circ n$ at 8 GeV/c.

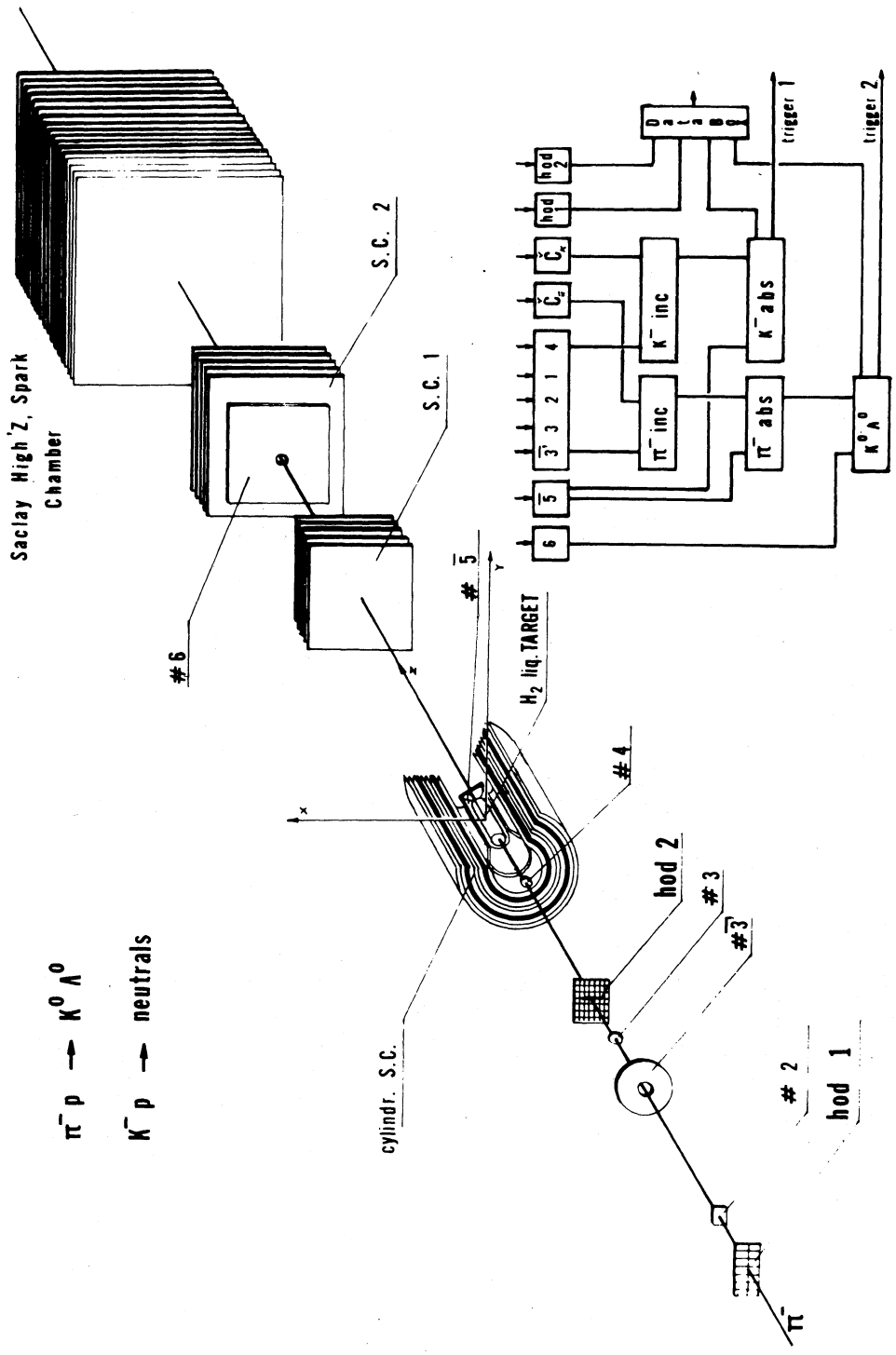
Saclay High'Z, Spark Chamber
S.C. 2
S.C. 1
#6
#5
H2 liq. TARGET
#4
hod 2
#3
#3'
2
hod 1
cylindr. S.C.
π⁻
π⁻ p → K⁰ Λ⁰
K⁻ p → neutrals
hod 2
hod 1
K⁻ inc
K⁻ abs
π⁻ inc
π⁻ abs
K⁰ Λ⁰
trigger 1
trigger 2
Data Bus

FIG. 1

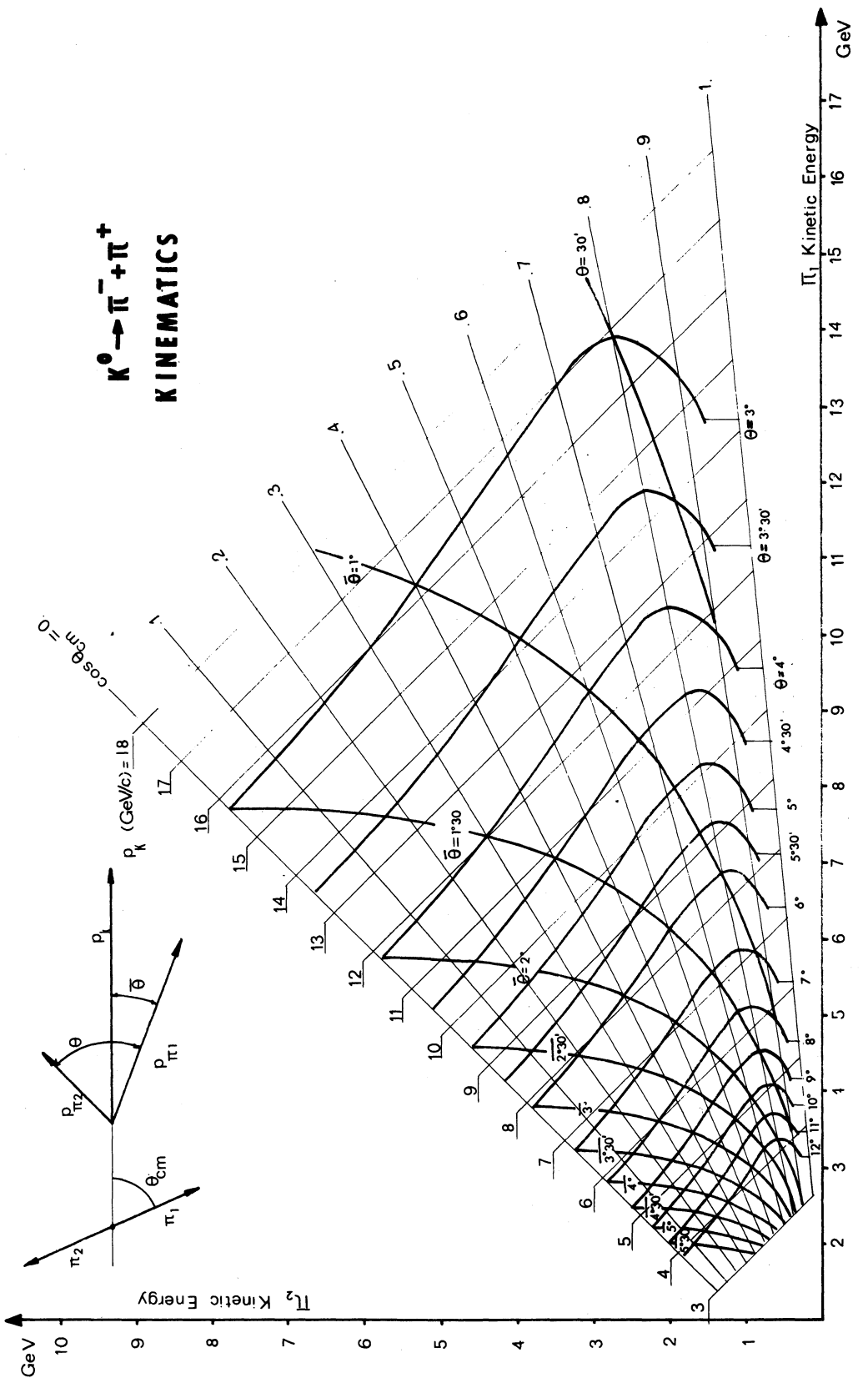
K⁰→π⁻+π⁺
KINEMATICS
Π₂ Kinetic Energy
Π₁ Kinetic Energy
GeV
p_K (GeV/c) = 18
cosθ_cm = 0
θ̄=1°
θ̄=1°30
θ̄=2°
2°30'
3°
3°30'
4°
4°30'
5°
5°30'
6°
7°
8°
9°
10°
11°
12°
θ=30'
θ=3°
θ=3°30'
θ=4°
p_t
θ̄
θ
p_π1
p_π2
θ_cm
π₁
π₂

Fig. 2

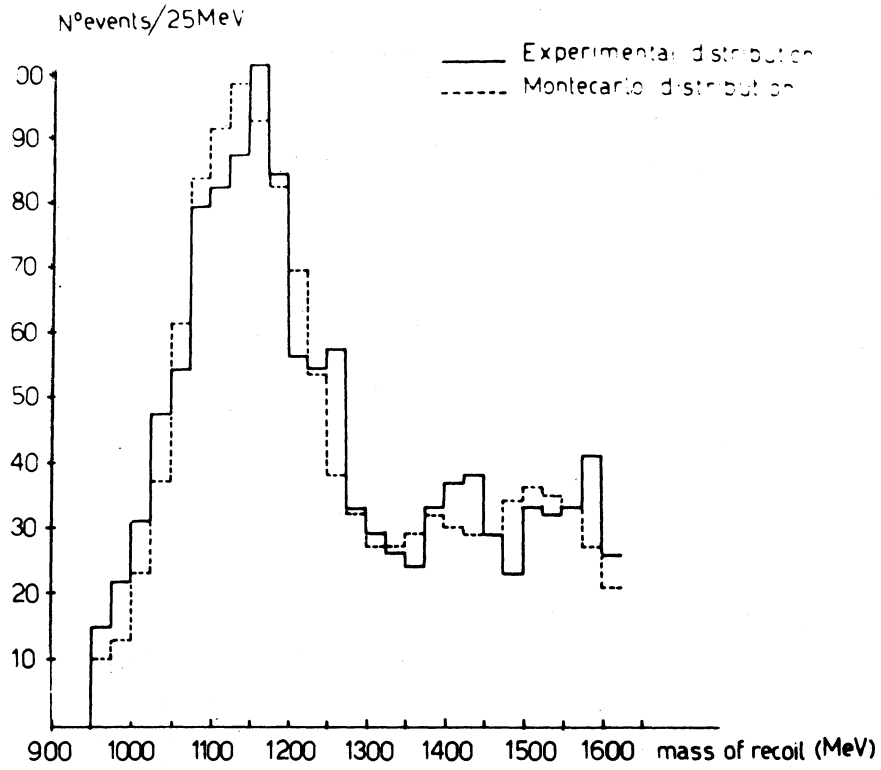
N°events/25MeV
Experimental distribution
Montecarlo distribution
30
90
80
70
60
50
40
30
20
10
900
1000
1100
1200
1300
1400
1500
1600
mass of recoil (MeV)

FIG. 3a

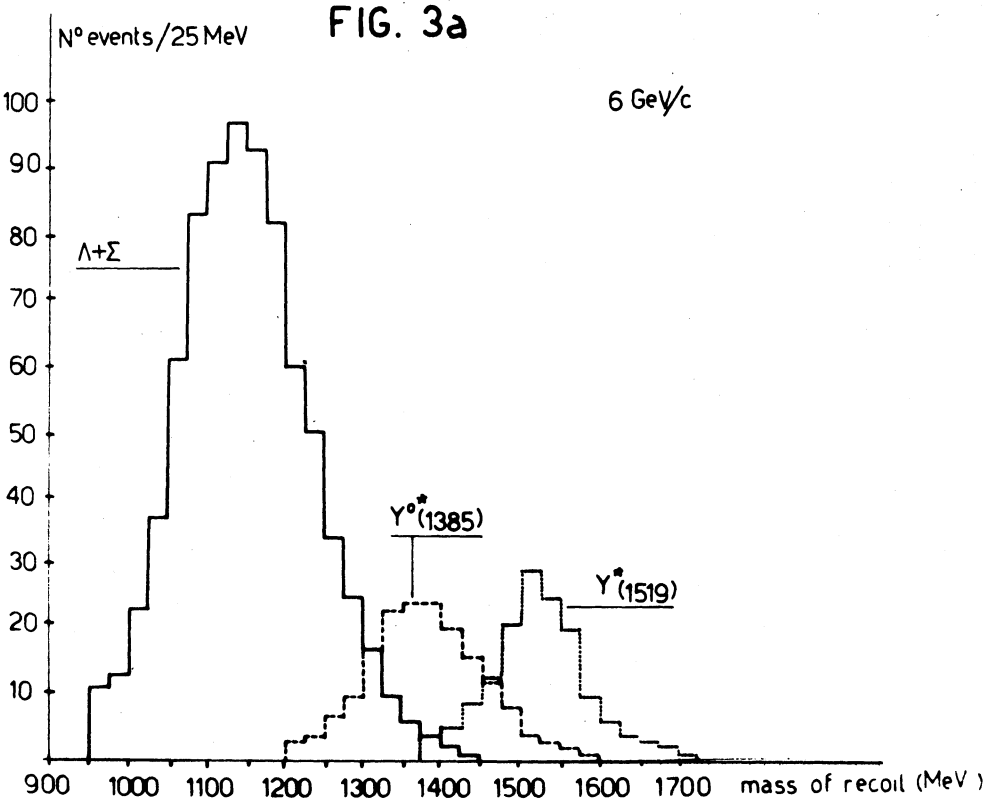
N° events/25 MeV
6 GeV/c
100
90
80
70
60
50
40
30
20
10
Λ+Σ
Y°*(1385)
Y*(1519)
900
1000
1100
1200
1300
1400
1500
1600
1700
mass of recoil (MeV)

FIG. 3b

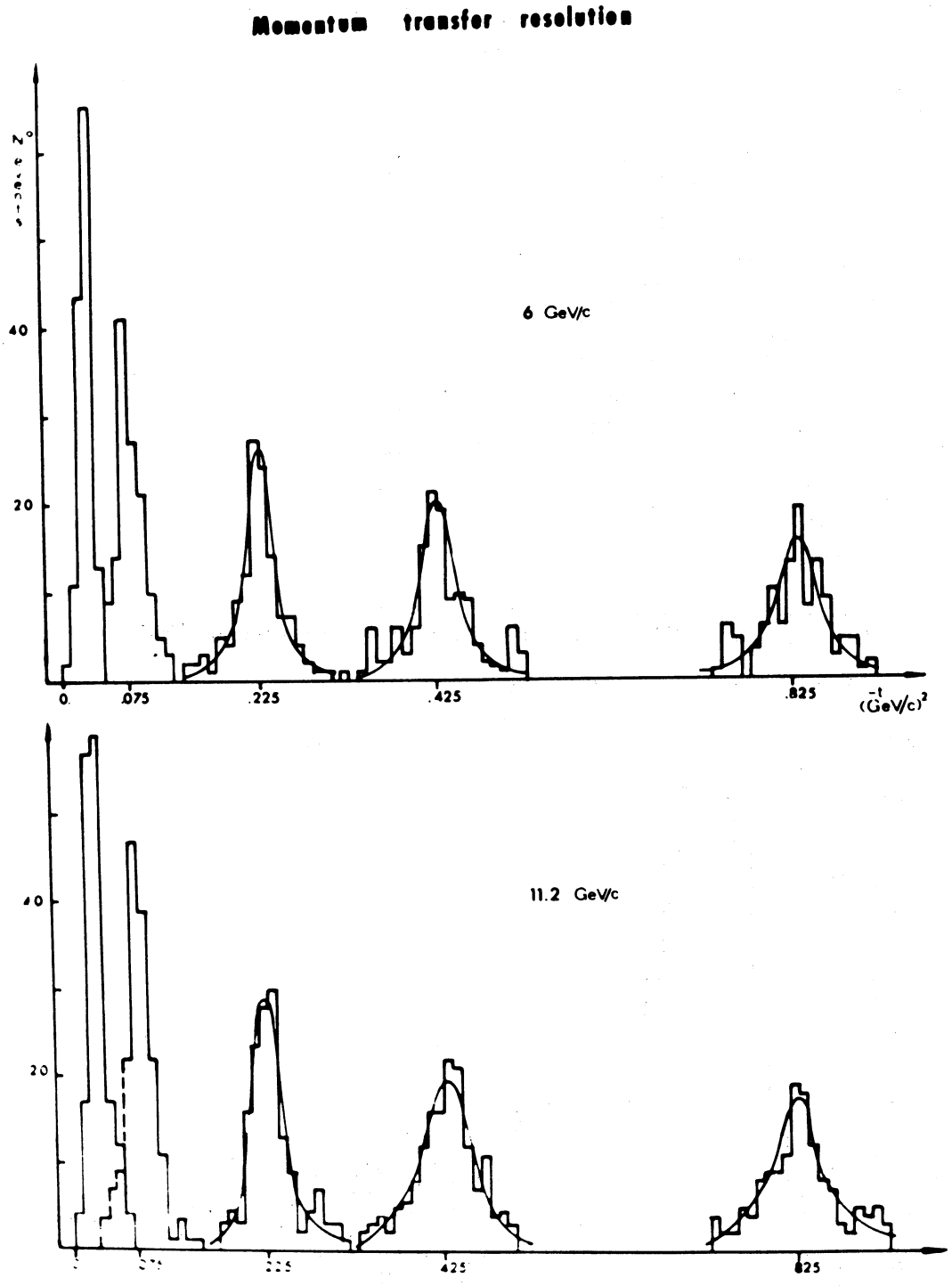
Momentum transfer resolution
6 GeV/c
40
20
0
.075
.225
.425
.825
(GeV/c)²
11.2 GeV/c
40
20
.425
.825

FIG. 4

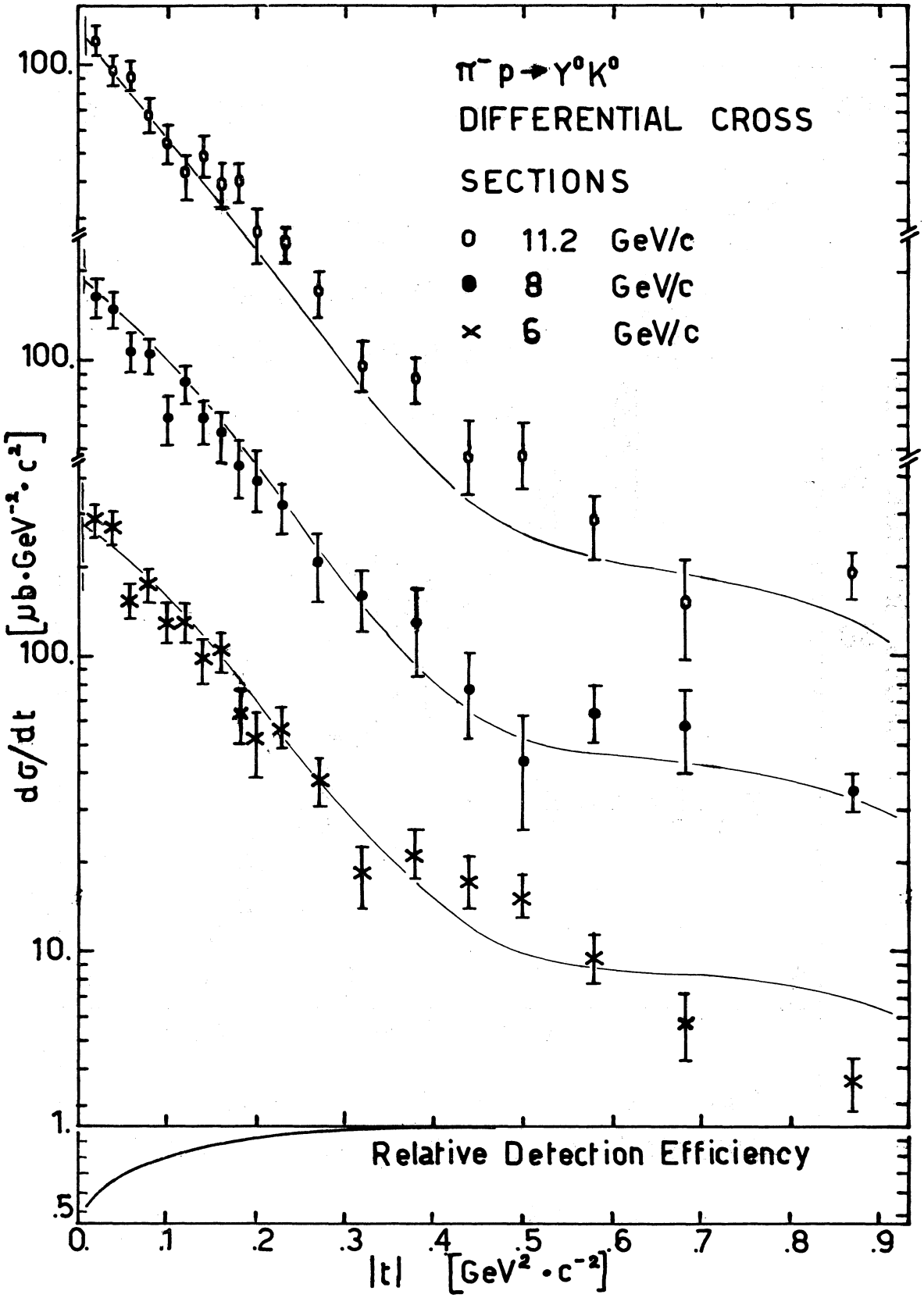
$\pi^- p \to Y^0 K^0$
DIFFERENTIAL CROSS SECTIONS
o 11.2 GeV/c
● 8 GeV/c
× 6 GeV/c
100.
100.
100.
10.
1.
.5
dσ/dt [μb·GeV⁻²·c²]
Relative Detection Efficiency
0.
.1
.2
.3
.4
.5
.6
.7
.8
.9
|t| [GeV²·c⁻²]

FIG. 5

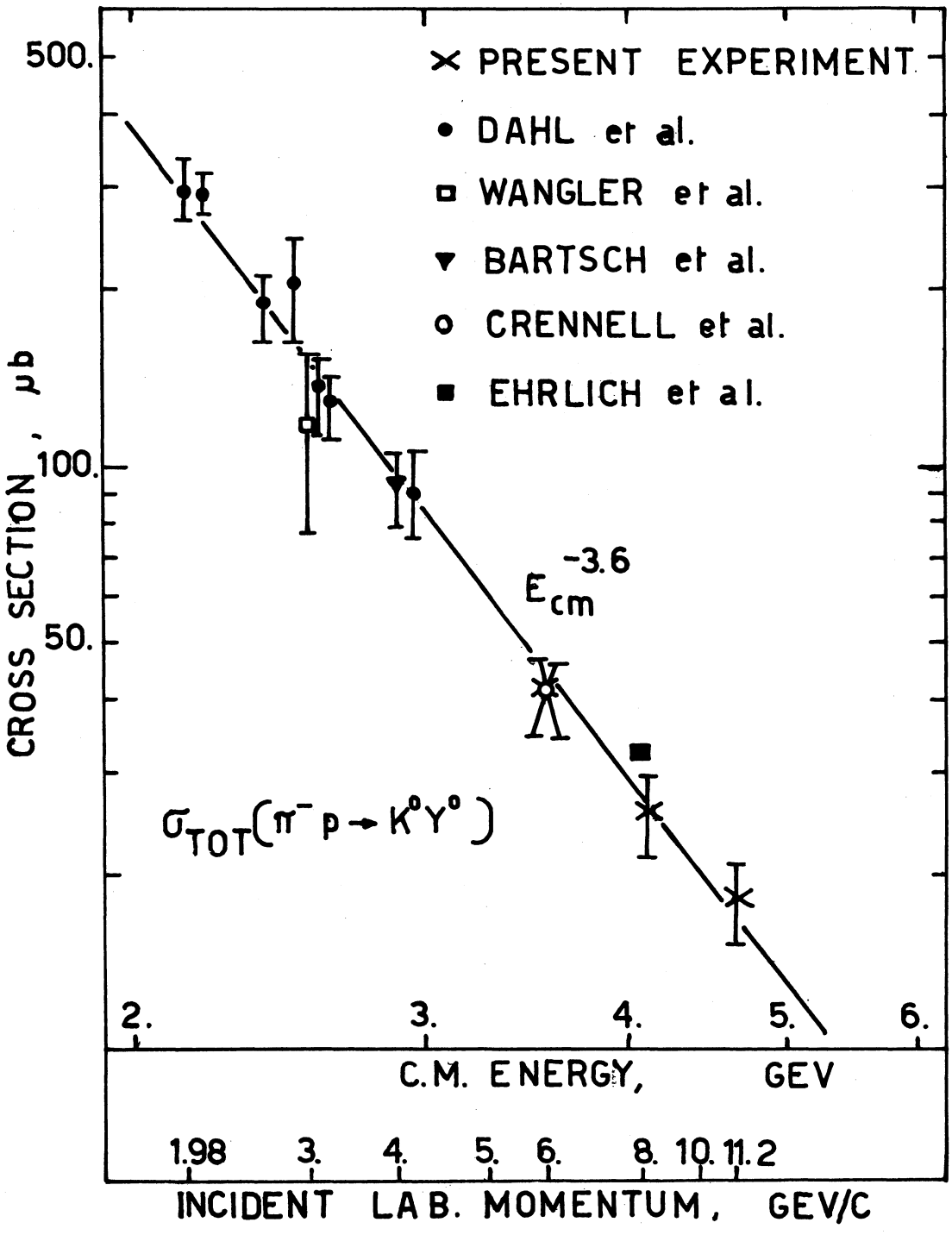
500.
100.
50.
CROSS SECTION, μb
× PRESENT EXPERIMENT
• DAHL et al.
□ WANGLER et al.
▼ BARTSCH et al.
○ CRENNELL et al.
■ EHRLICH et al.
$E_{cm}^{-3.6}$
$\sigma_{TOT}(\pi^- p \to K^0 Y^0)$
2.
3.
4.
5.
6.
C.M. ENERGY, GEV
1.98
3.
4.
5.
6.
8.
10.
11.2
INCIDENT LAB. MOMENTUM, GEV/C

FIG. 6

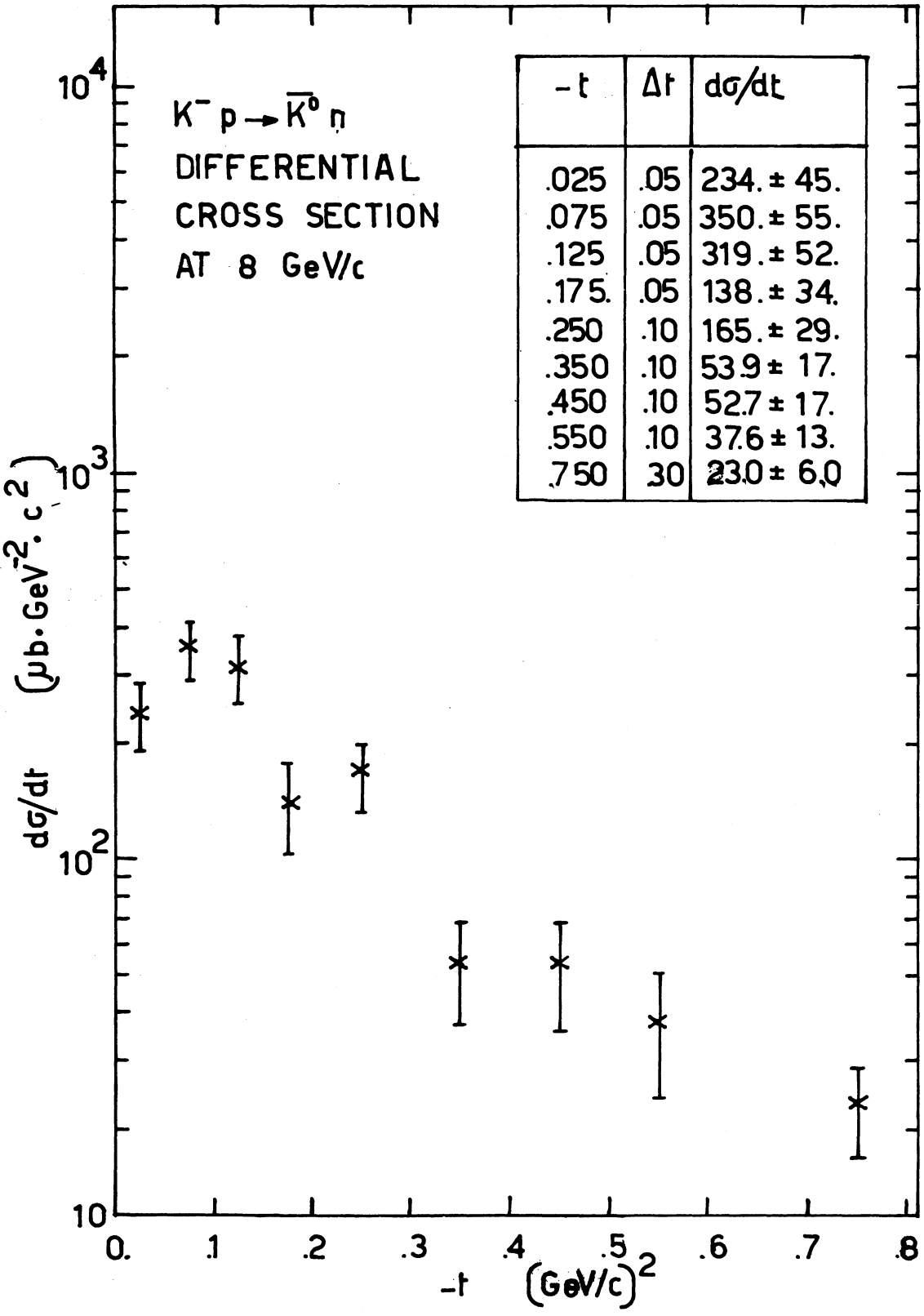

$-t$	Δt	$d\sigma/dt$
.025	.05	234. ± 45.
.075	.05	350. ± 55.
.125	.05	319. ± 52.
.175.	.05	138. ± 34.
.250	.10	165. ± 29.
.350	.10	53.9 ± 17.
.450	.10	52.7 ± 17.
.550	.10	37.6 ± 13.
.750	.30	23.0 ± 6.0

FIG. 7

THE STUDY OF 28.6 GeV/c p-p INTERACTIONS WITH 6 CHARGED PARTICLES IN THE FINAL STATES

P.L. Connolly, I.R. Kenyon, T.W. Morris and A.M. Thorndike†

Brookhaven National Laboratory, Upton, New York.
†Now on leave at CERN, Geneva, Switzerland.

1. INTRODUCTION

This paper describes results obtained so far in a continuing study of high multiplicity high energy pp interactions using pictures of the 80-inch Brookhaven National Laboratory Cryogenic Bubble Chamber filled with liquid hydrogen and exposed to a 28.6 GeV/c proton beam. Hand measurements on 29,500 pictures have yielded 5230 well reconstructed events having beam momenta within 2 standard deviations of the mean. We will be concerned here mainly with 6 prong events having 4 constraint fits. One constraint fits are in general found to be unreliable, but we will describe one technique which allows us to extract a more reliable subsample.

2. ANALYSIS

The measurement of these events has been simplified appreciably by introducing a track matching procedure[1] into the geometric reconstruction program TVGP. This now allows measurers to measure tracks in any order in each view. For kinematic fitting, the program QKIN, a derivative of SQUAW, was used. All events with fits of .1% probability or better have been reexamined at 10x magnification for consistency with

track densities. This eliminated some 30% of unique 1 constraint fits, many with low χ^2. Less than 5% of the unique 4c fits were rejected, however. The effective beam momentum profile was obtained from a large sample of beam tracks (in 4 prong events) measured with the Brookhaven National Laboratory Flying-Spot Digitizer[2]. This gave 28.6 GeV/c for the mean momentum with a spread of ±.3 GeV/c. A best input value for the beam momentum in each event was obtained by adding the measured value and the standard value suitably weighted. For the 4-constraint fits, we find the (missing mass)^2 is centered at -0.005 (GeV)^2 with a spread of .005 (GeV/c)^2; the χ^2 and stretch distributions show no gross aberrations; it appears, however, that our angle errors are overestimated due to the floors on the errors being set too large (.1^o in azimuth and .2^o in dip). After kinematic fitting and ionization checks, there are 230 events with 4-constraint fits with probability 1% or better. Of these, about 15% are ambiguous between more than one 4-constraint fit. (This represents a partial cross-section of .36±.02 mb.) In the following, we present results based mainly on these 4-constraint fits.

3. ISOBAR PRODUCTION

As we reported earlier[3], the most noticeable feature is the dominance of $\Delta(1236)$ production. Figures 1 and 2 show the effective mass distributions for the $(p\pi^+)$ and $(p\pi^-)$ systems for 4-momentum transfer ($|t|$) cuts of 1.0 and 2.0 (GeV/c)^2. The $(p\pi^+)$ plot shows almost pure $\Delta(1236)$ production whereas the $(p\pi^-)$ plot gives evidence of more background and an enhancement near 1.6 GeV/c which persists with tighter t cuts. This latter bump we tentatively associate with the neutral $N^*_{\frac{1}{2}}(1570)$[4]. We estimate that about one third of

all protons (counting both the beam and target protons) give rise to a $\Delta(1236)$. The ratio of Δ^{++} to Δ^{o} production is between 3:1 and 4:1. The t distribution of the $\Delta(1236)$ with respect to the initial state proton is shown in Figure 3. When compared with data from the study of $pp \to pN^*$ reactions at low momentum transfer[5], this slope is relatively small. This feature may reflect the fact that the $\Delta(1236)$ isobars are not the direct products of proton excitation. As an example, we show the effective mass plot for the $(p\pi^+\pi^-)$ system with $|t| < 2.0$ (GeV/c)^2 in Figure 4. When combinations not containing a $\Delta(1236)$ are excluded, we get the broken outline histogram. There is considerable enhancement in the low mass region from 1440 to 1760 GeV. This result is not inconsistent with the known large decay rates of the $N^*_{\frac{1}{2}}(1525)$, $N^*_{\frac{1}{2}}(1670)$ and $N^*_{\frac{1}{2}}(1688)$ into $N\pi\pi$. For $N^*_{\frac{1}{2}}(1525)$, it is also known that the preferred $N\pi\pi$ final state is $\Delta\pi$. No clear evidence has been seen for any boson resonance production; in the effective mass plot for $(\pi^+\pi^-)$, there is a shoulder around 650-800 MeV but this has not been explored in detail.

4. PRINCIPAL AXIS ANALYSIS

This technique was introduced by Brandt et al[6] to attempt to assign all outgoing particles in high energy collisions to two "intermediate bodies". In our case, this involves looking in turn at all combinations of final state particles into two groups, each group containing one proton; then we select the combination that gives the largest c.m. momentum to these groups. The groups so selected then correspond to the "intermediate bodies" of Brandt et al. Unlike Brandt et al, we find a marked forward-backward asymmetry in the π-meson angular distribution in the rest frame of the "intermediate bodies" with respect to the direction of motion

of the "intermediate body". This is shown by the full line histogram in Figure 5, where we have plotted the cosine of the angle (θ^{**}) the pion makes with the direction of the "intermediate body". A simple explanation of this effect is that backward emitted pions will tend to be assigned to the wrong "intermediate body". We have therefore investigated a somewhat different approach where we make the "intermediate bodies" by selecting the grouping that minimizes $|t|$ to the incident nucleons. The resulting $\cos\theta^{**}$ distribution is also shown in Figure 5 - it is much more symmetric. In Figure 6, we show the effective mass distributions of these "intermediate bodies" and in Figure 7 their $|t'|$ distribution. We plot t' (ie $t-t_{MIN}$) rather than t, since for the intermediate bodies t_{MIN} is frequently very large. Looking at Figure 6, we see a strong $\Delta(1236)$ signal and evidence for an enhancement in the 1.5 t0 1.8 GeV region. The semilogarithmic plot of the distribution is approximated rather well by a single line fit with exponent -5.8.

5. 1-CONSTRAINT FITS

It has been shown by Kernan et al[7] that 2-prong p-p interactions at 23 GeV/c yield many spurious 1-constraint fits and that only the class of fits with a fast neutron are reliable. In the high multiplicity events, there is also a background of spurious 1-constraint fits; this can most easily be seen by looking at the c.m. distributions of the nucleon momenta. These should be symmetric about zero but it is found that for 1-constraint fits there is a large excess of backward nucleons even if a tight χ^2 cut is imposed. It is possible to remove a good proportion of one type of spurious fits in the following way: In Figures 8 and 9, we show the angular correlation of the final state nucleons in the c.m.

frame for 4-constraint fits and 1-constraint fits (with a χ^2 cut of .2), respectively. The effect of the excess of slow nucleons in the 1-constraint case is to add a tail onto the sharp peak near a $\cos\theta^*_{NN}$ of -1. By cutting at some value, say -.8, in $\cos\theta^*_{NN}$, we can eliminate this tail and not appreciably cut into the more reliable peak. We are continuing to investigate this problem.

One very clean feature revealed by the 1-constraint fits is the presence of ω production in the reaction $pp \to 2p\, 2\pi^+2\pi^-\pi^o$. The effective mass plot is shown in Figure 10. Excluding events which have $\cos\theta^*_{pp} > 0$, we find the background is markedly reduced but the ω peak is virtually unaffected.

6. DISCUSSION AND CONCLUSIONS

In a recent paper, Morrison[8] has developed the idea that the I=O exchange mechanism ("Pomeron" exchange) tends to dominate reactions at high energies. The most important of these, after elastic scattering, is likely to be diffraction dissociation[9] in which one or both protons are excited into other $I=\frac{1}{2}$ states. It is interesting to see how far these ideas can be applied to high multiplicity final states. We restrict consideration to the reaction $pp \to pp\, 2\pi^+2\pi^-$. The very copious $\Delta(1236)$ production would in this view arise from the dissociation $p \to \Delta^{++}\pi^-$ or $p \to \Delta^o\pi^+$ or from decay of heavier isobars excited in the dissociation process. The ratio of around 3:1 for Δ^{++}: Δ^o production is certainly consistent with the simpler process. We have also found that part (~20%) of the Δ production can come from $N^*_{\frac{1}{2}}$ decays. The dominance of diffraction dissociation of the interaction should also lead to a sharp $|t|$ distribution. Our procedure described above for selecting "intermediate bodies" might be

expected to pick out the diffraction dissociation products. This will not always be the case because if we have our isobars produced which decay via a $\Delta(1236)$, then sometimes the $\Delta(1236)$ can have a lower $|t|$ value than the parent isobar and it will be selected as the "intermediate body". Such behaviour is apparent in Figure 6. The magnitude of the slope of the $|t'|$ distribution in Figure 7, although deliberately sharpened is somewhat surprising for high multiplicity events. If we remove all the $I\neq\frac{1}{2}$ "intermediate bodies" from the plot, we find the exponent is reduced to about 3.2. These slopes are comparable to those seen in 2 body reactions like $pp\rightarrow pN^*_{\frac{1}{2}}(1520)$ [5] at small $|t|$.

In summary, (at this preliminary stage of the analysis), we can say that the reaction $pp\rightarrow pp2\pi^+2\pi^-$ shows several simple features which are quite consistent with dominance of the reaction by diffraction dissociation of the protons. This dominance is obviously not established by these features, however.

REFERENCES

1. P.L. Connolly - unpublished.
2. "Study of pp interactions at 28.5 BeV/c in 2 and 4 prong final states" - P.L. Connolly, W.E. Ellis, P.V.C. Hough, D.J. Miller, T.W. Morris, C. Ouannes, R.S. Panvini, A.M. Thorndike, talk presented at the Third Topical Conference on Resonant Particles, Athens, Ohio, November 1967.
3. "The study of 28.6 GeV/c pp interactions with 6 or more charged particles in the final state" - P.L. Connolly et al, talk presented at the 1967 American Physical Society meeting in Washington, D.C.
4. The alternative decay of the neutral $N^*_{\frac{1}{2}}(1570)$ into $n\eta$ will be difficult to detect since it involves two neutrals.
5. E.W. Anderson, E.J. Bleser, G.B. Collins, T. Fujii, J. Menes, F. Turkot, R.A. Carrigan, R.M. Edelstein, H.C. Hien, T.J. McMahon, I. Nadelhaft, Phys. Rev. Lett. 16, 855(1966).
6. S. Brandt, Ch. Peyrou, R. Sosnowski, A. Wroblewski, Physics Letters 12, 57(1964).
7. "Investigation of kinematic fitting results for bubble chamber events involving neutral particles at high energies" - W.J. Kernan, T.L. Schalk, L.S. Schroeder and R.L. Wagstaff, AEC report UC-34 TID-4500(1967).
8. D.R.O. Morrison, to be published in Phys. Rev. Lett.(1967).
9. M.L. Good and W.D. Walker introduced the idea of diffraction dissociation on nuclei, Phys. Rev. 120, 1857(1960), and has been extended by S.D. Drell and K.Hiida to the formation of N^* isobars in $pp \rightarrow pN^*$ reactions, Phys. Rev. Lett. 7, 199(1961).

FIGURE CAPTIONS

1. Effective mass plot for $(p\pi^+)$ with $|t| < 2.0$ (GeV/c)^2 (dotted line) and $|t| < 1.0$ (GeV/c)^2 (full line) in the final state $pp\pi^+\pi^+\ \pi^-\pi^-$.

2. Effective mass plot for $(p\pi^-)$ with $|t| < 2.0$ (GeV/c)^2 dotted line) and $|t| < 1.0$ (GeV/c)^2 (full line) in the final state $pp\pi^+\pi^+\pi^-\pi^-$.

3. t to $\Delta(1236)$ in all $pp\pi^+\pi^+\pi^-\pi^-$ final states.

4. Effective mass plot for $(p\pi^+\pi^-)$ with $|t| < 2.0$ (GeV/c)^2 in the final state $pp\pi^+\pi^+\pi^-\pi^-$. All events (full line); events with $p\pi^+$ or $p\pi^-$ in $\Delta(1236)$ band (dotted line).

5. Angular distribution of the pions in the rest frame of the "intermediate body" chosen by principal axis technique. Full line represents the P-choice and the dotted line the t-choice.

6. Effective mass plot for "intermediate bodies" in the reaction $pp\to pp\pi^+\pi^+\pi^-\pi^-$ (116 cases have a proton as one "intermediate body").

7. t' to the "intermediate bodies" for the final state $pp\pi^+\pi^+\pi^-\pi^-$.

8. Angular correlation of the final state protons in the reaction $pp\to pp\pi^+\pi^+\pi^-\pi^-$.

9. Angular correlation of final state nucleons in the reactions "$pp\to pp\pi^+\pi^+\pi^-\pi^-\pi^o$" and "$pp\to pn\pi^+\pi^+\pi^+\pi^-\pi^-$" for a χ^2 cut of 0.2.

10. Effective mass plot of $(\pi^+\pi^-\pi^o)$ in the interaction $pp\to pp\pi^+\pi^+\pi^-\pi^-\pi^o$. All events with $\chi^2 \leq 2$ (broken line) and events with the protons in opposite hemispheres in the c.m. system (full line).

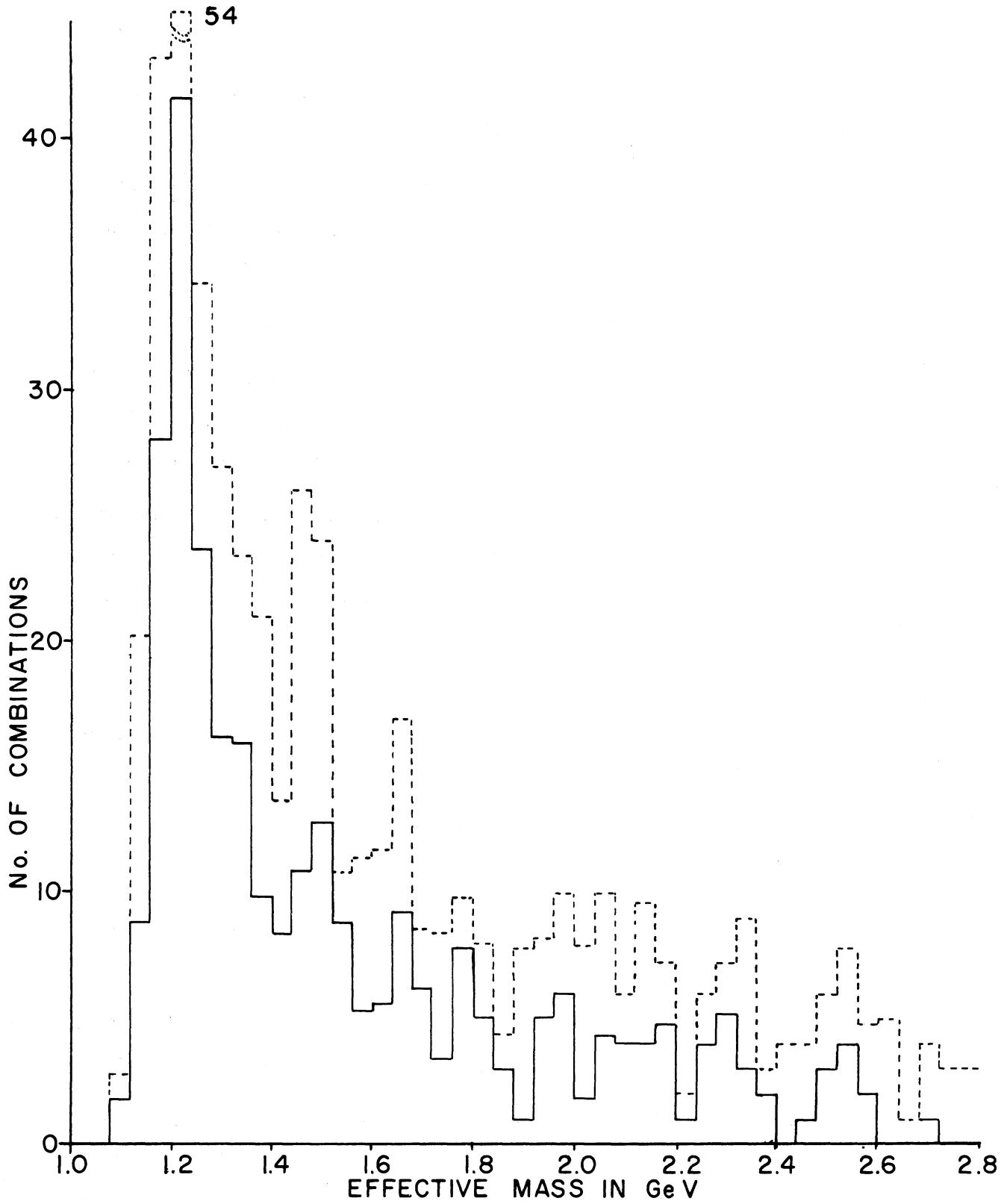
54
40
30
20
10
0
No. OF COMBINATIONS
1.0
1.2
1.4
1.6
1.8
2.0
2.2
2.4
2.6
2.8
EFFECTIVE MASS IN GeV

FIGURE 1.

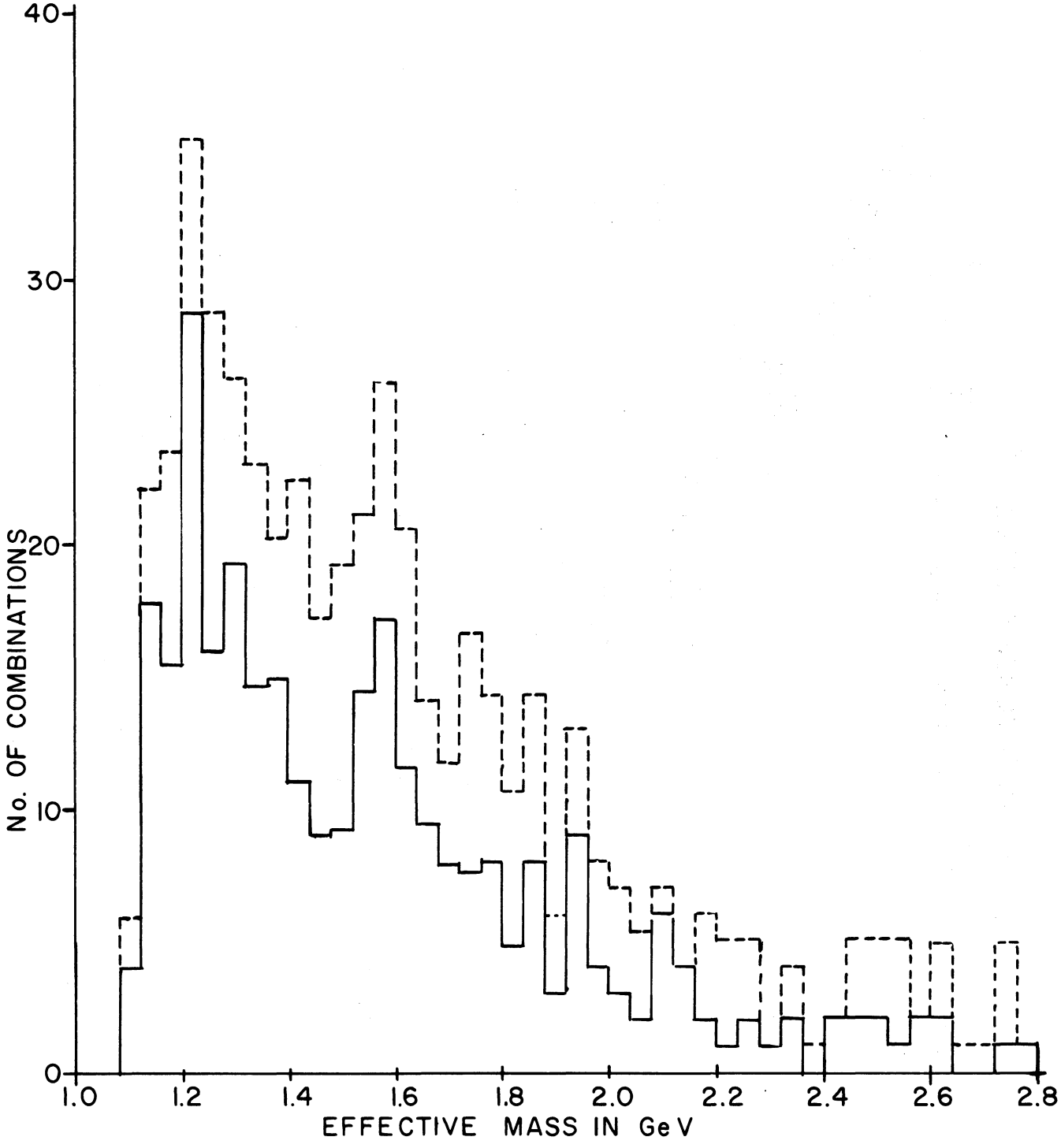
40
30
20
10
0
No. OF COMBINATIONS
1.0
1.2
1.4
1.6
1.8
2.0
2.2
2.4
2.6
2.8
EFFECTIVE MASS IN GeV

FIGURE 2.

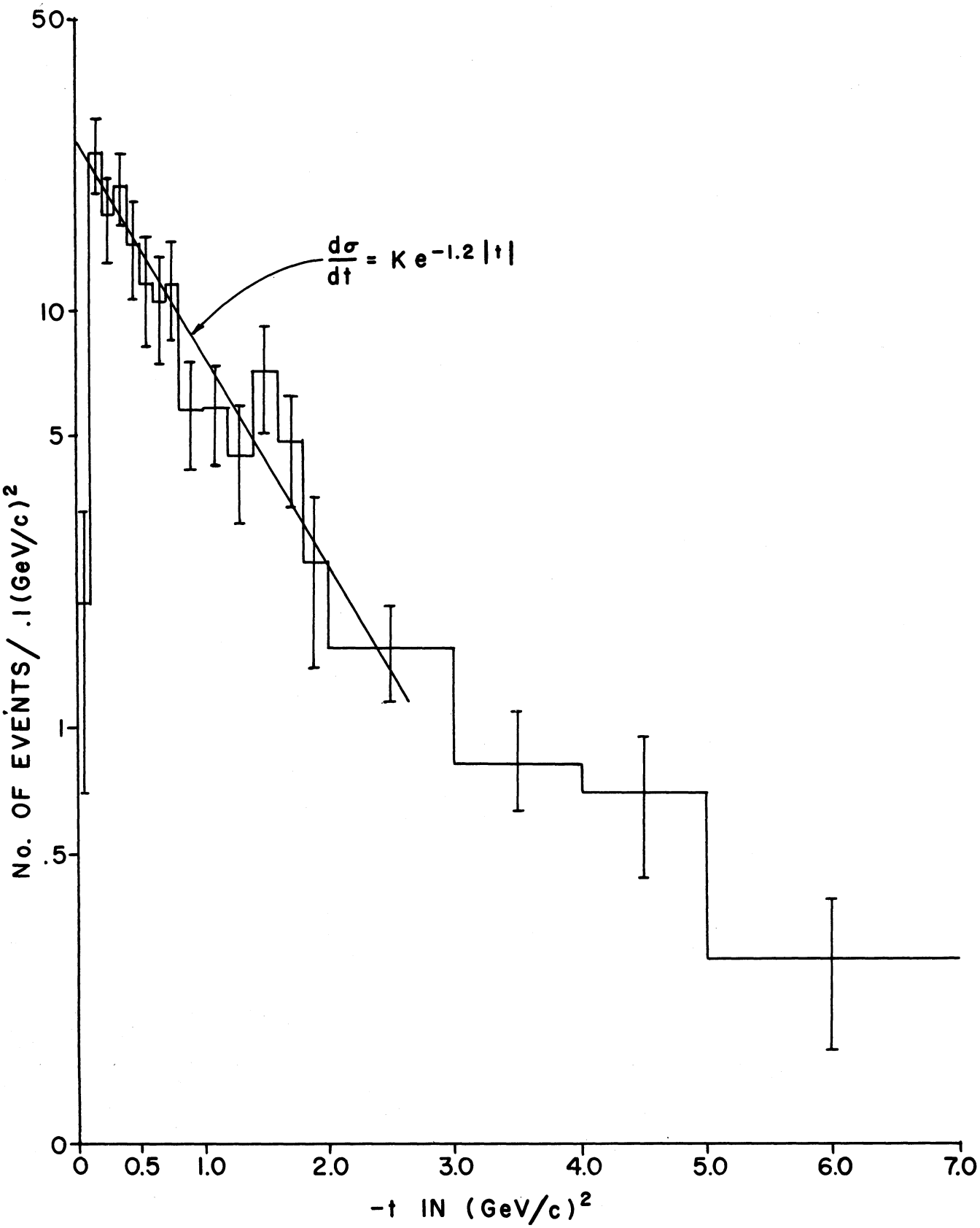
50
10
5
1
.5
0
No. OF EVENTS / .1 (GeV/c)²
$\frac{d\sigma}{dt} = K e^{-1.2|t|}$
0
0.5
1.0
2.0
3.0
4.0
5.0
6.0
7.0
-t IN (GeV/c)²

FIGURE 3.

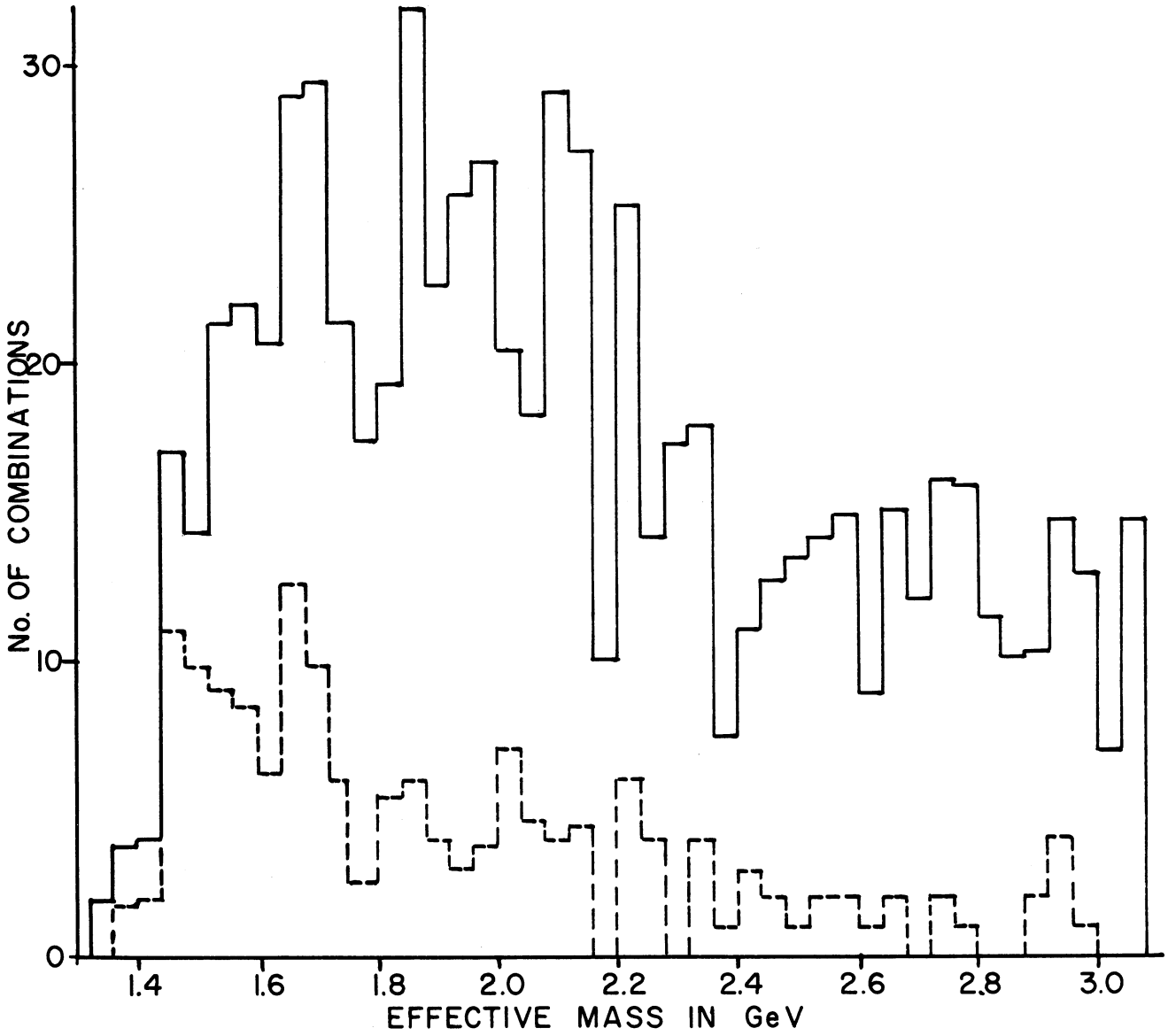
30
20
10
0
No. OF COMBINATIONS
1.4
1.6
1.8
2.0
2.2
2.4
2.6
2.8
3.0
EFFECTIVE MASS IN GeV

FIGURE 4.

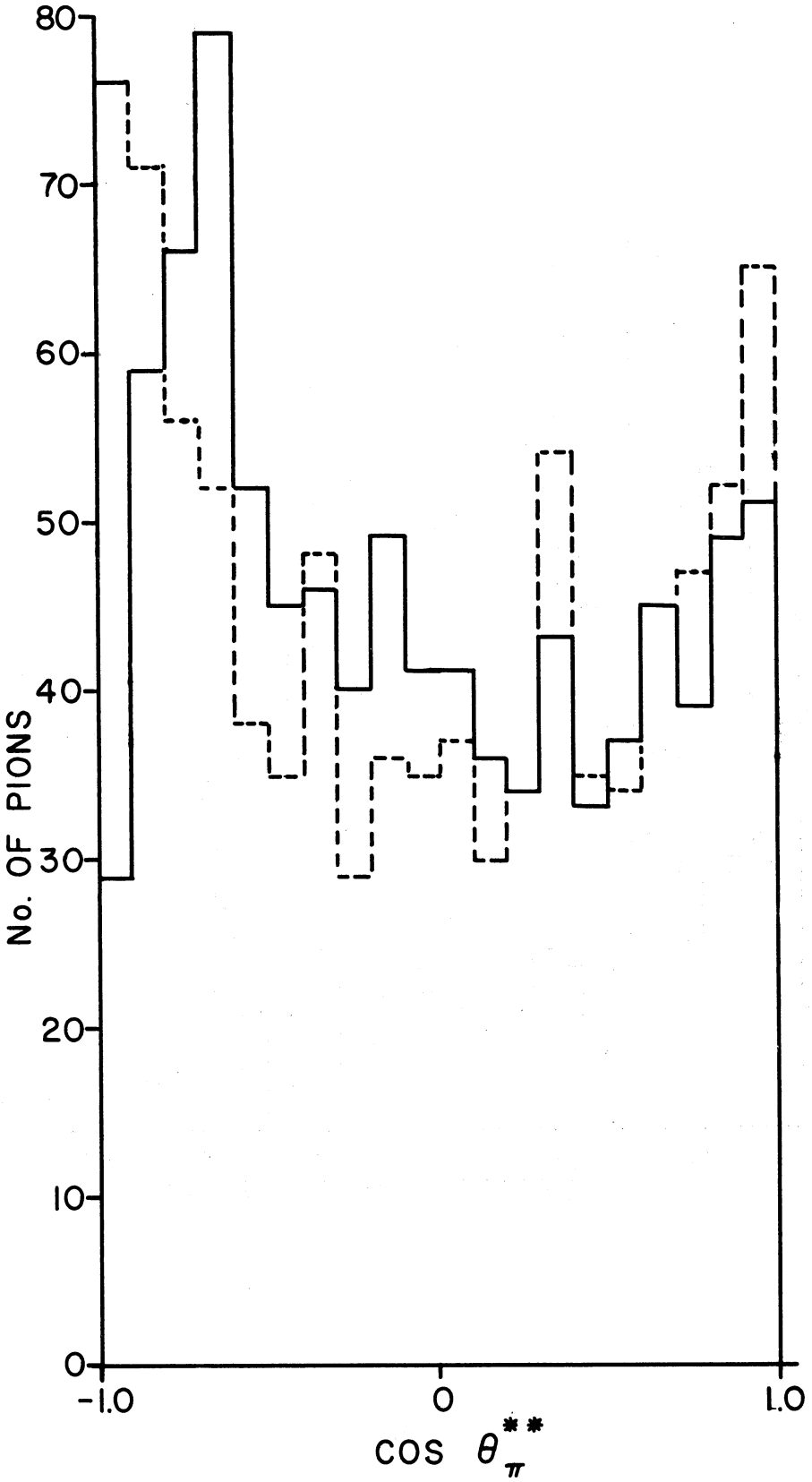

FIGURE 5.

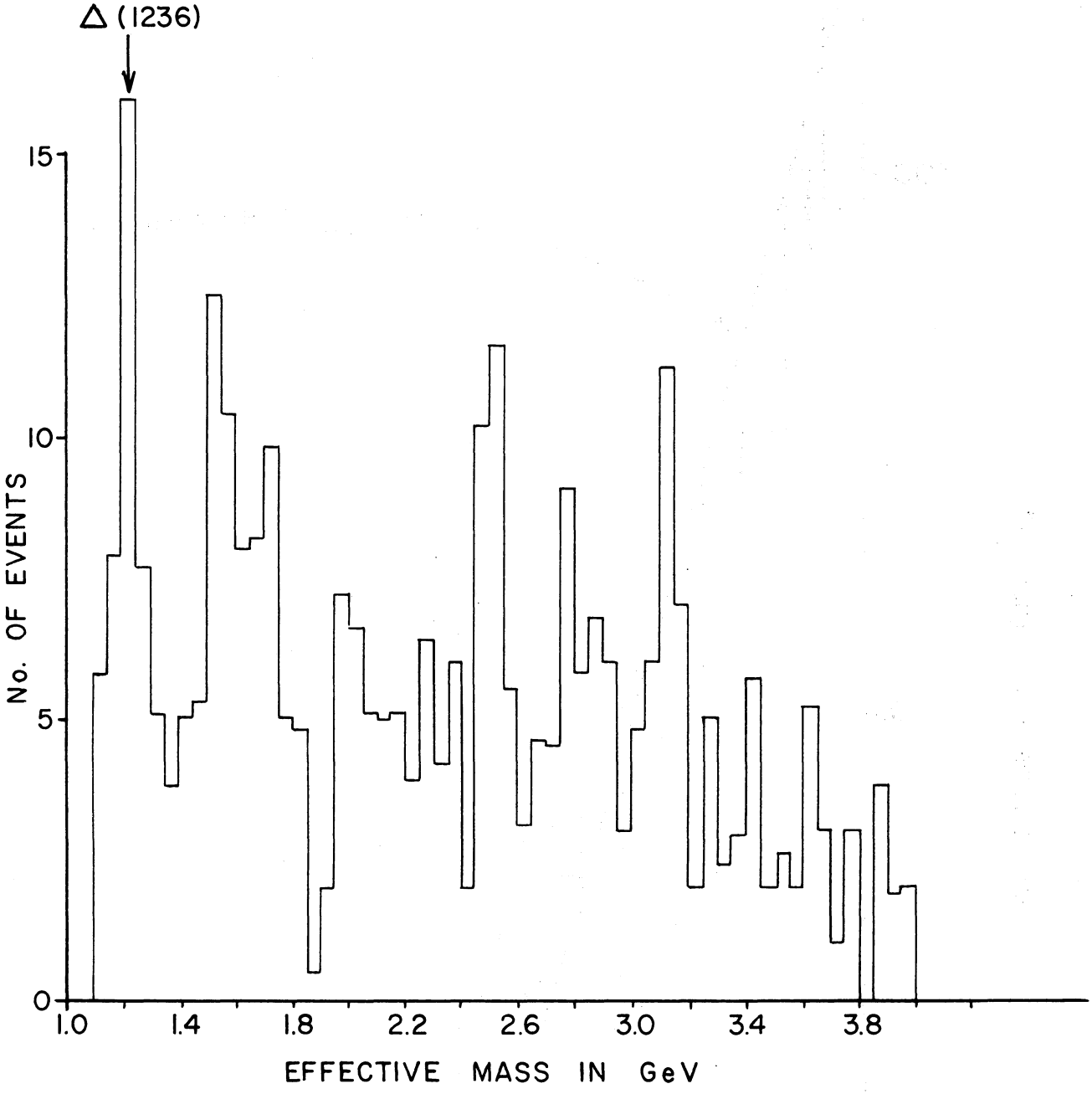
Δ (1236)
15
10
5
0
No. OF EVENTS
1.0
1.4
1.8
2.2
2.6
3.0
3.4
3.8
EFFECTIVE MASS IN GeV

FIGURE 6.

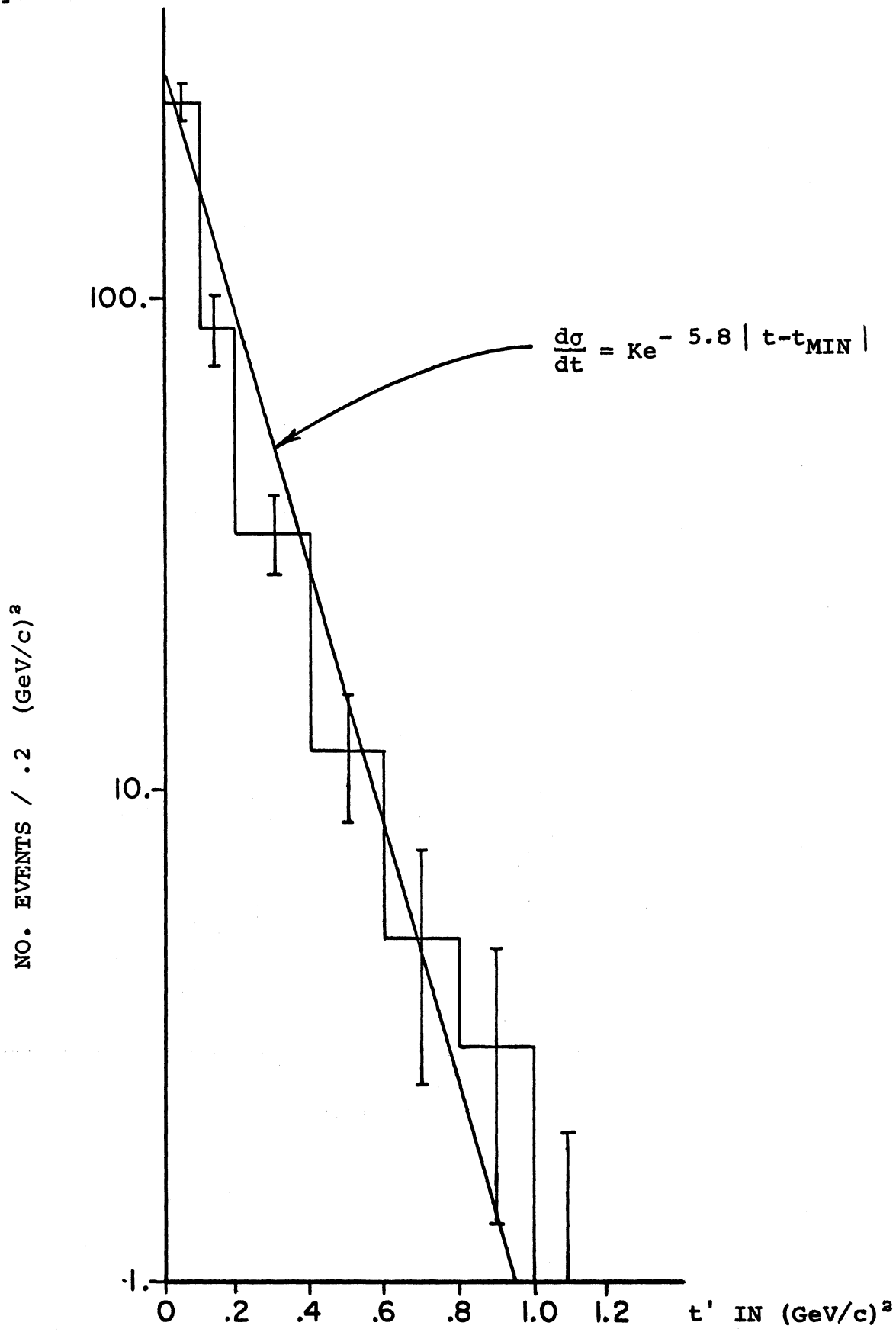
100.
10.
1.
$\frac{d\sigma}{dt} = Ke^{-5.8|t-t_{MIN}|}$
NO. EVENTS / .2 (GeV/c)²
0
.2
.4
.6
.8
1.0
1.2
t' IN (GeV/c)²

FIGURE 7.

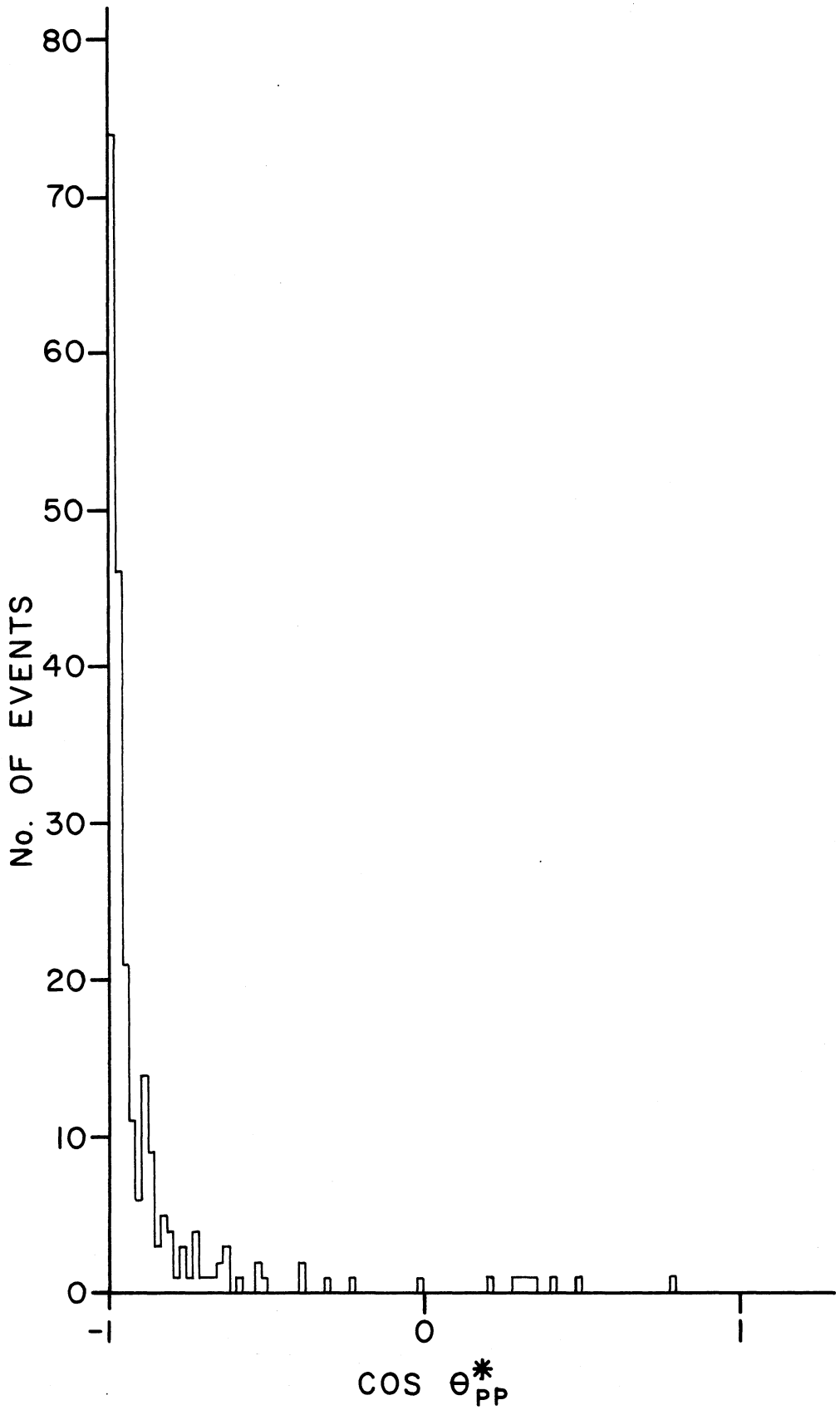

FIGURE 8.

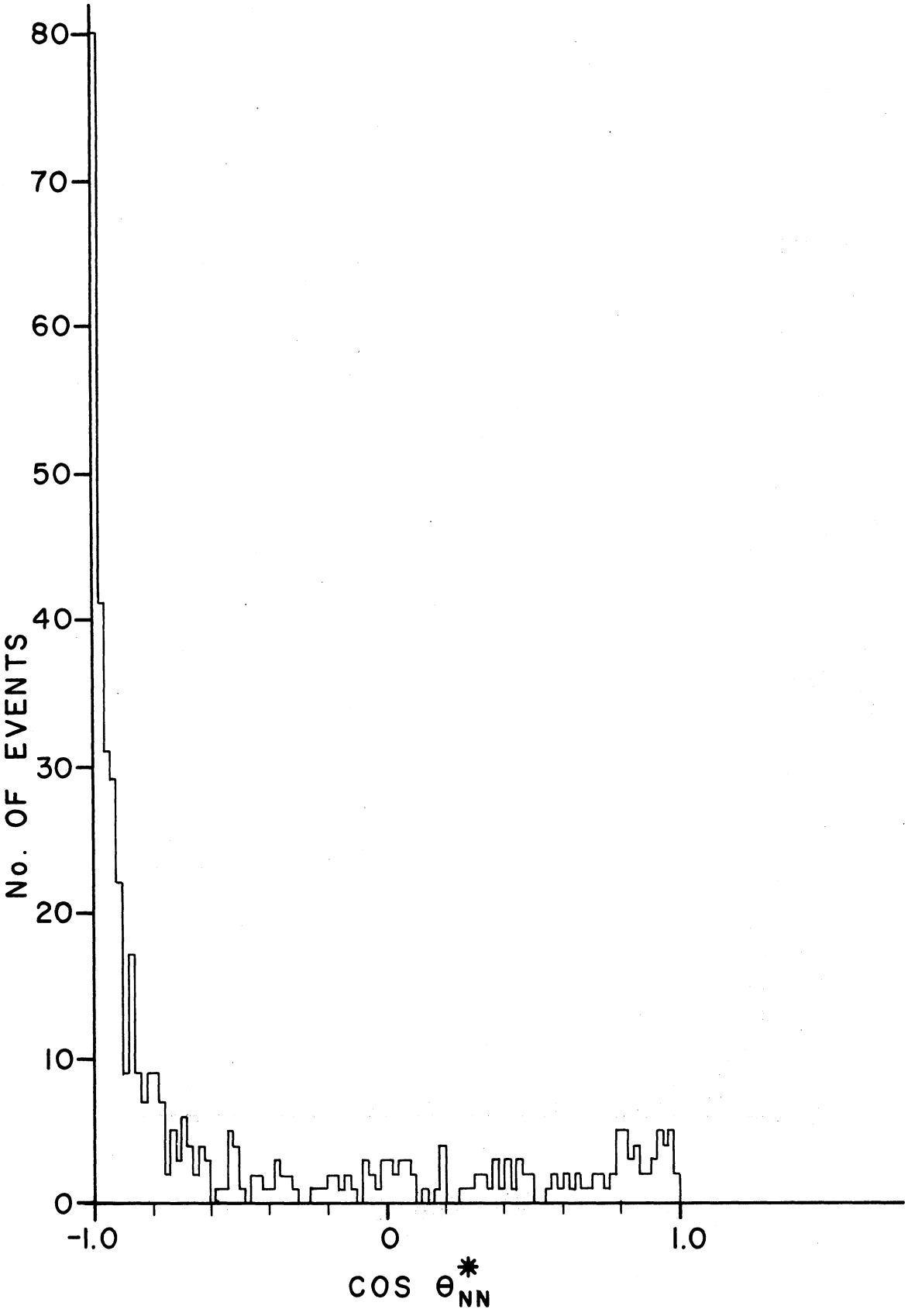

FIGURE 9.

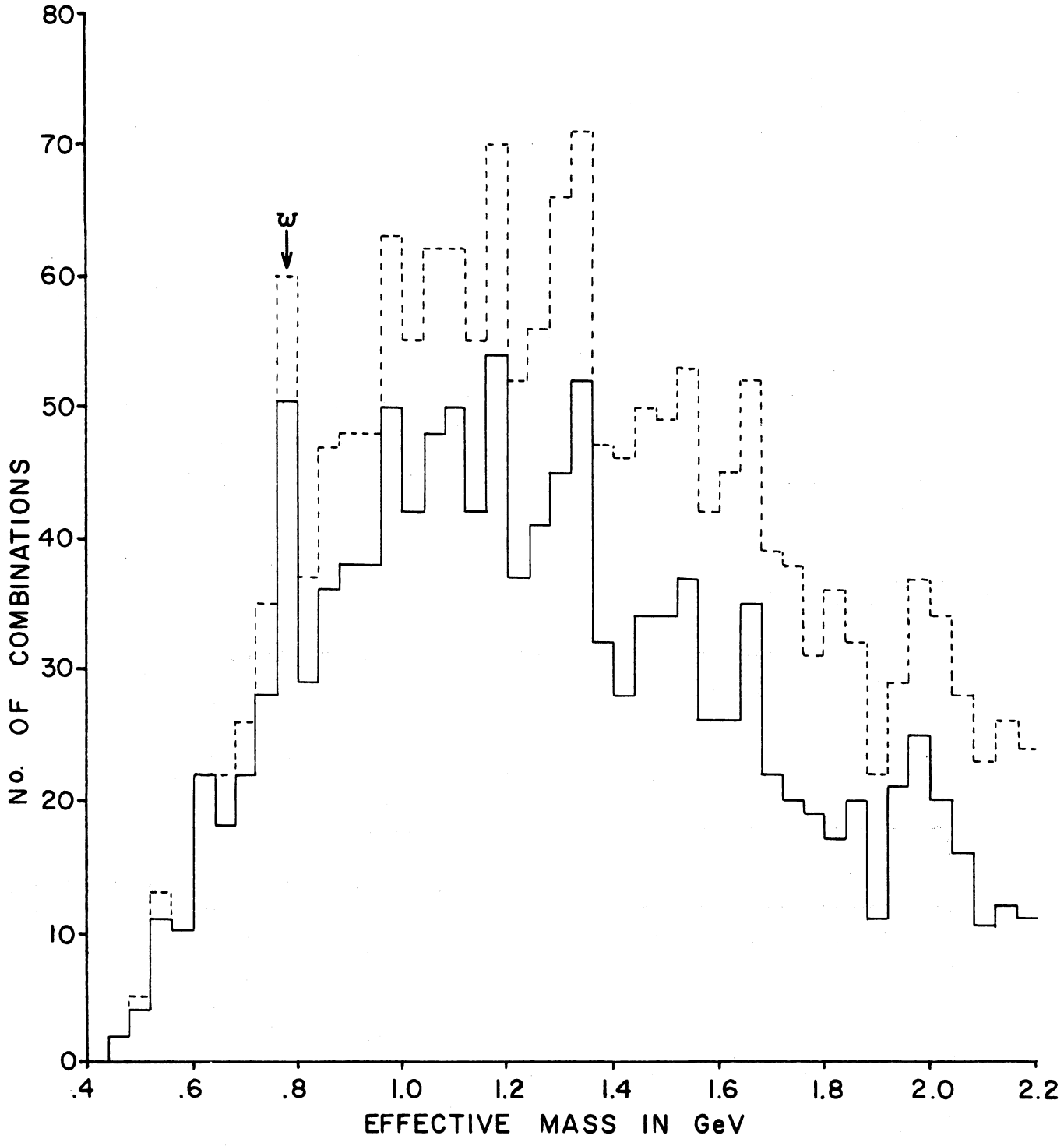
80
70
60
50
40
30
20
10
0
No. OF COMBINATIONS
ω
.4
.6
.8
1.0
1.2
1.4
1.6
1.8
2.0
2.2
EFFECTIVE MASS IN GeV

FIGURE 10.

SIX PRONG $\pi^- p$ INTERACTIONS AT 11 GeV/c INCOMING MOMENTUM

P. Daronian, A. Daudin, B. Gandois, C. Kochowski, L. Mosca,
Département de Physique des Particules Elémentaires,
CEN-Saclay, France.

Here we give some preliminary results on a partial sample of about 4000 six-prong events produced by negative pions of 11 GeV/c on protons in hydrogen bubble chambers (1.5 m BNHBC and 2 m CERN HBC).

1. CROSS SECTIONS

The cross sections of the different reactions studied are given in Table I.

TABLE I

Reactions	Cross sections (mb)
(1) $\pi^- p \to p\pi^-\pi^-\pi^-\pi^+\pi^+$	0.29 ± 0.03
(2) $\pi^- p \to p\pi^-\pi^-\pi^-\pi^+\pi^+\pi^\circ$	0.71 ± 0.07
(3) $\pi^- p \to n\pi^-\pi^-\pi^-\pi^+\pi^+\pi^+$	0.30 ± 0.03
(4) $\pi^- p \to p\pi^-\pi^-\pi^-\pi^+\pi^+ m\pi^\circ$ $(m \geq 2)$ (5) $\pi^- p \to n\pi^-\pi^-\pi^-\pi^+\pi^+\pi^+ m\pi^\circ$ $(m \geq 1)$	2.20 ± 0.25
All 6-prongs (without strange particles)	3.5 ± 0.30

These cross sections are compared in Fig. 1 with those obtained at others energies[1].

In the fitted reactions (1), (2) and (3) the percentage of ambiguous events is less than 15 %. However in 50 % of the NO FIT events one cannot discriminate between reaction (4) and (5). Indeed, Fig. 2 shows that the proton has a laboratory momentum often bigger than 1.5 GeV/c[2] and therefore cannot be identified by ionisation. The figure also shows that the strong peripherism observed at low multiplicities, is reduced but still present in reactions with 5 or 6 secondary pions.

2. RESONANCE PRODUCTION

2.1 Reaction $\pi^- p \to p\pi^-\pi^-\pi^-\pi^+\pi^+$ (286 events)

In reaction (1) a strong production of N^{*++} (40 % → $\sigma \simeq 0.12$ mb) and ρ° (40 % → $\sigma \simeq 0.12$ mb) is observed (Fig. 3a and b). The mutual interference of these resonances is not important, but their associated production is clear (Fig. 3d), so that the cross section of the reaction $\pi^- p \to N^{*++}\rho^\circ\pi^-\pi^-$ can be estimated ($\sigma \simeq 0.06$ mb). We can conclude that ~24 % of the pions produced in reaction (1) come from these two resonances.

In Fig. 3c the $(\rho^\circ\pi^-)$ mass distribution shows two separated enhancements in the A_1^- and A_2^- regions respectively.

The existence of a strong backward peaking in $\cos\theta^*(p)$ distribution (Fig. 4c) suggests the possibility of separating the events of reaction (1) in two samples : a "peripheral" one corresponding to a cut, of $\cos\theta^*(p) < -0.8$ and a "statistical" one corresponding to $\cos\theta^*(p) > -0.8$[+]. Fig. 5 (a, b, c, d) shows that the most important resonances

---

+) These cuts were found to be practically equivalent to the cuts : $\Delta^2_{P/p} \lesssim 1.3\ (\mathrm{GeV/c})^2$.

observed (N^{*++} and ρ^{o}) are essentially present only in the "peripheral" sample. The behaviour of the background is rather different in $(p\pi^{+})$ and $(\pi^{+}\pi^{-})$ mass distributions. The cut : $\cos\theta^{*}(p) < -0.8$, drastically reduces the background under the N^{*++} (see Fig. 5a) but not under the ρ^{o} (Fig. 5b). However the background under the ρ^{o} is considerably diminished by the cut, $\cos\theta^{*}(\pi^{+}\pi^{-}) > 0.85$, which also improves the evidence for the f^{o} meson (Fig. 6).

There is some indication of quasi-three body reactions, such as $\pi^{-}p \to N^{*+}_{1/2}\,\rho^{o}\pi^{-}$ or $\pi^{-}p \to N^{*++}A_2^{-}\pi^{-}$, but the corresponding cross sections seem to be weak. Search for quasi-two body reactions has not been successfull, so their eventual existence should not correspond to an important cross section.

2.2 Reactions (2) and (3)

The general features of these reactions are analogous to those of reaction (1), but less pronounced. In $(p\pi^{+})$, $(p\pi^{-})$, $(p\pi^{o})$, $(n\pi^{+})$, $(n\pi^{-})$ systems, isobar production is evident, generally enhanced in a "peripheral" sample of events. Meson resonances ($\rho^{\pm}$, and ω) are also observed but their study is made difficult mainly by the presence of a large number of combinations per event. Nevertheless ω production (Fig. 7) is very clear ($\sigma \simeq 0.12$ mb) and the corresponding background is reduced by the cut , $\cos\theta^{*}(\pi^{+}\pi^{-}\pi^{o}) > 0.85$ (Fig. 7) shaded histogram). One may note, in particular, the existence of the associated production $\pi^{-}p \to N^{*++}\omega\pi^{-}\pi^{-}$ ($\sigma \simeq 0.05$ mb).

3. INVESTIGATION ON SOME ASPECTS OF THE COLLISION MECHANISM

The strongly peripheral character of very high energy interactions has been known for some time : after their collision the incident particles keep their initial directed momentum almost unaltered, their transverse momentum being in

consequence small. In $\pi^- p$ interactions, the proton is essentially emitted backward in c.m.s. while one of the secondary π^- is projected energetically forward, contrary to the other $\pi^\pm$ emitted rather isotropically.

On the other hand, high multiplicity interactions are sometimes considered as due mainly to central collisions which should be compatible with the statistical model. Tests based on angular correlations between outcoming particles have been used to verify the validity of this model. The results of our experiment follow.

3.1 Asymmetry parameter of the proton

Fig. 4(a,b,c,d) shows the proton angular distribution $\cos\theta^*_p$, for various multiplicities in the 11 GeV/c $\pi^- p$ interactions [2]. The asymmetry parameter $As = \frac{F-B}{F+B}$ has been evaluated (F = number of forward events, and B = number of backward events). Fig. 8 compares our results with those obtained at 5.5 and 16 GeV/c [1]. At our energy "peripheral" events dominate when less than 6 secondary pions are produced, and with more than 7 secondary pions, "statistical" events are more important. Thus it seems that the 8-prong events study is more indicated to test the statistical model, the 10-prong cross section being very weak ($\sim$ 50 μb)

3.2 Correlation between longitudinal and transverse momenta

From a Peyrou plot, the mean transverse momentum $\langle P_T \rangle$ for various P_L^* bands has been determined. Fig. 9(a,b,c) shows the variation of $\langle P_T \rangle$ versus P_L^* for the P, π^+ and π^- in reaction (1). The results are comparable with those obtained with 10 GeV/c π^- [3]. But a difference between Fig. 9b and 9c is observed. The $\langle P_T \rangle$ variation seems less symmetrical for the π^- that for the π^+.

The Table II gives $\langle P_T \rangle$ for all events of the reaction (1), and also for the "statistical" sample ($\cos\theta^*_p > -0.8$). The results of the 10 and 16 GeV/c π^- experiments are reported for comparison

TABLE II

Average transverse momenta of secondary particles (MeV/c)

Reaction	Particle	$\langle P_T \rangle$ All events	$\langle P_T \rangle$ if $\cos\theta^*_p > -0.8$
$\pi^- p \to p 3\pi^- 2\pi^+$	p	10 GeV/c 420±20 11 " 460±32 16 " 466±18	640±66
	π^+	10 GeV/c 314±14 11 " 334±16 16 " 341±10	368±31
	π^-	10 GeV/c 365±11 11 " 376±15 16 " 387±10	410±26
$\pi^- p \to p 3\pi^- 2\pi^+ \pi^\circ$	p	11 GeV/c 480±20	
	π^+	" " 351±10	
	π^-	" " 382± 9	
	π°	" " 374±18	

3.3 The angular correlations between pions

Several studies on anti-protons annihilations and recently on $\pi^+ p$ interactions at 8 GeV/c [4] have shown that the distributions of the c.m. angles between pairs of pions depend on whether the pions have like or unlike charges : $\gamma^{++}_{--} < \gamma^{+-}$, γ being the ratio of the number of pairs with the opening angle larger than 90° to that with the opening angle smaller than 90°.

Table III gives our values of γ for reactions (1), (2), (3) and for the statistical sample in reaction (1) as well as γ values versus the difference $|\Delta P|$ between the momenta of the pion pairs [4] .

The γ^{++} is found smaller than γ^{--} for reaction (1) in agreement with the 16 GeV/c π^- results[1]. The 5.5 GeV/c π^+ experiment[5] has shown on the contrary that $\gamma^{--} < \gamma^{++}$. This effect could be attributed to the "leading π" that plays a more important role when the incident energy increases.

4. CONCLUSIONS

The most characteristic experimental features that follow from the study are :

a) The strong proton backward and the strong π^- forward collimations in c.m.s. observed at low multiplicities is still important with 5 or 6 secondary pions. (Fig. 4).

TABLE III

	$0 < \Delta P < 0.2$ GeV/c	$0.2 < \Delta P < 0.44$ GeV/c	$0.44 < \Delta P < 0.76$ GeV/c	$0.76 < \Delta P < 1.6$ GeV/c	Total
$\pi^- p \to p\, 2\pi^+\, 3\pi^-$					
γ^{++}	1.04±0.29	0.78±0.23	1.09±0.44	2.7 ±1.37	1.06±0.18
γ^{--}	0.88±0.16	1.30±0.25	1.64±0.33	1.94±0.41	1.35±0.13
γ^{+-}	1.13±0.14	1.16±0.15	1.30±0.19	1.44±0.23	1.22±0.08
$\pi^- p \to p\, 2\pi^+\, 3\pi^-$; $\cos\theta^*_p > -0.8$					
γ^{++}	0.93±0.56	1.10±0.49	1.00±0.63	1.73±1.15	1.12±0.31
γ^{--}	0.95±0.31	1.40±0.47	2.14±0.68	2.54±0.88	1.63±0.23
γ^{+-}	1.40±0.32	1.11±0.24	1.48±0.34	1.38±0.33	1.32±0.15
$\pi^- p \to p\, 2\pi^+\, 3\pi^-\, \pi^o$					
γ^{++}	1.43±0.22	1.38±0.25	1.48±0.33	1.43±0.55	1.42±0.14
γ^{--}	1.10±0.10	1.35±0.14	1.36±0.16	2.16±0.34	1.34±0.08
γ^{+o}	1.05±0.12	0.95±0.12	1.18±0.18	1.88±0.43	1.13±0.08
γ^{-o}	1.15±0.11	1.14±0.12	1.12±0.13	1.44±0.23	1.17±0.07
γ^{+-}	1.25±0.08	1.18±0.08	1.34±0.12	1.33±0.16	1.28±0.05
$\pi^- p \to n\, 3\pi^+\, 3\pi^-$					
γ^{++}	0.97±0.17	1.27±0.25	1.36±0.31	2.0 ±0.63	1.23±0.13
γ^{--}	1.06±0.19	1.14±0.22	1.44±0.35	1.58±0.42	1.22±0.13
γ^{+-}	1.20±0.13	1.43±0.16	1.37±0.19	1.47±0.25	1.34±0.08

b) The known N^{*++} , ρ^{o} , f^{o}, ω and A resonances are observed. The N^{*++} and ρ^{o} , especially abundant in reaction (1), are also collimated backward and forward respectively (in c.m.s.).

c) Little quasi-2-body and quasi-3-body production is observed ; but quasi-4-body production is more abundant. ($N^{*++}\rho^{o}\pi^{-}\pi^{-}$, 26 % of reaction (1) and $N^{*++}\omega\pi^{-}\pi^{-}$, 8 % of reaction (2)).

d) The $< P_T >$ is close to that found at other energies and it is sensibly smaller than for the "statistical" sample.

e) The angular correlations observed in other experiments (Goldhaber effect) are perturbed by the presence of resonances and the π^{-} leading effect ; so the interpretation is made difficult.

The experimental results suggest that it would be interesting to confront them with the existing models, in particular with the quark model recently proposed by Satz[6].

The authors are grateful to Professor A. BERTHELOT and Dr. A. ROGOZINSKI for their interest in this work.

REFERENCES

1) K. Böckmann, H. Drevermann, K. Sternberger, N. Stief, T. Hofmoki, L. Michejda, S. Orwinowski, H. Piotrowska, R. Sosnowski, M. Szeptycka, W. Wojcik, A. Wroblewski, Varsaw, Institute of Nuclear Research Report "P" 837/VI/PH.

2) Genova-Hamburg-Milano-Saclay Collaboration, Private communication.

3) M. Bardadin-Otwinowska, L. Michejda, S. Otwinowski, R. Sosnowski, Phys. Letters 21, 351 (1966).

4) J. Bartke, O. Czyzewski, J.A. Danysz, A. Eskreys, J. Loskiewicz, P. Malecki, J. Zaorska, K. Eskreys, K. Juszczak, D. Kisielewska, W. Zielinski, M. Szeptycka, K. Zalewski, G. Pichon, M. Rumpf, Phys. Letters 24B, 163 (1967).

5) a) H. Drevermann, U. Idschock, K. Bockmann, A.J. Apostolakis, G. Briggs, C.A. Kitchen, J.V. Major, C.L. Pols, J. Schotanus, D. Toet, R.T. van de Walle, R. Lestienne, P. Fleury, C. Grosso, B. Quassiati, G. Rinaudo, A. Werbrouck, Phys. Rev. 161, 1356 (1967).

b) R. Lestienne, Thesis 1967, Ecole Polytechnique, Paris.

6) H. Satz, Report Desy 67/19 (June 1967).

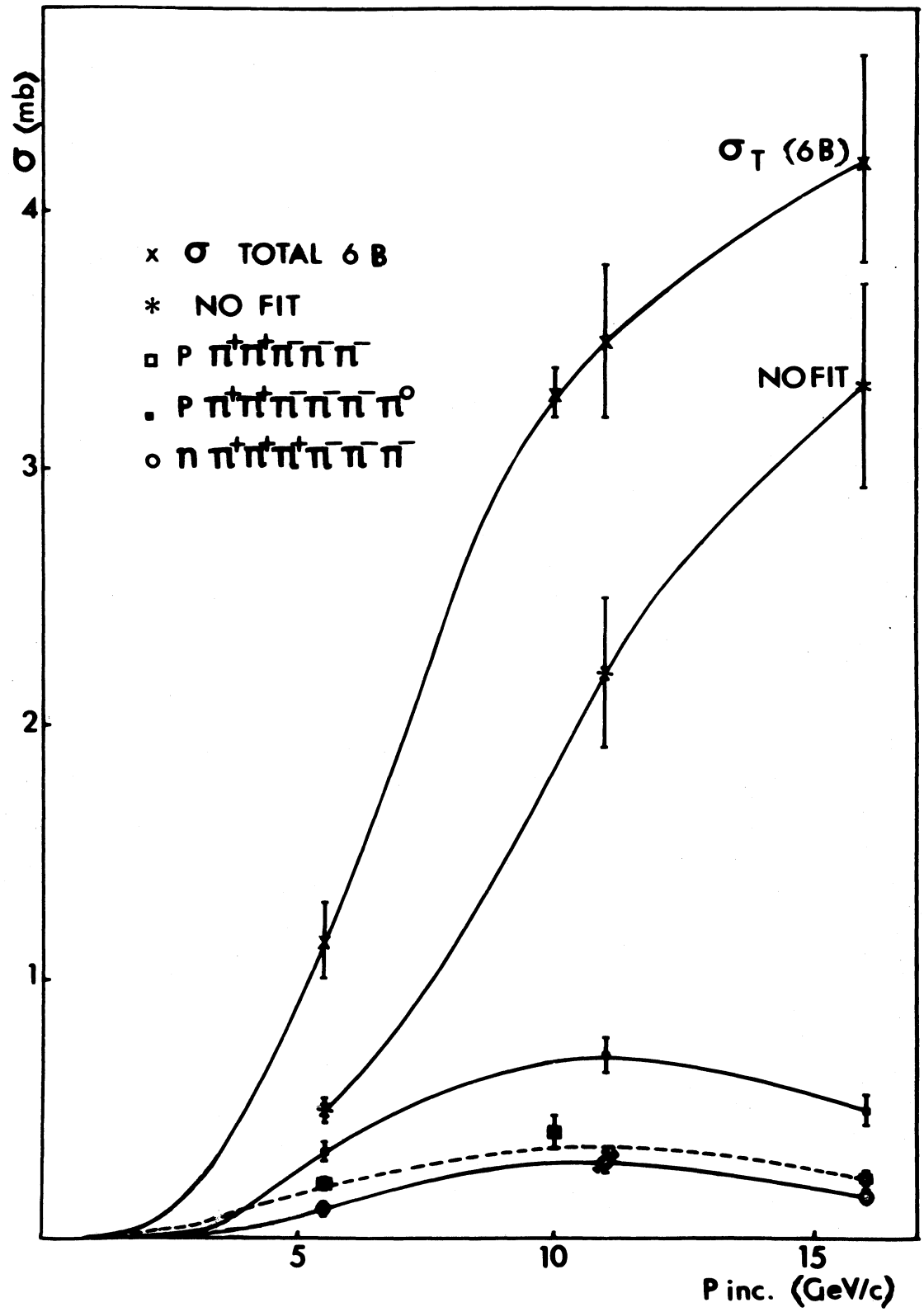

Fig. 1 : Cross sections for the various six charged prong reactions.

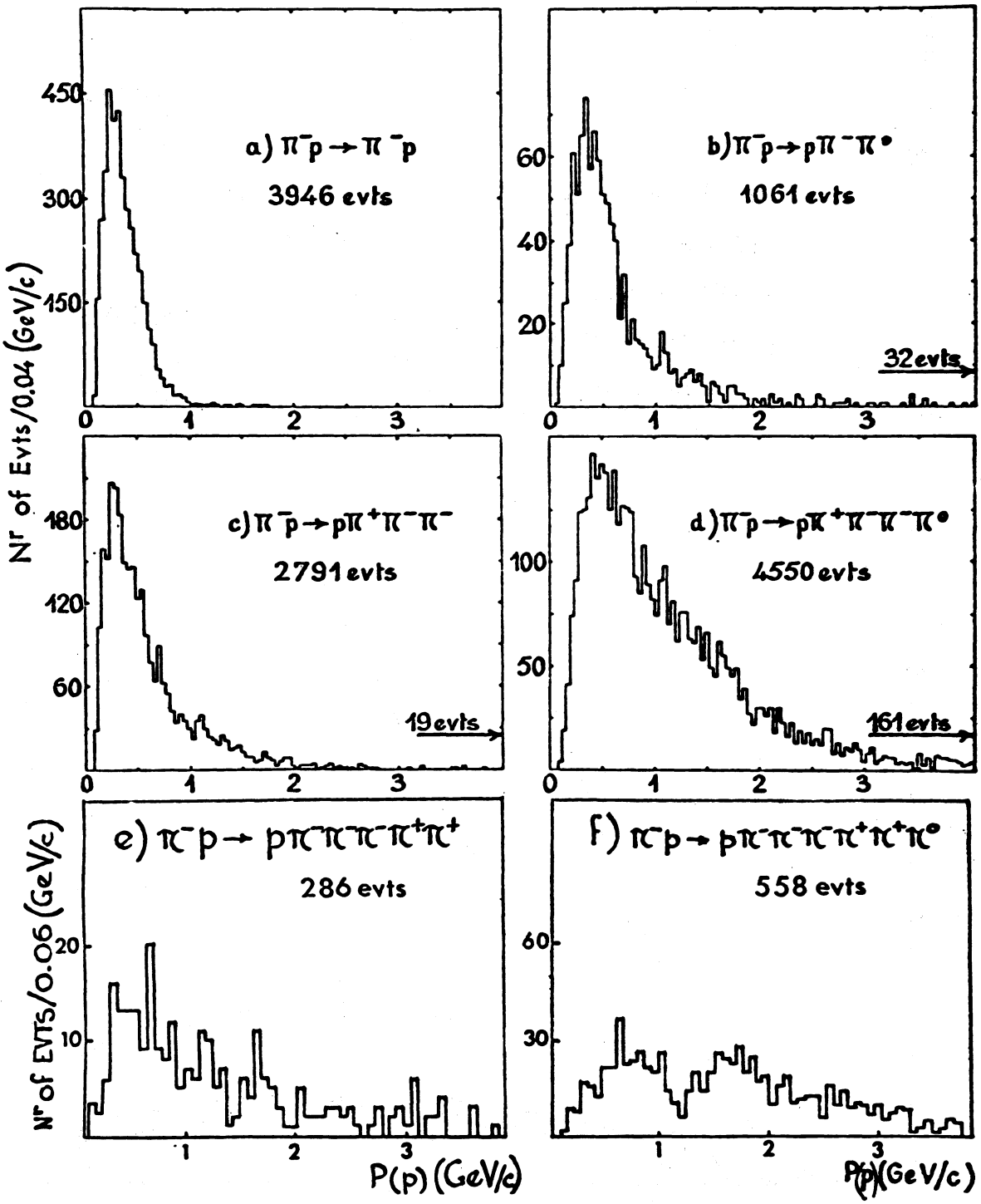

Fig. 2 : Laboratory momentum of the proton for various multiplicities.

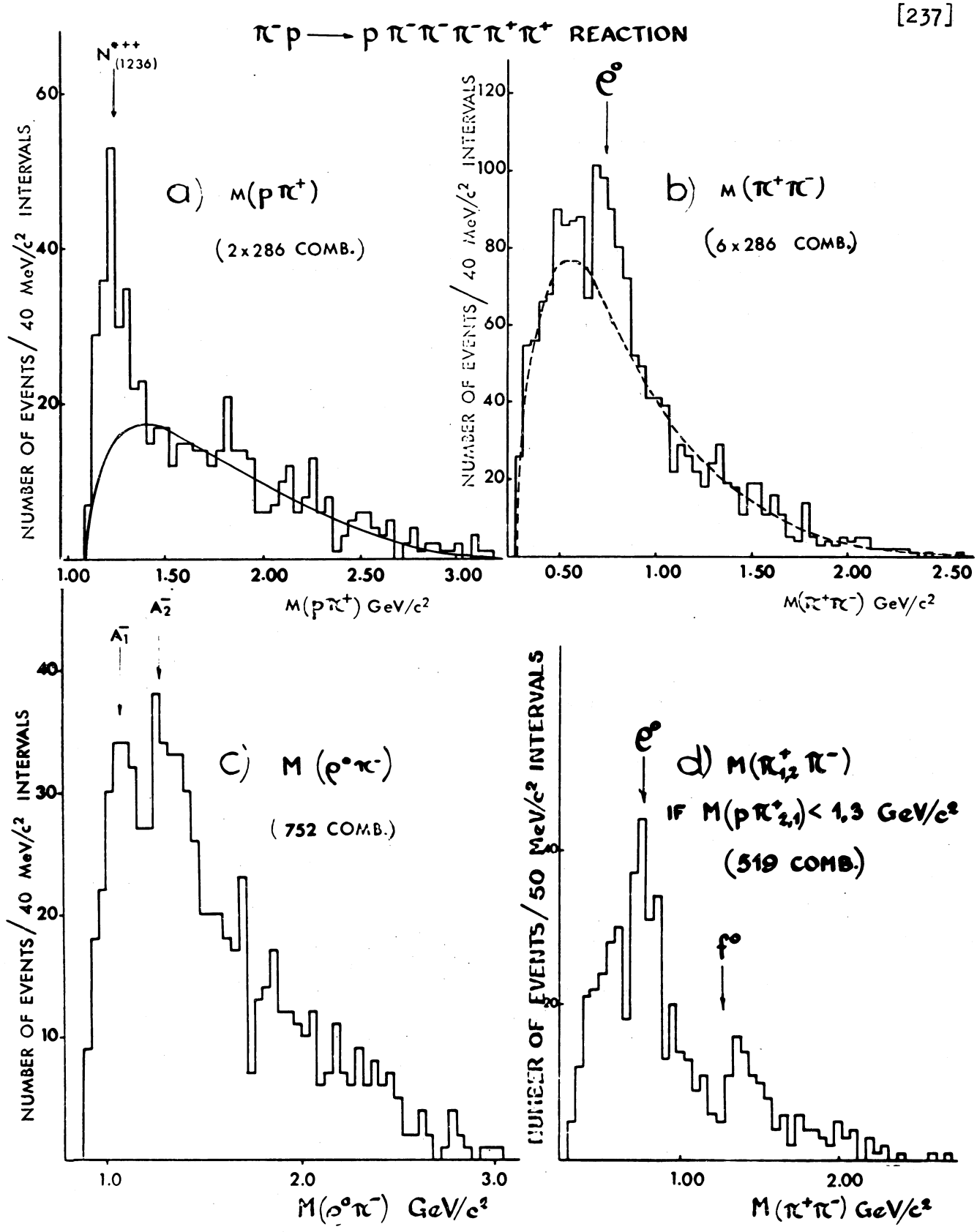

Fig. 3 (a, b, c, d) : Mass distributions in channel (1).
The full-line in a) shows the predictions of the statistical phase space. The dashed line in b) represents the experimental distributions of $M_{\pi^+\pi^+}$ + $M_{\pi^-\pi^-}$.

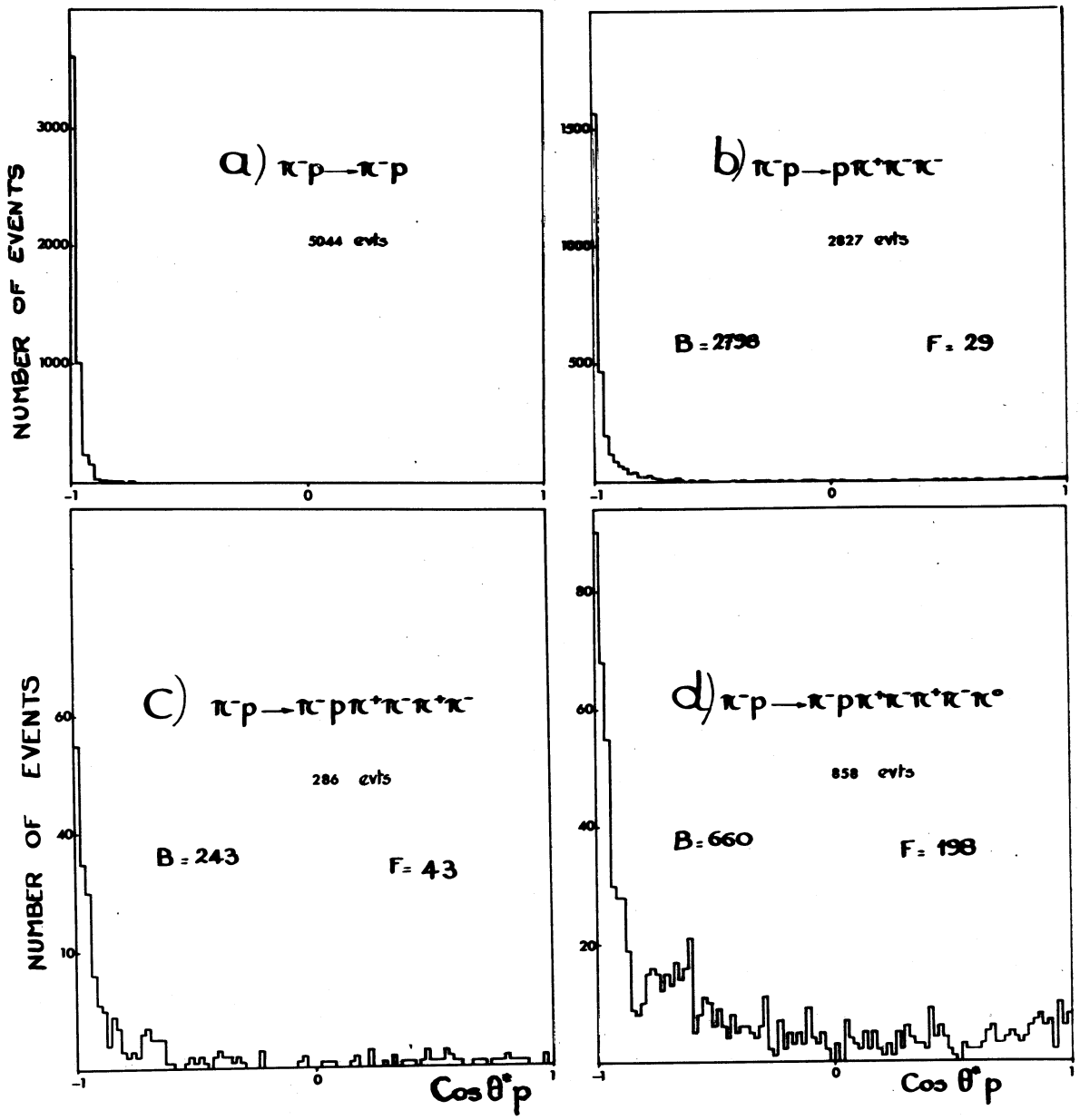

Fig. 4 : C.M. angular distributions of the protons.

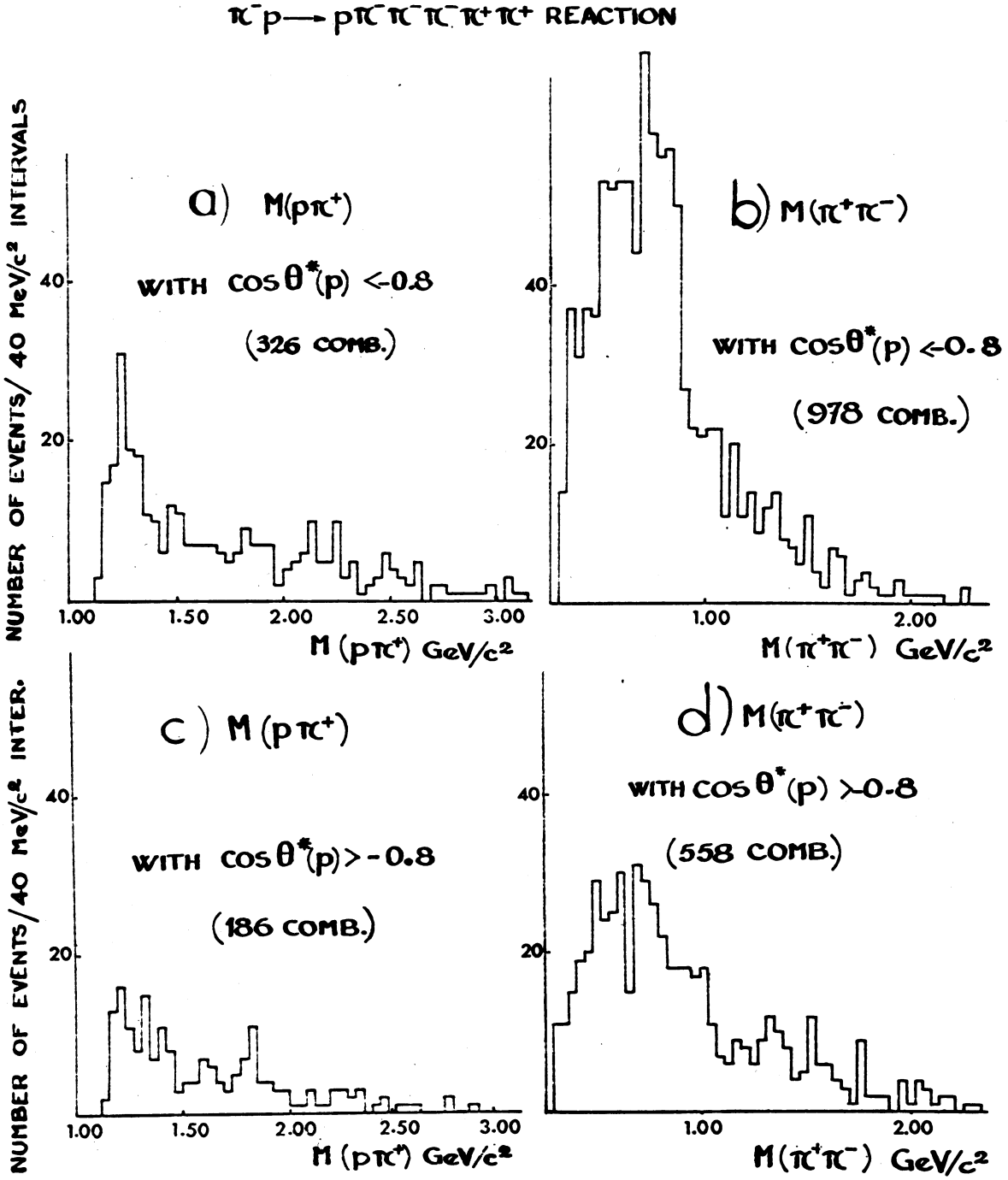

Fig. 5 : $(p\pi^+)$ and $(\pi^+\pi^-)$ mass distribution :

a, b, If $\cos\theta_p^* < -0.8$

c, d, If $\cos\theta_p^* > -0.8$

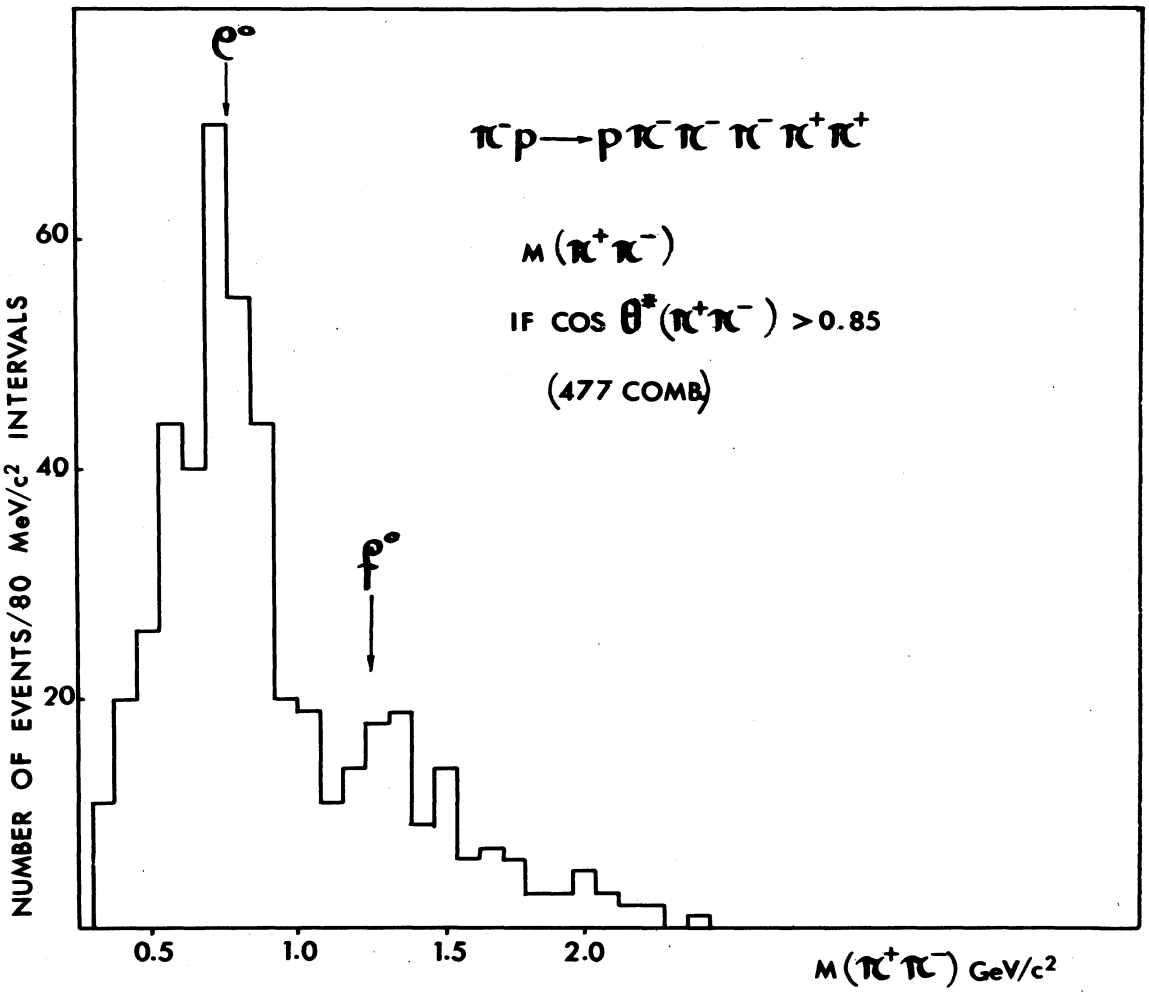

Fig. 6 : $(\pi^+\pi^-)$ mass distribution if $\cos\theta^*_{\pi^+\pi^-} > +0.85$.

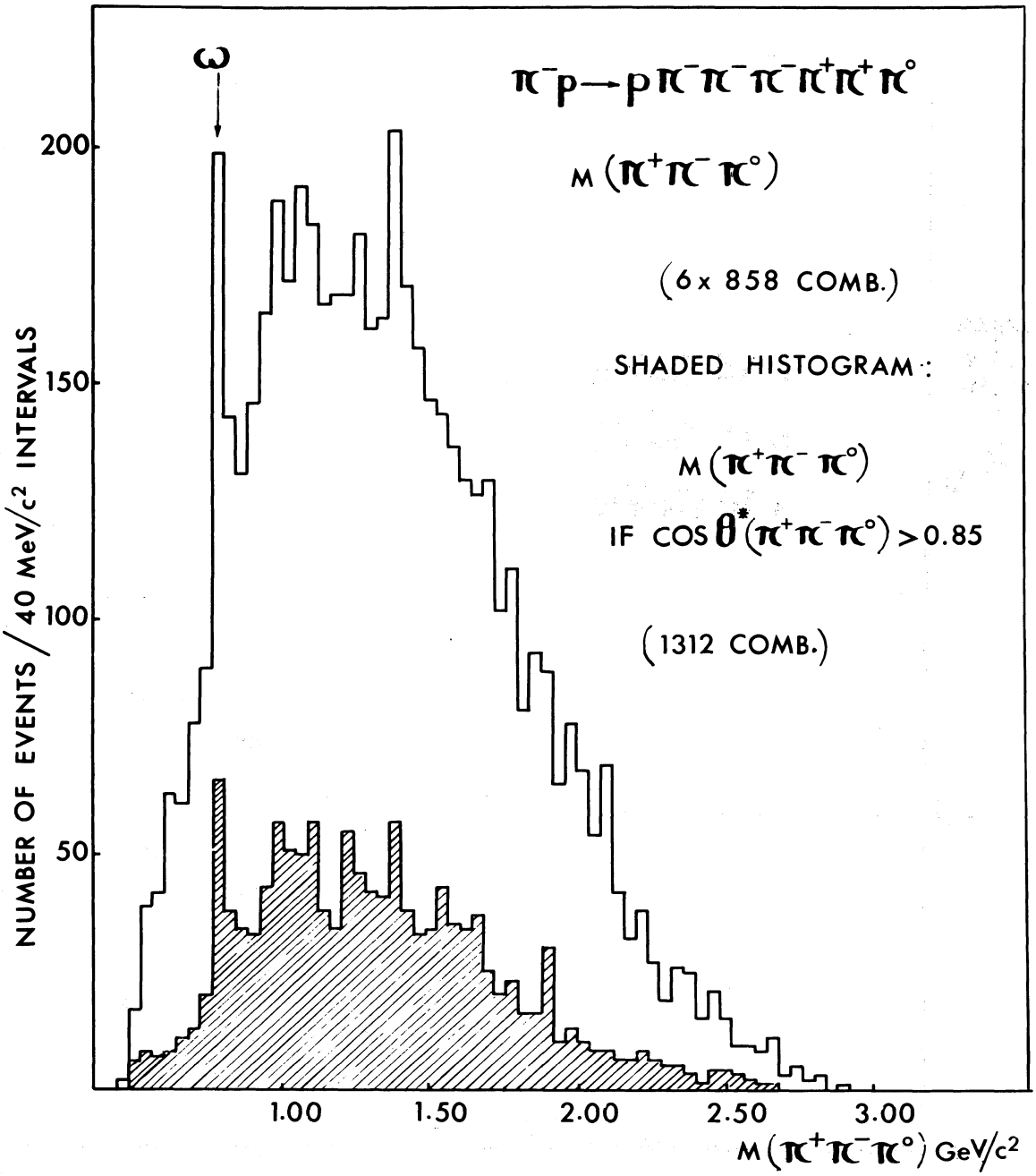

Fig. 7 : $(\pi^+\pi^-\pi^\circ)$ mass distribution.

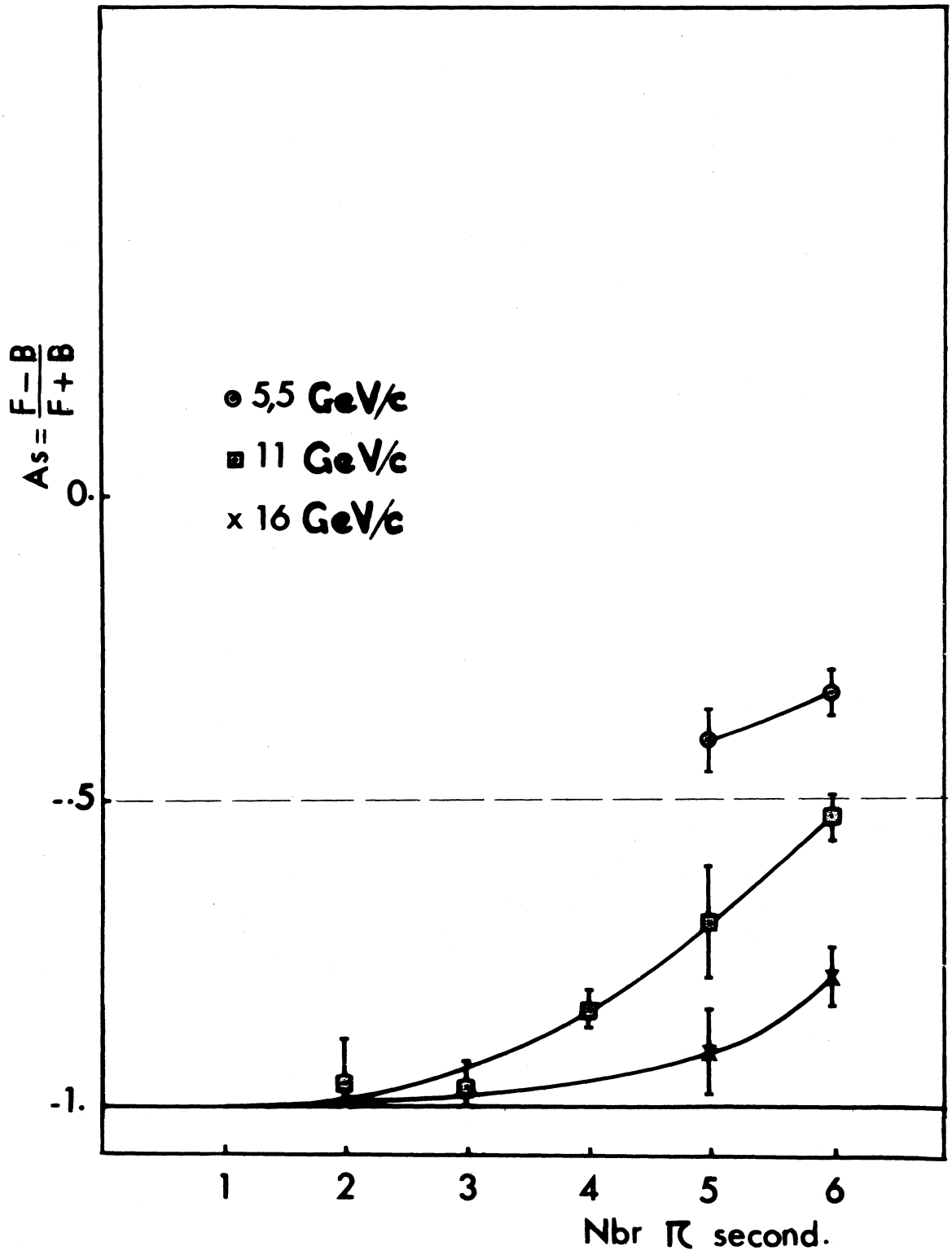

Fig. 8 : Asymmetry parameter As vs number of secondary pions.

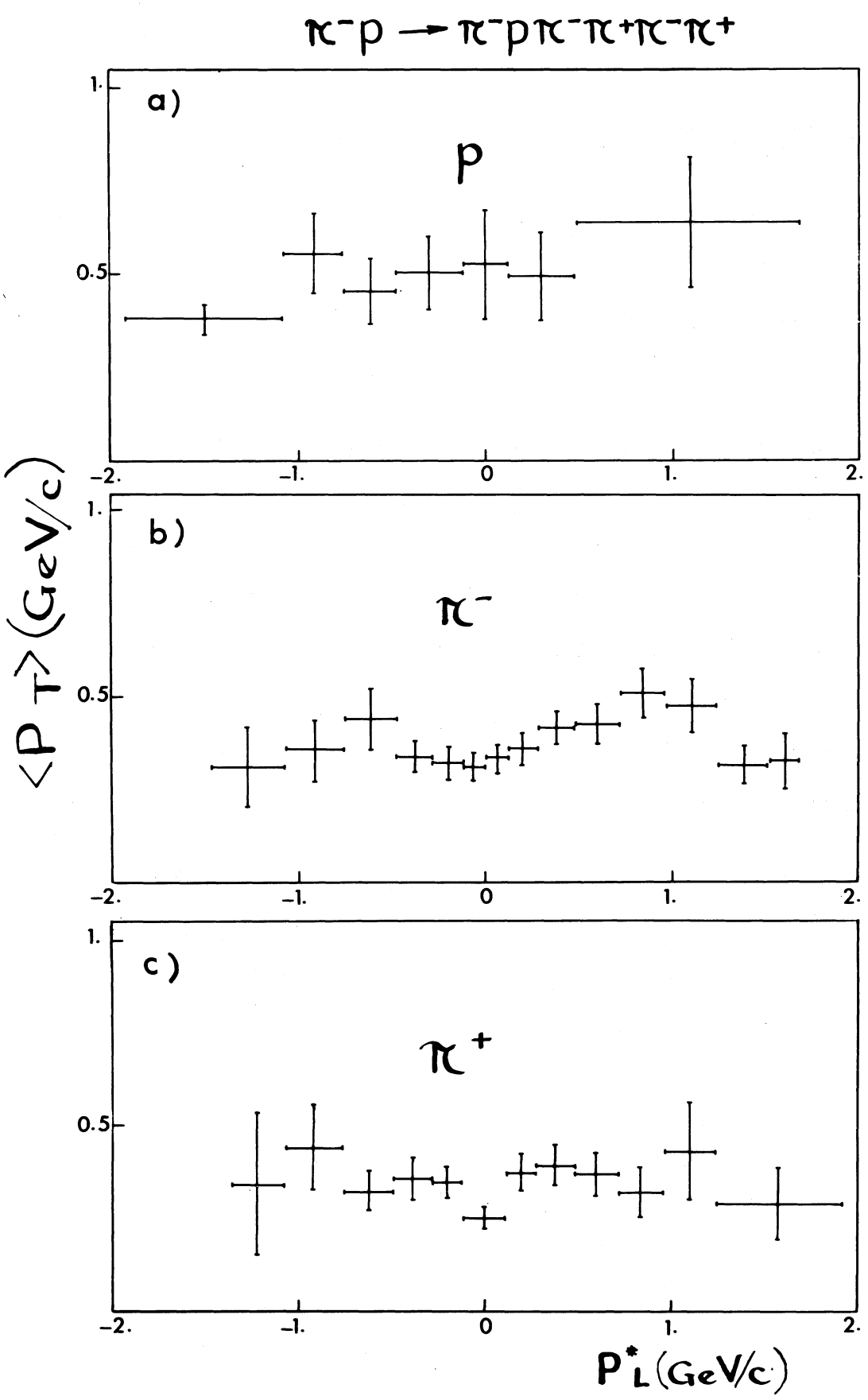

Fig. 9 : $\langle P_T \rangle$ vs P_L^* .

MULTIPRONG EVENTS IN 25 BEV/C π^-p COLLISIONS

J. W. Elbert, A. R. Erwin, S. Mikamo, D. Reeder, Y. Y. Chen, W. D. Walker, and A. Weinberg,

University of Wisconsin,
Madison, Wisconsin

Our group is currently analyzing multiprong events produced by 25 BeV/c π^- in the BNL 80 inch hydrogen chamber with a 1/4 inch thick Ta plate in the downstream end. We have measured data from 5,000 6-prongs down to 5 16-prongs, but many of the figures presented here are based on considerably smaller samples for the 6 and 8 prong events. The breakdown of the total cross section is approximately as follows in the table.

Number of Prongs	% of Total Cross Section
0	$.77 \pm .08$
2	$28.61 \pm .49$
4	$34.53 \pm .54$
6	$23.47 \pm .45$
8	$9.52 \pm .30$
10	$2.55 \pm .15$
12	$.44 \pm .06$
14	$.09 \pm .03$
16	$.003 \pm .002$

Figure 1 shows how the fraction of the total cross section has been going as a function of laboratory π^- momentum. This probably should be plotted as a function of most anything but straight lab momentum if one wishes to guess the processes responsible for the production. Our points at 25 BeV/c seem in agreement with p-p charged multiplicities at the same momentum, giving no clue of an essential difference between p-p and π^- - p interactions at higher multiplicities.

The difficulty in handling multiprong events in the usual way can probably be appreciated by noting that the number of effective mass combinations that should be computed for a 6 prong is 56, while the same number for a 16 prong event is 65,536. In most cases a resonance would probably be lost in the combinatorial background. A theoretical model then becomes a most important tool when it can guide the analysis and reduce the magnitude of the problem.

There are many such models, but most of them are statistical in nature and tend not to test very fundamental ideas. To date we have not found a statistical model that agrees well with the transverse and longitudinal momentum distributions observed. There is some hope therefore that the data contain more information than just some simple modification of phase space.

Although we will ultimately achieve kinematic fits to about 20% of our events as an upper limit, we currently are

using the larger sample of events without any particle identification. We do this by considering only tracks which transform into the forward hemisphere of the center of mass system when they are assumed to be pions. Events with obvious strange particle decays are not used since a serious effort has been made to constrain that sample of events kinematically. These forward tracks are, we hope, known to be pions with a fair degree of certainty. If π - p collisions are somehow different from p-p events, it would be expected that the difference would show up in the forward hemisphere.

Figure 2 is a plot of the longitudinal momenta in the center of mass for all particles in 6 prong events assuming each particle is a pion. The distribution in negative p_L probably must be disregarded because of proton misidentification. Positive values of p_L actually fall off with a very nice exponential in p_L for all multiplicities. There is no evidence for an articulate group of "screaming" pions in the forward direction with high momentum. By fitting the forward distribution of p_L to the form

$$dN \sim e^{-ap_L} dp_L$$

we can extract a coefficient $\underline{a}$ for each multiplicity. Typical fits can be seen in figure 3. The value of $\underline{a}$ as a function of multiplicity can be seen in figure 4. There is an obvious dependence here on multiplicity which probably escaped notice previously because of poor statistics.

The transverse momentum distribution of the forward hemisphere particles can be fit fairly well to the form

$$dN \sim p_T^{3/2} \, e^{-bp_T} \, dp_T$$

This is an approximation to what has been suggested by several statistical models.[1] Sample fits can be seen in figure 5. If one plots the coefficient b as a function of visible prongs, there is again a correlation which can be seen in figure 6.

These fits, which look pretty good at first glance, certainly don't tell the whole story. Figure 7 shows the extent to which the simple form used above for p_T fails when the events are plotted for various cuts in p_L ($P_{//}$ in the figure label). The product function of the two distributions does not do an especially good job of describing the data as may be seen by comparing the calculated and experimental angular distributions in figure 8.

The only attempts to look at effective masses so far have been rather crude and again involve only the unconstrained data for particles in the forward hemisphere. Figure 9 and 10 plot the effective mass of the group of charged particles in the forward hemisphere. Only events in which the missing momentum was in the backward hemisphere were used. About all one can say is that as the number of pions gets larger, the effective mass gets larger. When only two particles go forward in the 6 prongs, there is some evidence of rho and f° production. When three particles go forward, there is an

accumulation in the A region which almost always contains a rho-pi combination.

We have rather clear evidence that this is not the way to look at the higher multiplicities without some modification. If one transforms into the center of momentum system for the forward group of each event, one observes that all three components of the momentum have approximately the same distribution for 6-prongs. As the multiplicity increases, however, the longitudinal momentum distribution becomes distorted and depleted in the backward direction. The shape suggests that a forward going mass has decayed, throwing some of its products into the backward hemisphere.

We have made some attempt to compare our π-p data with the p-p counter data of Ratner et al.[2] at 12.5 BeV/c. This can be achieved with considerable loss in statistical accuracy by cutting the bubble chamber data to simulate the acceptance of the counter apparatus. The open circles of figure 11 represent about one third of our data. Considering the poor resolution and statistics of our "counters", and the limitation to 6 prongs only, one might conclude that π-p and p-p are not in disagreement at this stage of the experiment.

Better statistics can be obtained in our data by considering lower values of p_T than Ratner et al. The x's mark these points. They show the same dip for small values of p_L as the p-p data does for pion production.

Figure 12 compares the p-p data of Ratner et al. with our π-p data for the transverse momentum distribution. Agreement is especially good even though the comparison is just done for 6 prongs.

REFERENCES

1. See for example, G. A. Milekhin and I. L. Rozenthal, Soviet Physics JETP 6, 154 (1958). R. Hagedorn, Supplemento al Nuovo Cimento, No. 2, 147 (1965). J. R. Wayland and T. Bowen, Nuovo Cimento 48, 663 (1967).

2. L. G. Ratner, K. W. Edwards, C. W. Akerlof, D. G. Crabb, J. L. Day, A. D. Krisch, and M. T. Lin, Phys. Rev. Letters 18, 1218 (1967).

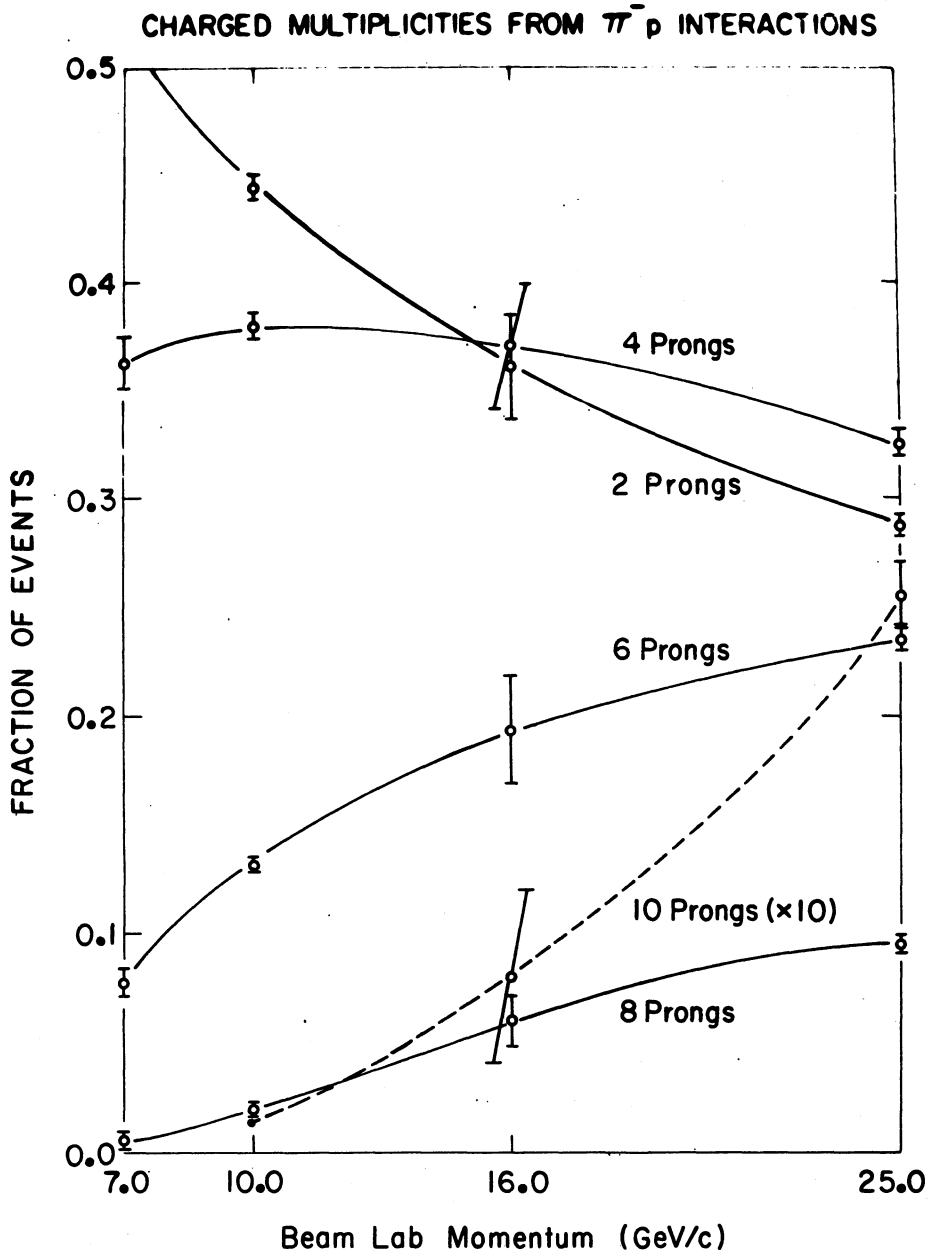
CHARGED MULTIPLICITIES FROM π⁻p INTERACTIONS
FRACTION OF EVENTS
0.5
0.4
0.3
0.2
0.1
0.0
4 Prongs
2 Prongs
6 Prongs
10 Prongs (×10)
8 Prongs
7.0
10.0
16.0
25.0
Beam Lab Momentum (GeV/c)

FIG. 1

C.M. LONGITUDINAL MOMENTUM

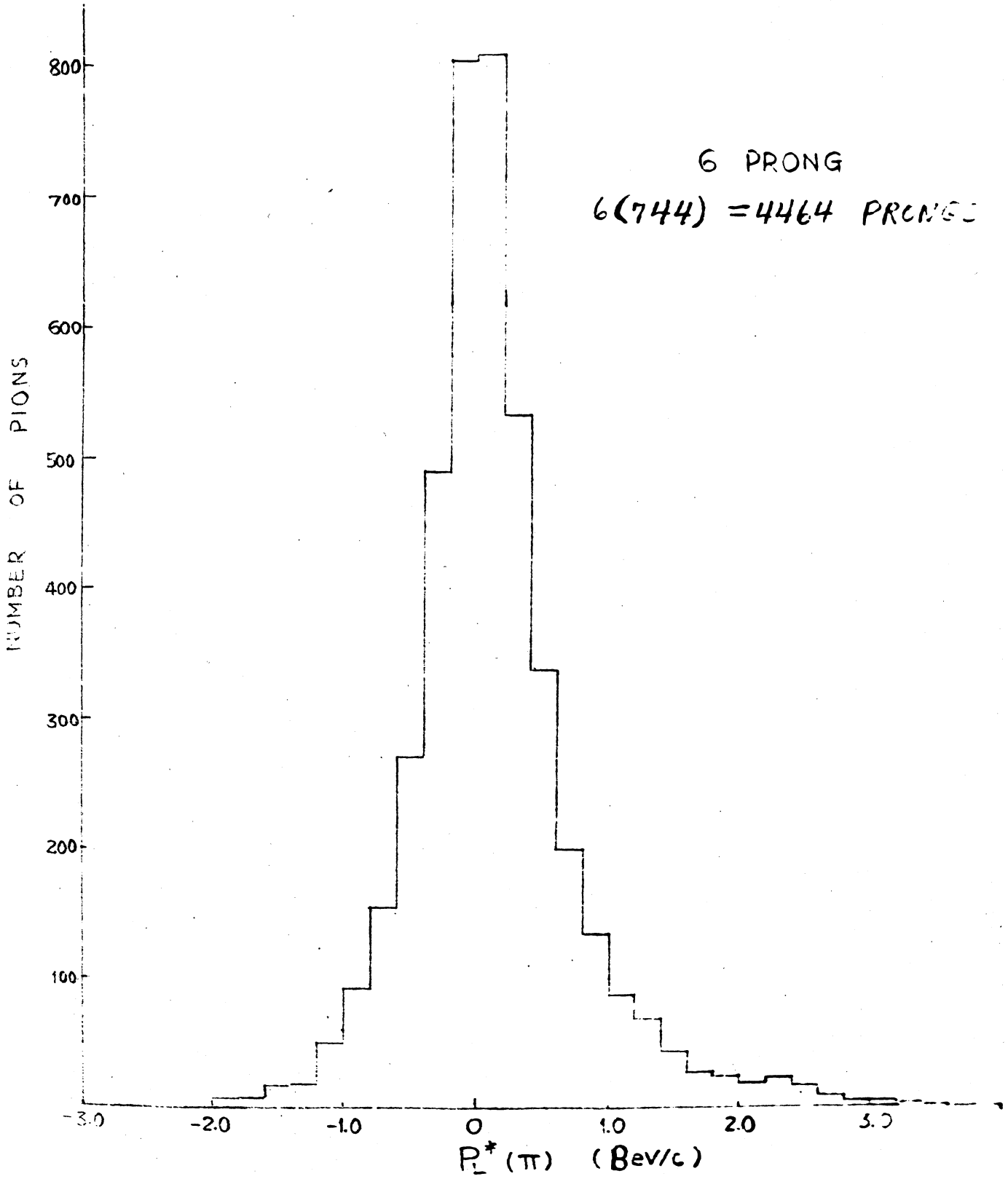

FIG. 2

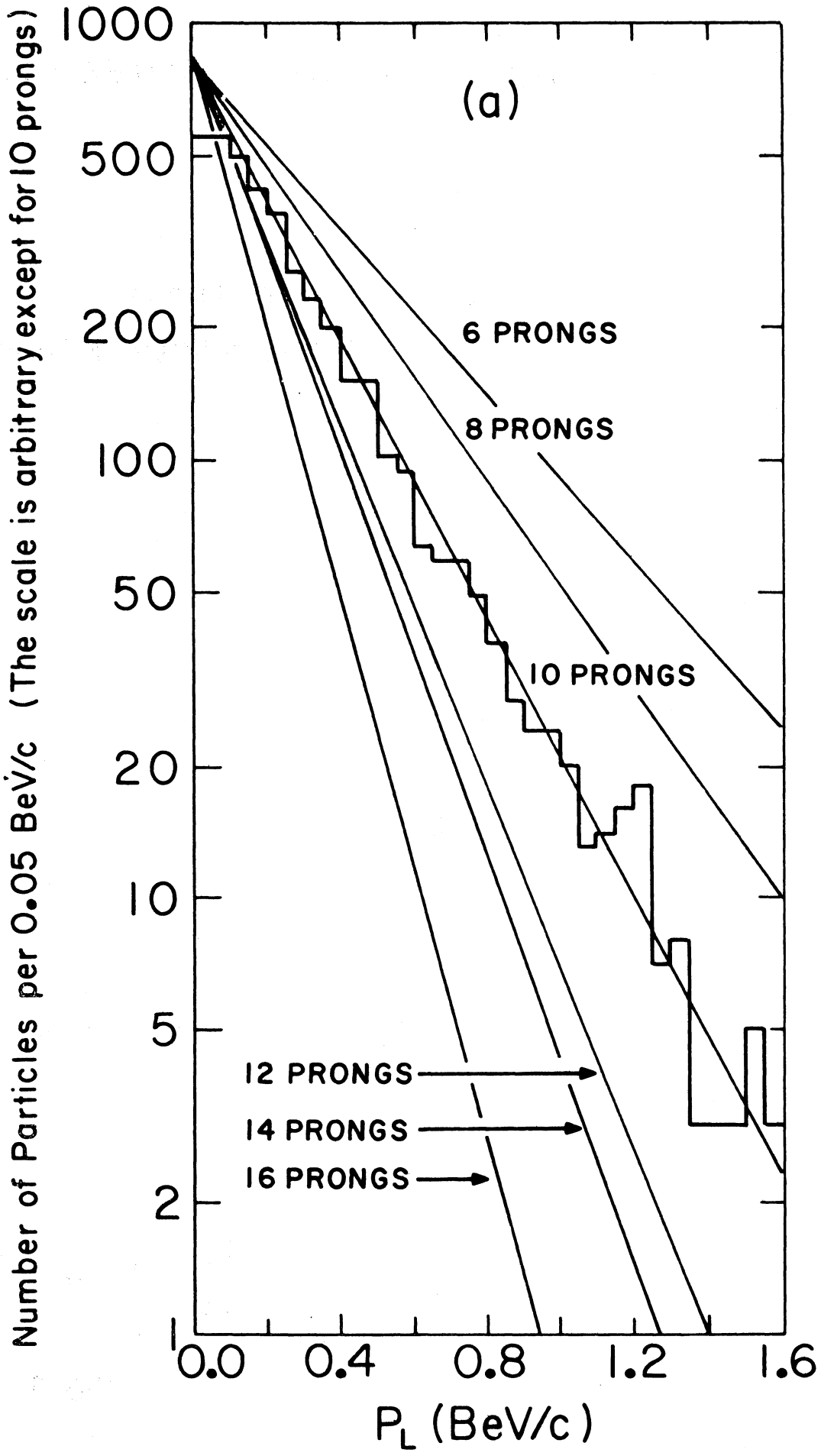
(a)
6 PRONGS
8 PRONGS
10 PRONGS
12 PRONGS
14 PRONGS
16 PRONGS
Number of Particles per 0.05 BeV/c (The scale is arbitrary except for 10 prongs)
1000
500
200
100
50
20
10
5
2
1
0.0
0.4
0.8
1.2
1.6
P_L (BeV/c)

FIG. 3

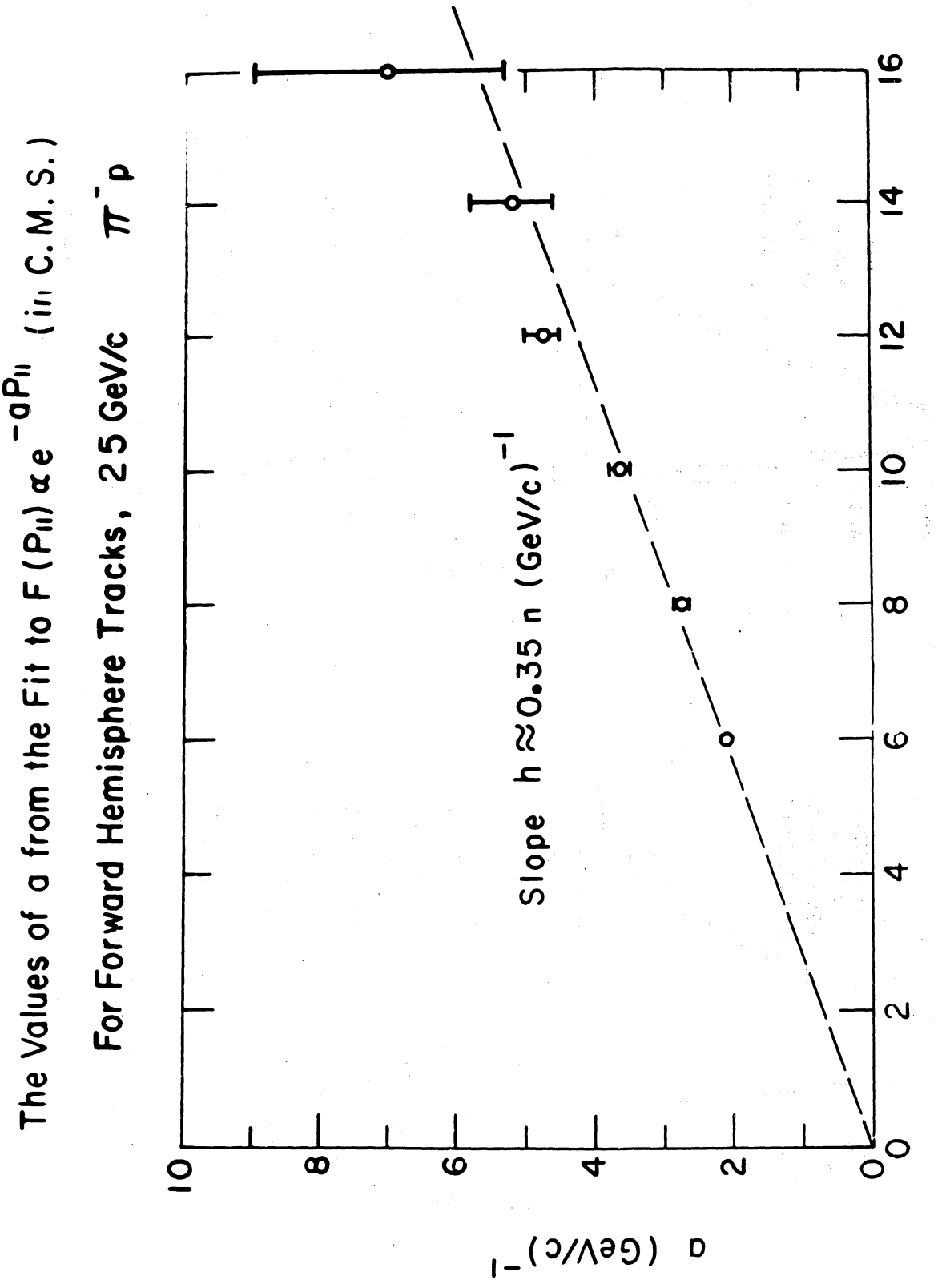
The Values of a from the Fit to $F(P_{II}) \propto e^{-aP_{II}}$ (i_{II} C.M.S.)
For Forward Hemisphere Tracks, 25 GeV/c $\pi^- p$
Slope $h \approx 0.35\ n\ (GeV/c)^{-1}$
a $(GeV/c)^{-1}$
Charged Particles (n)
0
2
4
6
8
10
12
14
16

FIG. 4

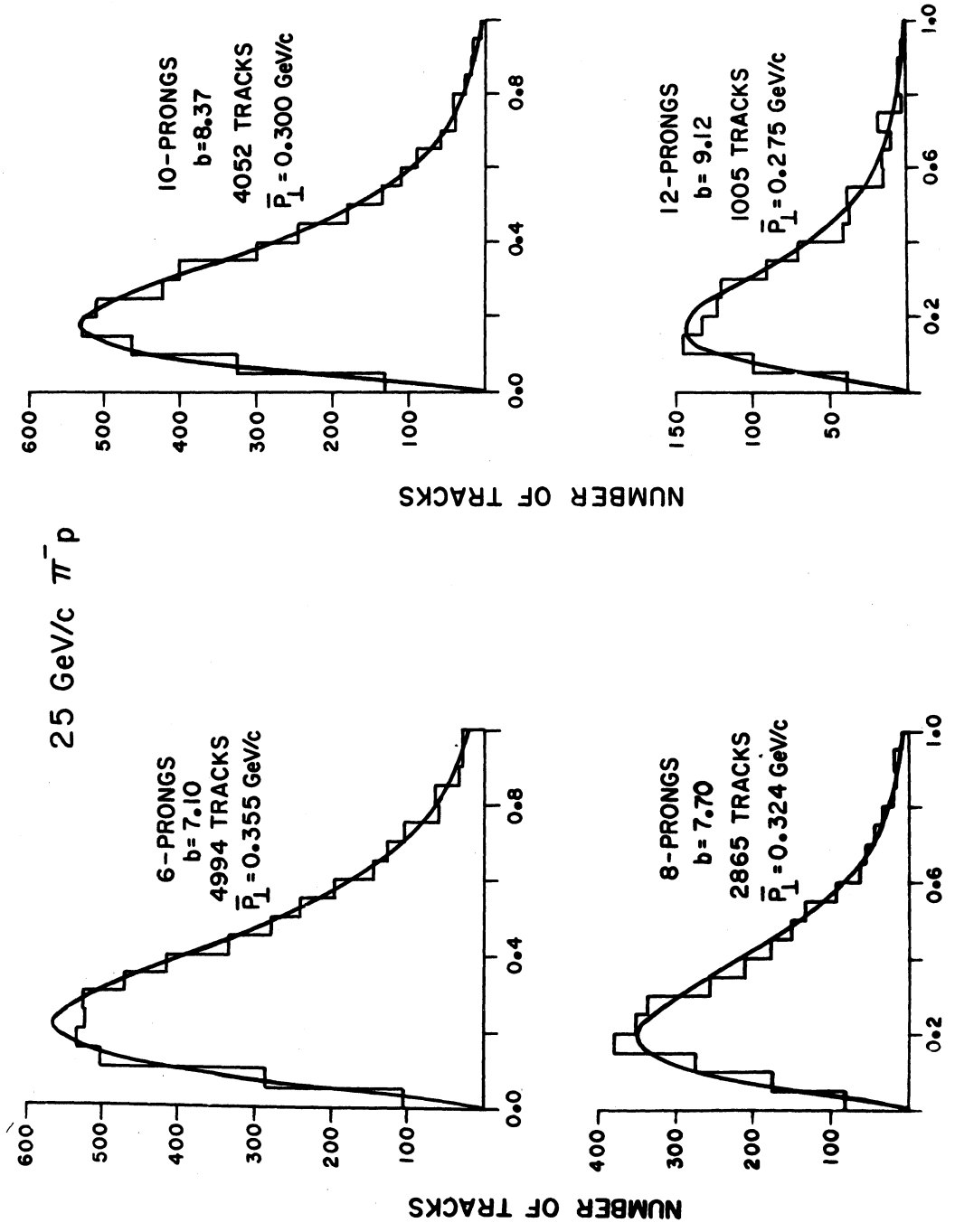
25 GeV/c π⁻ p
6-PRONGS
b= 7.10
4994 TRACKS
P̄⊥ = 0.355 GeV/c
8-PRONGS
b= 7.70
2865 TRACKS
P̄⊥ = 0.324 GeV/c
10-PRONGS
b=8.37
4052 TRACKS
P̄⊥ = 0.300 GeV/c
12-PRONGS
b= 9.12
1005 TRACKS
P̄⊥ = 0.275 GeV/c
NUMBER OF TRACKS
NUMBER OF TRACKS
P⊥ for Forward Particles and Best Fit to F(P⊥)dP ∝ P⊥^3/2 e^-bP⊥ dP⊥

FIG. 5

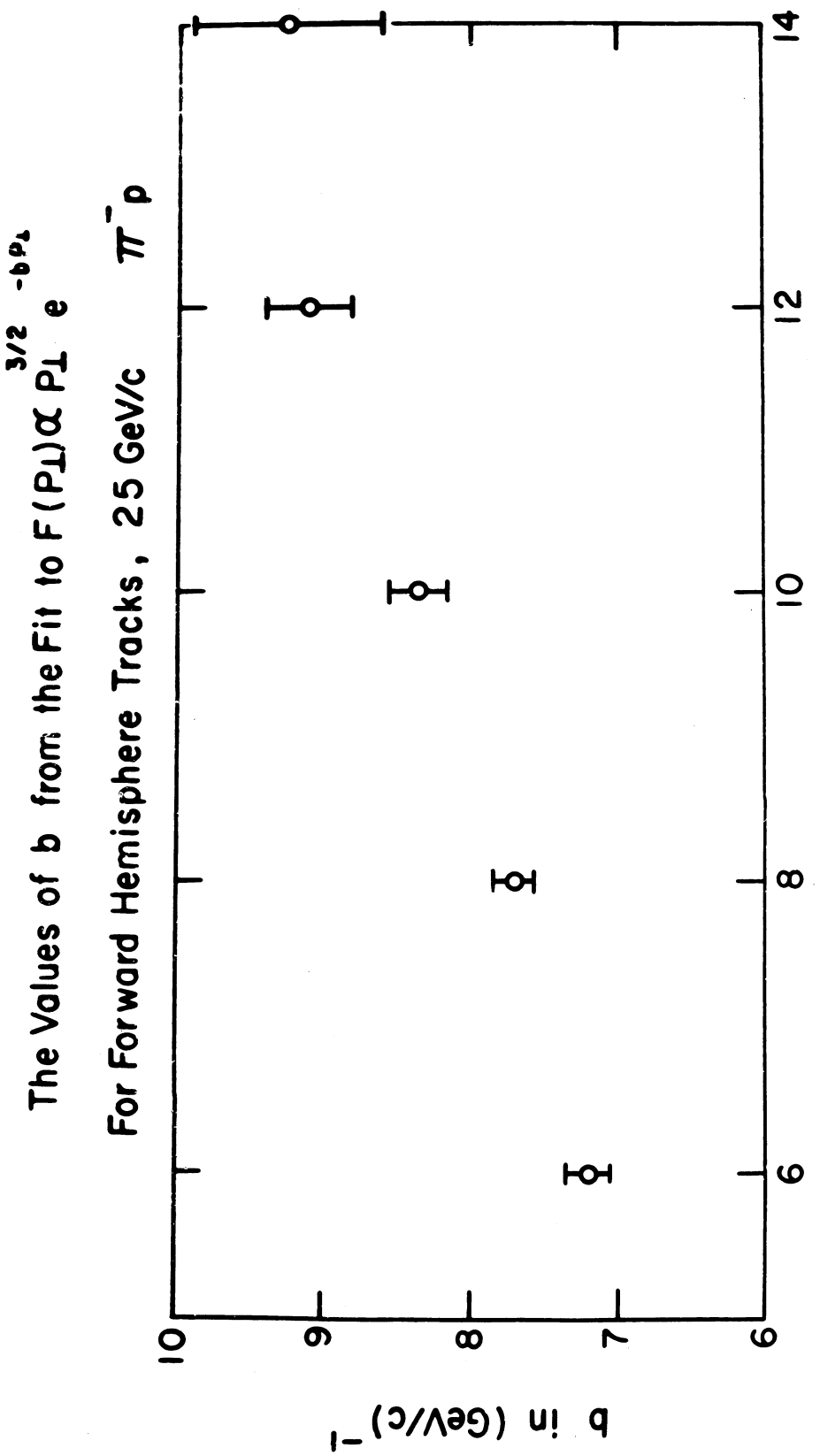
The Values of b from the Fit to $F(P_\perp)\alpha P_\perp^{3/2} e^{-bP_\perp}$
For Forward Hemisphere Tracks, 25 GeV/c $\pi^- p$
b in $(GeV/c)^{-1}$
NUMBER OF CHARGED PARTICLES
10
9
8
7
6
6
8
10
12
14

FIG. 6

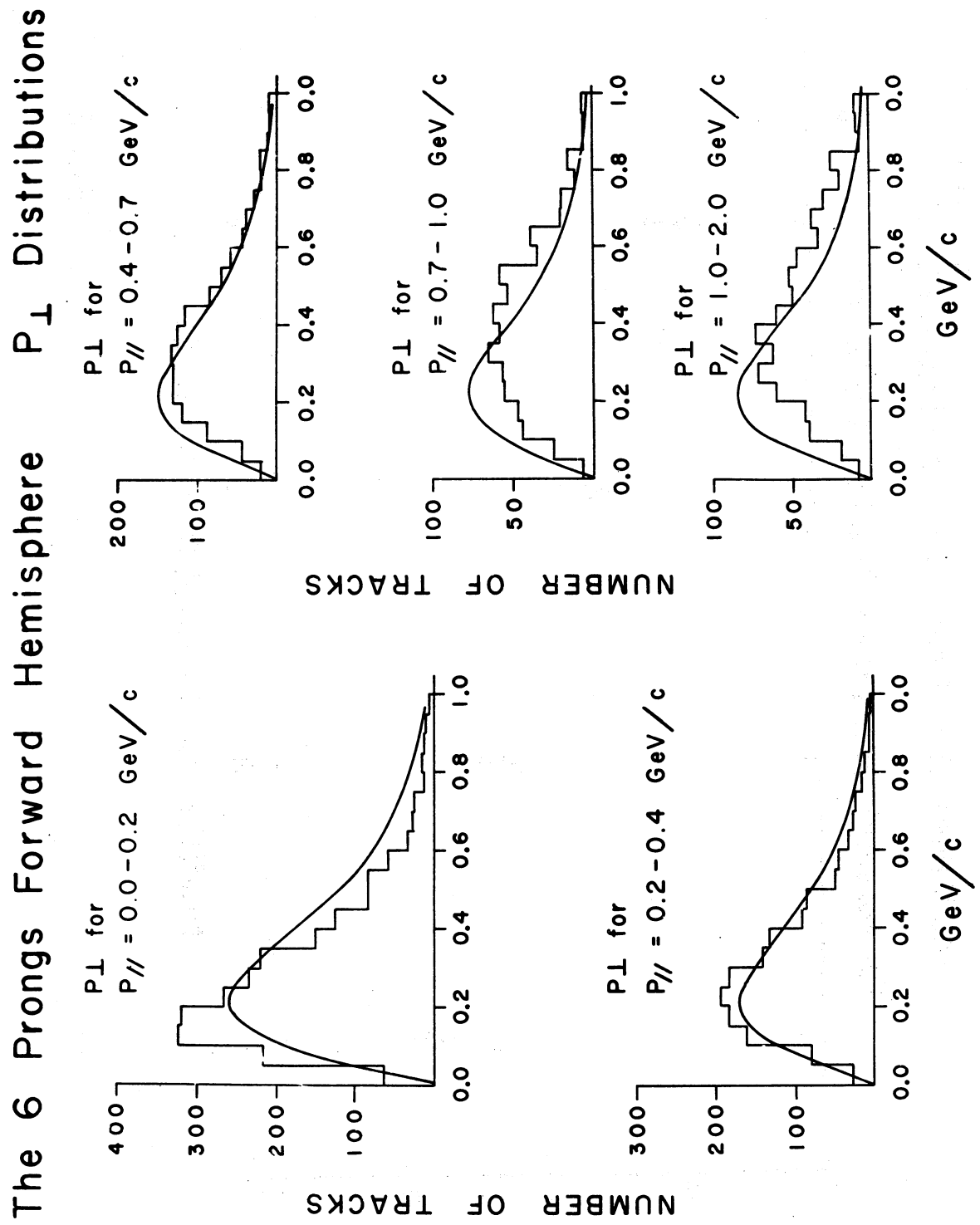
The 6 Prongs Forward Hemisphere $P_\perp$ Distributions
PT for
$P_{//}$ = 0.0-0.2 GeV/c
PT for
$P_{//}$ = 0.2-0.4 GeV/c
PT for
$P_{//}$ = 0.4-0.7 GeV/c
PT for
$P_{//}$ = 0.7-1.0 GeV/c
PT for
$P_{//}$ = 1.0-2.0 GeV/c
NUMBER OF TRACKS
GeV/c

FIG. 7

Forward Hemisphere Particle Angular Distribution Compared To That Given By $d\sigma/d\Omega \sim e^{-aP_{\parallel}} \cdot P_{\perp}^{3/2} e^{-bP_{\perp}}$

25 GeV/c $\pi^- p$

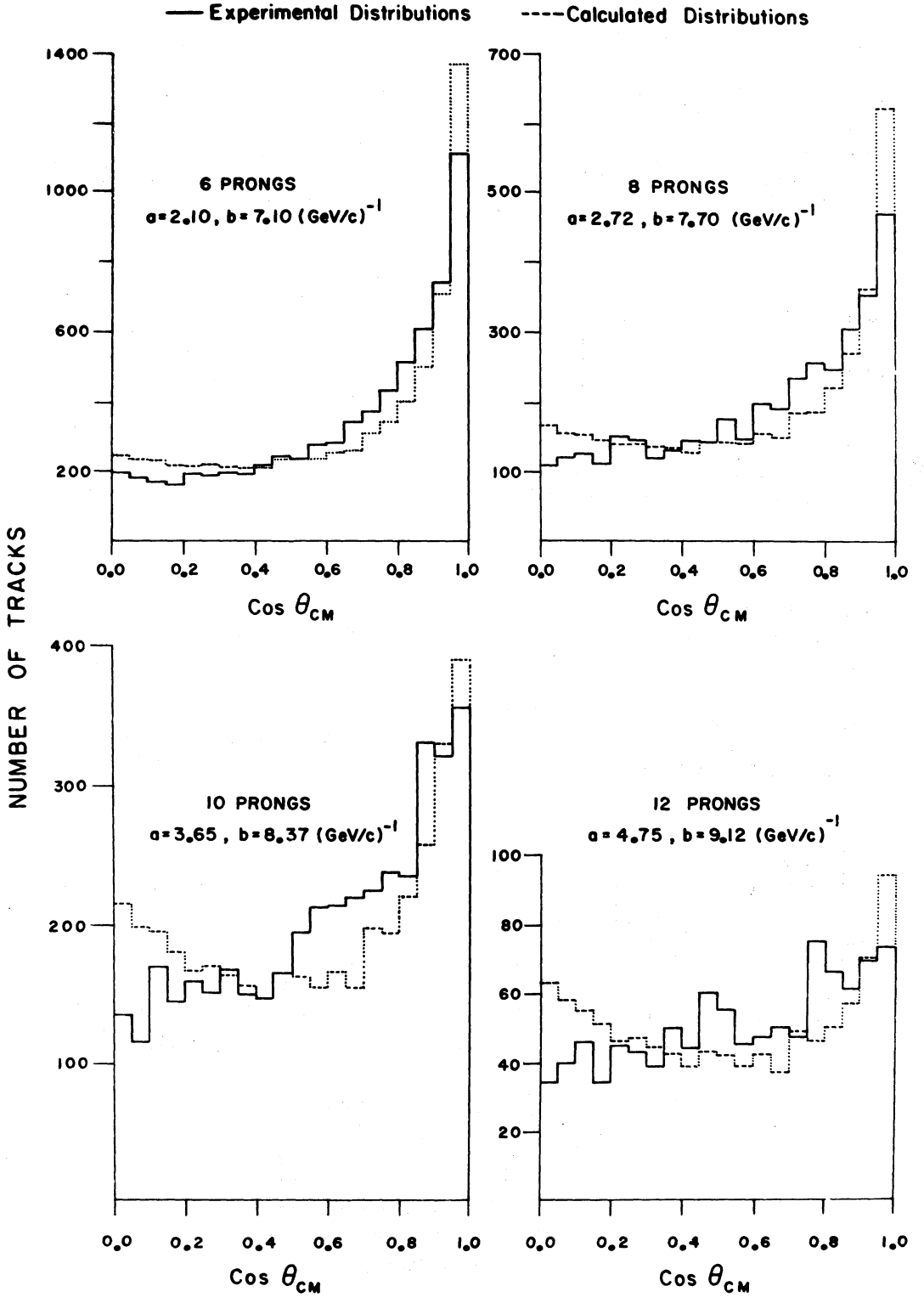

FIG. 8

FORWARD HEMISPHERE INVARIANT MASSES
(Net Charge = 0, Missing Momentum Backwards)

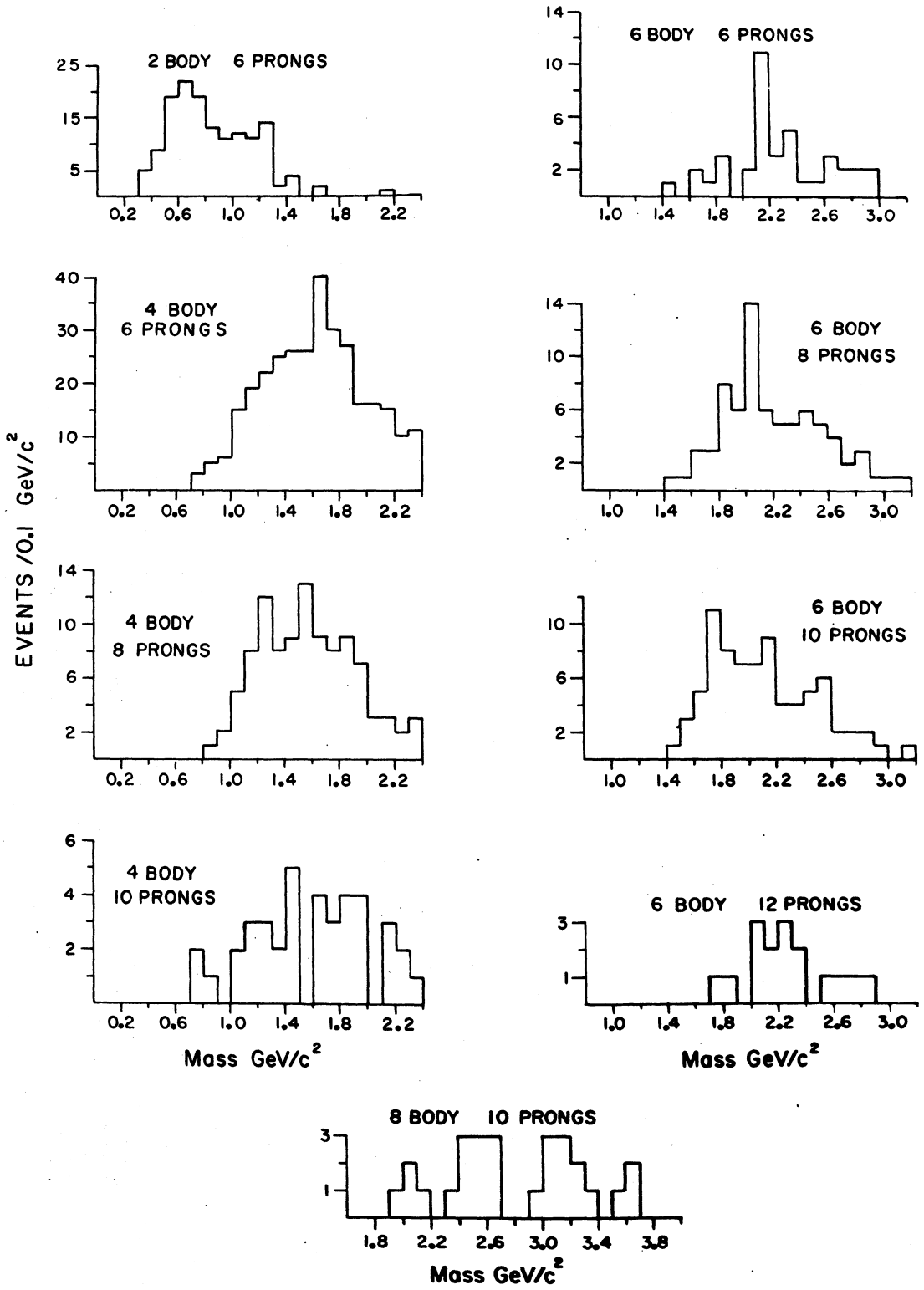

FIG. 9

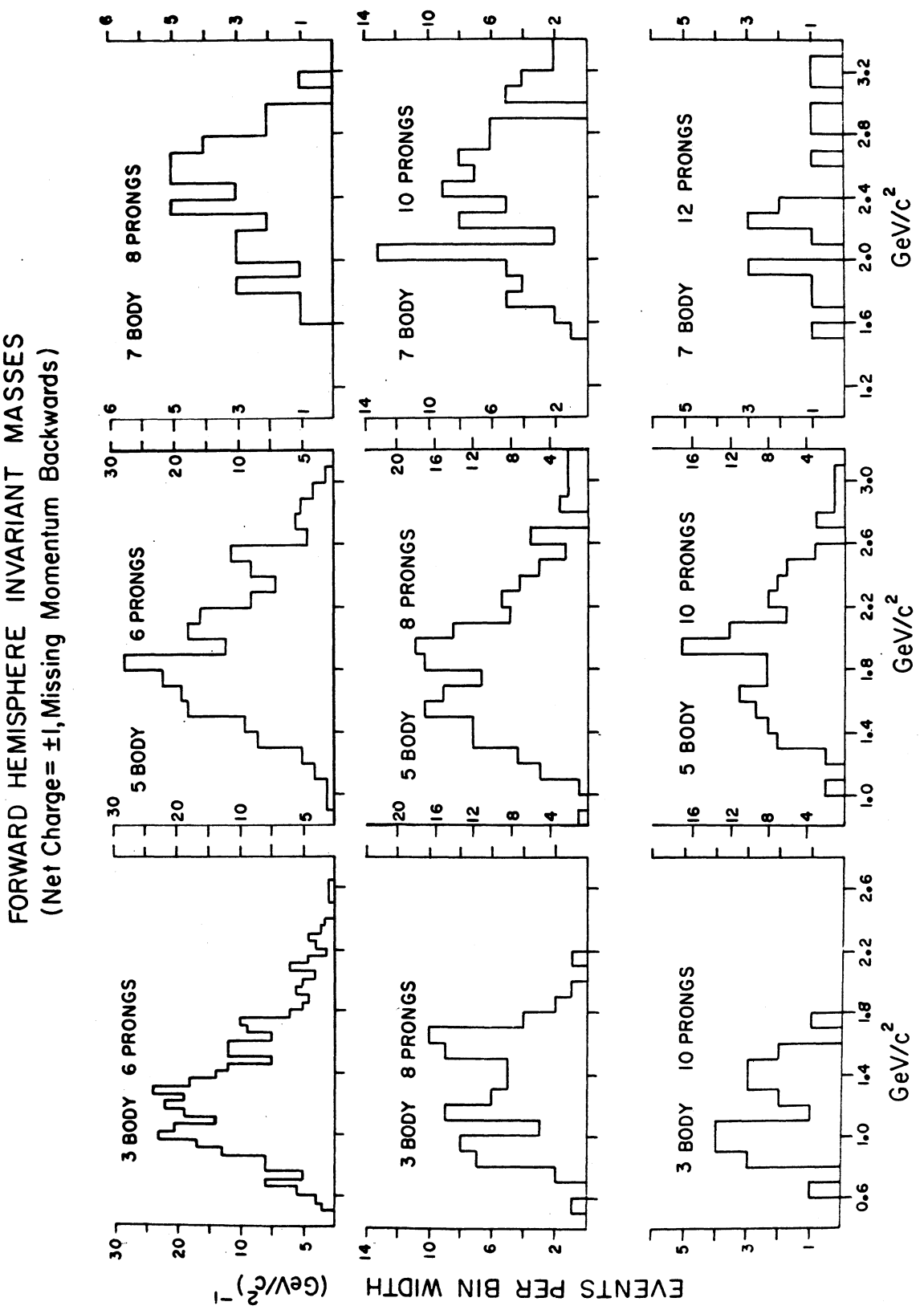
FORWARD HEMISPHERE INVARIANT MASSES
(Net Charge = ±1, Missing Momentum Backwards)
EVENTS PER BIN WIDTH (GeV/c²)⁻¹
3 BODY 6 PRONGS
5 BODY 6 PRONGS
7 BODY 8 PRONGS
3 BODY 8 PRONGS
5 BODY 8 PRONGS
7 BODY 10 PRONGS
3 BODY 10 PRONGS
5 BODY 10 PRONGS
7 BODY 12 PRONGS
GeV/c²

FIG. 10

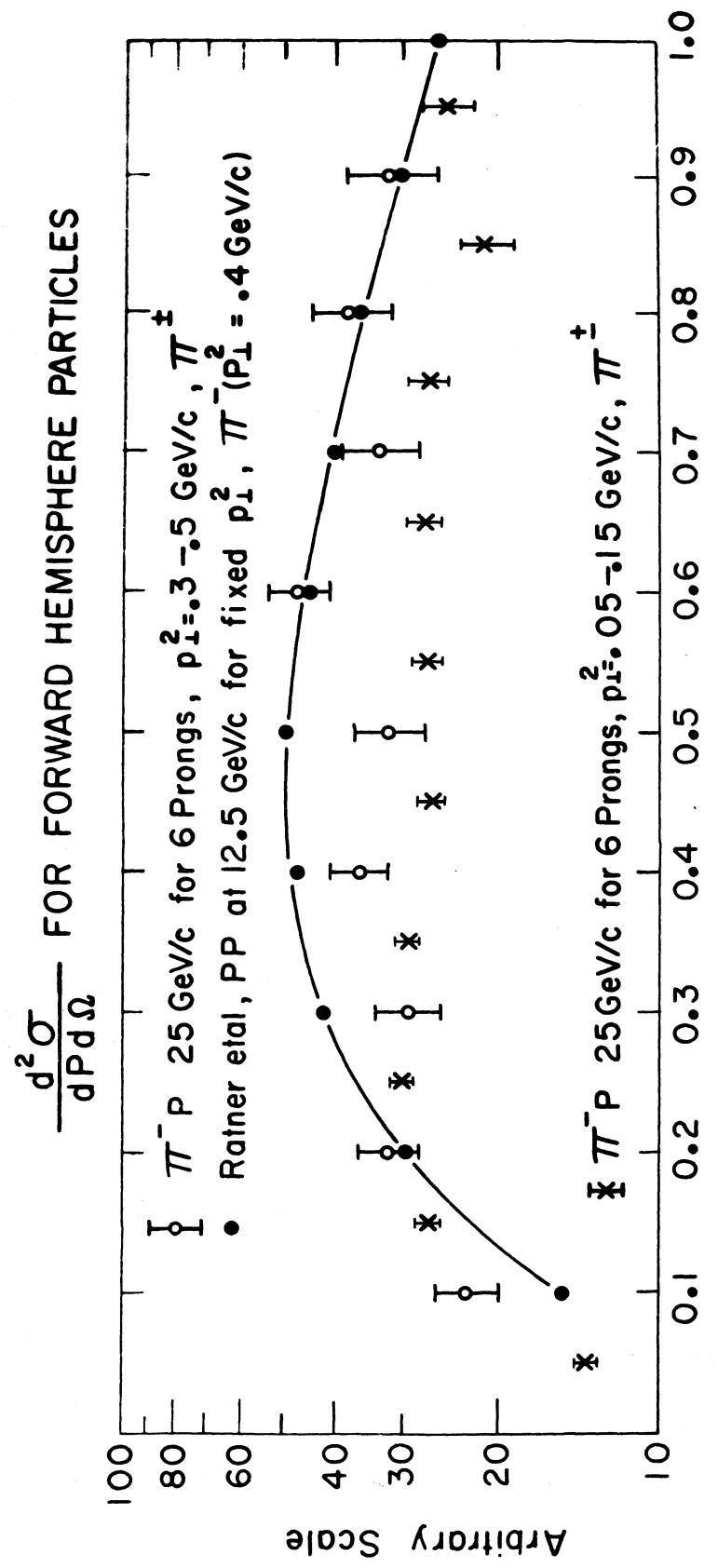
$\frac{d^2\sigma}{dP\,d\Omega}$ FOR FORWARD HEMISPHERE PARTICLES
π^- p 25 GeV/c for 6 Prongs, $p_\perp^2$=.3 -.5 GeV/c, $\pi^\pm$
Ratner etal, PP at 12.5 GeV/c for fixed $p_\perp^2$, π^- ($p_\perp^2$ = .4 GeV/c)
π^- p 25GeV/c for 6 Prongs, $p_\perp^2$=.05-.15 GeV/c, $\pi^\pm$
Arbitrary Scale
100
80
60
40
30
20
10
0.1
0.2
0.3
0.4
0.5
0.6
0.7
0.8
0.9
1.0
$p_{II}^{c.m.}$ (GeV/c)

FIG. 11

$\frac{d^2\sigma}{dP\,d\Omega}$ FOR FORWARD HEMISPHERE PARTICLES

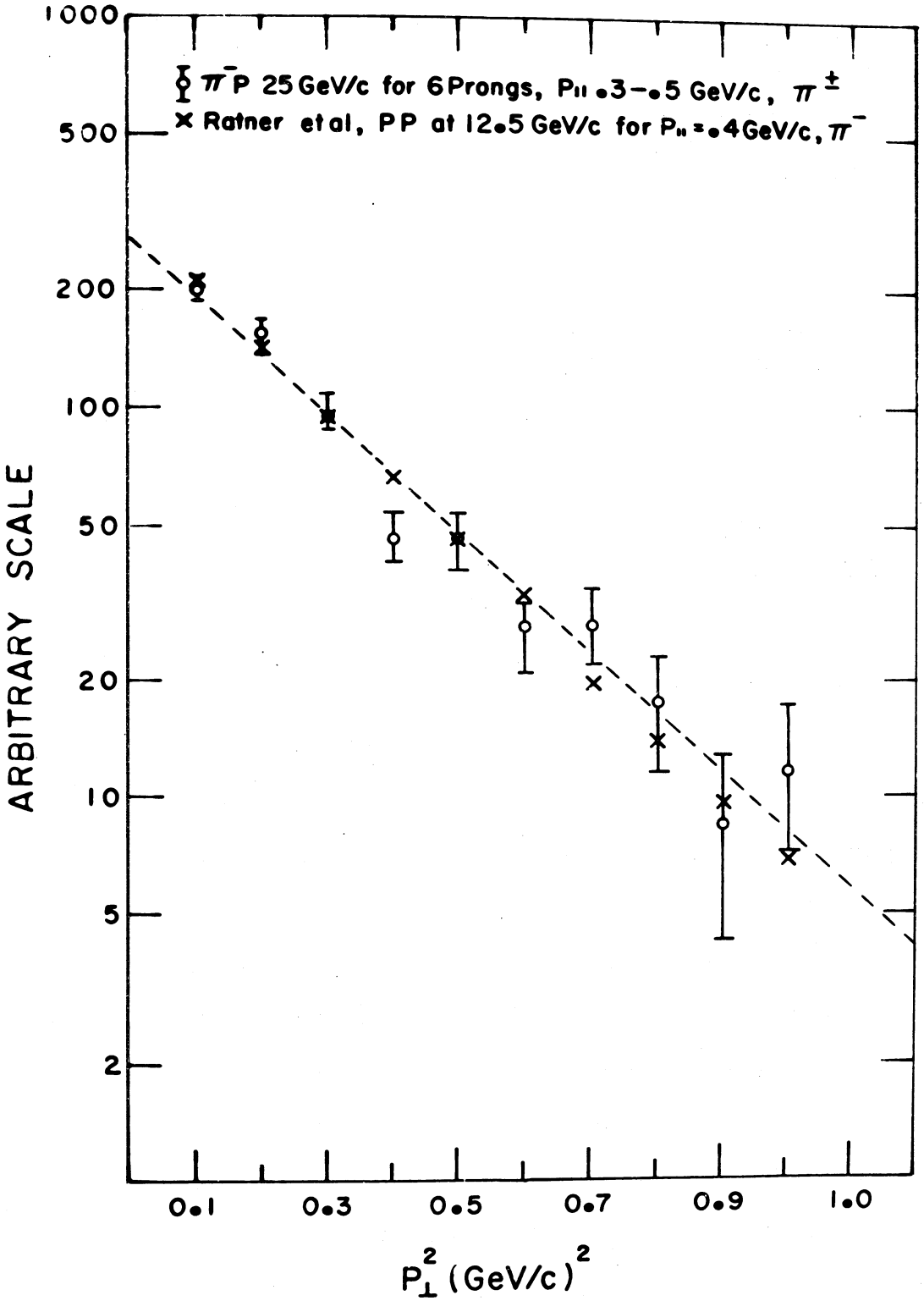

FIG. 12

PION, KAON, AND ANTIPROTON PRODUCTION IN THE CENTER OF MASS IN HIGH ENERGY PROTON PROTON COLLISIONS*

C. W. Akerlof, D. G. Crabb, J. L. Day, A. D. Krisch, and M. T. Lin,

Randall Laboratory of Physics,
University of Michigan,
Ann Arbor, Michigan

and

L. G. Ratner,

Particle Accelerator Division,
Argonne National Laboratory,
Argonne, Illinois

and

K. W. Edwards,†
Department of Physics,
University of Iowa,
Iowa City, Iowa

1. INTRODUCTION

In this paper we will describe a particle production experiment[1] performed last spring at Argonne National Laboratory. This experiment is a part of a continuing program to try to understand the nature of high energy proton-proton collisions with large momentum transfers.

The design of the experiment was based on the hope that if one viewed a proton-proton collision in the center of mass system, the distribution of any produced pions, kaons, or antiprotons might have a simple functional form which in turn might suggest a theoretical model. For this reason we chose to measure the particle production cross

section, $d\sigma/d\Omega dp$, in the center of mass as a function of the center of mass variables P_ℓ and $P_\perp$ which together completely define the produced particle momentum and direction.

The definition of P_ℓ and $P_\perp$ is shown schematically in Figure 1. We imagine that we are viewing a p-p collision in the center of mass frame. Just before the collision the two protons are heading directly towards each other. After collision a pion, kaon, or antiproton is emitted with a momentum P_ℓ along the incident proton direction and a momentum $P_\perp$ perpendicular to this direction.

The principal object of this experiment was to study the production cross section first as a function of $P_\perp$ for constant P_ℓ and second as a function of P_ℓ for constant $P_\perp$. This procedure was motivated by the suspicion that the cross section might behave as a simple function of these two variables. Our method differs from previous beam survey type experiments[2-6] in that we specifically do not make measurements at fixed laboratory angle and variable lab momentum; instead, we control both particle angle and momentum to fix the desired P_ℓ and $P_\perp$ in the center of mass.

2. THE EXPERIMENT

The apparatus which allowed us this freedom is shown in Figure 2. This is a layout drawing of the external proton beam at the Argonne ZGS. Protons at a momentum of 12.5 GeV/c from the ZGS are transported via a system of two quadrupole doublets to a 2" diameter liquid hydrogen target.

The particles produced in this target are detected in the single arm spectrometer consisting of the "C" magnet; scintillation counters S_1, S_2, and S_3 set at ten degrees to the incident proton beam; the "B" magnet; and finally the set of counters C_1, C_2, C_3, S_4, and S_5 outside the proton tunnel. Suppose for a moment that the "C" magnet is turned off. In this case any particle emitted at ten degrees in the laboratory will pass through S_1, S_2, and S_3 and be momentum analyzed by the combination of the "B" magnet and the momentum defining scintillation counter S_5. Now by turning on the "C" magnet we may steer particles of a fixed momentum which were produced either above or below the ten degree line into the angle defining counter S_3. In this way a coincidence between counters S_3 and S_5 together with the currents in the two bending magnets completely determines the particle angle and momentum. By appropriate choice of magnet currents we can essentially dial the values of P_ℓ and $P_\perp$ which our telescope is looking at.

Particle identification is carried out by the use of two threshold gas Cherenkov counters C_1 and C_2 filled with ethane. The operating points of these counters were set by running pressure curves every few data points. For the pion runs, C_1 was set to trigger only on pions and C_2 was not used at all. For the kaons, C_1 was set to anti out pions and C_2 was set to trigger on pions or kaons; a similar procedure was used to detect antiprotons.

The phase space, $\Delta\Omega\Delta p$, subtended by the telescope was

calculated directly from the experimental geometry and had a typical value of 5×10^{-6} steradian-GeV/c in center of mass. The incident proton flux was monitored with counter telescopes M and N and the exact normalization of counts in M and N was calibrated by separate runs with thin gold foils placed upstream of the hydrogen target. These foils were subsequently counted by the Argonne radiochemistry group and the incident proton flux obtained from the known spallation cross sections.

For each data point runs were made with the liquid hydrogen target both empty and full. The empty target rate was typically 30% of the full target rate so that the subtraction did not drastically increase the error in the true hydrogen cross section. For the case of the kaon and antiproton runs it was also necessary to take runs with the gas pressure in the Cherenkov counter C_2 lowered to find the number of pions that leaked through the anticoincidence Cherenkov counter C_1. This contamination effect amounted to about a 20% correction.

The accidental coincidence rate was determined by feeding a time to amplitude converter with signals from S_3 and S_5. The output of this circuit was analyzed and stored in a multichannel pulse height analyzer and this data enabled us to find the uncorrelated accidental rate. Finally the data were corrected for nuclear interactions in the counters and in-flight decay.

3. RESULTS

Figure 3 shows the cross section data taken at fixed P_ℓ for values of $P_\perp^2$ in the range of 0.1 to 1.5 $(GeV/c)^2$. For most of the runs shown, P_ℓ in the center of mass has been kept at 0.6 GeV/c. The exception is a run made at P_ℓ equal to 0.4 GeV/c for π^- production, and on this graph these points lie very close to the run at 0.6.

The most striking feature of this graph is that all of the data appear to lie along straight lines. Since $P_\perp^2$ is plotted along the horizontal axis and the vertical axis is logarithmic, we can conclude that our data are fit very well by the Gaussian function $e^{-aP_\perp^2}$. It seems remarkable that the slopes of all of these lines are so similar. The coefficient "a" has a value of 3.3, 3.5, and 3.5 for the π^+, π^-, and K^- data respectively. The K^+ data have significantly smaller slope with an "a" value of 2.7 $(GeV/c)^{-2}$. The reason for this anomalous behavior is not understood. As can be seen from Figure 3, the antiproton data are not very precise and they will be ignored throughout the rest of the discussion.

It should be pointed out that the Gaussian behavior of the production cross sections contradicts the conclusions of some previous lower precision beam experiments as well as the empirical parameterization for the data such as the one given by Cocconi, Koester, and Perkins.[7] The disagreement of these cross section formulas is serious only for particles emitted at relatively large angles and so is of

minor importance to the practical problem of secondary particle beam design.

The Gaussian nature of the cross section is interesting in itself and should be compared with a recent elastic proton proton scattering experiment[8] where a similar behavior was observed. Krisch and Krisch[9] have speculated that this behavior is the consequence of the convolution of a large number of independent processes all of which have a maximum probability at or near 0 degrees. Under quite general assumptions the Central Limit Theorem of statistics provides a proof that such convolutions would approach a Gaussian at high energies.

The similarity of the slopes of the data in Figure 3 offers something of a puzzle. Some time ago Krisch[10] postulated that for large momentum transfers the proton proton collision could be characterized by an interaction density of the form $\rho(R,r)$ where R represents an impact radius or distance of closest approach and r represents the point at which the massive quanta are emitted which are presumably responsible for the inter-nucleon forces. This picture found support in an elastic proton proton scattering experiment[8] in which it was observed that the cross section could be graphed with three straight lines on a semilogarithmic plot versus something like the transverse momentum squared. This behavior suggested that the proton proton interaction could be divided into three regions[11] each dominated by successively more massive quanta. Now in such

a picture it would be natural to expect that the interaction function $\rho(R,r)$ would behave differently depending on the nature of the quanta in question. In particular, one might expect that as the mass of the quanta increased from the mass of the pion to the mass of the kaon or antiproton, the interaction function would decrease in characteristic radius and the momentum, the variable conjugate to radius, would increase. This would imply that the cross section for K production would have a more gentle slope as a function of $P_\perp^2$ than the cross section for π production. This prediction has certainly not been borne out by this experiment. The mystery of the identical slopes remains, and we can only hope that some more sophisticated experiment can show the relation, if any, between the elastic and inelastic cross sections.

The results of the second part of this experiment are shown in Figure 4. Here we have held $P_\perp^2$ fixed at a value of 0.4 $(\text{GeV/c})^2$ and varied P_ℓ in the region of 0.0 to 1.0 GeV/c. Figure 4 is a plot of these production cross sections as a function of P_ℓ in the center of mass. Note that all four cross sections for π^+, π^-, K^+, and K^- production are very low at P_ℓ equal to zero, rise sharply to peak at about 500 MeV/c, and then droop slightly if at all.

The shape of these curves is strong evidence that the simple statistical model of proton proton interactions is inappropriate to describe particle production. In the statistical model[12] it is important that the two protons at

collision time form a compound state which later decays. Such a model would predict that the particle production probability should peak at P_ℓ equal to zero in contradiction to our data.

The symmetry of the initial two proton state insures that the curves for P_ℓ negative mirror the curves shown in Figure 4. The double peaked behavior may be characterized by saying that the produced particles have a preferred momentum of ±500 MeV/c in the center of mass. This description is equivalent to imagining that after collision the two initial baryons separate, each followed by its own cloud of excitation. These "fireballs" then decay more or less isotropically in their own rest frame.

The fireball rest frame may be found by searching for that frame in which the data of Figure 4 appear to peak at P_ℓ equal to zero. In Figure 5 the production cross sections are plotted in a fireball frame with a β for the fireball of 0.54 with respect to the center of mass. On the horizontal axis of Figure 5 is plotted P_ℓ^2 in the fireball frame. Thus a Gaussian behavior for the cross section as a function of P_ℓ would appear as a straight line.

Lines have been drawn on this graph corresponding to the slopes of the $P_\perp^2$ data shown in Figure 3. It can be seen that these lines describe reasonably well the pion data in the forward direction and the K^+ data in both forward and backward directions. The cross section for pions emitted in the backward hemisphere of the fireball appear to drop

very sharply with coefficients of 16.0 and 9.5 $(GeV/c)^{-2}$ for the π^+ and π^- data respectively. The reason for this very fast drop is not understood.

Thus we see that to a good approximation the positive kaons are emitted with an isotropic Gaussian distribution in the fireball frame while the pions are emitted isotropically in the forward hemisphere but suppressed in the backward half. The peak of the K^- data in this fireball frame clearly does not occur at P_ℓ equal to zero. In fact, this data may be symmetrized by sitting in a fireball frame moving somewhat slower with β of 0.4 with respect to the center of mass. This may be qualitatively understood by realizing that the K^- particles are always created in K^+K^- pairs and thus the available kinetic energy left over for the fireball is somewhat less. Assuming that the total available energy in the center of mass is split evenly between the forward and backward fireballs, we conclude that the fireball mass is about 2100 MeV for π^+, π^-, and K^+ production and 2300 MeV for K^- production.

One final comment should be made about the fireball kinematics. At first glance one might wonder why the cross section dip at low values of P_ℓ in the center of mass is so pronounced and yet this effect was never prominent in previous beam survey experiments. The answer probably lies in the fact that in this experiment $P_\perp^2$ was relatively large and far away from the region explored by most beam survey experiments. This means that for pion production, for

example, the peak of the cross section which occurs at $P_\ell = 0$ in the fireball frame will transform in the center of mass frame to $P_{\ell c.m.} = \beta\gamma \sqrt{P_\perp^2 + M_\pi^2}$. Thus when $P_\perp^2$ is small the peaks of the cross section lie close to zero P_ℓ in the center of mass, and when $P_\perp^2$ is large the peaks separate and become resolvable. This relation is shown graphically in Figure 6 where the two lines

$$P_{\ell c.m.} = \pm\beta\gamma \sqrt{P_\perp^2 + M_\pi^2}$$

are plotted.

Finally another supporting piece of evidence for this fireball description is provided in Figure 7. Here the pion production data for fixed $P_{\ell c.m.}$ is replotted so that the vertical axis represents the cross section, $\left.\frac{d\sigma}{d\Omega\, dp}\right|_{FIREBALL}$, and the horizontal axis represents $P^2_{FIREBALL}$. As can be seen, the π^- data taken at $P_{\ell c.m.} = 0.4$ and 0.6 appear to fall on the same straight line. For a plot of $\left.\frac{d\sigma}{d\Omega\, dp}\right|_{c.m.}$ versus $P^2_{c.m.}$ the same would not hold true.

*Supported by a research grant from the U. S. Atomic Energy Commission.

†Present address: Department of Physics, Carleton University, Ottawa, Canada.

REFERENCES

1. L. G. Ratner, K. W. Edwards, C. W. Akerlof, D. G. Crabb, J. L. Day, A. D. Krisch, and M. T. Lin, Phys. Rev. Letters 18, 1218 (1967).
2. W. F. Baker, R. L. Cool, E. W. Jenkins, T. F. Kycia, S. J. Lindenbaum, W. A. Love, D. Luers, J. A. Niederer, S. Ozaki, A. L. Read, J. J. Russell, and L. C. L. Yuan, Phys. Rev. Letters 7, 101 (1961).
3. A. N. Diddens, W. Galbraith, E. Lillethun, G. Manning, A. G. Parham, A. E. Taylor, T. G. Walker, and A. M. Wetherell, Nuovo Cimento 31, 961 (1964).
4. D. Dekkers, J. A. Geibel, R. Mermod, G. Weber, T. R. Willitts, K. Winter, B. Jordan, M. Vivargent, N. M. King, and E. J. N. Wilson, Phys. Rev. 137, B962 (1965).
5. R. A. Lundy, T. B. Novey, D. D. Jovanovic, and V. L. Telegdi, Phys. Rev. Letters 14, 504 (1965).
6. E. W. Anderson, E. J. Bleser, G. B. Collins, T. Fujii, J. Menes, F. Turkot, R. A. Carrigan, R. M. Edelstein, N. C. Hien, T. J. McMahon, and I. Nadelhaft, Phys. Rev. Letters 16, 855 (1966); 19, 198 (1967).
7. G. Cocconi, L. J. Koester, and D. H. Perkins, University of California Radiation Laboratory Report No. UCRL-10022 (1961), unpublished.

8. C. W. Akerlof, R. H. Hieber, A. D. Krisch, K. W. Edwards, L. G. Ratner, and K. Ruddick, Phys. Rev. Letters 17, 1105 (1966); Phys. Rev. 159, 1138 (1967).

9. A. D. Krisch and J. P. Krisch, paper presented at The Heidelberg International Conference on Elementary Particles, Heidelberg, September 20-27, 1967.

10. A. D. Krisch, Phys. Rev. 135, B1456 (1964); Lectures in Theoretical Physics, Vol. IX (University of Colorado Press, Boulder, Colorado, 1966).

11. The existence of these regions has recently been confirmed by J. V. Allaby, G. Cocconi, A. N. Diddens, A. Klovning, G. Matthiae, E. J. Sacharidis, and A. M. Wetherell, Phys. Letters 25B, 156 (1967).

12. G. Fast and R. Hagedorn, Nuovo Cimento 27, 203 (1963); G. Fast, R. Hagedorn, and L. W. Jones, Nuovo Cimento 27, 856 (1963).

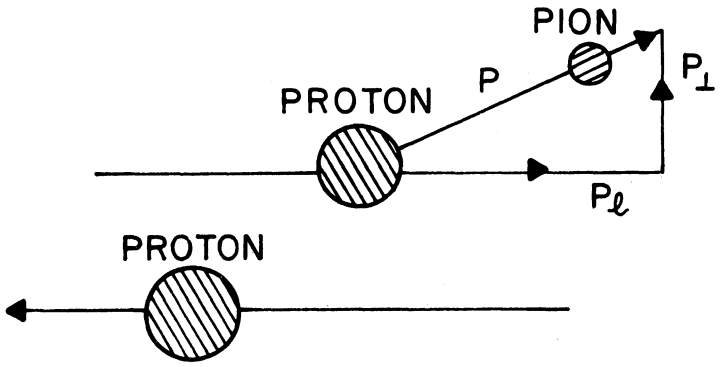

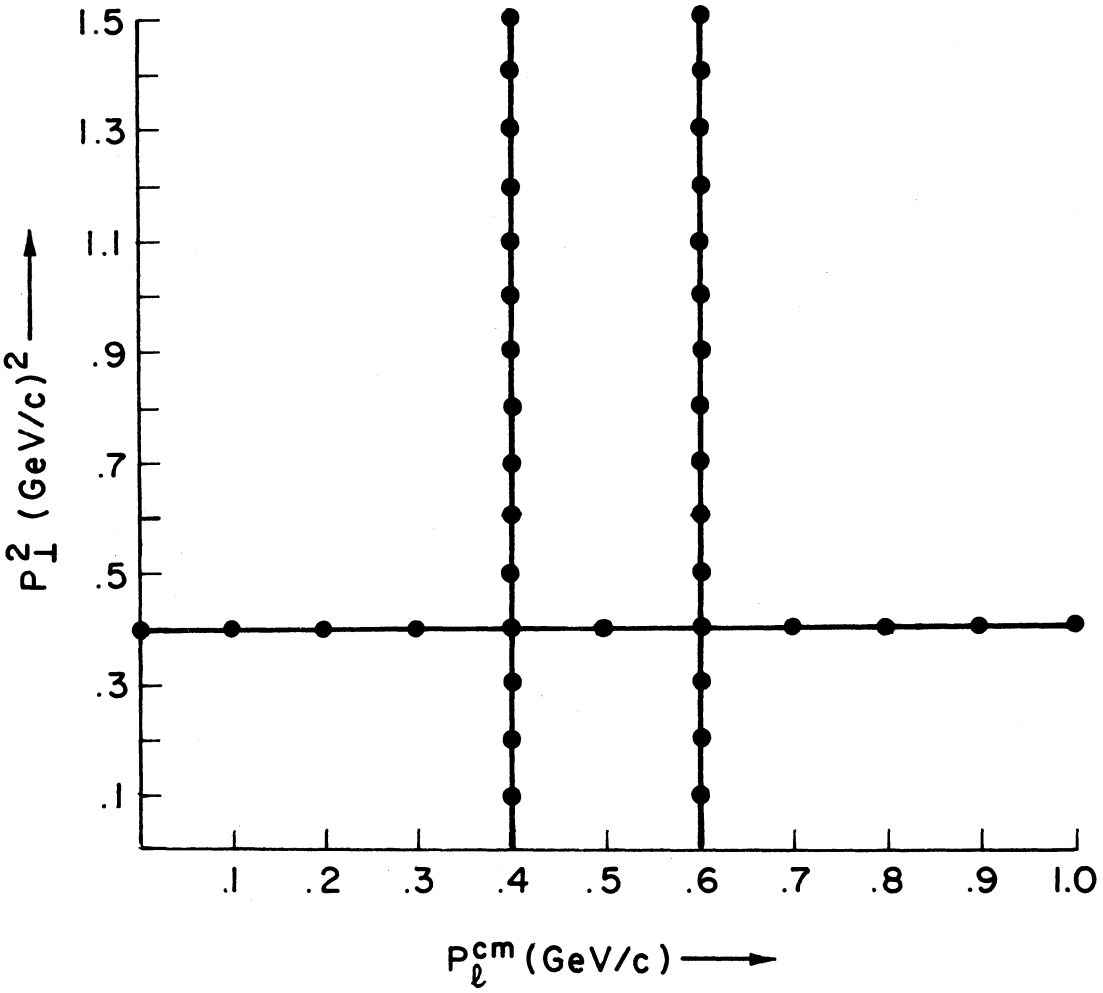

FIGURE 1. KINEMATICS

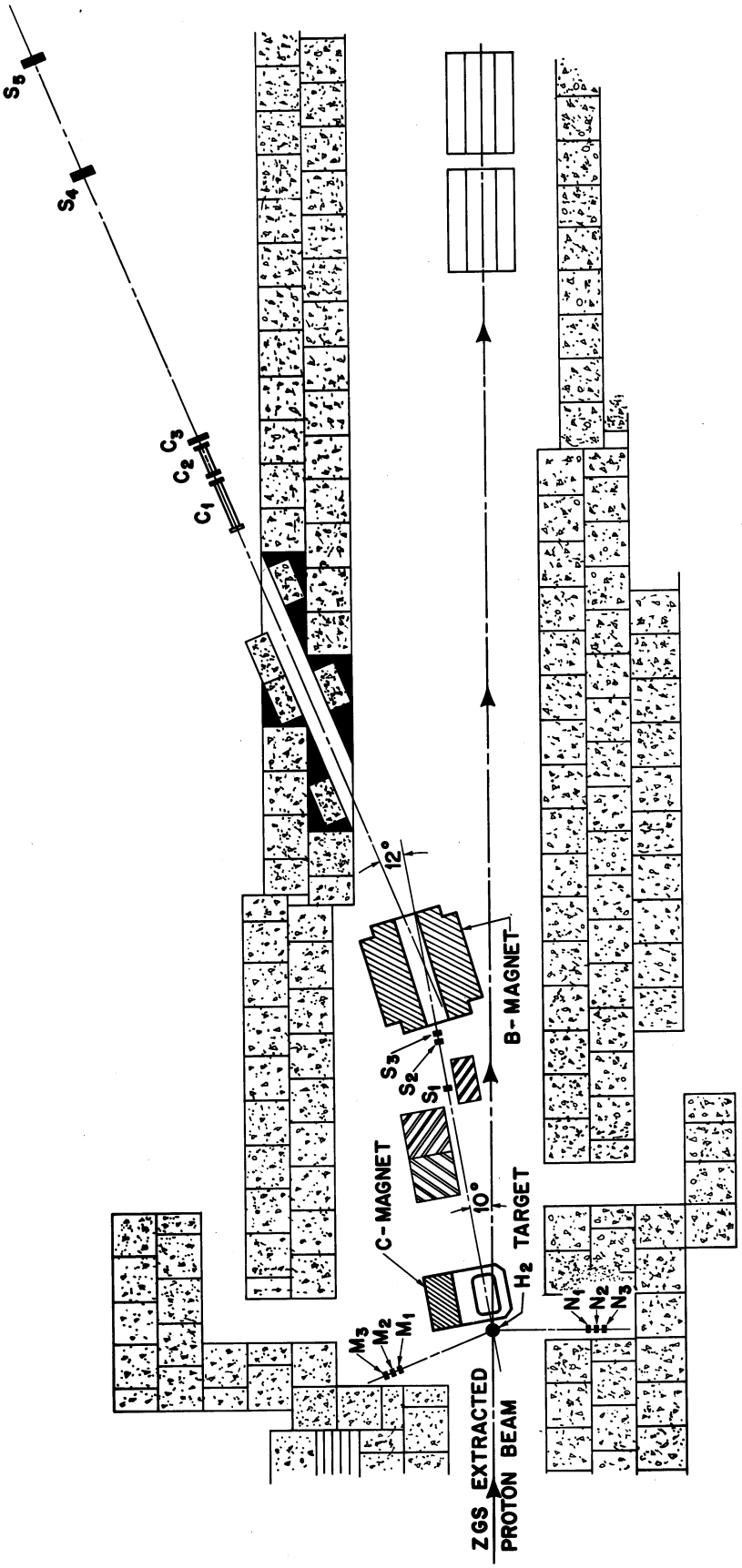

FIGURE 2. EXPERIMENTAL LAYOUT

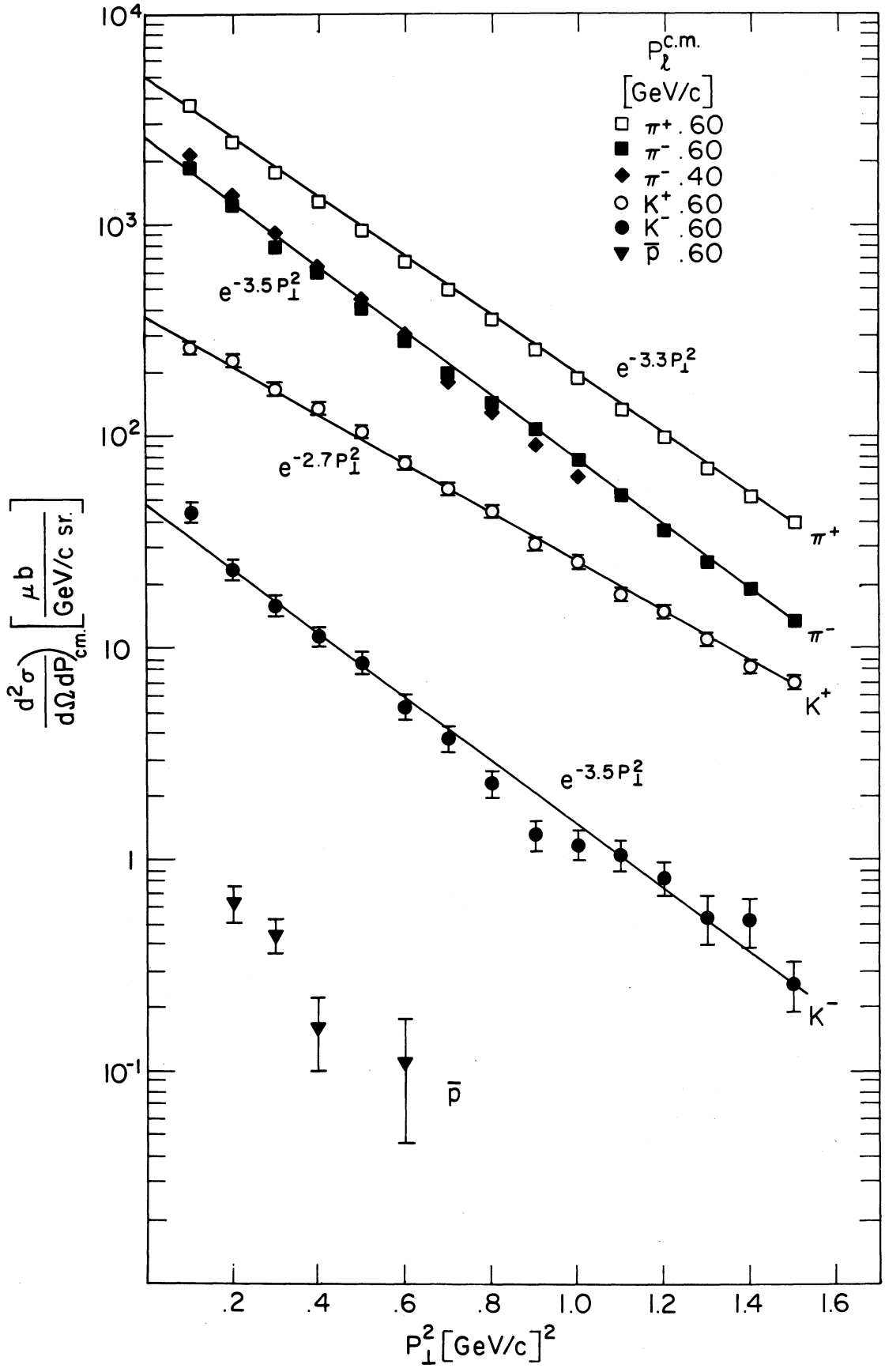

FIGURE 3. CROSS SECTION VS. $P_\perp^2$

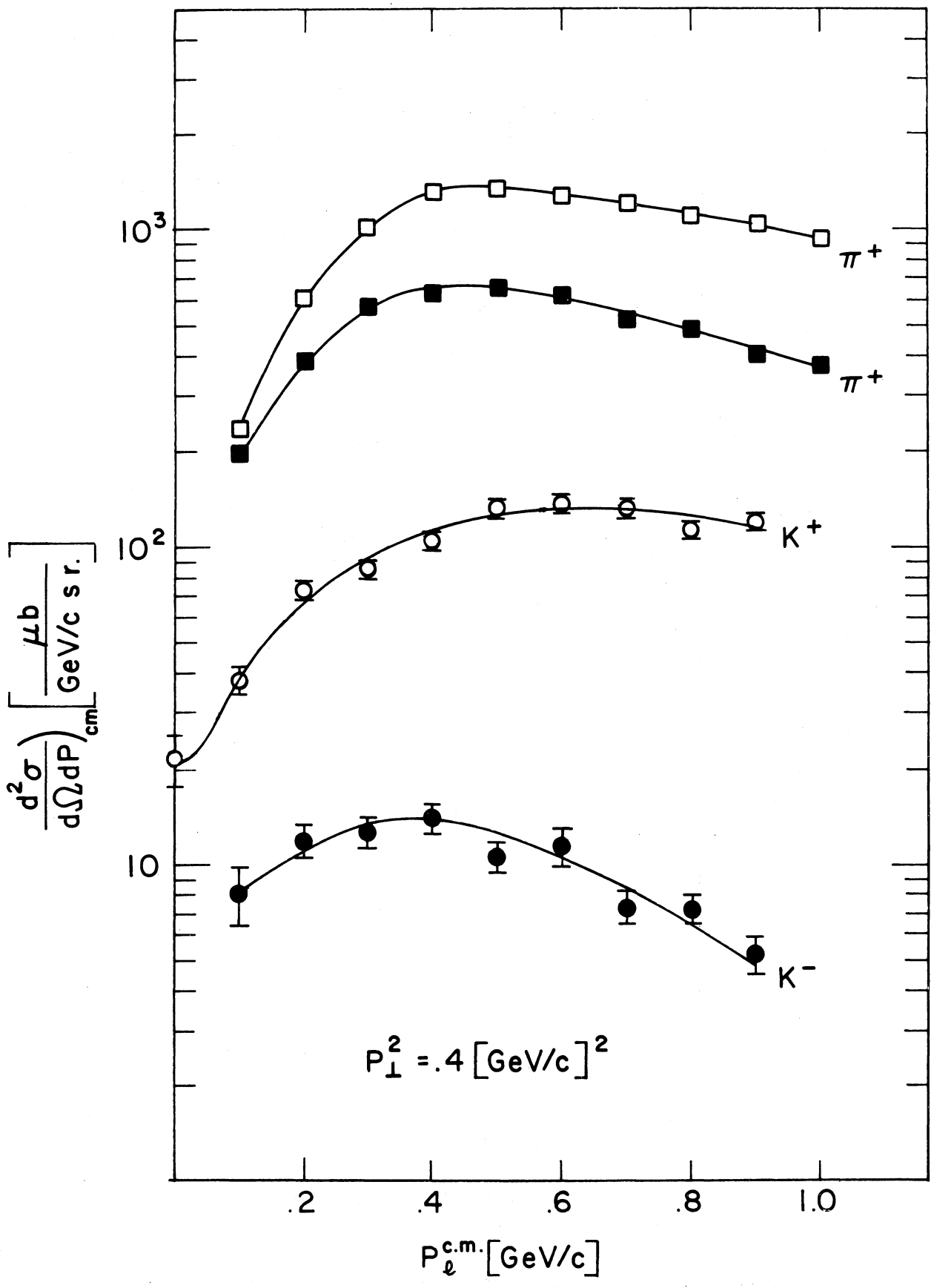

FIGURE 4. CROSS SECTION VS. $P_{\ell\ C.M.}$

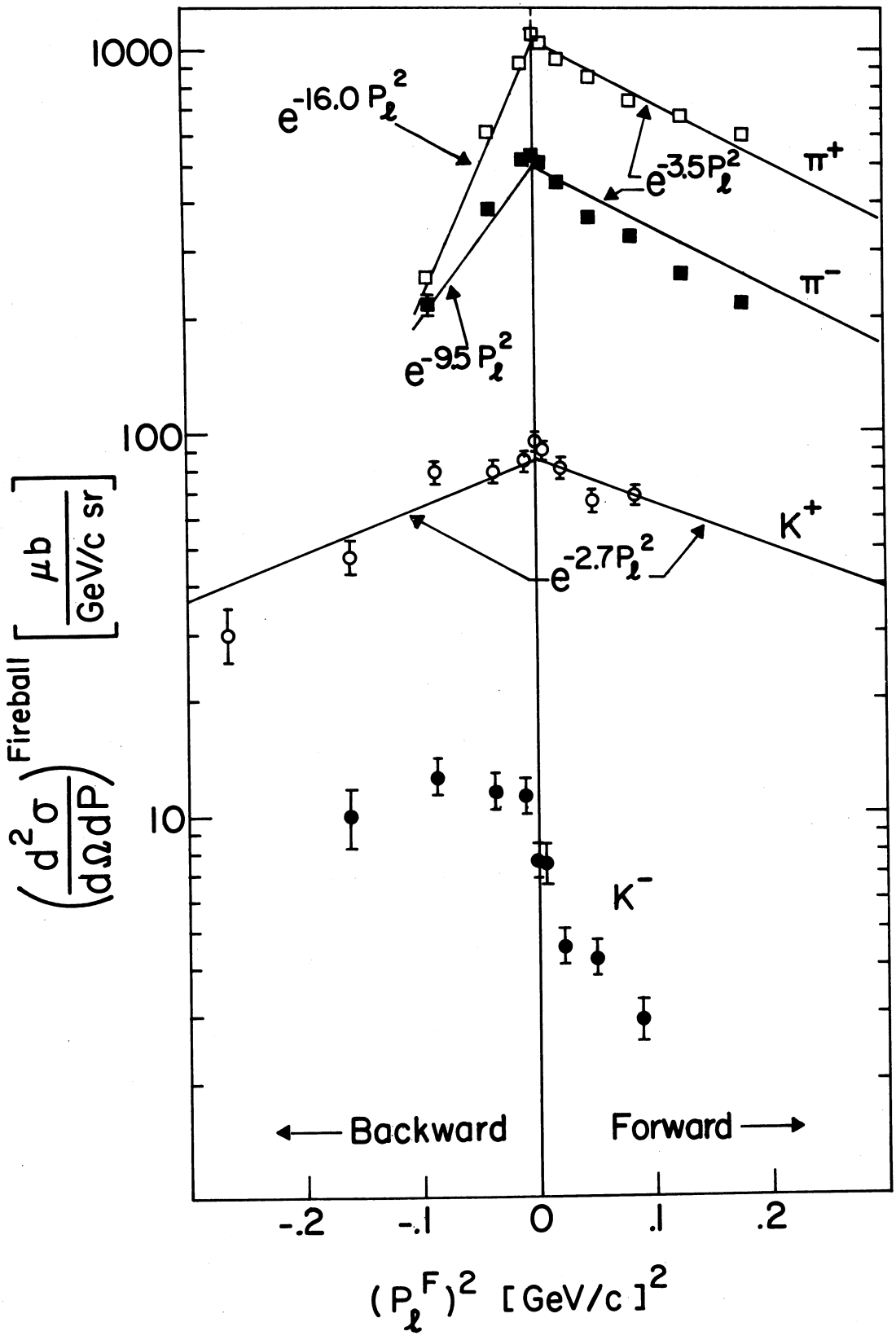

FIGURE 5. CROSS SECTION VS. $P_{\ell\ \text{FIREBALL}}^2$

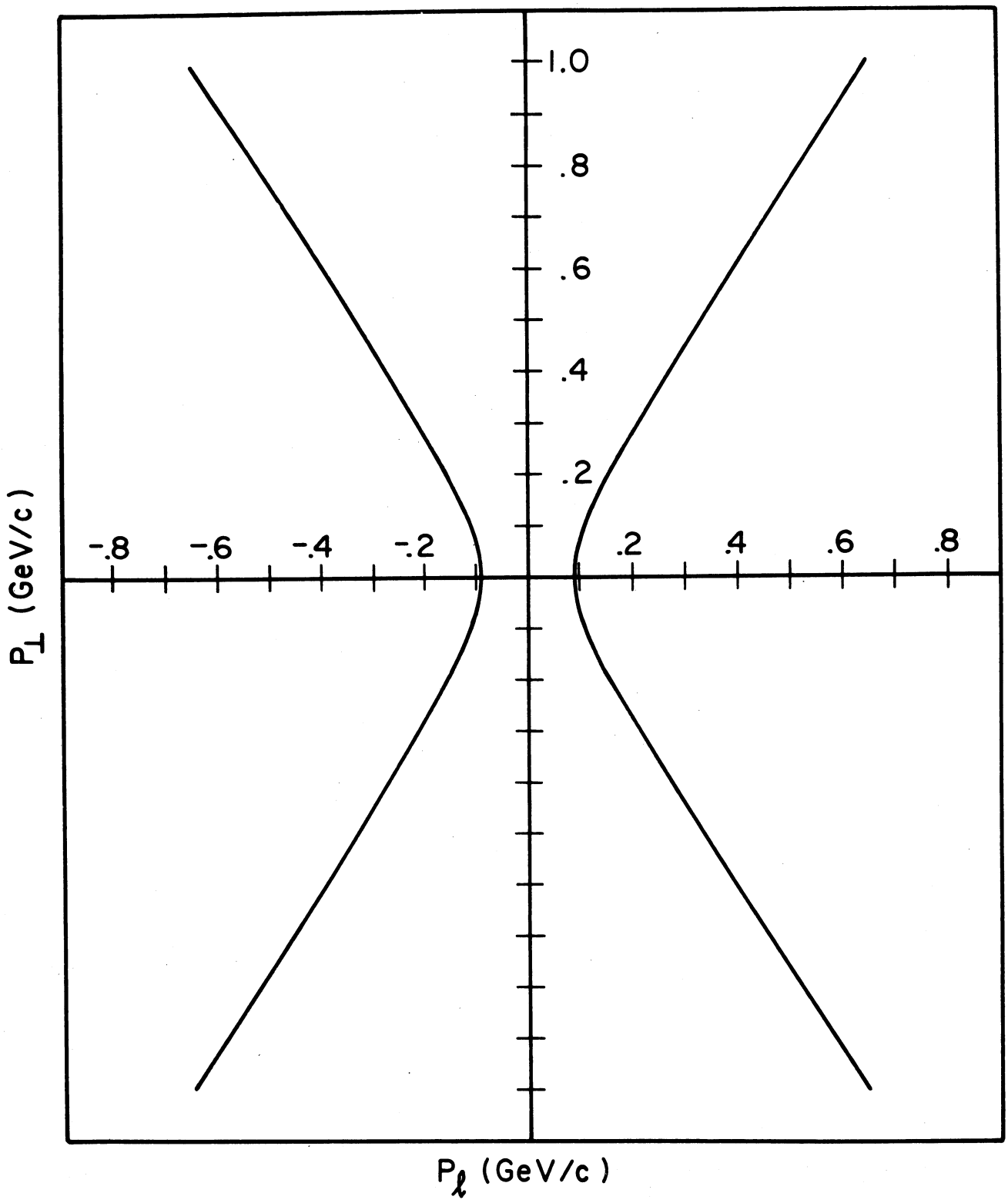

FIGURE 6. LOCUS OF THE MAXIMUM CROSS SECTION

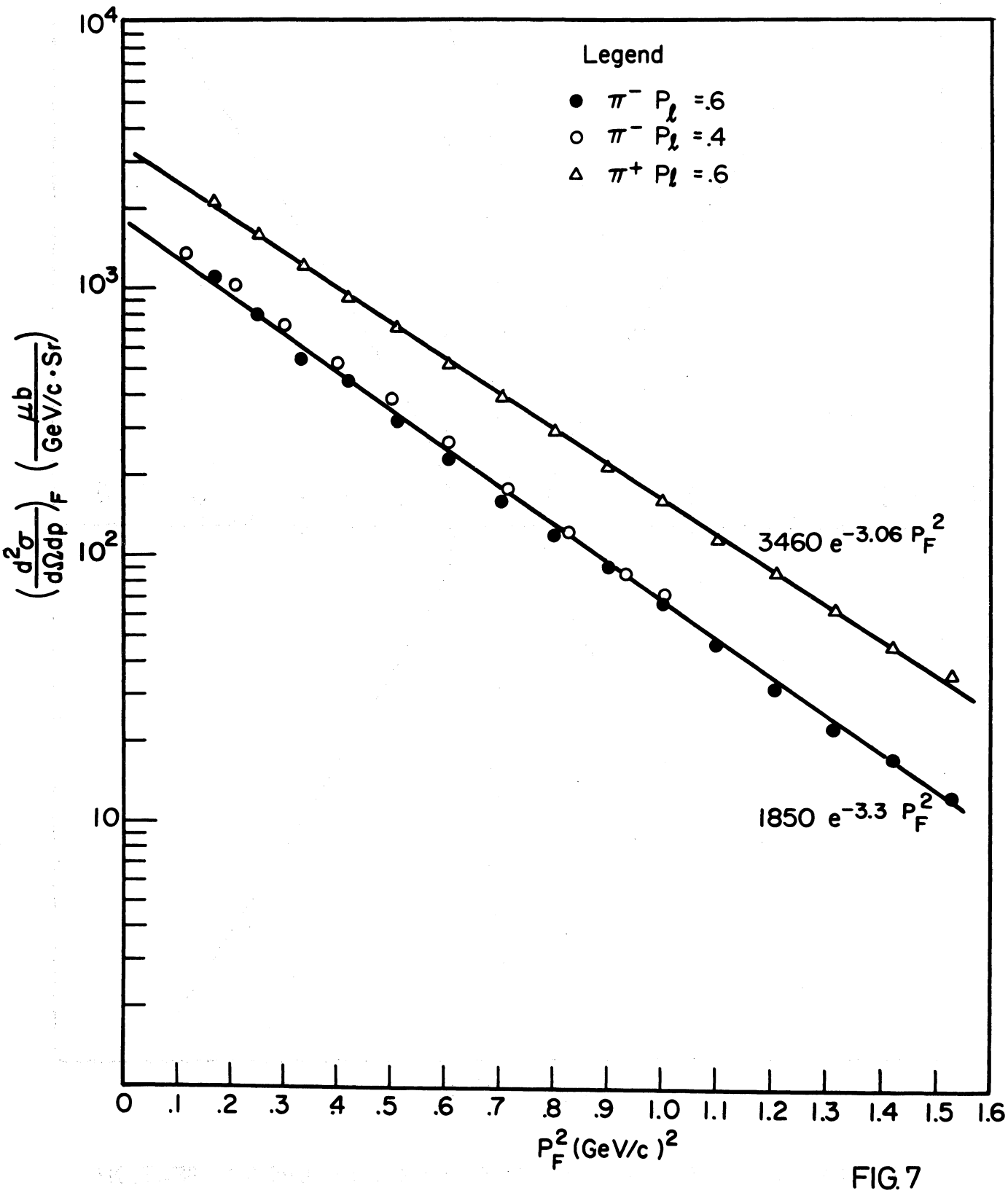
Legend
● π^- P_l =.6
○ π^- P_l =.4
△ π^+ P_l =.6
10^4
10^3
10^2
10
$\left(\frac{d^2\sigma}{d\Omega dp}\right)_F$ $\left(\frac{\mu b}{GeV/c \cdot Sr}\right)$
3460 $e^{-3.06\ P_F^2}$
1850 $e^{-3.3\ P_F^2}$
0 .1 .2 .3 .4 .5 .6 .7 .8 .9 1.0 1.1 1.2 1.3 1.4 1.5 1.6
P_F^2 (GeV/c)^2

FIG. 7

THE SEARCH FOR MESON RESONANCES IN HIGH MULTIPLICITY PROCESSES

J. Clayton, P. Mason, H. Muirhead and P. Renton.

Nuclear Physics Research Laboratory,
The University, Liverpool.

At high energies massive resonances can be produced in multiparticle final states

$$a + b \longrightarrow X + d + e + f \quad .....$$

where d, e, f are long lived particles (π, nucleon, hyperon) and X is a system which decays rapidly, perhaps through a chain of resonances, leading to more long lived particles

$$X \longrightarrow Y + ... \longrightarrow Z + ... \longrightarrow g + h + ...$$

Thus the experimenter is presented with a large number of possible combinations when trying to reconstruct possible resonances from the long lived particles observed in the final state, and any such resonances appear as small bumps on a large background with consequent problems of statistical resolution.

We illustrate this problem with data from our measurements on $p\bar{p} \rightarrow 3\pi^+ 3\pi^-$ at 2.5 GeV/c. In figure 1 we plot invariant mass distributions for $(2\pi^+ 2\pi^-)$ mesons; we have nine possible combinations per event. Small peaks can be seen at 1.6, 1.7 and 1.8 GeV; our

confidence in their existence is considerably reinforced by imposing a cut which demands that each system decays as

$$X \rightarrow \rho^0 \rho^0 \rightarrow 2\pi^+ 2\pi^-$$

where for our purposes a rho meson is defined as a $\pi^+\pi^-$ combination with mass in the interval 660 - 810 MeV. The result is shown in figure 2.

Now although the systems X appear as small peaks in figure 1 an analysis of the observed mass distribution indicates that they constitute $91 \begin{smallmatrix} + 26 \\ - 17 \end{smallmatrix}$ % of all events (i.e. $9 \times (10 \begin{smallmatrix} + 3 \\ - 2 \end{smallmatrix})$% of entries on the graph). We have therefore sought to find a way to improve the signal to background ratio.

Consider an initial state (i) leading to a final state (f) containing six pions via a system X containing four pions (figure 3). Then if we suppress irrelevant constants and kinematic terms the cross section σ_{fi} may be written as

$$\sigma_{fi} \propto \bar{\sum_i} \sum_f |T_{fi}|^2 \prod_{j=1}^{6} \frac{d\vec{p}_j}{2E_j} \delta(p_i - p_f)$$

$$\propto \bar{\sum_i} \sum_{f'} |\langle \pi_1 \pi_2 X | T_p | p\bar{p} \rangle|^2 \frac{\Gamma_{X \rightarrow 4\pi}}{(m_p^2 - m_X^2)^2 + m_X^2 \Gamma^2}$$

$$\cdot \, dm_p^2 \frac{d\vec{p}_1}{2E_1} \frac{d\vec{p}_2}{2E_2} \frac{d\vec{p}}{2E_p} \delta(p_i - p_1 - p_2 - p)$$

where T_p = operator for production of X

$$m_p^2 = -(p_1 + p_2 + p_3 + p_4)^2 = -P^2$$

Γ = total width of X

$\Gamma_{X \to 4\pi}$ = width for decay channel $X \to 4\pi$

We thus have an expression for $d\sigma_{fi}/dm_p^2$ in terms of a three body final state. The configurations of particles in the three body state will be determined by $\langle \pi_1 \pi_2 X | T | p\bar{p} \rangle$ and the phase space terms. We have therefore taken plausible forms for $|T|^2$ and determined its value for each of the possible combinations of pions. The combination which yielded the largest value for $|T|^2$ was then accepted as the most likely configuration and the corresponding mass m_p was determined.

In constructing possible forms for $|T|^2$ we have been guided by the principle that nature abhors a large four momentum transfer. Our angular distribution for π^+ and π^- appears to be partially correlated with the ingoing nucleons (figure 4). We therefore first examined our data with the diagrams shown in figure 5. Since our propagators had to be baryons we used the nucleon mass for m in our initial investigations.

No significant features emerged in our distribution for m_p when we used diagrams with two vertices only (figures 5(a) and 5(b)). However, we found that if we assumed three vertices (figure 5(c)) then peaks started to appear in our distributions. Briefly, the results obtained at this stage indicated that configurations placing any four pion system at the

centre vertex were unlikely (~ 50 events from a total of 736 events depending on the charge of q and r) furthermore no significant peaking occured in these events. In configurations which placed the four pion system at an extreme vertex peaking was observed in the distributions for m_p. The peaking appeared to be more pronounced if r was doubly charged than if it was neutral (the assignment of charge for r depends on the ordering of π^+ and π^- at π_1 and π_2). We illustrate the results at this stage in figure 6, where 6(a) and (b) indicates the mass distribution m_p for doubly charged and neutral systems respectively. It should be noted that both the magnitude for q and the sign of its charge is left undisturbed by either assignment of charge to π_1 and π_2.

In figure 6 (and subsequent diagrams) we show a comparison with phase space. We have used the CERN program FOWL to generate fictitious six pion events (i.e. events determined by phase space consideration alone) and then applied the same selection criteria as to our real events; the result is shown by the smooth curve in figure 6.

We next attempted to insert plausible factors in the numerator for T. Since large four momentum changes occur damping factors of the type exp. $- n\lambda(q^2 + r^2)$ were introduced for the vertex functions where $\lambda = 0.5$ GeV^{-2} and n = 0, 1, 2 ----. Peaking was found to be more pronounced if $|q^2|$ was used rather than q^2 (also for r^2). In figures 7 and 8 we illustrate the results for n = 3 and 6 for doubly charged and neutral r (figure 6 of course corresponds to n = 0). A notable feature in these figures is the relative magnitudes of the 1.7 and 1.8 GeV systems in the two curves.

The apparent occurence of doubly charged states for r encouraged us to believe that it might be the j = 3/2, T = 3/2 nucleon resonance at 1236 MeV (figures 6, 7, 8 in fact were determined with m_r = 1236 MeV). Now the angular distribution of pion scattering in the rest system of this resonance is $1 + 3\cos^2\Theta$. We therefore transformed all events to the rest system of r* and made the requirement that the product

$$T^2 \sim \cos^2\Theta \exp.\left[-n\lambda\left(|q|^2 + |r|^2\right)\right] / \left[(q^2 + m^2)(r^2 + m^2)\right]^2$$

should be a maximum. The results are shown in figs. 9, 10, 11.

Finally, we attempted to Reggeise the possible forms for T. We used a formulation suggested by Chan Hong-Mo, Kajantie and Ranft [1].

$$T \sim \exp.\left[-(\Omega_q q^2 + \Omega_r r^2)\right] \cdot s_{12}^{\alpha_q} s_{2X}^{\alpha_r}$$

---

* This could only be done in configurations in which r^2 was negative - these are the most likely configurations in any case.

where

$$\Omega_q = a_q + \alpha_q' \log s_{12}$$

$$\Omega_r = a_e + \alpha_r \log s_{2X}$$

$$s_{12} = -(p_1 + p_2)^2$$

$$s_{2X} = -(p_2 + P)^2$$

$$\alpha_q = \alpha_q(0) - \alpha_q' \cdot q^2$$

$$\alpha_r = \alpha_r(0) - \alpha_r' \, r^2$$

In the above expressions a_q and a_r are constants (equivalent to $n\lambda$ in our Feynman graphs) and α' are the slopes of Regge trajectories. We kept $a_q = a_r$ for simplicity, and assumed that α_r followed the trajectories containing either the $j = 3/2$, $T = 3/2$ resonance or the nucleon whilst α_q followed only the nucleon trajectory. Results for a value of $a_q = a_r = 5$ GeV^{-2} are shown in figures 12 and 13.

Our results therefore suggest that the selection of suitable forms for T can improve the signal to noise ratio in searching for resonances in systems of high multiplicity and at the same time give us some insight into the machanism whereby they are produced. It is perhaps of interest to note that Lipkin has suggested that the annihilation of proton-antiproton systems should proceed predominantly through the production of three nonstrange mesons if a quark picture is used. The present analysis suggests that the two pions produced with the resonances are separate entities, and thus if we take the figure of ~ 90% for resonance production quoted earlier, then three data for the channel $p\bar{p} \rightarrow 3\pi^+ 3\pi^-$ at 2.5 GeV/c would appear to support

the three meson hypothesis.

We are indebted to the Science Research Council for supporting this work.

Reference

(1) Chan Hong-Mo, K. Kajantie and G. Ranft, Nuovo Cimento 49, 157, 1967; see also F. Zachariesen and G. Zweig, Phys. Rev. 160, 1322, 1326, 1967.

Captions to figures

Figure 1. Mass distribution of any $(2\pi^+ 2\pi^-)$ combination in $p\bar{p} \to 3\pi^+ 3\pi^-$ at 2.5 GeV/c. Nine combinations per event.

Figure 2. Mass distribution of $\rho^0\rho^0$ from $p\bar{p} \to 3\pi^+ 3\pi^-$. We define a ρ^0 meson as any $\pi^+\pi^-$ system with a mass lying in the interval 660-810 MeV and impose the restriction that separate pairs of pions must form ρ's.

Figure 3. Schematic formulation of process

$$p\bar{p} \to X\,\pi^+\pi^- \downarrow 2\pi^+ 2\pi^-$$

Figure 4. Angular distribution of π^+ mesons with respect to proton and π^- with respect to antiproton in $p\bar{p} \to 3\pi^+ 3\pi^-$.

Figure 5. Possible forms for the matrix element $p\bar{p} \to X\,\pi^+\pi^-$.

Figure 6. Distribution of masses using

$$|T|^2 \sim \exp.\left[-n\lambda(|q|^2 + |r|^2)\right] / \left[(q^2 + m^2)(r^2 + m^2)\right]^2$$

with n = 0. Doubly charged baryons occur in (a) (r + + or --) and neutral in (b).

Figure 7. As for 6 with n = 3.

Figure 8. As for 6 with n = 6.

Figure 9. Distribution of masses using

$$T^2 \sim \cos^2\Theta \exp.\left[-n\lambda(|q|^2 + |r|^2)\right] / \left[(q^2 + m^2)(r^2 + m^2)\right]^2$$

with n = 0. Doubly charged baryons occur in (a) (r + + or ----) and neutral in (b).

Figure 10. As for 9 with n = 3.

Figure 11. As for 10 with n = 6.

Figure 12. Distribution of masses using Regge formulation given in the text with $a_q = a_r = 5\ \text{GeV}^{-2}$. (a) Assumption of doubly charged baryons for r, (b) neutral baryons for r. In both cases the Regge trajectories

$$\alpha_r = 0.15 - 0.9\ r^2 = \Delta_\delta$$

$$\alpha_q = -0.39 - 1.01\ q^2 = N_\alpha$$

were used.

Figure 13. Distribution of masses using Regge formulation given in text with $a_q = a_r = 5\ \text{GeV}^{-2}$. (a) Assumption of doubly charged baryon for r with Δ_δ trajectory and N_α trajectory for q (see caption to figure 12). (b) Assumption of neutral baryon for r and N_α trajectory for both r and q.

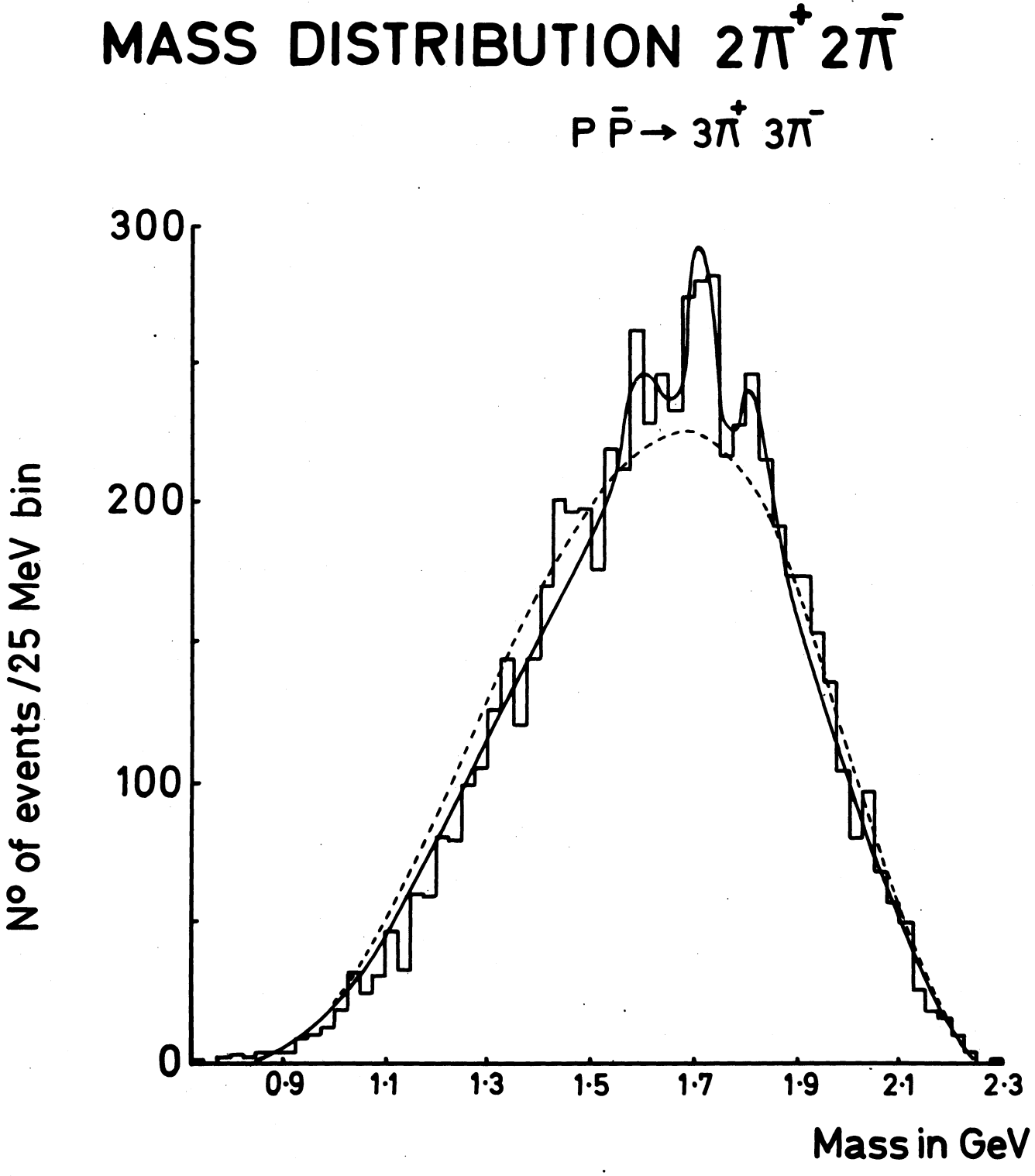
MASS DISTRIBUTION $2\pi^+ 2\pi^-$
$P\bar{P} \rightarrow 3\pi^+ 3\pi^-$
300
200
100
0
N° of events /25 MeV bin
0·9
1·1
1·3
1·5
1·7
1·9
2·1
2·3
Mass in GeV

FIGURE 1

MASS DISTRIBUTION $\rho^0 \rho^0$

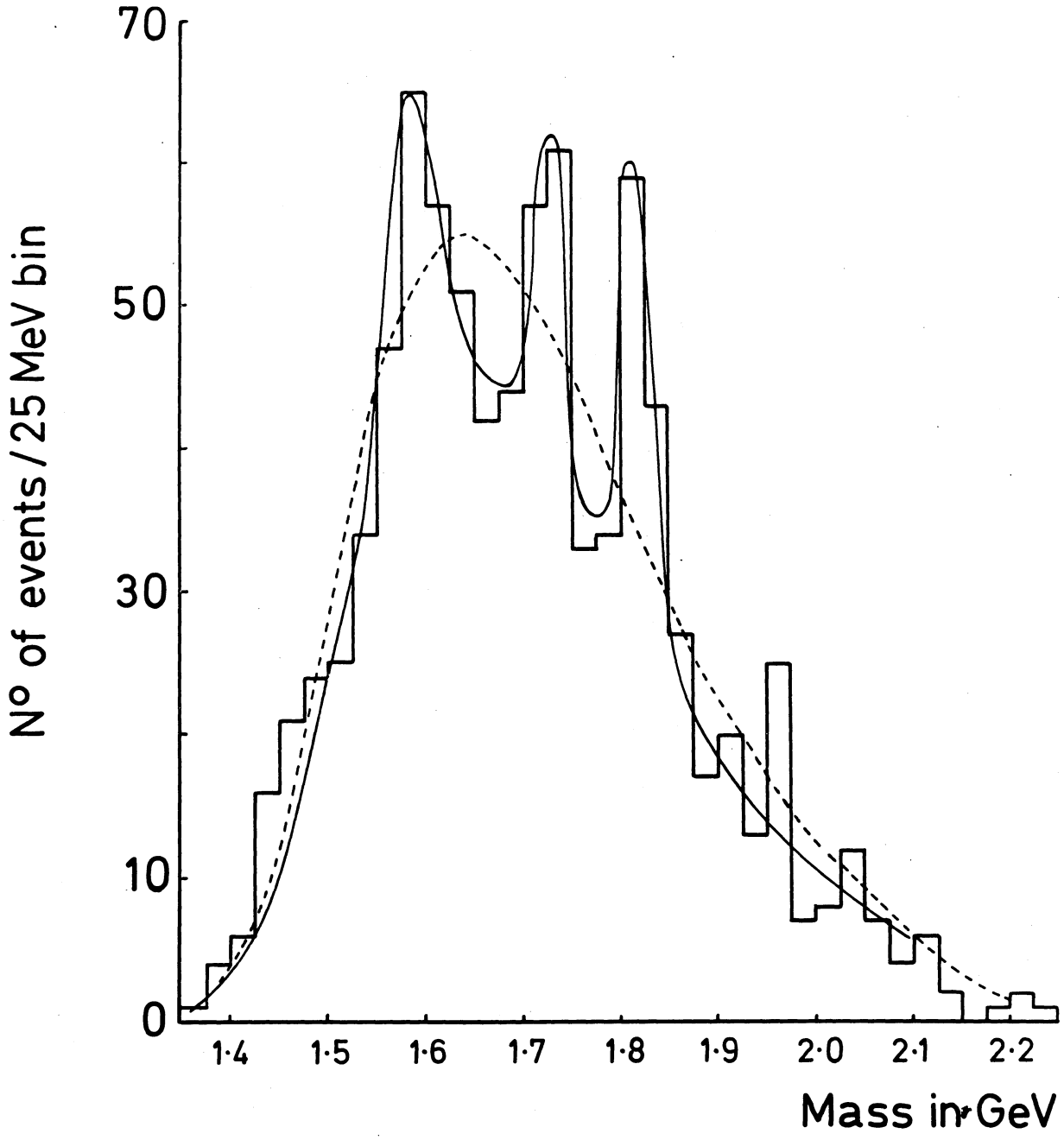

FIGURE 2

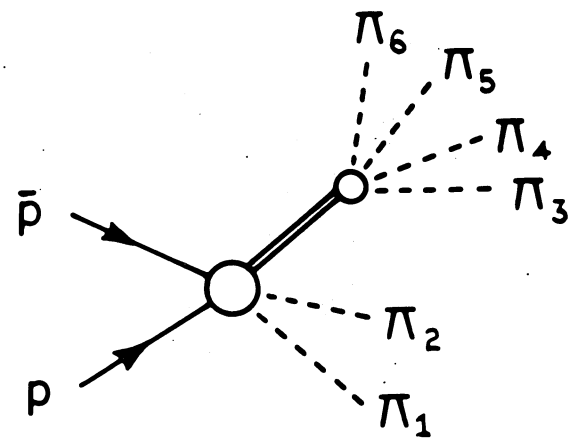

FIGURE 3

ANGULAR DISTRIBUTION π^+, π^- REFLECTED WITH RESPECT TO PROTON

$P\bar{P} \rightarrow 3\pi^+ 3\pi^-$

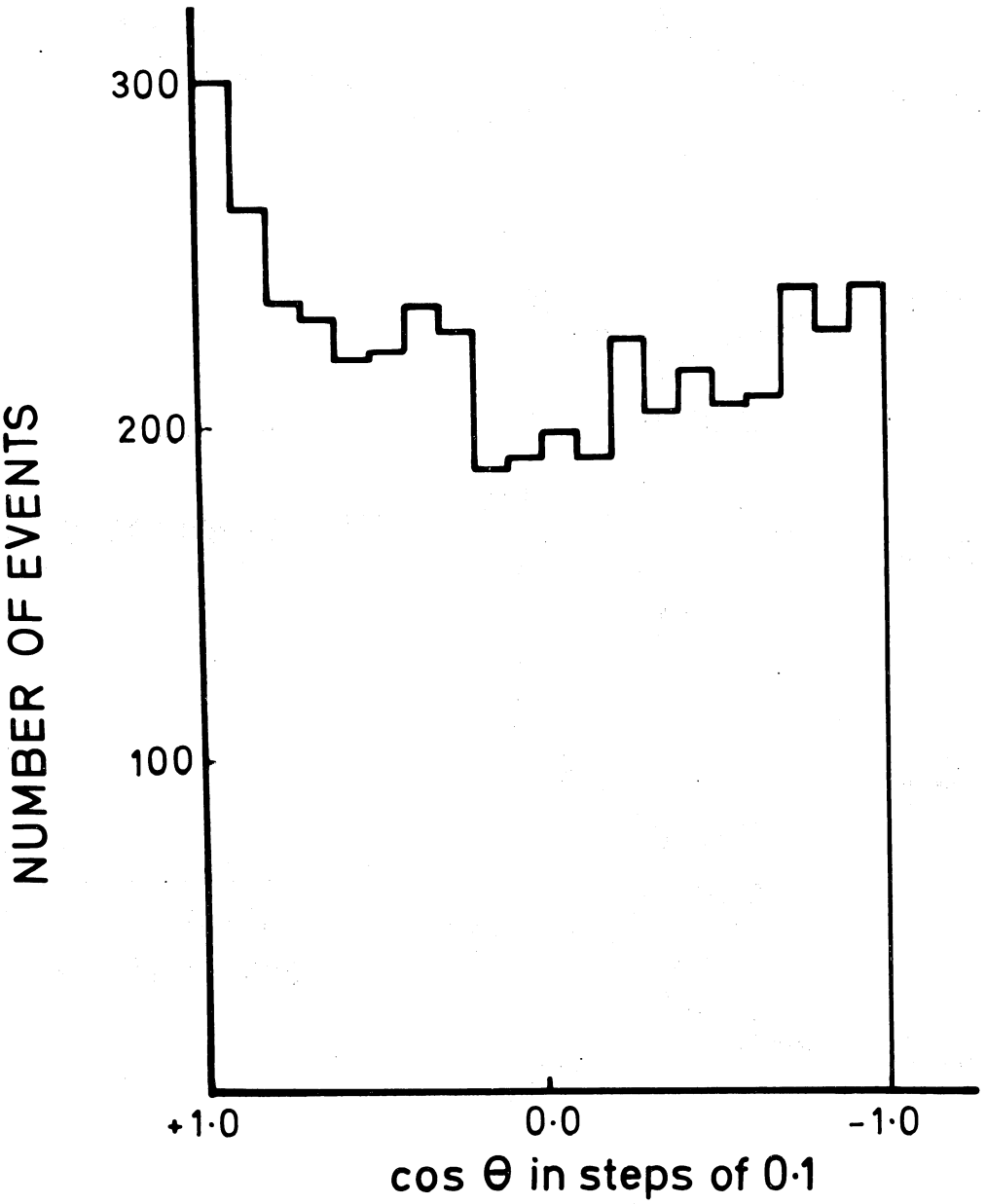

FIGURE 4

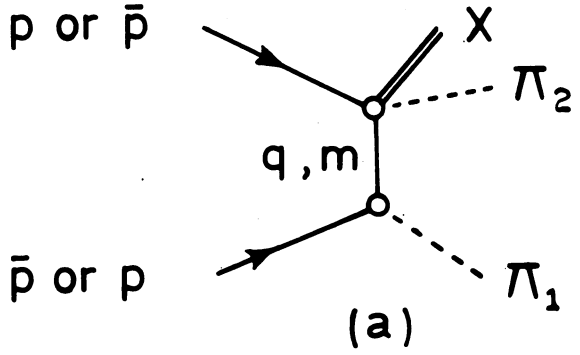

$$T \sim \frac{1}{q^2 + m^2}$$

18 combinations

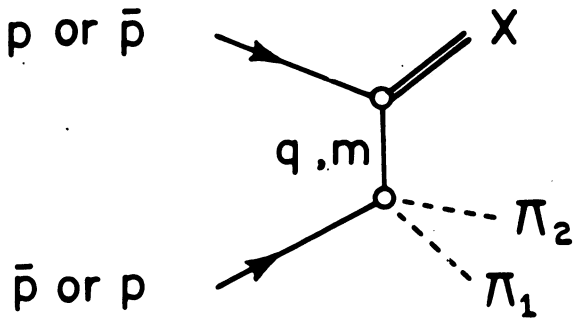

$$T \sim \frac{1}{q^2 + m^2}$$

18 combinations

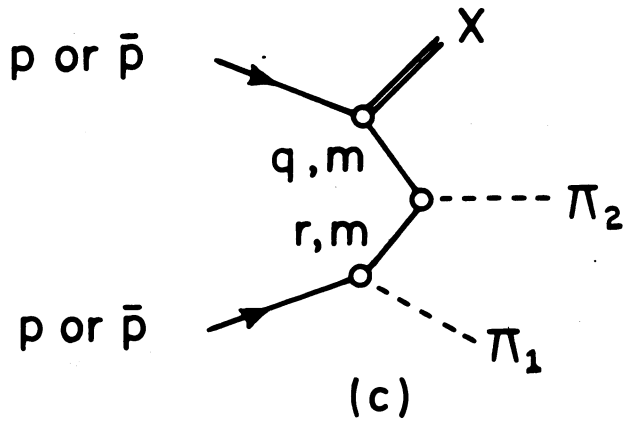

$$T \sim \frac{1}{q^2 + m^2} \cdot \frac{1}{r^2 + m^2}$$

54 combinations

FIGURE 5

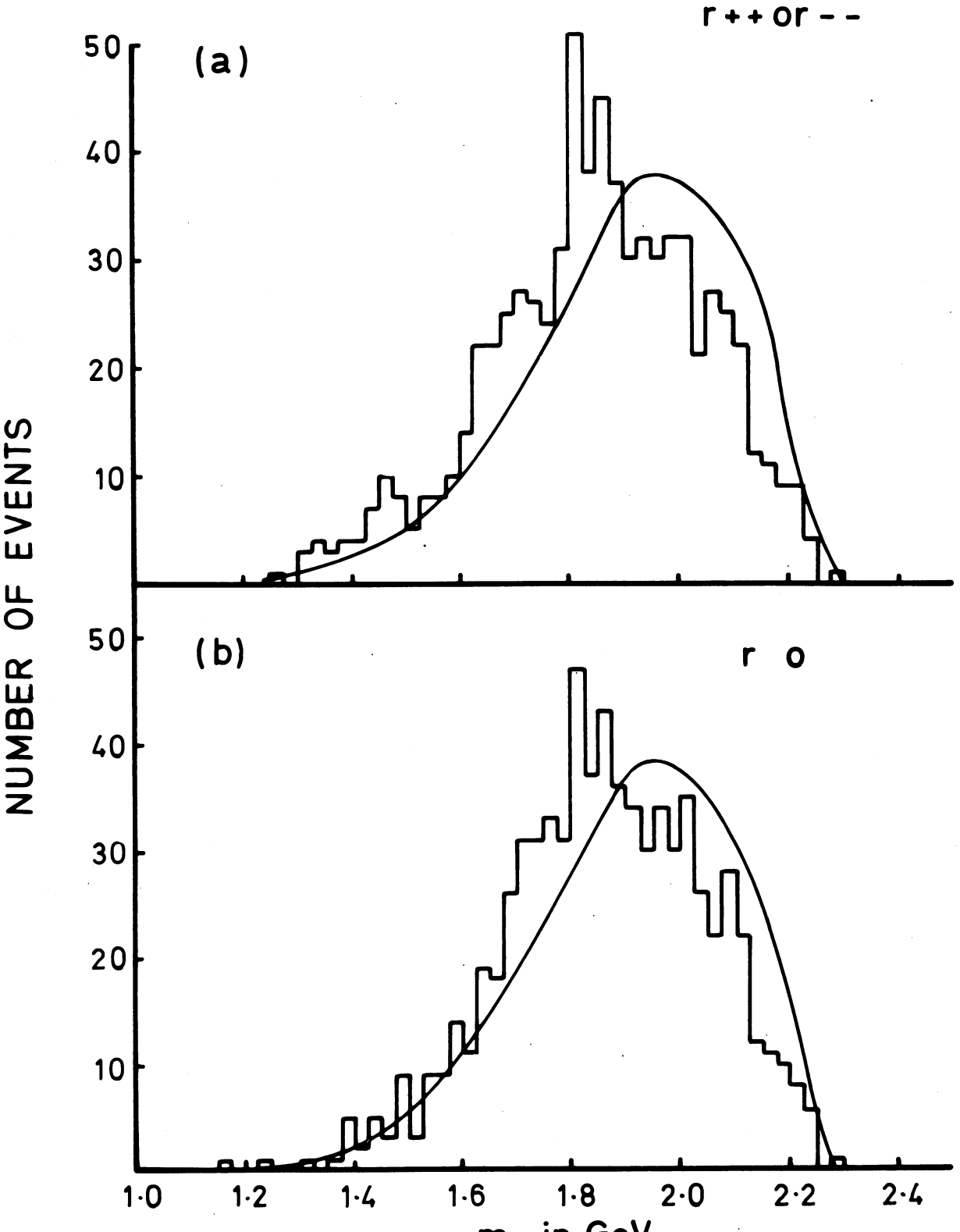
r++ or --
(a)
50
40
30
20
10
(b)
r o
50
40
30
20
10
NUMBER OF EVENTS
1·0
1·2
1·4
1·6
1·8
2·0
2·2
2·4
mp in GeV

FIGURE 6

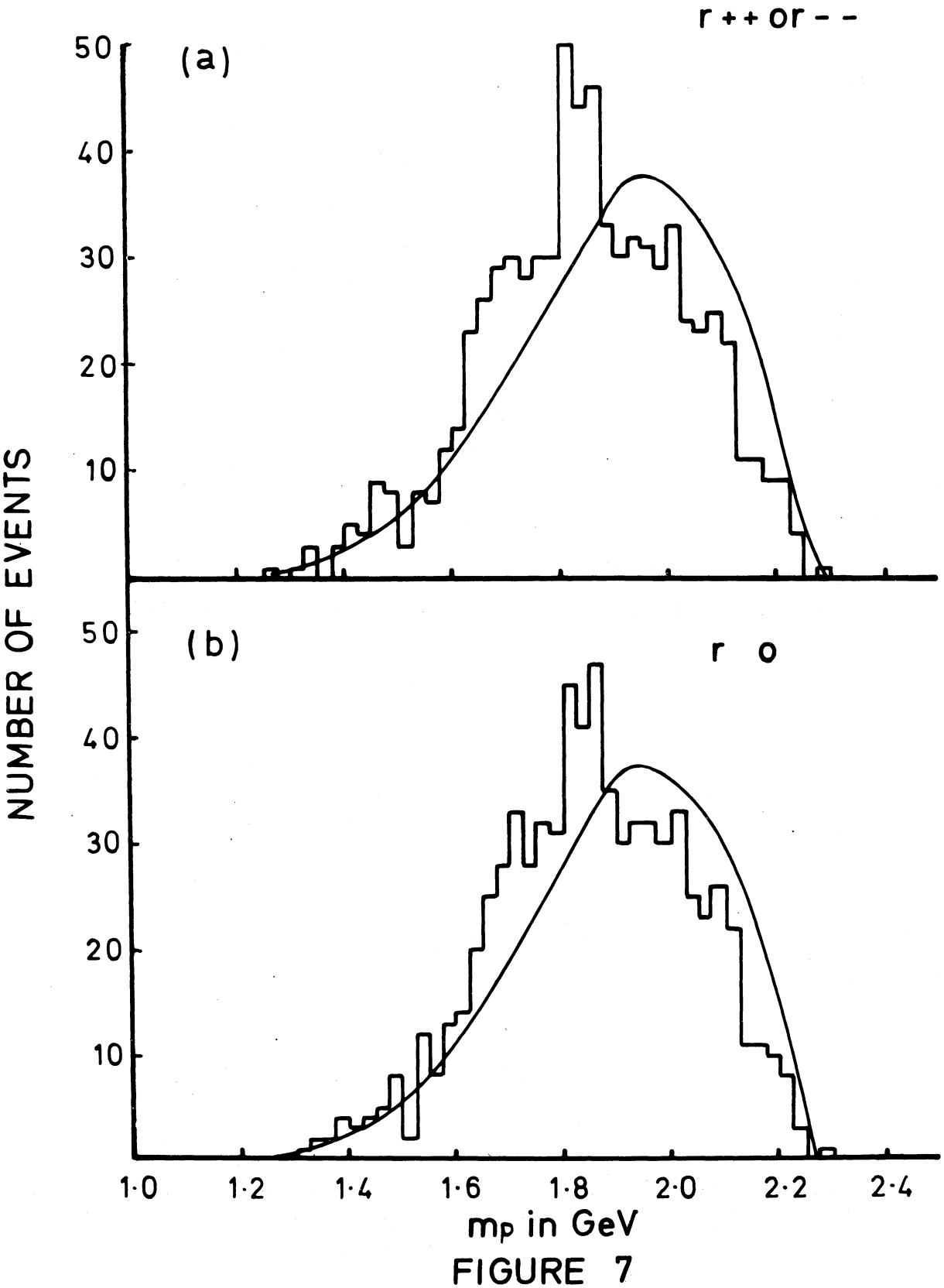
r ++ or - -
(a)
50
40
30
20
10
NUMBER OF EVENTS
(b)
r o
50
40
30
20
10
1·0
1·2
1·4
1·6
1·8
2·0
2·2
2·4
mp in GeV

FIGURE 7

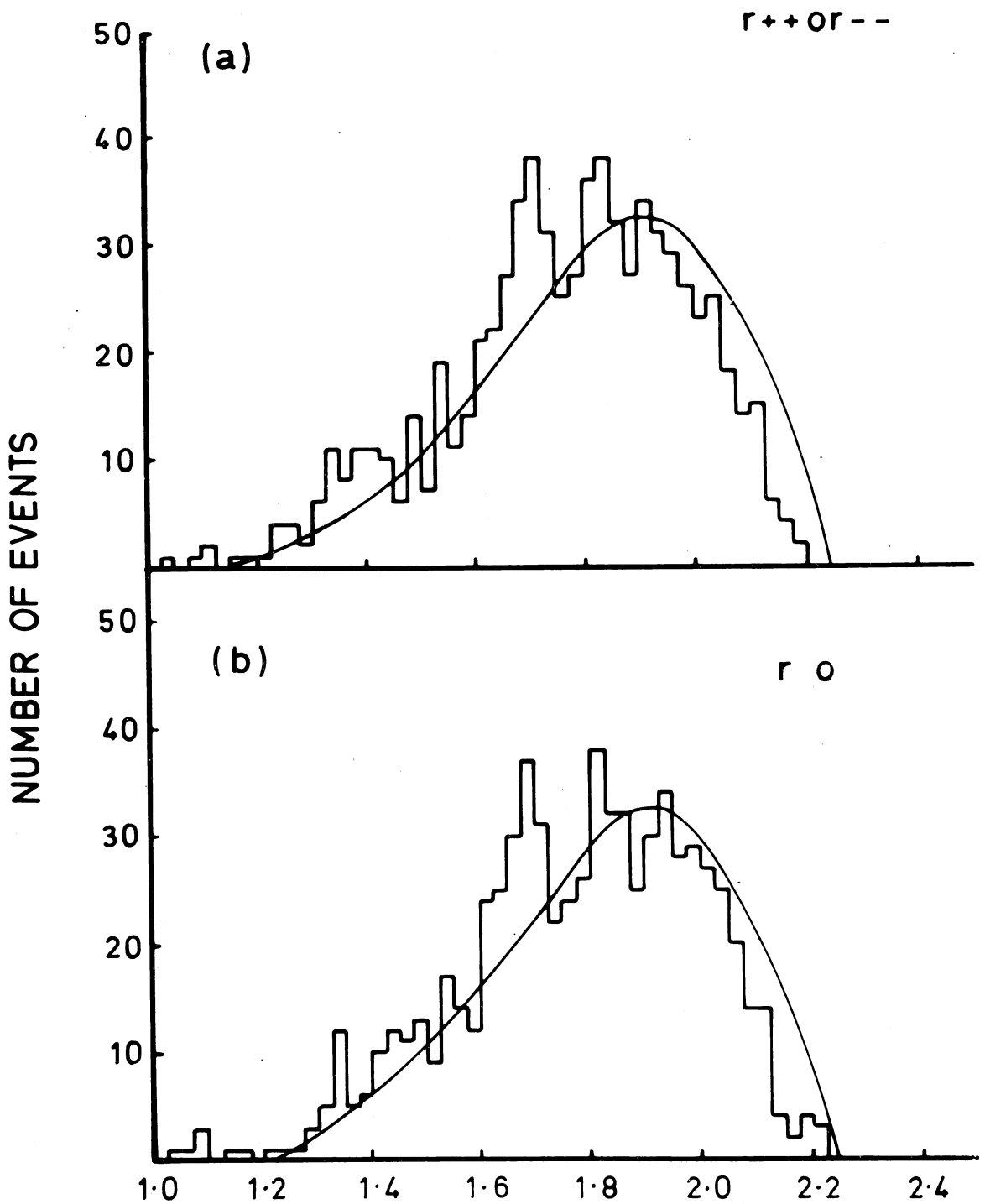
r++ or --
(a)
50
40
30
20
10
(b)
r o
NUMBER OF EVENTS
1·0
1·2
1·4
1·6
1·8
2·0
2·2
2·4
mp in GeV

FIGURE 8

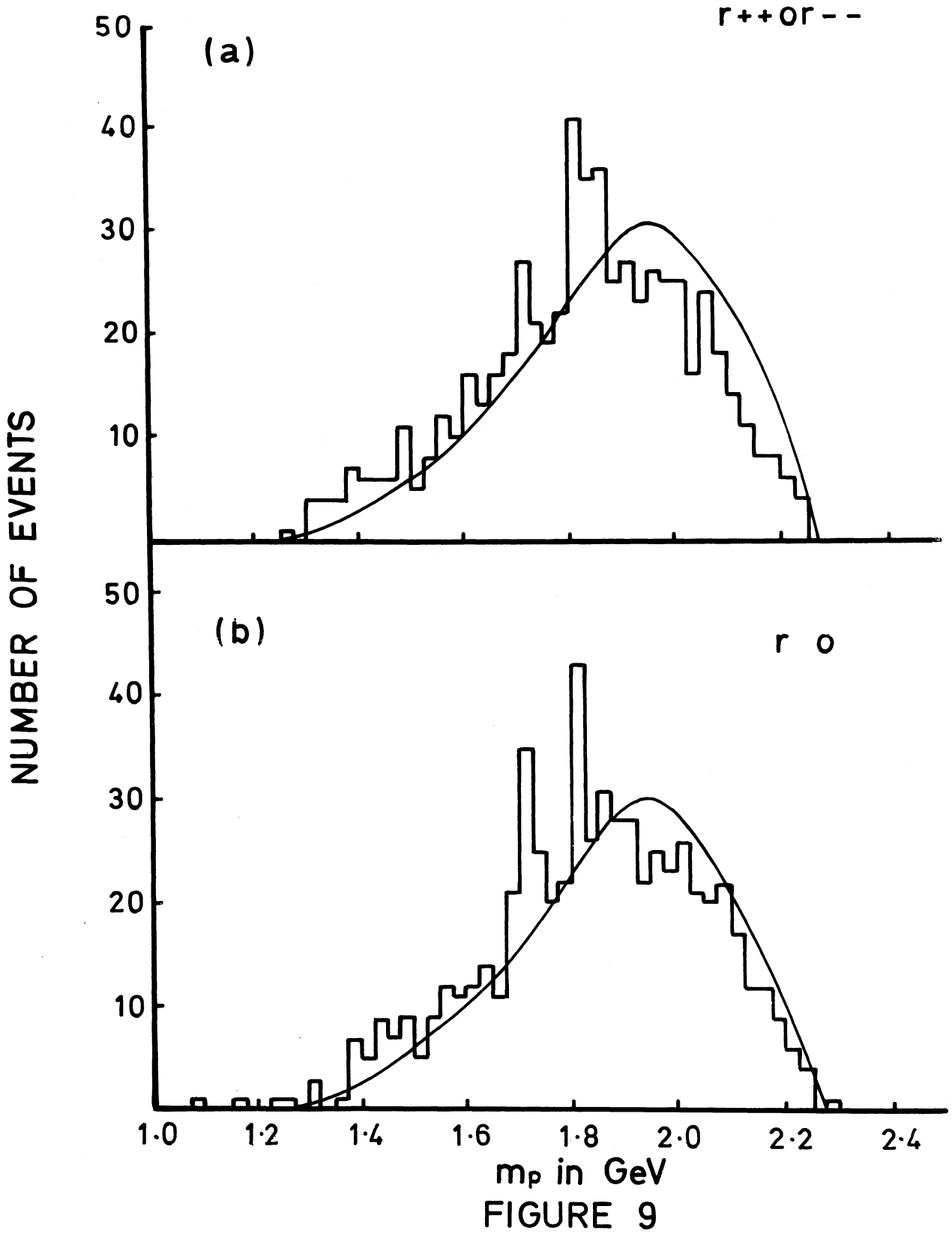
r++or--
(a)
50
40
30
20
10
NUMBER OF EVENTS
(b)
r o
50
40
30
20
10
1·0
1·2
1·4
1·6
1·8
2·0
2·2
2·4
mp in GeV

FIGURE 9

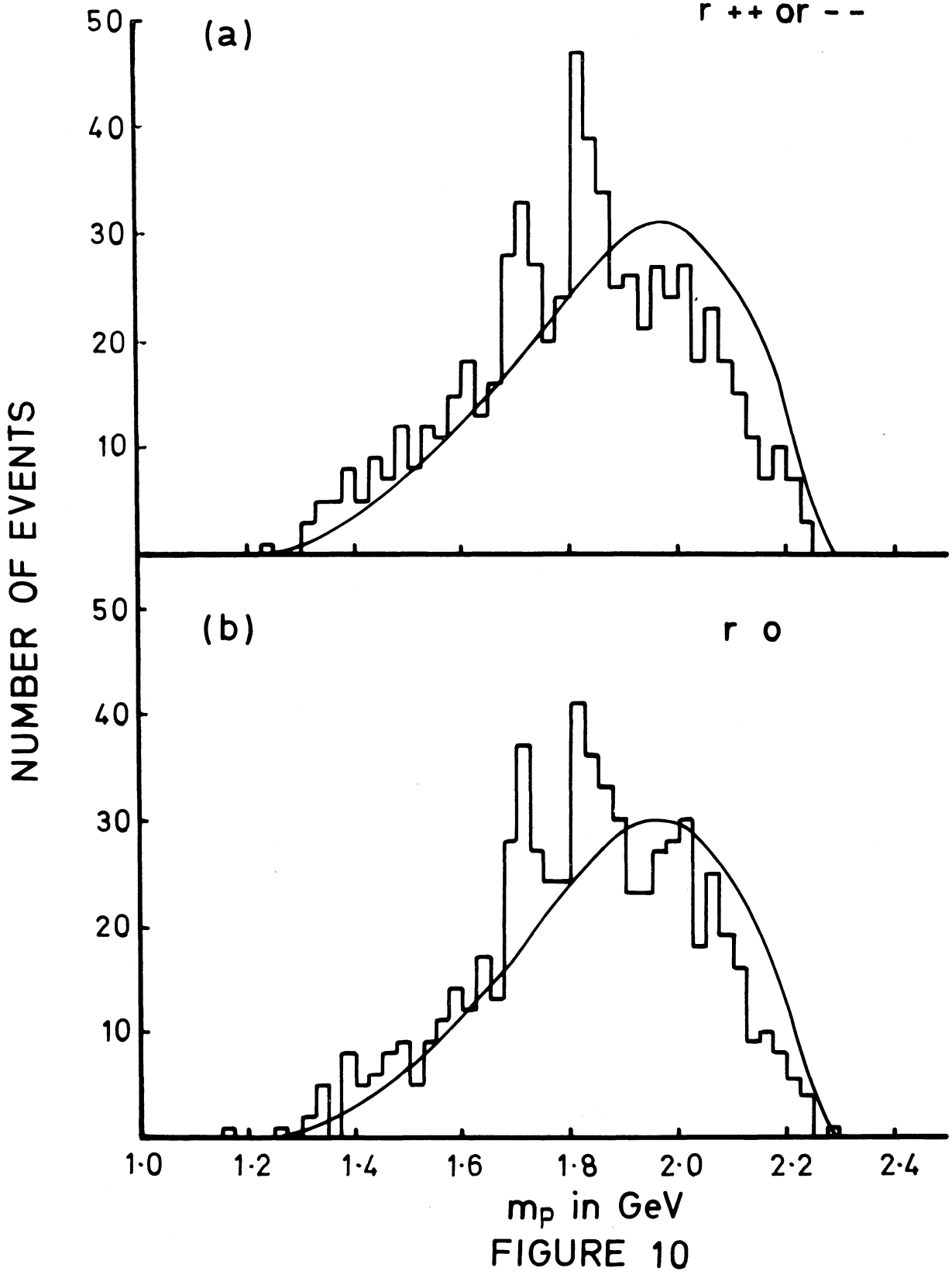
(a)
r ++ or - -
(b)
r o
NUMBER OF EVENTS
50
40
30
20
10
1·0
1·2
1·4
1·6
1·8
2·0
2·2
2·4
m_p in GeV

FIGURE 10

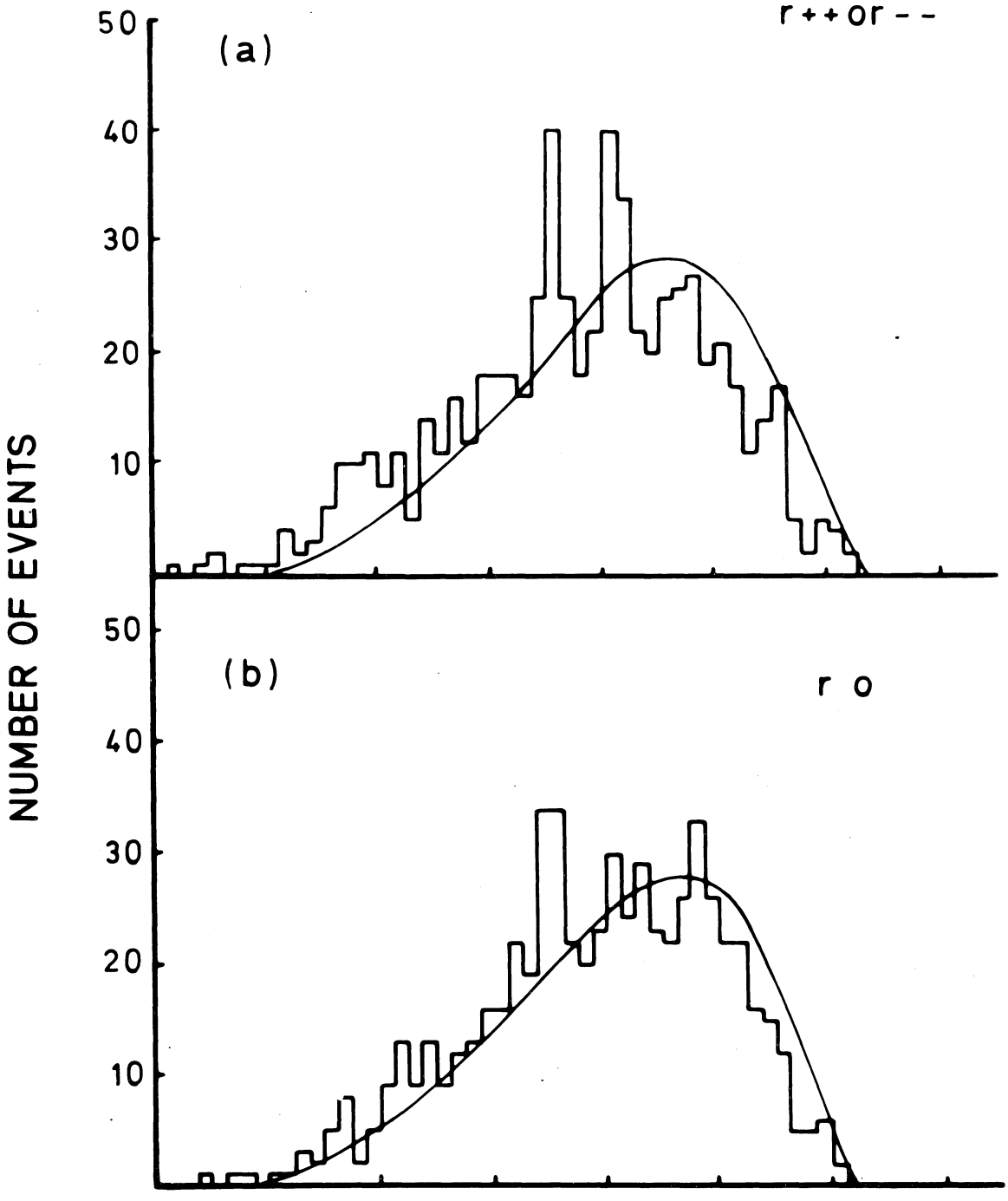
r++or--
(a)
50
40
30
20
10
(b)
r o
NUMBER OF EVENTS
1·0
1·2
1·4
1·6
1·8
2·0
2·2
2·4
m_p in GeV

FIGURE 11

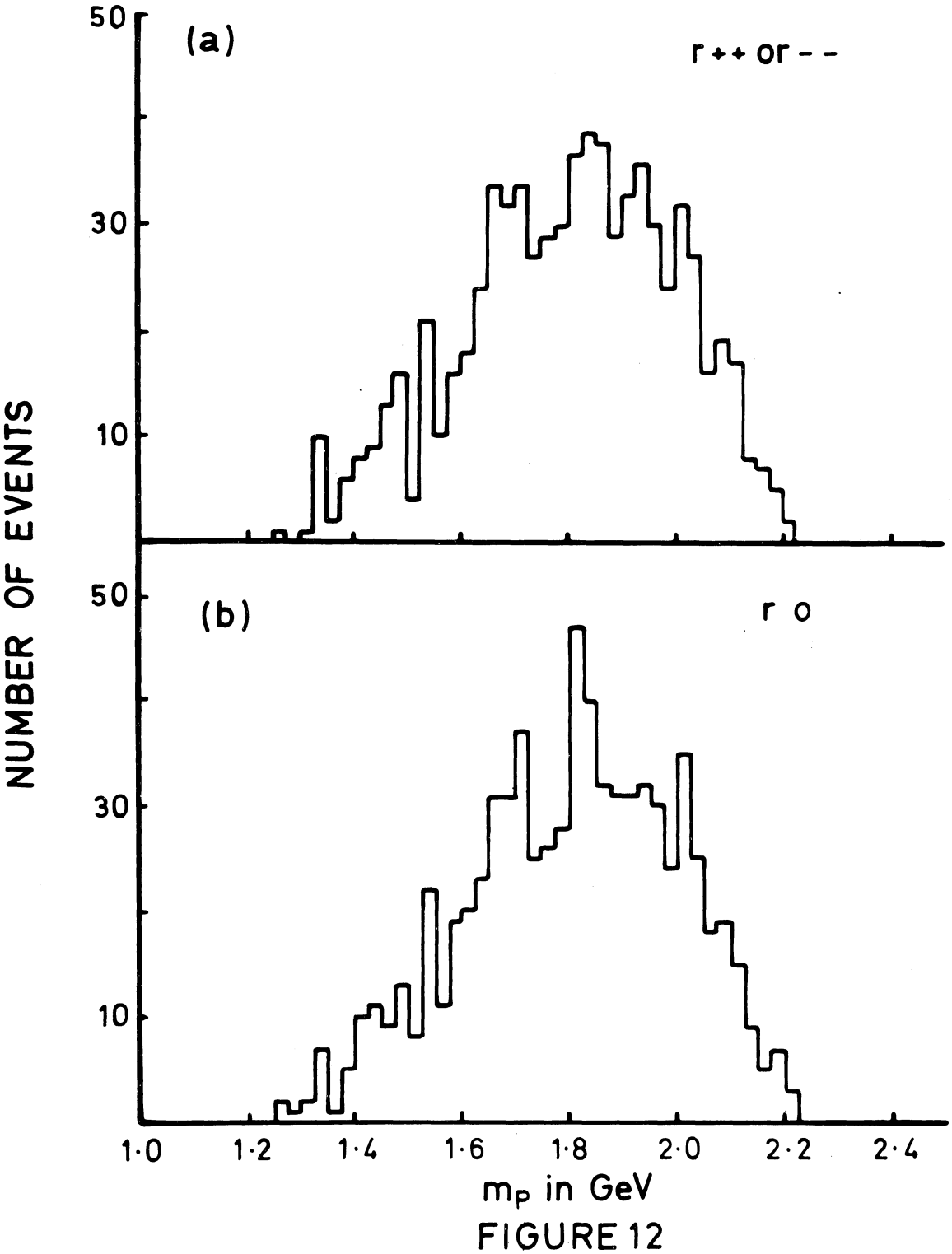
(a)
r++ or - -
50
30
10
(b)
r o
50
30
10
NUMBER OF EVENTS
1·0
1·2
1·4
1·6
1·8
2·0
2·2
2·4
mp in GeV

FIGURE 12

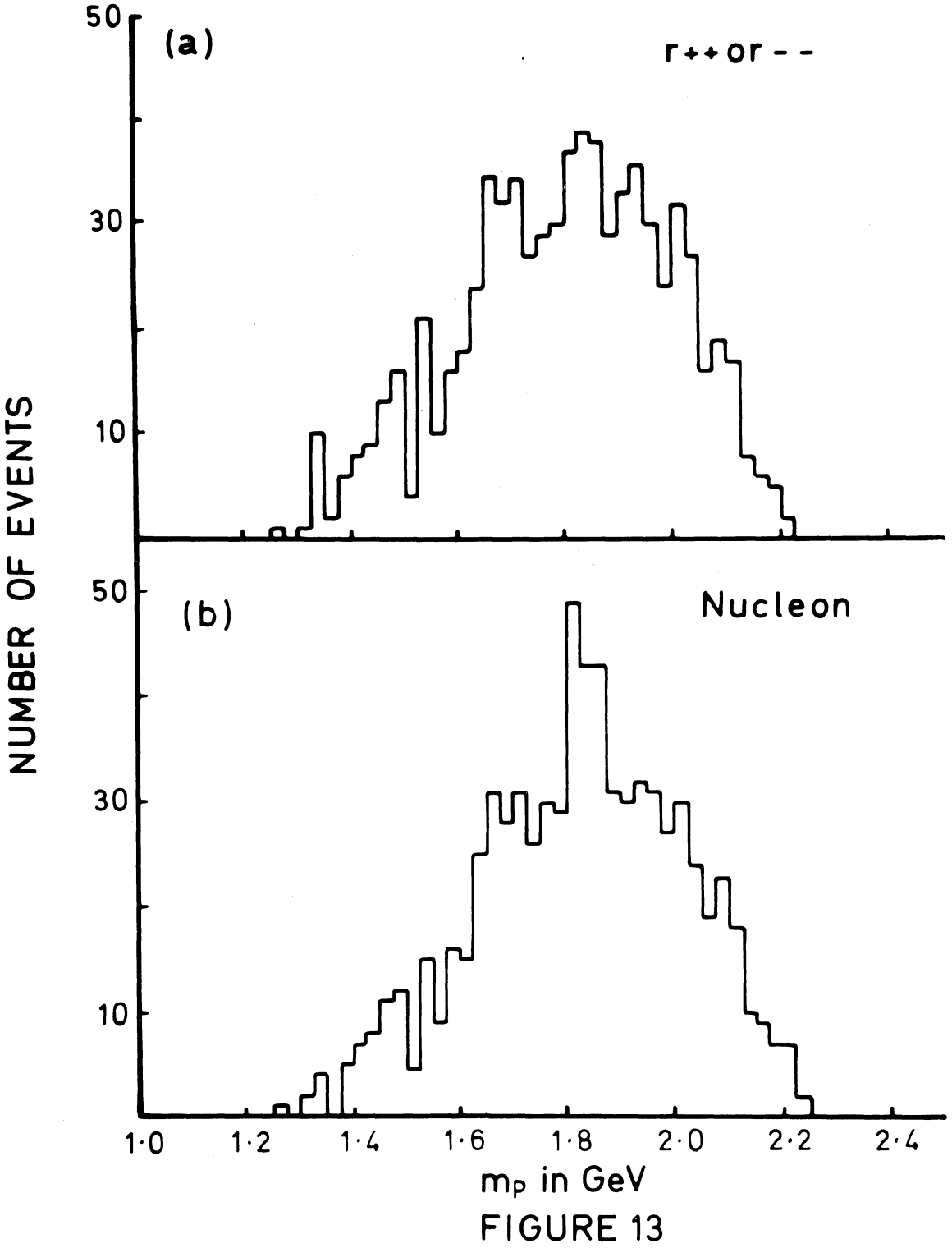
50
(a)
r++ or - -
30
10
NUMBER OF EVENTS
50
(b)
Nucleon
30
10
1·0
1·2
1·4
1·6
1·8
2·0
2·2
2·4
mp in GeV

FIGURE 13

CONTRIBUTED PAPERS NOT INCLUDED IN PROCEEDINGS

(Listed in order of arrival)

Kinematic singularities and threshold relations for helicity amplitudes
J.D. Jackson and G.E. Hite, Lawrence Radiation Laboratory, University of California, Berkeley, Cal., U.S.A.
(to be published in Physical Review)

Photoproduction of π^+, π^0 and K^+ near $t = 0$
Nina Byers and Gerald H. Thomas, Department of Theoretical Physics, Oxford, U.K. (previously Physics Department, University of California, Los Angeles, Cal., U.S.A.)
(published in Phys.Rev.Letters 20, 129 (1968))

Asymmetry moments of angular distributions
P. Kielanowski and J. Werle, Institute for Theoretical Physics, University of Warsaw, Warsaw, Poland
(to be published in Nuclear Physics)

"Proper helicity amplitude" for high energy collisions
Z. Koba, The Niels Bohr Institute, Copenhagen, Denmark

Observations on baryon resonance production in 28.5 GeV/c p-p interactions
P.L. Connolly, W.E. Ellis, P.V.C. Hough, D.J. Miller, T.W. Morris, C. Ouannes, R.S. Panvini, and A.M. Thorndike, Brookhaven National Laboratory, Upton, N.Y., U.S.A.
(Part of the material will be submitted to Phys.Rev. Letters)

Validity of the interference model for πN scattering
C.B. Chiu, CERN, Geneva, Switzerland, and A.V. Stirling, CEN-Saclay, France
(to be published in Phys.Letters)

Measurement of polarization in $\pi^- p \longrightarrow \pi^0 n$ and $\pi^- p \longrightarrow \eta n$
R.C. Lamb, R.A. Lundy, T.B. Novey, A. Yokosawa, and D.D. Yovanovitch, Argonne National Laboratory, Argonne, Ill., U.S.A.
(Partly published in Phys.Rev.Letters 20, 274 (1968)

Hadronic matter near the boiling point
R. Hagedorn, CERN, Geneva, Switzerland
(To be submitted to Nuovo Cimento)

Multi-Regge approach to high energy production processes
Naren F. Bali, Geoffrey F. Chew, and Alberto Pignotti, Department of Physics, University of Washington, Seattle, Washington, U.S.A.; Department of Physics and Lawrence Radiation Laboratory, University of California, Berkeley, Cal., U.S.A.

Why we need better high energy total cross section measurements
Harry J. Lipkin, The Weizmann Institute of Science, Rehovoth, Israel

Structure in backward π-p elastic scattering at 6, 10, and 14 GeV/c
J. Orear, D.P. Owen, F.C. Peterson, A.L. Read, D.G. Ryan, and D.H. White; A. Ashmore, C.J.S. Damerell, W.R. Frisken, and R. Rubinstein; Cornell University, Ithaca, N.Y., U.S.A.; and Brookhaven National Laboratory, Upton, N.Y., U.S.A.

The reaction $\pi^- p \longrightarrow n\pi^+\pi^-$ at 11 GeV/c
Genova - Hamburg - Milano - Saclay Collaboration

Abundances of kaons and η-mesons in high energy cosmic ray collisions
H. Pilkuhn, Department of Theoretical Physics, University of Lund, Lund, Sweden
(Will probably be published in Nuclear Physics B)

Pomeron exchange in inelastic two-body reactions
Douglas R.O. Morrison, CERN, Geneva, Switzerland
(to be submitted to Physical Review)

Production mechanisms and relations between spin density matrix elements
Gordon A. Ringland and Robert L. Thews, Lawrence Radiation Laboratory, University of California, Berkeley, Cal., U.S.A.

Dipion production in high energy π-p collisions
J.L. Davis, A.R. Erwin, A.F. Garfinkel, R.H. Hartung, Y.Y. Lee, B.Y. Oh, M.A. Thompson, W.J. Robertson, and W.D. Walker, Physics Department, University of Wisconsin, Madison, Wisconsin, U.S.A.
(published in Phys.Rev. Letters 20, 133 (1968))

On statistical large angle scattering
D.S. Chernavsky, E.L. Feinberg, P.N. Lebedev Physical Institute, Moscow, U.S.S.R.

Fit to $K^*(890)N$ production by means of reggeized helicity amplitudes
M. Markytan, CERN, Geneva, Switzerland
(to be submitted to Nuclear Physics)

Five prong interactions by 16 GeV/c π^- on light nuclei
Berkeley - Milano - Orsay Collaboration

The one pion exchange model and the $N^*_{1238} \longrightarrow p\pi^+$ decay, produced in $pp \longrightarrow nN^{*++}_{1238}$ between 2.8 and 10 GeV/c
B. Haber and G. Yekutieli, The Weizmann Institute of Science, Rehovoth, Israel
(to be published in Nuovo Cimento)